Universidade de Aveiro
2022

João Miguel Serras Dias

Bombas de calor por adsorção para aquecimento central e de águas domésticas

Adsorption heat pumps for space and domestic water heating

Universidade de Aveiro
2022

João Miguel Serras Dias

Bombas de calor por adsorção para aquecimento central e de águas domésticas

Adsorption heat pumps for space and domestic water heating

Tese apresentada à Universidade de Aveiro para cumprimento dos requisitos necessários à obtenção do grau de Doutor em Engenharia Mecânica, realizada sob a orientação científica do Doutor Vítor António Ferreira da Costa, Professor Catedrático do Departamento de Engenharia Mecânica da Universidade de Aveiro.

Apoio Financeiro da Fundação para a Ciência e Tecnologia (FCT) e do Fundo Social Europeu (FSE) no âmbito do III Quadro Comunitário de Apoio pela Bolsa de Doutoramento com ref.ª SFRH/BD/145124/2019, pelos projetos do Centro de Tecnologia Mecânica e Automação (TEMA): UIDB/00481/2020 e UIDP/00481/2020 da FCT, CENTRO-01-0145-FEDER-022083 do Centro2020.

O trabalho foi parcialmente desenvolvido no âmbito do projeto Smart Green Homes (SGH), POCI-01-0247-FEDER-007678, uma co-promoção entre a Bosch Termotecnologia S.A. e a Universidade de Aveiro.

o júri

presidente

Professor Doutor João Filipe Colardelle da Luz Mano
Professor Catedrático, Universidade de Aveiro

vogal

Professor Doutor José Joaquim da Costa
Professor Associado, Universidade de Coimbra

Professor Doutor José Carlos Fernandes Teixeira
Professor Catedrático, Universidade do Minho

Doutora Anabela Tavares Aguiar Valente
Investigadora Principal, Universidade de Aveiro

Doutora Ana Isabel Palmero Marrero
Investigadora Sénior, Universidade do Porto

Professor Doutor Celestino Rodrigues Ruivo
Professor Adjunto, Universidade do Algarve

Professora Doutora Mónica Sandra Abrantes de Oliveira Correia
Professora Associada com Agregação, Universidade de Aveiro

Professor Doutor Vítor António Ferreira da Costa (Orientador)
Professor Catedrático, Universidade de Aveiro

agradecimentos

Em primeiro lugar, ao meu orientador, o Professor Vítor Costa, pelos conhecimentos que me transmitiu, pelas imprescindíveis sugestões e críticas ao longo da orientação deste trabalho e pela relação pessoal que proporcionou uma excelente interação entre ambos.
Ao colega Francisco Lamas pelo companheirismo e por toda a ajuda e conhecimentos partilhados.
À Sílvia Coelho por todo o apoio ao longo desta etapa e pela ajuda em diversos momentos.
Aos meus pais pela educação que me proporcionaram ao longo da vida e pelo apoio incondicional.

A todos o meu muito obrigado!

palavras-chave

Sistemas térmicos de adsorção, bombas de calor por adsorção, modelação e simulação dinâmica, avaliação de performance, relação entre coeficientes de performance.

resumo

As tecnologias de aquecimento e refrigeração por adsorção podem ter um papel importante para alcançar um futuro mais verde e sustentável. As bombas de calor por adsorção (BCA) e os refrigeradores por adsorção (RA) podem funcionar com refrigerantes naturais com um potencial de aquecimento global nulo, podendo funcionar com recurso a calor residual e/ou fontes de energia renováveis. As BCA podem melhorar a eficiência energética dos edifícios e das habitações, tendo vindo a suscitar o interesse acrescido dos meios académico e industrial devido ao seu baixo impacte ambiental. Esta tese analisa e desenvolve tecnologias de aquecimento e refrigeração por adsorção, com principal destaque para os sistemas de BCA para aquecimento central ou de águas domésticas, com o objetivo de desenvolver e melhorar os modelos e ferramentas de simulação dinâmica, aumentando assim o seu nível de maturidade tecnológica (TRL).

É apresentada uma revisão da literatura e uma análise crítica do estado da arte das BCA, incluindo o seu princípio de funcionamento, modelos físicos, equilíbrio e cinétia de adsorção, propriedades físicas e termodinâmicas dos materiais adsorventes, pares adsorvente-adsorvato, configuração do leito adsorvente e condições de operação. São identificados e analisados os modelos físicos mais comumente usados para simulação de sistemas de aquecimento e refrigeração por adsorção.

São desenvolvidos e implementados modelos físicos detalhados para cada componente de uma BCA, tendo como objetivo principal a sua integração para a simulação precisa de um sistema de BCA completo. O adsorsor é o componente principal de qualquer sistema de adsorção, requerendo por isso maior atenção. São efetuadas análises da dimensionalidade do modelo e de independência de malha para identificar as combinações que conduzem aos resultados numéricos de maior precisão. Por essa via é possível concluir que são necessários modelos multidimensionais (de parâmetros distribuídos) para obter resultados mais precisos. Recorre-se a um modelo multidimensional para a simulação dinâmica e análise da performance de um adsorsor de tubos revestidos por uma camada (coating) de material adsorvente, a ser utilizado em sistemas de BCA e de RA. O novo modelo proposto para a simulação de sistemas de BCA inclui modelos numéricos validados para cada um dos seus componentes principais, considerando as suas interações e dinâmicas de modo integrado dentro de cada passo de tempo. O modelo físico desenvolvido preenche uma lacuna importante na literatura, sendo capaz de simular sistemas de BCA completos com elevada precisão. Os resultados obtidos por simulação dinâmica de sistemas de BCA completos forneceram a informação necessária para a construção de um protótipo de um sistema de BCA à escala real.

O modelo desenvolvido e implementado é utilizado para investigar a performance de sistemas de BCA e RA, mais concretamente através da obtenção dos seus coeficientes de performance (COP) e da potência específica de aquecimento (PEA) ou da potência específica de refrigeração (PER). O comportamento inverso do COP e da potência específica de aquecimento ou de refrigeração é explorado na procura de um critério que permita identificar a sua melhor combinação. O novo critério proposto baseia-se no mínimo custo da unidade do efeito térmico útil da BCA ou do RA: o tempo de ciclo que minimiza

o custo da unidade do efeito térmico útil da BCA ou do RA conduz ao melhor balanço entre o COP e a potência específica de aquecimento ou de refrigeração. Esta tese fornece uma melhor perspetiva de como modelar e simular sistemas de BCA e de RA com precisão acrescida. Os resultados dos modelos propostos e das simulações realizadas levam a uma melhoria nas previsões da performance, controlo e projeto de sistemas completos de BCA e de RA, contribuindo assim para melhorias futuras da sua performance e projeto, bem como para a redução dos custos de produção. Este trabalho incluiu a construção do protótipo de uma BCA adequada para aquecimento central ou de águas domésticas, que poderá ser utilizado para validação de modelos numéricos, bem como para o estabelecimento de estratégias de controlo e de integração com outros equipamentos.

keywords

Adsorption thermal systems, adsorption heat pumps, dynamic modelling and simulation, performance evaluation, relation between performance coefficients.

abstract

Adsorption heating and cooling technologies can play an important role towards the achievement of a greener and sustainable future. Adsorption heat pumps (AHPs) and adsorption refrigerators (ARs) can work with natural refrigerants that have zero global warming potential (GWP) and can be driven by waste heat and/or renewable energy sources. AHPs can improve household's energy efficiency and given their low environmental impact they have recently gathered increased academic and industrial attention. This thesis analyses and develops adsorption heating and cooling technologies, focusing mainly on AHPs systems suitable for central or domestic water heating applications, aiming to develop and improve their dynamic modelling and simulation, and thus contribute to increase its technology readiness level (TRL).

A literature review and critical analysis of the AHPs is carried out, which includes the working principle, physical models, adsorption equilibrium and kinetics, adsorbent materials physical and thermodynamic properties, adsorbent-adsorbate pairs, adsorbent bed design and operating conditions. The physical models commonly used to simulate adsorption heating and cooling systems are identified and critically analysed.

Detailed physical models of each component of an AHP are developed and implemented, the main objective being their integration for the accurate dynamic simulation of a complete AHP system. The adsorber is the core component of any adsorption system, which deserves major attention. Dimensional and grid independence analyses are conducted to identify their most suitable combinations for more accurate adsorber dynamic simulations. That allowed to conclude that multidimensional (distributed parameters) models are required to obtain more accurate results. A multidimensional model is used for the dynamic simulation and performance evaluation of a coated tube adsorber used in AHPs or ARs systems. The proposed novel model for the simulation of complete AHPs system includes validated numerical models for each of its main components, their interactions and dynamics within each time step being considered in an integrated way. The developed physical model capable of accurately simulating complete AHPs systems fulfils a major literature gap. Based on the results obtained from the dynamic simulations of the complete AHPs systems, a real scale prototype of an AHP system has been constructed.

The developed and implemented model is used to investigate the performance of AHPs and ARs systems, more specifically by obtaining their coefficients of performance (COP) and specific heating power (SHP) or specific cooling power (SCP). The inverse behaviour of the COP and the specific (heating or cooling) powers is explored on the search of a criterion leading to their best combination. Such a novel criterion is proposed, based on the minimum cost of the unit of thermal useful effect of the AHP or AR: the cycle time that minimizes the cost of the unit of thermal useful effect provides the best balance between the COP and the SHP or SCP.

This thesis provides better insights on how to more accurately model and simulate AHPs and ARs systems. Results from the proposed models and simulations allow improved performance prediction, control, and design of complete AHPs and ARs systems, thus contributing to their future performance

and design improvements and manufacturing costs reduction. This work included the construction of an AHP prototype suitable for space and domestic water heating that can be used in the future for numerical models' validation, as well as for design of control strategies and integration with other equipment.

TABLE OF CONTENTS

1. GENERAL INTRODUCTION ---------- 3

1.1. SCOPE ---------- 5
1.2. RESEARCH OBJECTIVES ---------- 7
1.3. OUTLINE OF THE THESIS ---------- 9
1.4. REFERENCES ---------- 13

2. ADSORPTION HEAT PUMPS FOR HEATING APPLICATIONS: A REVIEW OF CURRENT STATE, LITERATURE GAPS AND DEVELOPMENT CHALLENGES. ---------- 19

2.1. INTRODUCTION ---------- 23
2.2. WORKING PRINCIPLE ---------- 24
2.3. BRIEF STATE OF THE ART ---------- 28
2.3.1. Physical models and numerical methods ---------- 28
2.3.2. Adsorption equilibrium ---------- 29
2.3.3. Adsorbent-adsorbate working pairs ---------- 30
2.3.4. Adsorbent physical and thermodynamic properties ---------- 33
2.3.5. Bed specifications ---------- 36
2.3.6. Operating conditions ---------- 37
2.4. AHP DEVELOPMENT CHALLENGES ---------- 38
2.4.1. The physical model for the entire AHP system ---------- 39
2.4.2. On the adsorbent-adsorbate working pair ---------- 41
2.4.3. Regeneration of the adsorbent material ---------- 42
2.4.4. How to improve an AHP system performance? ---------- 42
2.4.5. What are the system's major limitations? ---------- 46
2.5. CONCLUSIONS ---------- 46
2.6. REFERENCES ---------- 49

3. WHICH DIMENSIONAL MODEL FOR THE ANALYSIS OF A COATED TUBE ADSORBER FOR ADSORPTION HEAT PUMPS? ---------- 57

3.1. INTRODUCTION ---------- 61
3.2. AHP'S DIMENSIONAL MODELS ---------- 65
3.2.1. General assumptions ---------- 69
3.2.2. Lumped parameter model (0D model) ---------- 69
3.2.3. 1D distributed parameter model (radial) ---------- 72
3.2.4. 2D distributed parameter model (radial and longitudinal) ---------- 74
3.3. COMPARISON AND SENSIBILITY ANALYSIS OF THE DIMENSIONAL MODELS ------ 76
3.3.1. Reference parameters ---------- 77
3.3.2. Metal-adsorbent interface heat transfer coefficient ---------- 81
3.3.3. Adsorber tube length ---------- 81
3.3.4. Heat transfer fluid velocity ---------- 82
3.3.5. Metal mass ---------- 84
3.4. CONCLUSIONS ---------- 85
3.5. REFERENCES ---------- 87

4. MODELING AND ANALYSIS OF A COATED TUBE ADSORBER FOR ADSORPTION HEAT PUMPS ---------- 95

4.1. INTRODUCTION ---------- 99
4.2. ADSORBER'S DESIGN ---------- 101
4.3. PHYSICAL MODEL ---------- 104

4.4. RESULTS AND DISCUSSION ---- 109
4.4.1. Influence of the evaporator temperature ---- 111
4.4.2. Influence of the condenser temperature ---- 112
4.4.3. Influence of the regeneration temperature ---- 113
4.4.4. Influence of the cycle time ---- 114
4.4.5. Influence of the metal-adsorbent heat transfer coefficient ---- 115
4.4.6. Influence of the adsorbent coating thickness ---- 116
4.4.7. Influence of the tube diameter ---- 117
4.4.8. Influence of the heat transfer fluid velocity ---- 118
4.5. ADSORPTION HEAT PUMP SYSTEM ---- 119
4.6. CONCLUSIONS ---- 122
4.7. REFERENCES ---- 125

5. EVALUATING THE PERFORMANCE OF A COATED TUBE ADSORBER FOR ADSORPTION COOLING ---- 131

5.1. INTRODUCTION ---- 135
5.2. COATED TUBE ADSORBER ---- 138
5.3. ADSORBER MODEL ---- 139
5.4. RESULTS AND DISCUSSION ---- 145
5.4.1. Evaporator temperature ---- 147
5.4.2. Condenser temperature ---- 149
5.4.3. Regeneration temperature ---- 149
5.4.4. Cycle time ---- 150
5.4.5. Regeneration time ---- 151
5.4.6. Tube-adsorbent heat transfer coefficient ---- 152
5.4.7. Adsorbent coating thickness ---- 153
5.4.8. Tube diameter ---- 154
5.4.9. Heat transfer fluid velocity ---- 155
5.5. CONCLUSIONS ---- 156
5.6. REFERENCES ---- 159

6. MODELLING AND ANALYSIS OF A COMPLETE ADSORPTION HEAT PUMP SYSTEM 165

6.1. INTRODUCTION ---- 169
6.2. ADSORPTION HEAT PUMP SYSTEM ---- 174
6.3. PHYSICAL MODEL ---- 180
6.3.1. Evaporator ---- 181
6.3.2. Condenser ---- 182
6.3.3. Electric heater ---- 183
6.3.4. Water reservoir ---- 183
6.3.5. Adsorber ---- 185
6.3.6. Model's solution ---- 191
6.4. RESULTS AND DISCUSSION ---- 192
6.4.1. Temperature, pressure, and uptake fields ---- 194
6.4.2. System's time evolution ---- 198
6.4.3. System's performance evaluation ---- 205
6.5. CONCLUSIONS ---- 206
6.6. REFERENCES ---- 209

7. ON THE BEST COEFFICIENT OF PERFORMANCE AND SPECIFIC HEATING OR COOLING POWER COMBINATION FOR ADSORPTION REFRIGERATORS AND HEAT PUMPS ---- 217

7.1. INTRODUCTION ---------- 221
7.2. PROPOSED METHODOLOGY AND CRITERION ---------- 224
7.3. APPLICATION EXAMPLES ---------- 228
7.3.1. Application example 1 ---------- *229*
7.3.2. Application example 2 ---------- *233*
7.4. CONCLUSIONS ---------- 237
7.5. REFERENCES ---------- 239

8. GENERAL CONCLUSIONS ---------- 243

8.1. SUMMARY OF RESEARCH AND FINDINGS ---------- 245
8.2. FUTURE CHALLENGES ---------- 250

LIST OF FIGURES

Figure 2.1 – Schematics of a common adsorption heat pump. 25
Figure 2.2 – Adsorption heat pump thermodynamic cycle. (Adapted from (Demir et al. 2008)). 25
Figure 2.3 – Types of adsorption isotherms according to the IUPAC classification. In Type IV and Type V graphs, the red and blue lines represent adsorption and desorption, respectively. (Adapted from (Sing 1985)). 30
Figure 2.4 – Adsorber module (on the left) and its representative element (on the right). 40
Figure 2.5 – Schematics of the representative element for the development of physical models. 41
Figure 2.6 – Possible AHP system schematics. 45
Figure 3.1 – Energy scheme of a common adsorption heat pump (Dias and Costa 2018). ... 62
Figure 3.2 – a) Adsorber module containing several metal tubes with an external adsorbent material coating; b) Adsorber module cross section view. 66
Figure 3.3 – Representative element for the development of the physical models (on the left) and schematics (on the right) (Dias and Costa 2018)..... 66
Figure 3.4 – COP and SHP as function of the metal-adsorbent heat transfer coefficient obtained with the 1D and 2D models..... 81
Figure 3.5 – COP and SHP deviations as function of the tube length. 82
Figure 3.6 – COP percent deviation as function of the axial and radial direction resolutions, respectively Δz and Δr, and the heat transfer fluid velocity. 83
Figure 3.7 – SHP percent deviation as function of the axial and radial direction resolutions, respectively Δz and Δr, and the heat transfer fluid velocity. 84
Figure 4.1 – a) Coated tube adsorber schematics. b) Ideal thermodynamic cycle of the AHP (Adapted from (Dias and Costa 2018) with permission from Elsevier)..... 103
Figure 4.2 – The AHP coated tube adsorber, without the sealing metal joint (left) and with the sealing metal joint (right)..... 104
Figure 4.3 – Effect of the evaporator temperature on the adsorber performance for scenarios A and B. 112
Figure 4.4 – Influence of the condenser temperature on the adsorber performance for scenarios A and B. 113
Figure 4.5 – Adsorber performance as a function of the regeneration temperature for scenarios A and B. 114
Figure 4.6 – Influence of the cycle time on the adsorber performance for scenarios A and B. 115
Figure 4.7 – COP and SHP as function of the metal-adsorbent heat transfer coefficient for scenarios A and B. 116
Figure 4.8 – Effect of the adsorbent coating thickness on the adsorber performance for scenarios A and B. 117
Figure 4.9 – Impact of the inner tube's diameter on the adsorber performance for scenarios A and B. 118
Figure 4.10 – Influence of the heat transfer fluid's velocity on the adsorber performance for scenarios A and B. 119
Figure 4.11 – AHP system during the adsorption phase. 121
Figure 4.12 – AHP system during the regeneration phase. 121
Figure 5.1 – a) Schematics of the adsorber module containing several metal tubes with an external adsorbent coating; b) Adsorber module cross section view. (Reproduced from (Dias and Costa 2019) with permission from Elsevier). 139

Figure 5.2 – a) Representative metal tube externally coated with the adsorbent material; b) Coated tube schematics. (Reproduced from (Dias and Costa, 2018) with permission from Elsevier). **140**
Figure 5.3 – Influence of the evaporator temperature on the adsorber's performance. **148**
Figure 5.4 – Effect of the condenser temperature on the adsorber's performance. **149**
Figure 5.5 – COP_c and SCP as function of the regeneration temperature. **150**
Figure 5.6 – Influence of the cycle time on the adsorber's performance. **151**
Figure 5.7 – Effect of the regeneration time on the adsorber's performance. **152**
Figure 5.8 – Tube-adsorbent heat transfer coefficient's impact on the adsorber's performance. **153**
Figure 5.9 – Adsorber's performance as function of the adsorbent coating thickness. **154**
Figure 5.10 – Influence of the tube's diameter on the adsorber's performance. **155**
Figure 5.11 – HTF's velocity impact on the adsorber's performance. **156**
Figure 6.1 – Inner metal tube and an assembled adsorber tubular unit. **175**
Figure 6.2 – Schematics of the adsorber built and modelled. **176**
Figure 6.3 – Pictures of the developed adsorber: a) Three assembled tubular units assembled in the adsorber; b) Fifty tubular units assembled in the adsorber; c) Adsorber sealed with the sealing joint; d) Adsorber assembled with the top HTF collector steel lid. **177**
Figure 6.4 – The AHP system: a) During the adsorption phase, and b) During the regeneration (desorption) phase. **179**
Figure 6.5 – Finite volume discretization of the water reservoir. **184**
Figure 6.6 – Schematics of an adsorber's single tubular unit (figure not to scale). **186**
Figure 6.7 – Time evolution of the uptake, including the warming up period, for the bottom, middle, and top layers, a) mean axial uptake; b) mean radial uptake. **192**
Figure 6.8 – Temperature, pressure, and uptake distributions in the adsorbent bed at selected instants a) during pre-cooling; b) during adsorption. **196**
Figure 6.9 – Temperature, pressure, and uptake distributions in the adsorbent bed at selected instants, a) during pre-heating b) during regeneration. **197**
Figure 6.10 – Time evolution of the adsorbent's bed temperature for the bottom, middle and top layers, a) mean axial temperature; b) mean radial temperature. **199**
Figure 6.11 – Time evolution of the adsorbent's bed pressure for the bottom, middle and top layers, a) mean axial pressure; b) mean radial pressure. **200**
Figure 6.12 – Time evolution of the adsorbent's bed uptake for the bottom, middle and top layers, a) mean axial uptake; b) mean radial uptake. **201**
Figure 6.13 – Time evolution of, a) the evaporator's temperature; and b) the adsorbate mass in the evaporator. **203**
Figure 6.14 – Time evolution of, a) the condenser's temperature and mean water temperature in the reservoir's control volumes that contain the condenser; and b) the reservoir's mean water temperature. **204**
Figure 7.1 – Dependence of the dimensionless *COP (C)* and *SHP (S)* on the dimensionless cycle time τ. **230**
Figure 7.2 – Dependence of the dimensionless function F on the dimensionless cycle time τ for some selected values of β, for $\gamma = 0.1$. **231**
Figure 7.3 – Dependence of the dimensionless function F on the dimensionless cycle time τ for some selected values of β, for $\gamma = 0.1$. **232**
Figure 7.4 – Dependence of the dimensionless function F on the dimensionless cycle time τ for some selected values of γ for $\beta = 1$. **233**
Figure 7.5 – Dependence of the dimensionless *COP* (C) and *SHP* (S) on the dimensionless cycle time τ. **234**

Figure 7.6 – Dependence of the dimensionless function F on the dimensionless cycle time τ for some selected values of β, for $\gamma = 0.1$..... 235
Figure 7.7 – Dependence of the dimensionless function F on the dimensionless cycle time τ for some selected values of β, for $\gamma = 0.1$..... 235
Figure 7.8 – Dependence of the dimensionless function F on the dimensionless cycle time τ for some selected values of γ, for $\beta = 0.2$..... 236

LIST OF TABLES

Table 3.1 – Standard parameters used in the simulations. 78
Table 3.2 – Results comparison for the different dimensional models using constant parameters. 80
Table 3.3 – Deviations of COP and SHP due to disregarding the tube metal mass. 85
Table 4.1 – Dimensions of the coated tube adsorber. 104
Table 4.2 – Reference values for the parameters and thermophysical properties used in the simulations. 111
Table 5.1 – Parameters used as references. 147
Table 6.1 – Reference parameters used in the simulations. 193
Table 7.1 – Set of parameters used to obtain the *COP* and *SHP*. 229

LIST OF ORIGINAL PUBLICATIONS

The following original publications resulted from this PhD work, this thesis being the result of their compilation:

I. **Dias JMS**, Costa VAF (2018) Adsorption heat pumps for heating applications: A review of current state, literature gaps and development challenges. *Renewable and Sustainable Energy Reviews* 98:317–327. https://doi.org/10.1016/j.rser.2018.09.026

II. **Dias JMS**, Costa VAF (2019) Which dimensional model for the analysis of a coated tube adsorber for adsorption heat pumps? *Energy* 174:1110–1120. https://doi.org/10.1016/j.energy.2019.03.028

III. **Dias JMS**, Costa VAF (2021) Modeling and Analysis of a Coated Tube Adsorber for Adsorption Heat Pumps. Energies 14:6878. https://doi.org/https://doi.org/10.3390/en14216878

IV. **Dias JMS**, Costa VAF (2020) Evaluating the performance of a coated tube adsorber for adsorption cooling | Évaluation de la performance d'un adsorbeur à tube enrobé pour le refroidissement par adsorption. *International Journal of Refrigeration* 118:21–30. https://doi.org/10.1016/j.ijrefrig.2020.06.023

V. **Dias JMS**, Costa VAF (2022) Modelling and analysis of a complete adsorption heat pump system. Appl Therm Eng 118782. https://doi.org/https://doi.org/10.1016/j.applthermaleng.2022.118782

VI. Costa VAF, **Dias JMS,** (2022) On the best coefficient of performance and specific heating or cooling power combination for adsorption refrigerators and heat pumps. Applied Thermal Engineering (Under Revision)

ABBREVIATIONS

AHP	Adsorption heat pump
COP	Coefficient of performance
COP_c	Cooling coefficient of performance
EU	European Union
GHG	Greenhouse gases
GWP	Global warming potential
HCFC	Hydrochlorofluorocarbons
HFC	Hydrofluorocarbons
HP	Heat pump
HTF	Heat transfer fluid
IEA	International Energy Agency
SCI	Science Citation Index
SCP	Specific cooling power
SHP	Specific heating power
TRL	Technology readiness level
VCHP	Vapor compression heat pumps

CHAPTER 1

1. GENERAL INTRODUCTION

This Chapter presents the general scope of the PhD work. The importance of adsorption heat pumps towards the achievement of a greener future and implementation of environmentally friendly technologies is highlighted. The advantages and setbacks of the technology, as well as its position in the heating and cooling market are presented. Research needs in the field of adsorption heat pumps are identified and the research questions are formulated. Furthermore, the research objectives and the scientific contributions of the thesis are described. Finally, the outline of the thesis is presented, connecting all the papers that resulted from the PhD work.

1.1. SCOPE

Moving towards a greener planet is crucial to maintain citizens' life quality in fully developed countries and to improve living conditions in underdeveloped regions. In Europe, this process is already on the march through goal settings, rules and legislation, and population's mindsets. The European Union (EU) is focused on an ambitious growth strategy that aims to achieve zero greenhouse gases (GHG) emissions by 2050. To comply with this objective, priority has been set by the European Commission to carry out the European Green Deal from 2019 to 2024, which focuses on several key actions like environmentally friendly technologies, decarbonization of the energy sector, and improvement of buildings' energy efficiency, among others (European Commission 2019).

As the biggest energy end-use sector in Europe, heating and cooling accounted for 51% of the EU's energy consumption in 2019, from which approximately 75% were obtained from burning fossil fuels. In 2017, buildings stood for 33% of the EU total energy consumption, 86.4% still coming from non-renewable sources (REN21 2020). Space and water heating represent 79% of European households' final energy consumption (European Commission 2021). During recent years, most focus is being addressed to include and increase the share of renewables in the energy sector; however, considering residential and industrial buildings and processes, the heating and cooling sector is causing a bigger impact on the environment than the electricity production sector itself. Efforts must be strengthened to diminish the harmful impacts of thermal energy needs and move towards the achievement of the key energy goals set for the following years, by introducing new technologies and improving those that are already available.

Heat pumps are among the most environmentally friendly technologies that can be integrated with intermittent renewable energy sources (Yunna and Ruhang 2013). Since heat pumps can contribute to lessen GHG emissions, its importance has been recently growing. Nonetheless, heat pumps market share is still meagre, having accounted for just 5% of the buildings heating sector in 2019. Under the Sustainable Development Scenario, heat pumps representation in the market is required to triple by 2030, which will require several technological improvements, installation and purchase costs reduction, increased energy performance, removal of market barriers, and enforce the use of alternative refrigerants (International Energy Agency (IEA) 2020). Policy makers from several countries are setting incentives towards the embracement and diffusion of heat pumps throughout the

society, recognizing and promoting the benefits they can provide to the desired low carbon future, in the transition to a more sustainable energy society (Gaur et al. 2021).

The common and most used heat pumps in the market are electricity driven conventional vapor compression heat pumps (VCHP). Although many efforts have been carried out to reduce their global warming potential (GWP), VCHP still mostly rely on refrigerants (HFCs and HCFCs) with significant GWP. Due to their low environmental impact, adsorption heat pumps (AHP) have captivated the interest of researchers and attracted the heating and cooling market's attention over the last years. Their importance has been rising mainly due to two key characteristics. Firstly, they can work with natural refrigerants, such as water and ammonia, with zero GWP, which are environmentally friendly, abundant in nature, and are easy to deal with (Dawoud 2014). Secondly, unlike VCHP that are driven by electricity, AHP are driven by thermal energy, that can result from waste heat and renewable energies like solar, biomass and geothermal energy (Demir et al. 2008). One of the concerns with VCHP that is recently worrying their manufacturers and customers, especially in the residential market of the more developed countries, is the significant compressor noise. Since AHP do not require moving parts, they do not generate noise, making them ideal for applications for which noise and vibration are concerns, like the residential sector. Despite the clear environmental and acoustic and vibration advantages, AHP also have some setbacks, which are mainly the high manufacturing costs associated with new technologies, lower coefficient of performance (COP) and low power density. More research and innovation are needed to diminish the hindrances of AHP technology and create favourable conditions to truly introduce this technology in the market and make it appealing.

However, directly comparing the performance of AHP and VCHP is more complex than what commonly assumed (Boruta et al. 2021). The COP for adsorption technologies should not be directly compared to that of VCHP since there is a significant difference between them. AHP are directly driven by thermal energy that can be freely obtained, or obtained from processes with high energy efficiencies close to 100% (e.g., waste heat, solar collectors, gas and biomass burners). On the other hand, VCHP rely on electricity and their COP is obtained as the ratio between the thermal energy obtained and the electric energy required to operate the heat pump, disregarding the thermal energy lost during the thermal to electric energy conversion processes, which have low efficiencies (30-40% for steam turbines and 10-14% for photovoltaic panels). To truly compare the AHP's and VCHP's COPs, the primary energy lost during electric energy production process should be included

as an input for the VCHP, which will result in much lower COPs than those commonly reported. Only under these conditions the COP comparison between these two different heat pump technologies can be more effectively made. This must be taken into consideration, and it is important to make use of the financial incentives, decided by policy makers, to carry out further research on AHP technology to minimize its well-identified disadvantages and improve its technology readiness level (TRL).

A simple AHP must include an adsorber, an evaporator, a condenser, an expansion valve and a heat transfer system to provide/withdraw heat to/from the adsorber (Dias and Costa 2018). Several studies focus on adsorbent-adsorbate working pairs selection (e.g. (Freni et al. 2016; Boman et al. 2017)), development of new adsorbent materials (e.g. (Pinheiro et al. 2015; Calabrese et al. 2017a, b; Henninger et al. 2017; Kim et al. 2017)), adsorbent materials' physical and thermodynamic properties (e.g. (Poyelle et al. 1999; Zhang and Wang 1999; Freni et al. 2013)), adsorber configurations (e.g. (Girnik et al. 2017; Mohammadzadeh Kowsari et al. 2017; Rivero-Pacho et al. 2017; Wittstadt et al. 2017)) and operating conditions (e.g. (Dawoud 2014; Sapienza et al. 2016; Palomba et al. 2017a)). However, physical models describing a complete AHP system cannot be found in the literature (Dias and Costa 2018). Furthermore, a system level study considering the simultaneous optimization of the adsorber configuration and the system's operating conditions is lacking (Pesaran et al. 2016). Considering the advancements in computational power, it is now possible to carry out complex and detailed simulations much faster than before, what enables the development of extensive and reliable models that consider the dynamics of complete AHP systems.

1.2. RESEARCH OBJECTIVES

Following the identified research needs, this work aims to contribute to the development of accurate models for complete AHP systems and the improvement of their performance, fulfilling the literature gap for system level studies. The developed tool will be able to simulate the dynamics of a complete AHP system, enabling the optimization and better prototypes designs, accelerating the achievement of generous performance coefficients at lower costs and shorter times. In this context, this work will enrich the knowledge in the field by providing answers for the following main questions: How to develop and implement a physical model for an entire AHP system? How to improve the AHP systems' performance?

This work follows the 2030 Agenda goals 7, 11 and 12. More specifically, AHPs will help increasing the share of renewable energy (goal 7.2) and improve the energy efficiency of the residential sector (goal 7.3). Furthermore, using performance optimized AHPs will reduce the emissions caused by gas and petrol burning, contributing to better air quality in cities, and allow the re-use of wasted energy in households, lowering the amount of primary energy consumed (goal 11.6). Additionally, replacing conventional heat pumps that can release greenhouse gases by AHPs will mitigate the release of these harmful substances to the environment (goal 12.4), minimizing the harmful effects of space and domestic water heating on global warming.

The main objective of this work is to model, simulate and develop a complete AHP system for space and domestic water heating. More specifically, the objectives are as follows:

- Understand the dynamics of AHP systems suitable for space and domestic water heating. Identify and select a suitable design and adsorbent-adsorbate working pair for an AHP for space and water heating;
- Establish and develop models capable of describing the selected adsorber design. Implement the developed models to carry out parametric studies and sensitivity analyses, aiming to identify the key parameters and dynamics of AHP suitable for space and domestic water heating;
- Based on the outcomes of the previous objective, develop a complete AHP system to be used for domestic space and water heating. Develop physical models capable of simulating the dynamics of whole AHP systems, considering not only the adsorber, as usual in the literature, but also all their main components and the interactions between them. Perform parametric studies and sensitivity analyses for the whole AHP system, identifying the key parameters, considering different working modes, system configurations and control techniques;
- Considering the results and conclusions obtained from the accurate and detailed simulation of the complete AHP system, build a representative prototype of the AHP and conduct experimental tests to validate/calibrate the developed models.

These objectives help overcoming the existing gaps in this scientific domain and provide a powerful tool that can be used to develop AHPs with better performances at lower costs in shorter times. In addition, it will be possible to use the developed model to test several working pairs, physical and thermodynamic properties of adsorbents and adsorbates, different adsorber configurations and operation conditions. The proposed model for the whole AHP system represents a major scientific accomplishment since a system level approach is still lacking.

This work began within the Smart Green Homes project (POCI-01-0247-FEDER-007678), a co-promotion between Bosch Termotecnologia S.A. and the University of Aveiro. The initial plan included building and testing prototypes of AHP by Bosch Termotecnologia S.A. and their testing, which ended up not being possible within the useful timeline of the project due mainly to several delays in delivering the necessary materials during the Covid-19 pandemic. A base prototype was still built, and preliminary tests carried out to assess its operability under the required vacuum conditions, but there was no time left for its fine tuning and detailed and complete operation testing.

1.3. OUTLINE OF THE THESIS

This document presents the main results and the discussions of the PhD thesis entitled “Adsorption heat pumps for space and domestic water heating”, which arose from a set/sequence of scientific papers on the AHP subject, and it is structured as follows.

Chapter 1 presents a brief scope of AHP technologies, identifying and discussing their advantages and hindrances, current position on the market, performance criteria and coefficients and the trends and focus of recent investigations. These topics will be extensively discussed in Chapter 2.

Chapter 2 presents a literature review and critical analysis of the most relevant work on the field of AHP, covering the working principle, physical models, adsorption equilibrium and kinetics, adsorbent material physical and thermodynamic properties, adsorbent bed design and operating conditions. This work helped pointing out the literature gaps in AHP technologies, formulating the research questions, and delineating the research objectives of this thesis. The lack of system level studies and of detailed models for whole AHP systems was quickly identified as a major gap in the literature. The best adsorbent-adsorbate working pairs that would be used throughout this work were also identified, adsorbent coatings being the most promising adsorbent bed design.

Being the lack of detailed models for AHP technologies identified as a major gap, Chapter 3 discusses in detail the common physical models used to describe adsorption technologies. Dimensional analysis and grid independence studies were carried out using a lumped parameter model (0D), a 1D distributed parameter model (radial direction), and a 2D distributed parameter model (radial and longitudinal directions). A comparison and sensibility analyses of the three-dimensional models (0D, 1D and 2D) is also carried out, considering variations of some parameters and analysing the results deviations. This study concludes that the 2D distributed parameter model must be used in order to more accurately describe the adsorber dynamics of AHP systems and identified the adsorbent bed mesh resolution that must be used to conduct accurate analyses and performance predictions. Thus, the 2D distributed parameter model is selected for the following studies.

Since adsorbent coatings had been identified in Chapter 2 as the most promising solutions to achieve higher AHP performance coefficients, a coated tube adsorber is modelled and analysed in Chapter 4. A coated tube adsorber suitable for space and domestic water heating is proposed and discussed. The 2D distributed parameter model discussed in Chapter 3 is implemented to the proposed design and application. This paper focus on the effect of several governing parameters on the coated tube adsorber performance, more specifically on its COP and SHP. The analysed parameters are the regeneration, condenser and evaporator temperatures, the heat transfer fluid velocity, the heat transfer tube diameter, the adsorbent coating thickness, the metal-adsorbent heat transfer coefficient, and the cycle time. Considering the analysis carried out for the coated tube adsorber, a proposal for a complete adsorption heat pump system is presented.

The needs of both heating and cooling is common in the residential sector. In Chapter 5, the coated tube adsorber is analysed for cooling applications aiming to evaluate its performance for such working conditions. The 2D distributed parameter model is used to analyse the influence of several governing parameters such as the evaporator, condenser and regeneration temperatures, cycle time, metal-adsorbent heat transfer coefficient, metal tube diameter, coating thickness and heat transfer fluid (HTF) velocity on the adsorber's performance. The cycle time was identified as a system-controlling parameter to tune the COP_c and the specific cooling power (SCP). A regeneration temperature of approximately 70 °C results on the highest cooling coefficient of performance (COP_c), which makes the system suitable for regeneration using solar thermal collectors. The possibility to generate a cooling effect resorting on freely obtained thermal energy is the major advantage of adsorption cooling.

The information obtained from the previous Chapters culminated on the development and modelling of an entire AHP system. The AHP system that has been proposed in Chapter 4 was improved. In Chapter 6, a detailed and accurate model for the whole AHP system suitable for space and domestic water heating is presented, fulfilling the major literature gap for detailed models capable of simulating all the dynamics of whole AHP systems, identified in Chapter 2. This novel approach implements validated numerical models for each of the main components of the AHP system, connecting and integrating all the components considering their interactions and dynamics within each time step. As a result, a deeper understanding of AHP's dynamics and more accurate performance predictions can be achieved. The improved model can provide better insights on how to design and control the AHP systems, contributing to future performance improvements and manufacturing costs reduction.

The inverse behaviour of the performance parameters COP and SCP or SHP was common in all the investigations carried out throughout this work. An objective criterion that allows setting the best balance between the COP and SCP or SHP was found to be essential for the optimization of adsorption heating and cooling technologies, not being available in the literature. Such criterion is proposed in Chapter 7, based on the minimum cost of the unit of obtained useful effect in adsorption refrigerators or heat pumps. For a system operating under a given set of operating conditions the dependence of COP and SCP or SHP on the cycle time can be obtained from numerical simulations using the model for the complete system, presented in Chapter 6, and once known these dependencies it is found the cycle time leading to the minimum cost of the unit of obtained useful effect. The best balance between COP and SCP or SHP corresponds to the COP and SHP associated with that cycle time. Two examples are presented to show the application of the (new) proposed criterion.

Finally, Chapter 8 summarizes the main outcomes achieved in this thesis, analysing the progresses made in the modelling and simulation of AHP systems. In addition, Chapter 8 provides suggestions of possible tasks and future works to be developed following the research presented throughout this thesis.

This thesis is based on slightly modified versions of published and on submitted to publication papers in peer-reviewed journals from the Science Citation Index (SCI). The slight papers modifications concern the harmonization of: i) References, since the papers were published in different journals, using different references styles, ii) Harmonization and document formatting to make the text easier to read, and iii) Minor spelling corrections and

nomenclature updates. The references used in this work are compiled at the end of each chapter. Given that this work is published in several different scientific journals, with difference formatting and styles, each Chapter has its own nomenclature, which is presented before the Introduction Section of each Chapter. In all the (published and submitted) papers, the author was responsible for the study conception and design, as well as for the results analysis and for the manuscript writing. Professor Vítor Costa, as co-author and supervisor of this work, was responsible for the orientation of all the steps related to the successful development of the thesis.

1.4. REFERENCES

Boman DB, Hoysall DC, Pahinkar DG, et al (2017) Screening of working pairs for adsorption heat pumps based on thermodynamic and transport characteristics. Appl Therm Eng 123:422–434. https://doi.org/10.1016/j.applthermaleng.2017.04.153

Boruta P, Bujok T, Mika Ł, Sztekler K (2021) Adsorbents, Working Pairs and Coated Beds for Natural Refrigerants in Adsorption Chillers—State of the Art. Energies 14:. https://doi.org/10.3390/en14154707

Calabrese L, Bonaccorsi L, Freni A, Proverbio E (2017a) Silicone composite foams for adsorption heat pump applications. Sustain Mater Technol 12:27–34. https://doi.org/10.1016/j.susmat.2017.04.002

Calabrese L, Brancato V, Bonaccorsi L, et al (2017b) Development and characterization of silane-zeolite adsorbent coatings for adsorption heat pump applications. Appl Therm Eng 116:364–371. https://doi.org/10.1016/j.applthermaleng.2017.01.112

Dawoud B (2014) On the development of an innovative gas-fired heating appliance based on a zeolite-water adsorption heat pump; System description and seasonal gas utilization efficiency. Appl Therm Eng 72:323–330. https://doi.org/10.1016/j.applthermaleng.2014.09.008

Demir H, Mobedi M, Ülkü S (2008) A review on adsorption heat pump: Problems and solutions. Renew. Sustain. Energy Rev. 12:2381–2403

Dias JMS, Costa VAF (2018) Adsorption heat pumps for heating applications: A review of current state, literature gaps and development challenges. Renew Sustain Energy Rev 98:317–327. https://doi.org/10.1016/J.RSER.2018.09.026

European Commission (2019) A European Green Deal. https://ec.europa.eu/info/strategy/priorities-2019-2024/european-green-deal_en

European Commission (2021) Heating and Cooling. https://ec.europa.eu/energy/topics/energy-efficiency/heating-and-cooling_en

Freni A, Frazzica A, Dawoud B, et al (2013) Adsorbent coatings for heat pumping applications: Verification of hydrothermal and mechanical stabilities. In: Applied Thermal Engineering. pp 1658–1663

Freni A, Maggio G, Sapienza A, et al (2016) Comparative analysis of promising adsorbent/adsorbate pairs for adsorptive heat pumping, air conditioning and refrigeration. Appl Therm Eng 104:85–95. https://doi.org/10.1016/j.applthermaleng.2016.05.036

Gaur AS, Fitiwi DZ, Curtis J (2021) Heat pumps and our low-carbon future: A comprehensive review. Energy Res. Soc. Sci. 71:101764

Girnik IS, Grekova AD, Gordeeva LG, Aristov YI (2017) Dynamic optimization of adsorptive chillers: Compact layer vs. bed of loose grains. Appl Therm Eng 125:823–829. https://doi.org/10.1016/j.applthermaleng.2017.06.141

Henninger SK, Ernst SJ, Gordeeva L, et al (2017) New materials for adsorption heat transformation and storage. Renew Energy 110:59–68. https://doi.org/10.1016/j.renene.2016.08.041

International Energy Agency (IEA) (2020) Heat Pumps. In: IEA, Paris. https://www.iea.org/reports/heat-pumps

Kim C, Cho K, Kim SK, et al (2017) Alumina-coated ordered mesoporous silica as an efficient and stable water adsorbent for adsorption heat pump. Microporous Mesoporous Mater 239:310–315. https://doi.org/10.1016/j.micromeso.2016.10.014

Mohammadzadeh Kowsari M, Niazmand H, Tokarev MM, et al (2017) Bed configuration effects on the finned flat-tube adsorption heat exchanger performance: Numerical modeling and experimental validation. Appl. Energy

Palomba V, Vasta S, Freni A (2017) Experimental testing of AQSOA FAM Z02/water adsorption system for heat and cold storage. Appl Therm Eng 124:967–974. https://doi.org/10.1016/j.applthermaleng.2017.06.085

Pesaran A, Lee H, Hwang Y, et al (2016) Review article: Numerical simulation of adsorption heat pumps. Energy 100:310–320

Pinheiro JM, Valente AA, Salústio S, et al (2015) Application of the novel ETS-10/water pair in cyclic adsorption heating processes: Measurement of equilibrium and kinetics properties

and simulation studies. Appl Therm Eng 87:412–423. https://doi.org/10.1016/j.applthermaleng.2015.05.011

Poyelle F, Guilleminot J-JJ, Meunier F (1999) Experimental Tests and Predictive Model of an Adsorptive Air Conditioning Unit. Ind Eng Chem Res 38:298–309. https://doi.org/10.1021/ie9802008

REN21 (2020) Renewables 2020 Global Status Report. Paris

Rivero-Pacho AM, Critoph RE, Metcalf SJ (2017) Modelling and development of a generator for a domestic gas-fired carbon-ammonia adsorption heat pump. Renew Energy 110:180–185. https://doi.org/10.1016/j.renene.2017.03.089

Sapienza A, Gullì G, Calabrese L, et al (2016) An innovative adsorptive chiller prototype based on 3 hybrid coated/granular adsorbers. Appl Energy 179:929–938. https://doi.org/10.1016/j.apenergy.2016.07.056

Wittstadt U, Füldner G, Laurenz E, et al (2017) A novel adsorption module with fiber heat exchangers: Performance analysis based on driving temperature differences. Renew Energy 110:154–161. https://doi.org/10.1016/j.renene.2016.08.061

Yunna W, Ruhang X (2013) Green building development in China-based on heat pump demonstration projects. Renew. Energy 53:211–219

Zhang LZ, Wang L (1999) Effects of coupled heat and mass transfers in adsorbent on the performance of a waste heat adsorption cooling unit. Appl Therm Eng 19:195–215. https://doi.org/10.1016/S1359-4311(98)00023-4

CHAPTER 2

This Chapter has been published as:

Dias JMS, Costa VAF (2018) Adsorption heat pumps for heating applications: A review of current state, literature gaps and development challenges. Renew Sustain Energy Rev 98:317–327. https://doi.org/10.1016/j.rser.2018.09.026

2. ADSORPTION HEAT PUMPS FOR HEATING APPLICATIONS: A REVIEW OF CURRENT STATE, LITERATURE GAPS AND DEVELOPMENT CHALLENGES.

Abstract

A review of the most relevant work on the field of adsorption heat pumps with emphasis on heating applications is presented, covering the working principle, physical models, adsorption equilibrium and kinetics, adsorbent material physical and thermodynamic properties, adsorbent bed designing and operating conditions. The major literature gaps and development challenges of adsorption heat pumps for heating applications are identified and discussed. A bridge between materials and system level studies is lacking. The simultaneous investigation of the adsorption kinetics, adsorbent bed specifications, operating conditions and interaction between all the system components is missing in the literature. Detailed information required for the development and validation of physical models is often not provided in the experimental studies. A physical model that considers an entire adsorption heat pump system, which is required for performance predictions and system's optimization, cannot be found in the literature. To improve the adsorption heat pump system's performance the heat and mass transfer resistances need to be minimized by developing new adsorbent materials and better interaction between the adsorbent bed and the wall of the duct where the heat transfer fluid flows. In addition, operation modes optimized for the desired application can also contribute to improving the system's performance.

Keywords: Adsorption heat pump, Heating applications, Renewable energy, Adsorption heating, System's performance, Physical model

NOMENCLATURE

C	Specific heat (J/kg.K)
C_p	Constant pressure specific heat (J/kg.K)
H	Enthalpy (J)
m	Mass (kg)
P	Pressure (Pa)
Q	Heat (J)
T	Temperature (absolute) (K)
X	Adsorbate concentration in the adsorbent (uptake) ($kg_a.kg_s^{-1}$)

Greek letters

τ	Cycle time (s)

Subscripts

a	Adsorbate
ads	Adsorption
bed	Adsorbent bed
c	Condenser /Cooling
cyc	Cycle
des	Desorption
e	Evaporator
h	Heating
ic	Isosteric cooling
ih	Isosteric heating
s	Adsorbent
v	Vapour/Vaporization

2.1. INTRODUCTION

Due to their low environmental impact, adsorption heat pumps (AHPs) have attracted researchers and heating market attention over the last years. Compared to the conventional vapour compression heat pumps, which rely on high global warming potential (GWP) refrigerants (HFCs and HCFCs), AHPs may work with natural refrigerants that have zero GWP such as water and ammonia (Dawoud 2014). Moreover, contrary to the vapour compression heat pumps that run on electrical energy, AHPs can make mainly use of waste heat and renewable energies like solar and geothermal energy (Demir et al. 2008).

Nowadays, almost 50% of Europe's energy consumption is channelled to heat and cold production. More than 35% of the overall consumption is used by the building sector alone, from which 75% is employed on domestic hot water production and room heating (Pinheiro et al. 2016). Since most of this energy is from non-renewable and environmentally harmful energy sources, AHPs can significantly contribute to decrease humanity's dependence on these harmful energy sources.

AHP's application was first demonstrated by Tchernev (1976) for domestic hot water production and space heating. Since then, much research has been done in order to increase their coefficient of performance (COP), operating with lower desorption temperatures and providing continuous heating or cooling process. Finding new working pairs or enhance the existing pairs to increase the COP, the adsorption rate and to decrease desorption temperature are among the most studied subjects at the adsorbent material level. In addition, the development of more accurate and efficient numerical models, optimization of heat and mass transfer by designing of adsorbent beds and operating conditions have also been investigated (Demir et al. 2008). However, studies of a complete AHP system considering all its aspects and components cannot be found in literature.

In the following sections, an overview of the recent studies on adsorption heat pumps with emphasis on heating applications is presented. The main objective is to identify the bridges that need to be built between the adsorption kinetics, bed designing, operating conditions and remaining system components instead of being a repertory of previous work on the field. Thus, the identification of the major challenges and setting directions for the development of future work, attempting to fill the existing gaps, are discussed in this review. In addition, this paper comprises information about the AHP working principle, physical models, adsorption equilibrium and kinetics of typical and new adsorbent-adsorbate working

pairs, adsorbent material thermodynamic and physical properties, adsorbent bed designing and operating conditions. Overall, it can help researchers working on the field or it can be used as a guide for researchers that are new to the AHPs subject, covering the main usually dispersed information required to start developing work in AHP systems.

2.2. WORKING PRINCIPLE

Heat pumps work by extracting heat from a low temperature level and delivering it at an intermediate temperature level, driven by a third energy source (Ulku 1986). In AHPs, this third energy source is heat from a higher temperature level source that in practice can be, for example, waste heat, gas burners, electricity, geothermal and solar energy. A simple AHP consists of an adsorbent material packed or coated on an adsorbent bed (metallic structure where the adsorbent is placed), an evaporator, a condenser, an expansion valve and a heat transfer system or fluid to provide/withdraw heat to/from the adsorbent bed. In heating applications, the evaporator makes use of a free of charge low temperature level heat source (ambient, geothermal or waste heat) to vaporize the adsorbate, which is fed to the adsorbent bed during the adsorption phase. Useful heat of adsorption is collected by the heat transfer system, normally through a heat transfer fluid (HTF). On the other hand, during desorption phase heat has to be provided to the bed in order to release the adsorbate from the adsorbent in vapour state. The adsorbate is driven through the condenser, where it condenses before returning to the evaporator. Useful heat of condensation, Q_c, is released during the process. A scheme of an AHP system is presented in Figure 2.1.

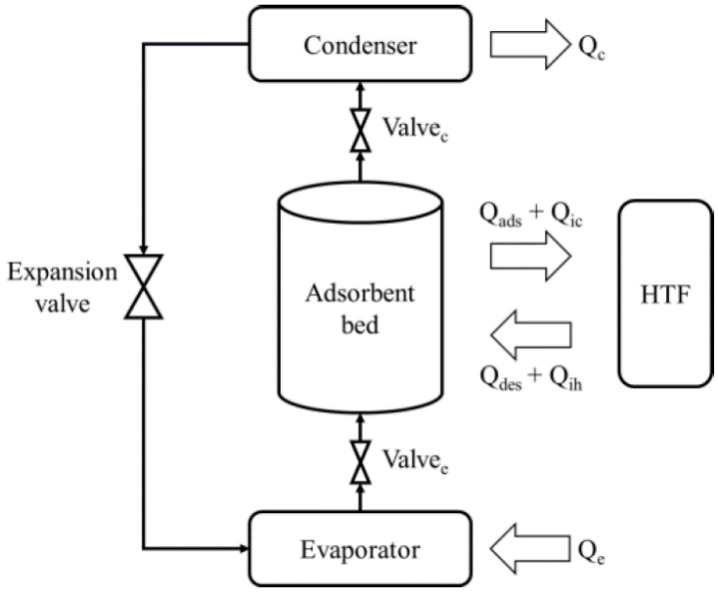

Figure 2.1 – Schematics of a common adsorption heat pump.

The ideal thermodynamic cycle of an AHP is presented in Figure 2.2. in the Clapeyron diagram. It consists of four phases, namely isobaric adsorption (1-2), isosteric heating (2-3), isobaric desorption (3-4) and isosteric cooling (4-1).

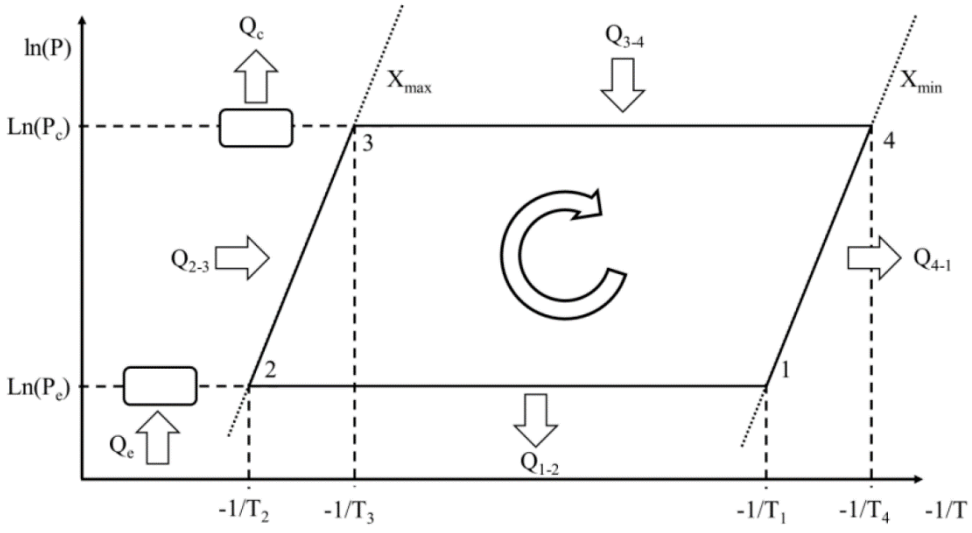

Figure 2.2 – Adsorption heat pump thermodynamic cycle. (Adapted from (Demir et al. 2008)).

During the isobaric adsorption phase (1-2) the valve between the evaporator and the adsorbent bed is open and the valve between the adsorbent bed and the condenser is closed. The vaporized adsorbate is adsorbed by the adsorbent releasing heat Q_{1-2} in the

process, which has to be removed until the bed temperature reaches T_2 (~T_c). The cycle maximum adsorbate uptake, X_{max}, is achieved at the end of the phase and it is dependent on the bed pressure, which is normally at the evaporator pressure, P_e. The heat released by the adsorbent bed during this phase can be calculated through the following equation (Demir et al. 2008):

$$-Q_{1-2} \approx \int_{T_1}^{T_2} \left[m_s\left(C_s + XC_{p,a}\right) + m_{bed}C_{bed}\right]dT - \int_{X_{min}}^{X_{max}} m_s \Delta H_{ads} dX \quad 2.1$$

After the isobaric adsorption phase (1-2), the isosteric heating phase (2-3) starts. The valve between the evaporator and the adsorbent bed is closed and heat is provided to the bed. Since both bed valves are closed, the adsorbate uptake remains constant throughout this phase. The pressure inside the bed increases with temperature until it reaches the condenser pressure, P_c, when the phase is terminated. The amount of heat provided during this process is given by (Demir et al. 2008):

$$Q_{2-3} \approx \int_{T_2}^{T_3} \left[m_s\left(C_s + X_{max}C_{p,a}\right) + m_{bed}C_{bed}\right]dT \quad 2.2$$

The isobaric desorption phase (3-4) follows continuing the heating process with the valve between the bed and the condenser open. The adsorbate is desorbed and flows from the bed to the condenser, where it condenses releasing useful heat of condensation, Q_c. The pressure remains constant during this phase, being at the condenser pressure. When desorption temperature, $T_{des} = T_4$, is achieved the valve is closed and the next phase follows. The heat that must be provided to the bed during this phase is given by (Demir et al. 2008):

$$Q_{3-4} \approx \int_{T_3}^{T_4} \left[m_s\left(C_s + XC_{p,a}\right) + m_{bed}C_{bed}\right]dT - \int_{X_{max}}^{X_{min}} m_s \Delta H_{ads} dX \quad 2.3$$

The last phase of the cycle is the isosteric cooling (4-1). The valves between the adsorbent bed and the condenser and evaporator are closed and the temperature of the bed is lowered. The uptake remains constant during the process and the pressure inside the bed decreases along with the temperature. When the pressure drops to the evaporator

pressure, P_e, the phase ends and the subsequent isobaric adsorption phase follows. The heat withdrawn from the bed during the isosteric cooling is (Demir et al. 2008):

$$-Q_{4-1} \approx \int_{T_4}^{T_1} \left[m_s \left(C_s + X_{min} C_{p,a} \right) + m_{bed} C_{bed} \right] dT \quad 2.4$$

The required heat for the vaporization of the adsorbate in the evaporator, Q_e, taken from the low-level heat source during adsorption, and the heat of condensation, Q_c, obtained during desorption phase, can be described as (Demir et al. 2008):

$$Q_e = m_s \Delta X \Delta H_v + \int_{T_c}^{T_e} m_s \Delta X C_{p,a} dT \quad 2.5$$

$$Q_c = m_s \Delta X \Delta H_v \quad 2.6$$

Although it is not the objective of an adsorption heat pump for heating applications, a cooling effect is provided by the evaporator as it withdraws heat from its surroundings.

The performance of an adsorption heat pump is usually evaluated considering its coefficient of performance and specific heating or cooling power (SHP/SCP). For heating applications, COP_h is defined as the ratio of the heat released by the adsorbent bed during isosteric cooling and adsorption phases ($Q_{4\text{-}1} + Q_{1\text{-}2}$), plus the heat of condensation Q_c, to the heat required during isosteric heating and desorption ($Q_{2\text{-}3} + Q_{3\text{-}4}$). For cooling purposes, COP_c is the ratio of the heat of evaporation to the heat provided to the bed (Demir et al. 2008).

$$COP_h = \frac{Q_c + Q_{4-1} + Q_{1-2}}{Q_{2-3} + Q_{3-4}} \quad 2.7$$

$$COP_c = \frac{Q_e}{Q_{2-3} + Q_{3-4}} \quad 2.8$$

The SHP is obtained as the ratio of useful heat to the adsorbent mass and cycle time. SCP is simply the heat of evaporation divided by the adsorbent mass and cycle time. The specific heating/cooling power is characteristic that highly depends on the system design, allowing comparison of different system setups and designs (Demir et al. 2008).

$$SHP = \frac{Q_c + Q_{4-1} + Q_{1-2}}{m_s \tau_{cyc}} \quad 2.9$$

$$SCP = \frac{Q_e}{m_s \tau_{cyc}} \quad 2.10$$

2.3. BRIEF STATE OF THE ART

2.3.1. Physical models and numerical methods

Numerical models can predict the system's performance with a given accuracy without the need of an experimental setup. Additionally, system's parameters and operating conditions can be easily set. The agreement between the model outputs and the real system's performance highly depends on its assumptions, numerical accuracy and knowledge of the necessary thermodynamic and physical properties. For adsorption heat pumps, three types of modelling are normally implemented, namely thermodynamic, lumped-parameter and distributed-parameter models. Thermodynamic models are the less accurate type, disregarding heat and mass transfer kinetics inside the adsorbent bed, considering that the bed is in thermodynamic equilibrium. Since the computations are straightforward, it allows a simple and fast evaluation of the system's performance upper limit. Lumped-parameter models are concentrated models, only accounting for the heat and mass transfer between the system's components but not inside the system's components themselves. Although these models do not consider temperature or pressure gradients inside the adsorbent and external mass transfer resistance, some describe the internal mass transfer resistance through the linear driving force (LDF) model (Sircar 1983). The

LDF model usually underestimates the adsorption kinetics (Chahbani et al. 2002). The most accurate type of models are the distributed-parameter model. However, these models are computationally expensive since they involve solving coupled partial differential equations' systems. Nevertheless, in order to obtain accurate predictions for the system's performance the distributed-parameter models are essential. Normally, LDF model is used for the intra-particle mass transfer resistance whereas the inter-particle mass transfer resistance is described by Darcy's Law. An extensive review on numerical models for adsorption heat pump modelling can be found in (Pesaran et al. 2016). The most common methods for numerically solving the physical model equations are alternating difference implicit (ADI), finite difference, Crank-Nicholson and Runge-Kutta methods. The method of lines is commonly used to transform the partial differential equations' systems into a system of ordinary differential equations by discretizing the spatial coordinate.

2.3.2. Adsorption equilibrium

Concerning the adsorption equilibrium, there are four equations that are commonly used: Dubinin equations (normally Dubinin-Astakhov equation), Langmuir equation, Freundlich equation and Toth equation. An extensive description of the adsorption equilibrium theory and equations is presented in (Hassan et al. 2015). Recently, a comparison between several adsorption equations predictions and experimental data was made for the AQSOA zeolite-like adsorbent (Teo et al. 2017). Accordingly to the IUPAC (International Union of Pure and Applied Chemistry) (Sing 1985) the equilibrium isotherms can be classified in six types (Type I – Type VI) and are presented in Figure 2.3. Type IV and Type V isotherms show a hysteresis, which is presented by red and blue lines for adsorption and desorption, respectively. For AHP applications an S-shaped isotherm represents a major advantage since the majority of the adsorbate uptake occurs for low relative pressures (Ehrenmann et al. 2011). For the adsorption kinetics, the LDF (Linear Driving Force) model was proven to be a valid tool to describe the evolution of the adsorption uptake in time (Sakoda and Suzuki 1984; Sircar and Hufton 2000), being used in almost all simulation models.

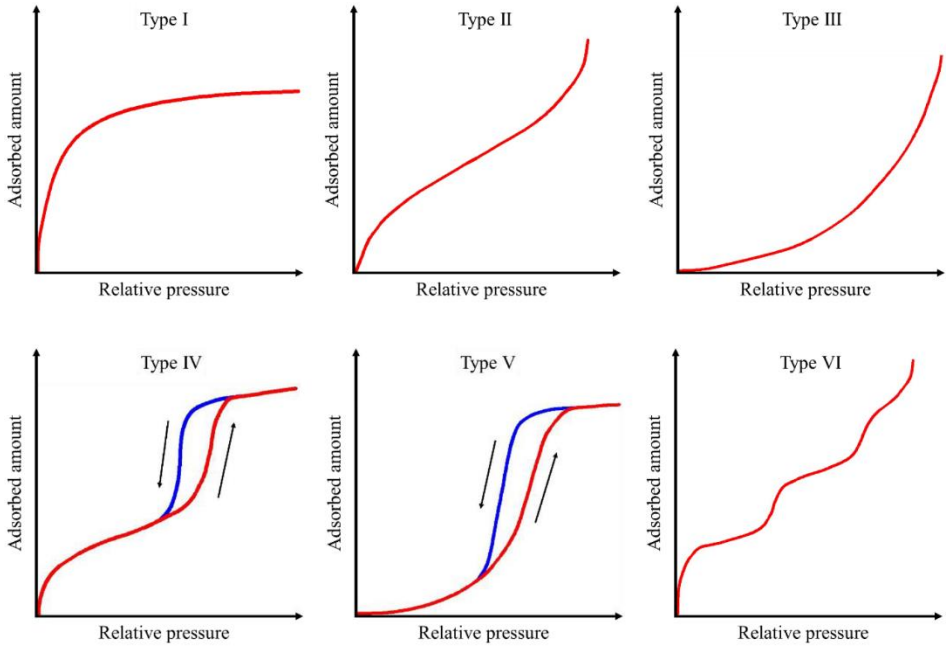

Figure 2.3 – Types of adsorption isotherms according to the IUPAC classification. In Type IV and Type V graphs, the red and blue lines represent adsorption and desorption, respectively. (Adapted from (Sing 1985)).

2.3.3. Adsorbent-adsorbate working pairs

Much work has been done and still is being done aiming to characterize and compare adsorbent-adsorbate working pairs, normally using typical operating conditions (Demir et al. 2008; Wang et al. 2009; Frazzica et al. 2014; Freni et al. 2016; Goyal et al. 2016; Pinheiro et al. 2016; Cabeza et al. 2017; Frazzica and Freni 2017). Concerning the adsorbate, water is by far the most used but ammonia, methanol and ethanol can also be used. Ammonia is commonly used with activated carbon adsorbents, having a high specific heating power due to the high pressure during the adsorption phase. On the other hand, in case of leakage it is toxic and releases an intense smell. Ethanol and methanol are mostly used for refrigeration applications due to their low vaporization temperature (Cabeza et al. 2017).

The typical adsorbent materials used for AHPs are zeolites, silica gels, activated carbons and zeolite-like AlPOs (aluminophosphates) and SAPOs (silico-aluminophosphates). The adsorbent-adsorbate pair selection is one of the key issues for a reliable adsorption heat pump. Although many studies have been conducted on working pairs, most consider only the adsorbate and adsorbent material kinetics and performances, disregarding its applicability in a practical or commercial system. Many working pairs with

excellent adsorption capacity have been reported recently, however, most of them still possess low hydrothermal stability or show hysteresis associated to the material aging over few cycles. Another aspect is the material readiness to market since even though some adsorbent materials show good uptake capacity, hydrothermal stability and long life cycle time, they cannot be produced in mass scale or the cost for their production is unsustainable.

2.3.3.1. Silica gel

Silica gel is a classical water adsorbent that has been studied and implemented in several adsorption systems over the last years. The advantages of silica gel adsorbents are the low regeneration temperatures (60-100 °C), low cost and reliability in practical applications (Freni et al. 2016). Unfortunately, most of the water adsorption occurs at high relative pressures. Many alternatives to overcome this problem have been investigated, namely the increase of silanol groups on the surface and the reduction of the pore size. The alternative with the most water adsorption capacity is the mesoporous silica containing impurities, such as aluminium or other metals (Jeremias et al. 2014).

2.3.3.2. Zeolites

Although zeolites can be combined with many refrigerants water is undoubtedly the most common. Similar to silica gel, zeolites have been the most studied adsorbents and implemented on experimental systems. The water uptake capacity of the zeolites is relatively high, as well as its adsorption heat. On the other hand, a high desorption temperature (200-300 °C for natural zeolites) represents a major setback for the use of zeolites as adsorbent material on adsorption heat pumps. Some improvements with the objective of reducing the desorption temperature have been made over the years (Jeremias et al. 2014; Freni et al. 2016).

2.3.3.3. AIPO and SAPO

AIPOs (aluminophosphates) and SAPOs (silico-aluminophosphates) are zeolite-like materials that possess high water uptake capacity and are capable of working with low desorption temperatures (60-100 °C). These materials have S-shaped isotherms meaning that they have a high water exchange capacity for low temperature differences (Jeremias et al. 2014; Freni et al. 2016; Boman et al. 2017). Recently, Mitsubishi Plastic Inc. developed and commercialized new adsorbent materials, AQSOA®-FAM-Z01 and AQSOA®-FAM-Z02

(Kakiuchi et al. 2005a, b). Both materials work with desorption temperatures in the range of 60-90^{0}C and seem to be a promising solution for heating applications.

2.3.3.4. Activated carbons

Activated carbons have been widely implemented with methanol and ammonia as adsorbate. They can be used in the form of powder, fibre, granular, compact and monolithic carbon. The temperature ranges for the activated carbons are very wide and depend on its form and on the used adsorbate. An extensive study on activated carbons was performed in (Tamainot-Telto et al. 2009).

2.3.3.5. Composite adsorbents

The composite adsorbents are normally formed by inorganic salts inserted in porous matrices. These adsorbents can be combined with water, methanol, ethanol or ammonia as the adsorbate (Gordeeva and Aristov 2012; Freni et al. 2016). Some of these materials, based on mesoporous silica impregnated with $CaCl_2$ (SWS-1L) and LiBr (SWS-2L), possess a high water uptake (0.75 kg/kg) and a relatively low desorption temperature (70-120 °C) (Aristov et al. 2002). The composite SWS-8L allows a water uptake of 0.2 kg/kg and an even lower desorption temperature (75-80 °C) (Simonova et al. 2009). As for the utilization of methanol and ethanol as adsorbate, some studies can be found in references (Aristov et al. 2007; Gordeeva et al. 2008; Gordeeva and Aristov 2010).

2.3.3.6. Metal-Organic frameworks (MOFs)

Although MOFs demonstrate a high water, ethanol and methanol uptake capacity under common operating conditions, their hydrothermal instability, degradation over time and high cost are still some major obstacles (Freni et al. 2016). Nevertheless, accordingly to recent studies like reference (Henninger et al. 2017), MOFs are very promising materials for future use as adsorbents. In order to implement these materials on practical systems, improvements must be made to their hydrothermal stability and hysteresis behaviour.

New materials are being investigated every day and some are very promising for future applications, namely composite adsorbents and MOFs (Metal Organic Frameworks) (Pinheiro et al. 2015; Elsayed et al. 2016; Calabrese et al. 2017b, a; Henninger et al. 2017; Gediz Ilis 2017; Kim et al. 2017; Zhu et al. 2018). Although some of these adsorbents demonstrate very good uptake capacities, they also show hydrothermal instability, degradation over time and high cost, which are still some major obstacles (Freni et al. 2016).

Furthermore, they are difficult to produce in a large scale, which makes them still not suitable nor available for final applications that require mass production.

Some recent reviews include a summary of the research done on adsorption materials (Demir et al. 2008; Cabeza et al. 2017). Recently, Boman et al. (Boman et al. 2017) performed a screening of potential working pairs for AHPs based on the thermodynamic and transport characteristics. In addition to the working pairs comparison, an extensive list of more than one hundred adsorbent-adsorbate uptake equations are listed and referenced, serving as a useful database for future research (Boman et al. 2017).

2.3.4. Adsorbent physical and thermodynamic properties

In order to obtain a system with reasonable SHP, efforts have to be done to lower the heat and mass transfer resistances. These parameters depend on the adsorbent-adsorbate pair and the bed design (i.e. adsorbent thickness, use of thermal enhancing material between adsorbent and bed structure, fins configuration, etc.).

Poyelle et al. (Poyelle et al. 1999) investigated the effect of the convective heat transfer coefficient and adsorbent permeability on the COP for cooling mode (COP_c) and SCP (Specific Cooling Power) of an adsorptive air conditioning unit. A high conductive adsorbent composite was developed and implemented in an adsorber, resulting in considerable improvements of the effective thermal conductivity and convective heat transfer coefficient, respectively, when compared to a common zeolite granular bed. However, the effective permeability is decreased from 10^{-9} m^2 to 10^{-12} m^2 due to material consolidation, increasing the mass transfer resistance. Experimental tests were performed for different evaporation temperatures, T_e. For T_e = 4 °C the mass transfer resistance dictates the system performance whereas for T_e in the range of 25 – 30 °C the performance is controlled mostly by the heat transfer resistance inside the adsorbent, resulting in a gain of 0.27 and 38 W/kg for the COP_c and SCP, respectively. This enhancement is a consequence of the pressure raise in the adsorber inherent to the increase of T_e, which accelerates the adsorption process. An analogous analysis for the condenser temperature, T_c, was not reported but if the same dynamics take place in desorption process, if T_c increases the process duration will probably increase also, penalizing the performance.

Zhang and Wang (1999) presented a parametric study on heat and mass transfer dynamics of an adsorption cooling system for automobile applications, resorting on waste heat from the exhaust gas to regenerate the adsorbent. The effects on the system

performance, based on finite difference computational simulations, were the objective of their research. Simulations indicated that if the adsorbent permeability is beneath a critical point value of $5 \times 10^{-11}\ m^2$ the system's performance severely decreased. In addition, a strong influence of the heat transfer coefficients and bed thickness on the performance was noticed. Increasing the bed thickness will decrease the heat transfer and consequently decrease the system's performance. Finally, they also reported that for systems with short cycle times the internal mass transfer resistance can be limiting.

Restuccia et al. (2002) demonstrated that there is a commitment between the heat and mass transfer in the adsorbent. Four shapes of zeolite were used as adsorbent: grains, brick, powder and coated layer. Using a numerical model and a Yate's analysis to the data, a comparison based on the specific cooling power was done. Results showed that the parameters that mostly affect the system's performance are the bed permeability and thickness. Furthermore, although increasing the adsorbent material consolidation will increase the heat transfer coefficients, the permeability will decreases, which means that a balance between these parameters is needed to maximize the system's specific power. This effect was demonstrated in this study since grain (lowest heat transfer coefficient and highest permeability) and brick (lowest permeability and higher heat transfer coefficients) shaped adsorbent beds showed worse performance than the powder adsorbent bed (medium permeability and heat transfer coefficients). In addition, since the system‘s bed thickness also influences the heat and mass transfers, it strongly influences the system's performance. This effect makes the zeolite coating (lower thickness) the adsorbent configuration that has the best performance.

Pinheiro et al. (2015) presented a study of an adsorption heating system based on the ETS-10- water pair. The developed model accounts for the adsorption equilibrium, heat and mass transfer in one dimension, heat transfer between the vapour and the adsorbent and intra-particle mass transport. Heat transfer resistances in the adsorbent material and adsorbent bed interface, as well as between the heating/cooling fluid and the adsorbent bed were neglected. Their research demonstrated that by decreasing the adsorbent thickness, the SHP increases and the COP slightly decreases. Furthermore, the system COP reaches its maximum when the HTF temperature is equal to the temperature at the end of the isobaric desorption. In fact, the HTF temperature should be higher than the desired regeneration temperature since heat loss occurs in the metal/adsorbent interface, which was disregarded in this model.

Since adsorbent coatings seem to be the best configuration for AHPs (Restuccia et al. 2002), it is important to study their hydrothermal and mechanical stabilities. This was done by Freni et al. (2013) using experimental methods on zeolite-based (AQSOA-Z02 from Mitsubishi Plastics) coatings over aluminium substrates, manufactured by the Institute for Advanced Energy Technologies of the Italian Research Council (CNR-ITAE) using the dip coating technique. The manufactured coating was compared with a coating prepared by Mitsubishi Plastics (MP) and the hydrothermal stability was successfully verified after 35000 cycles, for both adsorbents. Concerning the mechanical strength, it was found that for the MP coating it is already satisfying. On the other hand, the CNR-ITAE coating still needs to be improved to achieve satisfactory mechanical stability. In (Teo et al. 2017), detailed data about the AQSOA type zeolites is presented.

A comparison between a coated and a granular adsorbent was performed in (Freni et al. 2015a) using a SAPO-34 zeolite. The comparison was based on the differential water loading, mass SCP (W/kg_s), volumetric SCP (VSCP) (W/dm^3_s) and COP_c. The coated adsorber presented higher differential water loading, mass SCP, and lower volumetric SCP (VSCP) and COP_c. The difference on the COP_c is due to the higher metal to adsorbent mass ratio of the coated adsorber, which has to be decreased to obtain better COP_c.

A three-dimensional coupled heat and mass transfer numerical model was proposed by Radu et al. (2017) to study the effects of different adsorbent particle sizes and packing configurations. Their work suggest that particles with smaller diameters and configurations with fewer layers present faster sorption kinetics. Desorption phase was proven faster than adsorption by the numerical model since it occurs at a higher temperature, resulting in faster diffusion. As previously stated by other works, it was also concluded that a small adsorbent bed thickness leads to better performance.

Girnik et al. (2017) used a binder on a commercial active carbon to enhance the adsorption kinetics. The volumetric large temperature jump (V-LTJ) method was used to measure the adsorbate amount in the adsorbent. It was also demonstrated that for smaller particle sizes the performance is bettered due to faster ad/desorption dynamics. Ramji et al. (2014) used a CFD (Computational Fluid Dynamics) model to study the effect of the adsorber external wall thickness, which affects the capacity of the adsorber to maintain the optimum temperature during the desorption phase. The CFD model results were compared to experimental data and a good agreement was achieved. The results suggest the optimal thickness of the stainless-steel wall for the adsorber external wall.

2.3.5. Bed specifications

Several studies have been conducted aiming at the modelling and experimental testing of adsorbent bed/heat exchanger configurations. The common parameters investigated are flat or circular tube configurations, the use of fins, fin height, fin pitch and number of fins. Núñez et al. (2007) developed a prototype of an adsorption chiller and heat pump for domestic applications capable of delivering a nominal power of 3-8 kW (COP = 0.5) and 16 kW (COP = 1.5) for cooling and heating modes, respectively. However, to achieve this power level two beds of silica gel with 35 kg were used, corresponding to SCP of 86-229 W/kg and SHP of 457 W/kg. As a result, a big machine that might not be adequate for domestic applications is needed. Therefore, further improvements should be made to the bed design in order to maximize the heat and mass transfer kinetics that were disregarded in this study.

Kowsari et al. (2017) presented a parametric study of a heat exchanger (HEx) to be used as adsorbent bed using a numerical model, which was validated with an experimental set up. Rectangular and trapezoidal bed geometries were explored using different fin heights and pitch and the results were compared based on SCP, VSCP, COP_c, adsorbent mass and metal mass. The rectangular geometry showed the best SCP when compared to a similar configuration for the trapezoidal geometry. As reported by previous studies, higher metal mass leads to a lower COP_c and large adsorbent thickness provides poor SCP.

Rivero-Pacho et al. (2017) performed a parametric study of a carbon-ammonia adsorber for a gas fired AHP operating under room heating conditions, using two 2-D finite difference simulation models programmed in Matlab™. The adsorber is made of 1700 tubes with 1.2 mm outer diameter and a pitch of 3 mm, with a mixture of carbon grains and powder packed between the tubes. A finned tube and shell and tube geometries were compared and no major differences in the COP were reported. However, according to the authors by using the finned tube geometry the number of tubes can be decreased seven times, reducing the manufacturing costs.

A novel adsorber structure with aluminium sintered metal fibres was reported by Wittstadt et al. (2017). Results obtained by a driving temperature difference analysis showed that this new type of HEx reaches a very high-volume specific power density for a reasonable adsorbent to HEx mass ratio.

Graf et al. (2016) presented an experimentally calibrated dynamic model to predict the SCP and COP of AHPs. Gravimetric large temperature jump (G-LTJ) experiments were

conducted on a representative adsorber part in order to calibrate the adsorber model, which is then used to simulate an AHP and predict its SCP and COP. The heat and mass transfer coefficients were determined by least-square fitting the measured and simulated adsorbate uptake. The model was validated for a small representative adsorber part, allowing a fast evaluation of design and operating parameters, such as fin geometry, cycle times and operating temperatures. However, the model was not validated for a real AHP system and the question of whether it successfully predicts the performance of a real sized adsorber remains. (San and Tsai 2014; Frazzica et al. 2016a) describe the designing and testing of AHP systems based on previous parametric analysis of single system components. These approaches are purely experimental and provide accurate characterizations of a system for a given experimental scenario. However, these kinds of experimental approaches are limited to the implemented setup, making it difficult to perform a parametric analysis of the entire system since the whole setup would have to be dismantled and built over again in order to change some parameters.

2.3.6. Operating conditions

Sapienza et al. (2016) developed an adsorption chiller prototype with three flat tube HExs coated with the AQSOA-Z02 adsorbent and simultaneously packed with silica gel grains. The prototype was tested in a test bench for adsorption chillers at CNR-ITAE Testing Centre under two different operating temperatures sets. The temperatures of the evaporator and condenser in/outlet were monitored and the effect of the cycle time on the average cooling power (ACP) and COP_c was investigated for the two different working conditions. The cycle times that result in maximum ACP were identified as well as the cycle times that lead to maximum COP_c. The results show that maximum ACP and maximum COP_c cannot be obtained simultaneously and the balance between them can be controlled by adjusting cycle times.

An experimental study of an adsorption heat storage system using AQSOA-Z02-water pair was presented by Palomba et al. (2017a). The system was tested under different operating conditions for cold storage, daily heat storage and seasonal heat storage working modes. The temperatures in the adsorber, evaporator and condenser in/outlets were monitored. The results demonstrated that desorption temperature is the parameter with higher repercussions on the storage capacity of the system. Furthermore, the evaporator temperature has a significant influence on the system's performance while in the range of 5-10 ^{0}C, having little effect for temperatures above this range.

Dawoud (2014), from Viessmann Werke Allendorf GmbH, presented a gas-fired adsorption heat pump for heating appliance and described the system, dividing it in four modes. The concept is to use adsorption and desorption phases to sustain the low heat demand operation modes. In the medium heat demand mode, the adsorption and desorption processes can only deliver the required heat to the heating net at the beginning of each phase. To achieve the desired supply temperature, the gas burner is used to heat backup the adsorption heat pump when the adsorption and desorption phases are close to their ends. Even when the processes are close to their ends, they are still used to pre-heat the return cold water, reducing the temperature lift needed in the gas burner. When in high heat demand mode, the water is heated using solely the gas burner. The system was implemented in two one-family houses in Germany and showed 27% more efficient seasonal gas utilization, which results in 20% less CO_2 emissions when compared to the stand-alone gas condensing boiler technology. As a result, Viessmann has launched a commercial product called Vitosorp 200-F. The heat pump adsorption module is composed by a HEx coated with zeolite adsorbent and it is regenerated by a water circuit heated by a gas-fired boiler. However, Vitosorp 200-F remains a confidential solution and detailed information about it is not available. A performance-predicting model, which can provide designing and dimensioning details to guide in the construction of a similar system, does not exist or is unavailable to outsiders. Furthermore, the system's components are not specifically described, which makes it impossible to develop a physical model that represents the system.

2.4. AHP DEVELOPMENT CHALLENGES

Although several studies on the adsorption kinetics, adsorbent bed specifications and operating conditions are reported in literature, a system-level approach considering an entire AHP system would be a valuable contribution towards the development of the AHP technology. The optimization of a single or few parameters, isolated components and working pairs can have only a slight effect on the performance of the complete system. System-level studies including simultaneously the optimization of the adsorption kinetics, adsorbent bed specifications, operating conditions and relationship between all system components is lacking (Pesaran et al. 2016). Furthermore, detailed experimental data to allow the validation of physical dynamic models that consider an entire AHP system are still unavailable. Future research must be done to consolidate the individual optimizations into

a practical and commercial AHP in order to identify and distinguish the highly sensitive parameters from the more irrelevant ones.

The main challenges that are yet to be overcome in order to develop an AHP system for heating appliances are discussed below. The objective of this work is not to present concrete solutions but to identify the major challenges and make way for future work to be developed as an attempt to overcome them. Nevertheless, some ideas and possible approaches that have been considered as promising by the authors are reported.

2.4.1. The physical model for the entire AHP system

A physical model that can be used as a dimensioning and optimization tool for an AHP system for heating applications is currently inexistent or unavailable in the literature. A possible approach aiming at the development of such a tool, with the ability to describe an entire AHP system, is to consider that the adsorber module can be described by a simple transient lumped-parameter model. Although the external mass transfer resistance and the temperature gradient inside the adsorbent material are neglected, the lumped-parameter analysis can account for the internal mass transfer resistance through the LDF model. A lumped-parameter model can provide some knowledge about the system's dynamics, enabling one to make some preliminary observations. Moreover, some key parameters with influence on the system's performance can be identified by this simpler model. This kind of approach was made by Fernandes et al. (2016a, b) to describe a thermal energy storage system with an adsorption module and perform a viability study. This methodology was proven suitable for the proposed system since its dynamics were slow enough to consider thermal equilibrium inside the adsorber. For shorter cycle times, as occurs when gas burners are used as heating elements, the equilibrium state inside the adsorber cannot be assumed blindly. A more complicated one-dimensional, bi-dimensional or tri-dimensional distributed-parameter analysis of the adsorber module needs to be considered. By comparing the results from both approaches, assuming that the tri-dimensional distributed-parameter model as the exact solution, the accuracy of the lumped-parameter model can be verified for different operating modes/conditions. Finally, after the physical model of the adsorber module is consolidated it has to be interconnected with the remaining system's components resulting in a tool capable of describing an AHP system as a whole.

A possible hypothesis for the development of a physical model for a complete AHP system is to use the type of models referred in the previous paragraph to describe an element that can be representative of an adsorber module. A possible adsorber module can

be made by several metal tubes coated with an adsorbent material enclosed in a chamber that is connected to the evaporator and the condenser. The heat transfer fluid is circulated inside the metal tubes, providing/withdrawing heat to/from the adsorbent material. By circulating the heat transfer fluid inside the metal tubes where the coating exists in their outer surface, the only heat transfer is to the adsorbent material, which is an advantage when compared to other designs where the heat transfer fluid circulates on an outer shell with the adsorbent material packed inside. A possible adsorber module and its representative element are presented in Figure 2.4. A distributed-parameter model considering the radial and axial directions should be sufficient to model the purposed adsorber since it is essentially symmetric along the angular direction. The schematics of the representative element for the development of a physical model is presented in Figure 2.5.

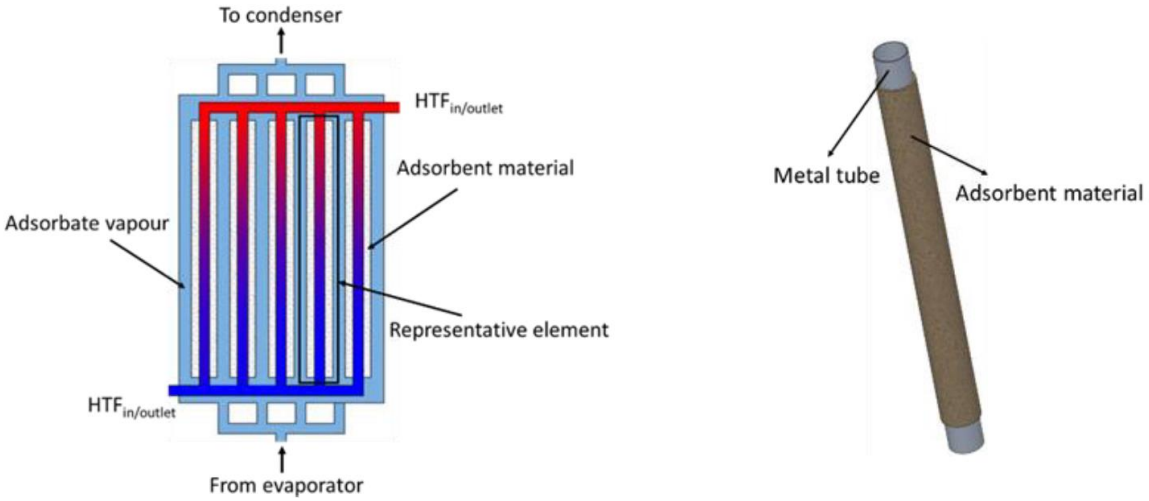

Figure 2.4 – Adsorber module (on the left) and its representative element (on the right).

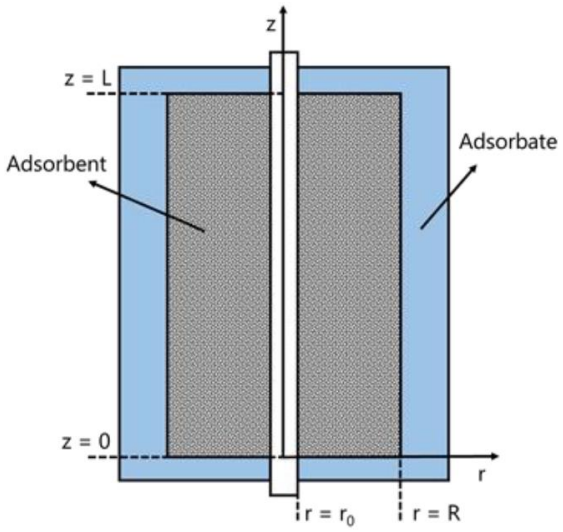

Figure 2.5 – Schematics of the representative element for the development of physical models.

2.4.2. On the adsorbent-adsorbate working pair

As previously stated in this paper, there are several adsorbent-adsorbate working pairs that can be used in an AHP system for heating applications. However, many of these working pairs are not available in the amounts needed for application in a real size AHP or their cost is unsustainable. From the available literature, the following adsorbent-adsorbate working pairs show interesting characteristics and readiness to market for being used in a real AHP system for heating applications:

- ✓ Silica gel – Water
- ✓ Activated carbon – Ammonia
- ✓ Zeolite 4A – Water
- ✓ Zeolite 13X – Water
- ✓ AQSOA-Z02 – Water

These are the most studied working pairs and there is much information about the adsorbent physical and thermodynamic properties. Furthermore, hydrothermal stability and material aging for these few particular materials are already well established and considered suitable. Thus, these working pairs are the safest options for usage in an AHP system for heating appliances. Furthermore, the emphasis that is currently being made by the industry on environmentally friendly systems makes the usage of water as adsorbate very desirable.

2.4.3. Regeneration of the adsorbent material

There are several ways of regenerating the adsorbent material being the most common solar thermal energy, waste heat and gas burners. Waste heat is normally used in applications where it is abundant at low cost, such as industrial processes or thermal engines. However, for domestic applications it is normally unavailable in a useful amount. Solar thermal energy is commonly used for adsorption heat storage, which can store energy during the day. However, these systems just regenerate the material when solar energy is available, storing heat of adsorption to be used later. In order to control the cycle time, the adsorbent material must be regenerated whenever the system requires, which varies for different operating conditions and system's configuration. Gas burners can be used anytime, providing a solution for cycle time control. Unfortunately, unlike solar energy, natural gas is not free and releases CO_2 to the atmosphere. A combination of the two technologies might be a good solution since by using solar energy when it is available and the gas burner only when the solar energy is unavailable or it is not self-sufficient. Therefore, the operational costs and CO_2 emissions inherent to the burning of natural gas can be lowered while maintaining the cycle time control. In addition, the gas burner can be directly used to provide heat when the heat power demands are too high to be satisfied by the adsorption process alone. It can also be used to elevate the temperature effectively over 50 ^{0}C, which is very difficult to achieve through the adsorption process.

The usage of electricity for water heating has recently captured the market's interest (Sawin et al. 2017), as it can be obtained from renewable energy sources. Using electricity for the adsorbent material regeneration still requires future investigation, comparing it to the common adsorbent regeneration options in order to identify its advantages and disadvantages.

2.4.4. How to improve an AHP system performance?

Three main areas can be improved in order to better an AHP system performance, which are adsorbent material physical and thermodynamic properties, adsorber configuration and operating modes.

2.4.4.1. Adsorbent physical and thermodynamic properties

Regarding the adsorbent material physical and thermodynamic properties, the simultaneous enhancement of the adsorbent material permeability and thermal conductivity would be a major improvement. However, from (Poyelle et al. 1999) it is concluded that by

improving one of these parameters the other is deteriorated. Finding the right balance between these two parameters comprises a good chance of improving the system's performance. Furthermore, the convective heat transfer coefficient between the adsorber metal wall and the adsorbent material directly influences the heat flux that is transferred between them, hardly affecting the cycle time and consequently the SHP. This parameter is influenced by the effective contact between the adsorbent material and the adsorber metal wall. In order to enhance the effective contact better coating techniques that bind the adsorbent material to the metal wall without compromising the adsorbent permeability can contribute to the system's performance improvement. All these parameters are currently being developed at lab scale but their sustainable production for the market is still a challenge.

Larger contact areas between the adsorbent material and the adsorber metal wall will enhance the heat transfer between them. In order to increase this heat transfer area it is common to include fins in the adsorber. However, it is also common to disregard the adsorber metal mass in the performance calculation, which needs to be taken into account in the physical models to obtain accurate results. Recent studies (Freni et al. 2016; Frazzica and Freni 2017) have demonstrated that the metal to adsorbent material mass ratio affects the performance of AHP systems. Higher metal to adsorbent mass ratios lead to lower performances, which was verified for several working pairs. Thus, by using an adsorber configuration with fins with the objective of enhancing the heat transfer in the bed the metal to adsorbent mass ratio is considerably increased. The added fins will not only increase the total metal mass but also occupy precious space that could be otherwise filled with adsorbent material, lowering the adsorbent mass when compared to a similar configuration without fins.

2.4.4.2. Adsorber configurations

There are several packing techniques and adsorber configurations such as shell packing, which was used in (Pinheiro et al. 2016), plate-finned, tube, finned tube, fin plate, flat pipe, spiral plate and coated tube, which are described in (Li et al. 2015). All the different configurations result in different adsorbent-metal wall contact areas, metal to adsorbent mass ratios, adsorbent area exposed to the adsorbate and heat losses to the environment. As result, a lot of work as to be done in order to select the best adsorber configuration, which may be different for each application and dependent on the adsorber metal and adsorbent-adsorbate working pair thermodynamic and physical properties. For example, shell configuration has less adsorbent-adsorbate contact area but it has more adsorbent-

metal contact area when compared to the tube configuration. Nevertheless, in the shell configuration the HTF circulates around the adsorbent material whereas in the tube configuration the adsorbent material is packed around the tube, which will minimize heat losses since the heat can only be transferred from the tube to the adsorbent material. Finned HExs will have more adsorbent-metal contact area but will have less adsorbent-adsorbate contact area and higher metal to adsorbent mass ratio. When designing an adsorber one should take into account the following aspects: maximization of the heat transfer between adsorbent material and the heat transfer fluid, maximization of the adsorbent surface exposed to the adsorbate, minimization of the metal to adsorbent mass ratio, guarantee of a good thermal contact between the adsorbent bed and the metal (for example using thermal interface material paste), and keep a simple design that can be built using vacuum technology elements. Selecting the best configuration and designing the optimum adsorber is a hard task, requiring further investigation aiming at the best balance of all these parameters.

2.4.4.3. Operation modes

The operation mode of an AHP system will influence the system's performance and the best operation mode for one application is not necessarily the best for different applications. Deciding how to use the system and selecting the best operation mode for a given application can be challenging. As previously mentioned, (Dawoud 2014) presents four different working modes for a specific heating appliance. For example, in case of an integration with a solar panel it could be used during the day to regenerate the adsorbent and after, directly heat the water in a tank, storing sensible heat in the water tank and adsorption heat in the adsorbent material that can both be used later. The AHP system can be used as a heat storage system by using high adsorbent mass and long cycle times, which can be advantageous if the energy source driving it is available or cheaper during a given time period. On the other hand, if the application requires high powers it might be a best option to define an operation mode that results in faster/shorter cycles.

A possible system configuration is presented in Figure 2.6. This system uses the adsorber module from Figure 2.4 to heat the water inside the water tank. The water is used as heat transfer fluid and a gas burner is used for the adsorbent regeneration. Thus, the major components of the system are the adsorber module, evaporator, condenser, gas burner, expansion valve (EV) and the water tank.

During the adsorption phase, the adsorber is receiving adsorbate vapour coming from the evaporator and the valve to the condenser is closed. As the adsorbent material uptakes the adsorbate, heat of adsorption is released. In order to retrieve this heat, cold water is taken from the bottom of the water tank, or from the supply network, and circulated inside the tubes of the adsorber. After leaving the adsorber, the warmed water is returned to the tank. The process continues until a pre-determined uptake value is achieved or a certain time is passed. Afterwards, desorption process starts and water is taken from the water tank, heated by the gas burner and circulated inside the tubes of the adsorber. The adsorbent material releases the adsorbate, which circulates through the condenser releasing the heat of condensation to the water inside the tank. The process continues until a pre-determined uptake value is achieved or a certain time is passed. At the end of the desorption phase, the hot water that was circulated inside the tubes of the adsorber is returned to the water tank.

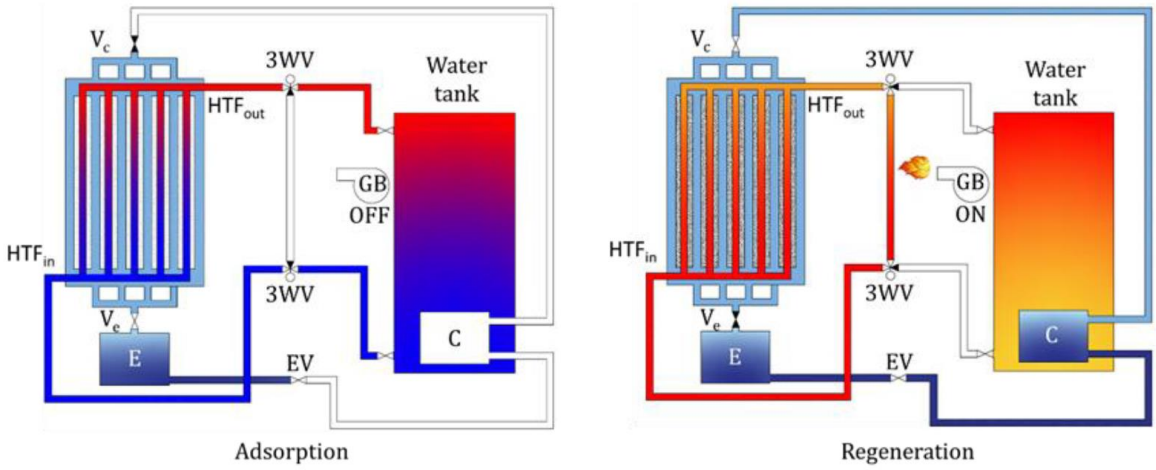

Figure 2.6 – Possible AHP system schematics.

This system can work in three different modes: low power demand, medium power demand and high power demand. In the low power demand mode, the gas burner is only used to regenerate the adsorbent material and the heat delivered to the water tank is solely obtained by the adsorption and regeneration processes. In the medium peak demand mode, the gas burner is used not only for the regeneration of the adsorbent but also to heat the water that leaves the adsorber during the adsorption process, boosting its temperature to a higher level. Finally, in the high power demand mode the system works as a gas boiler, using the gas burner to heat the water directly, providing instant hot water.

2.4.5. What are the system's major limitations?

An AHP system has some limitations, some easier to overcome than others. The major limitations that have been identified are the following:

- Low COP;
- A large mass of adsorbent material is needed to produce the required heating powers for most applications;
- The materials used in the system (valves, joints, welding, etc.) need to be adequate for vacuum operating conditions;
- Difficult to provide heat at temperatures over 55 °C;
- The adsorbent-adsorbate working pairs with higher COP and capable of delivering higher heating powers require high regeneration temperatures;
- Many cautions have to be taken when regeneration temperatures higher than the heat transfer fluid's boiling temperature are used due to the possible resulting high pressure inside the pipes.

2.5. CONCLUSIONS

A review on AHP systems with emphasis on heating applications was presented. The most relevant studies in the field are reported and the major gaps in the literature were identified and discussed. The essential subjects to the understanding of an AHP namely its working principle, physical models, adsorption equilibrium and kinetics of typical and new adsorbent-adsorbate working pairs, adsorbent material thermodynamic and physical properties, adsorbent bed designing and operating conditions were discussed. Overall, a help to researchers working on the field or a guide for new researchers approaching the AHP subject was presented, highlighting the hindrances and work that still has to be done in order to develop a physical model and an optimized solution for an AHP system.

Despite all the research performed on new adsorbent-adsorbate working pairs, not many are ready to market, easily accessed and produced, hydrothermal stable and with a long life cycle. A bridge between the material's level and system's level studies is yet to be built. The LDF model and Darcy's Law are the most common models to account for the internal and external mass transfer resistances, respectively.

A physical model that considers a whole AHP system cannot be found in the literature. Many experimental studies and numerical simulations do not provide detailed information that can be used to validate new models. Furthermore, simultaneous optimization of the

bed specifications, operating conditions and adsorbent material thermodynamic and physical properties is not reported in the literature. The development of a physical model that describes an entire AHP system would be welcome. In addition, adsorbent-adsorbate working pairs with low heat and mass transfer resistances, which can regenerated at lower temperatures would be ideal for the most applications. New operating modes that can improve the performance of the entire AHP system are valuable towards achieving competitive AHP solutions.

2.6. REFERENCES

Aristov YI, Gordeeva LG, Pankratiev YD, et al (2007) Sorption equilibrium of methanol on new composite sorbents “caCl 2/silica gel.” Adsorption 13:121–127. https://doi.org/10.1007/s10450-007-9012-x

Aristov YI, Restuccia G, Cacciola G, Parmon VN (2002) A family of new working materials for solid sorption air conditioning systems. Appl Therm Eng 22:191–204. https://doi.org/10.1016/S1359-4311(01)00072-2

Boman DB, Hoysall DC, Pahinkar DG, et al (2017) Screening of working pairs for adsorption heat pumps based on thermodynamic and transport characteristics. Appl Therm Eng 123:422–434. https://doi.org/10.1016/j.applthermaleng.2017.04.153

Cabeza LF, Solé A, Barreneche C (2017) Review on sorption materials and technologies for heat pumps and thermal energy storage. Renew Energy 110:3–39. https://doi.org/10.1016/j.renene.2016.09.059

Calabrese L, Bonaccorsi L, Freni A, Proverbio E (2017a) Silicone composite foams for adsorption heat pump applications. Sustain Mater Technol 12:27–34. https://doi.org/10.1016/j.susmat.2017.04.002

Calabrese L, Brancato V, Bonaccorsi L, et al (2017b) Development and characterization of silane-zeolite adsorbent coatings for adsorption heat pump applications. Appl Therm Eng 116:364–371. https://doi.org/10.1016/j.applthermaleng.2017.01.112

Chahbani MH, Labidi J, Paris J (2002) Effect of mass transfer kinetics on the performance of adsorptive heat pump systems. Appl Therm Eng 22:23–40. https://doi.org/10.1016/S1359-4311(01)00067-9

Dawoud B (2014) On the development of an innovative gas-fired heating appliance based on a zeolite-water adsorption heat pump; System description and seasonal gas utilization efficiency. Appl Therm Eng 72:323–330. https://doi.org/10.1016/j.applthermaleng.2014.09.008

Demir H, Mobedi M, Ülkü S (2008) A review on adsorption heat pump: Problems and solutions. Renew. Sustain. Energy Rev. 12:2381–2403

Ehrenmann J, Henninger SK, Janiak C (2011) Water adsorption characteristics of MIL-101 for heat-transformation applications of MOFs. Eur J Inorg Chem 471–474. https://doi.org/10.1002/ejic.201001156

Elsayed E, Al-Dadah R, Mahmoud S, et al (2016) Aluminium fumarate and CPO-27(Ni) MOFs: Characterization and thermodynamic analysis for adsorption heat pump applications. Appl Therm Eng 99:802–812. https://doi.org/10.1016/j.applthermaleng.2016.01.129

Fernandes MS, Brites GJVN, Costa JJ, et al (2016a) Modeling and parametric analysis of an adsorber unit for thermal energy storage. Energy 102:83–94. https://doi.org/10.1016/j.energy.2016.02.014

Fernandes MS, Brites GJVN, Costa JJ, et al (2016b) A thermal energy storage system provided with an adsorption module – Dynamic modeling and viability study. Energy Convers Manag 126:548–560. https://doi.org/10.1016/j.enconman.2016.08.032

Frazzica A, Freni A (2017) Adsorbent working pairs for solar thermal energy storage in buildings. Renew Energy 110:87–94

Frazzica A, Füldner G, Sapienza A, et al (2014) Experimental and theoretical analysis of the kinetic performance of an adsorbent coating composition for use in adsorption chillers and heat pumps. Appl Therm Eng 73:1020–1029. https://doi.org/10.1016/j.applthermaleng.2014.09.004

Frazzica A, Palomba V, Dawoud B, et al (2016) Design, realization and testing of an adsorption refrigerator based on activated carbon/ethanol working pair. Appl Energy 174:15–24. https://doi.org/10.1016/j.apenergy.2016.04.080

Freni A, Bonaccorsi L, Calabrese L, et al (2015) SAPO-34 coated adsorbent heat exchanger for adsorption chillers. Appl Therm Eng 82:1–7. https://doi.org/10.1016/j.applthermaleng.2015.02.052

Freni A, Frazzica A, Dawoud B, et al (2013) Adsorbent coatings for heat pumping applications: Verification of hydrothermal and mechanical stabilities. In: Applied Thermal Engineering. pp 1658–1663

Freni A, Maggio G, Sapienza A, et al (2016) Comparative analysis of promising adsorbent/adsorbate pairs for adsorptive heat pumping, air conditioning and refrigeration. Appl Therm Eng 104:85–95. https://doi.org/10.1016/j.applthermaleng.2016.05.036

Gediz Ilis G (2017) Influence of new adsorbents with isotherm Type V on performance of an adsorption heat pump. Energy 119:86–93

Girnik IS, Grekova AD, Gordeeva LG, Aristov YI (2017) Dynamic optimization of adsorptive chillers: Compact layer vs. bed of loose grains. Appl Therm Eng 125:823–829. https://doi.org/10.1016/j.applthermaleng.2017.06.141

Gordeeva L, Aristov Y (2010) Novel sorbents of ethanol “salt confined to porous matrix” for adsorptive cooling. Energy 35:2703–2708. https://doi.org/10.1016/j.energy.2009.04.001

Gordeeva LG, Aristov YI (2012) Composites “salt inside porous matrix” for adsorption heat transformation: A current state-of-the-art and new trends. Int J Low-Carbon Technol 7:288–302. https://doi.org/10.1093/ijlct/cts050

Gordeeva LG, Freni A, Krieger TA, et al (2008) Composites “lithium halides in silica gel pores”: Methanol sorption equilibrium. Microporous Mesoporous Mater 112:254–261. https://doi.org/10.1016/j.micromeso.2007.09.040

Goyal P, Baredar P, Mittal A, Siddiqui AR (2016) Adsorption refrigeration technology - An overview of theory and its solar energy applications. Renew. Sustain. Energy Rev. 53:1389–1410

Graf S, Lanzerath F, Sapienza A, et al (2016) Prediction of SCP and COP for adsorption heat pumps and chillers by combining the large-temperature-jump method and dynamic modeling. Appl Therm Eng 98:900–909

Hassan HZ, Mohamad AA, Alyousef Y, Al-Ansary HA (2015) A review on the equations of state for the working pairs used in adsorption cooling systems. Renew Sustain Energy Rev 45:600–609. https://doi.org/10.1016/j.rser.2015.02.008

Henninger SK, Ernst SJ, Gordeeva L, et al (2017) New materials for adsorption heat transformation and storage. Renew Energy 110:59–68. https://doi.org/10.1016/j.renene.2016.08.041

Jeremias F, Fröhlich D, Janiak C, et al (2014) Water and methanol adsorption on MOFs for cycling heat transformation processes. New J Chem 38:1846. https://doi.org/10.1039/c3nj01556d

Kakiuchi H, Shimooka S, Iwade M, et al (2005a) Novel water vapor adsorbent FAM-Z01 and its applicability to an adsorption heat pump. Kagaku Kogaku Ronbunshu 31:361–364. https://doi.org/10.1252/kakoronbunshu.31.361

Kakiuchi H, Shimooka S, Iwade M, et al (2005b) Water Vapor Adsorbent FAM-Z02 and Its Applicability to Adsorption Heat Pump. KAGAKU KOGAKU RONBUNSHU 31:273–277. https://doi.org/10.1252/kakoronbunshu.31.273

Kim C, Cho K, Kim SK, et al (2017) Alumina-coated ordered mesoporous silica as an efficient and stable water adsorbent for adsorption heat pump. Microporous Mesoporous Mater 239:310–315. https://doi.org/10.1016/j.micromeso.2016.10.014

Kowsari MM, Niazmand H, Tokarev MM (2017) Bed configuration effects on the finned flat-tube adsorption heat exchanger performance: Numerical modeling and experimental validation. Appl. Energy

Li XH, Hou XH, Zhang X, Yuan ZX (2015) A review on development of adsorption cooling - Novel beds and advanced cycles. Energy Convers. Manag. 94:221–232

Núñez T, Mittelbach W, Henning HM (2007) Development of an adsorption chiller and heat pump for domestic heating and air-conditioning applications. Appl Therm Eng 27:2205–2212. https://doi.org/10.1016/j.applthermaleng.2005.07.024

Palomba V, Vasta S, Freni A (2017) Experimental testing of AQSOA FAM Z02/water adsorption system for heat and cold storage. Appl Therm Eng 124:967–974. https://doi.org/10.1016/j.applthermaleng.2017.06.085

Pesaran A, Lee H, Hwang Y, et al (2016) Review article: Numerical simulation of adsorption heat pumps. Energy 100:310–320

Pinheiro JM, Salústio S, Rocha JJ, et al (2016) Analysis of equilibrium and kinetic parameters of water adsorption heating systems for different porous metal/metalloid oxide adsorbents. Appl Therm Eng 100:215–226. https://doi.org/10.1016/j.applthermaleng.2016.01.142

Pinheiro JM, Valente AA, Salústio S, et al (2015) Application of the novel ETS-10/water pair in cyclic adsorption heating processes: Measurement of equilibrium and kinetics properties and simulation studies. Appl Therm Eng 87:412–423. https://doi.org/10.1016/j.applthermaleng.2015.05.011

Poyelle F, Guilleminot J-JJ, Meunier F (1999) Experimental Tests and Predictive Model of an Adsorptive Air Conditioning Unit. Ind Eng Chem Res 38:298–309. https://doi.org/10.1021/ie9802008

Radu AII, Defraeye T, Ruch P, et al (2017) Insights from modeling dynamics of water sorption in spherical particles for adsorption heat pumps. Int J Heat Mass Transf 105:326–337

Ramji HR, Leo SL, Abdullah MO (2014) Parametric study and simulation of a heat-driven adsorber for air conditioning system employing activated carbon-methanol working pair. Appl Energy 113:324–333. https://doi.org/10.1016/j.apenergy.2013.07.017

Restuccia G, Freni A, Maggio G (2002) A zeolite-coated bed for air conditioning adsorption systems: Parametric study of heat and mass transfer by dynamic simulation. In: Applied Thermal Engineering. pp 619–630

Rivero-Pacho AM, Critoph RE, Metcalf SJ (2017) Modelling and development of a generator for a domestic gas-fired carbon-ammonia adsorption heat pump. Renew Energy 110:180–185. https://doi.org/10.1016/j.renene.2017.03.089

Sakoda A, Suzuki M (1984) Fundamental study on solar powered adsorption cooling system. J Chem Eng Japan 17:52–57. https://doi.org/10.1252/jcej.17.52

San JY, Tsai FK (2014) Testing of a lab-scale four-bed adsorption heat pump. Appl Therm Eng. https://doi.org/10.1016/j.applthermaleng.2014.05.014

Sapienza A, Gullì G, Calabrese L, et al (2016) An innovative adsorptive chiller prototype based on 3 hybrid coated/granular adsorbers. Appl Energy 179:929–938. https://doi.org/10.1016/j.apenergy.2016.07.056

Sawin JL, Seyboth K, Sverrisson F (2017) Renewables 2017: Global status report

Simonova IA, Freni A, Restuccia G, Aristov YI (2009) Water sorption on composite “silica modified by calcium nitrate.” Microporous Mesoporous Mater 122:223–228. https://doi.org/10.1016/j.micromeso.2009.02.034

Sing KSW (1985) Reporting physisorption data for gas/solid systems with special reference to the determination of surface area and porosity (Recommendations 1984). Pure Appl Chem 57:603–619

Sircar S (1983) Linear-driving-force model for non-isothermal gas adsorption kinetics. J Chem Soc Faraday Trans 1 Phys Chem Condens Phases 79:785. https://doi.org/10.1039/f19837900785

Sircar S, Hufton JR (2000) Why Does the Linear Driving Force Model for Adsorption Kinetics Work?

Tamainot-Telto Z, Metcalf SJ, Critoph RE, et al (2009) Carbon-ammonia pairs for adsorption refrigeration applications: ice making, air conditioning and heat pumping. Int J Refrig 32:1212–1229. https://doi.org/10.1016/j.ijrefrig.2009.01.008

Tchernev DI (1976) Solar app. of natural zeolites. In: Mumpton LBS and FA (ed) Proc. Natural Zeolites Oc. Prop. Use. Pergamon Press, Oxford

Teo HWB, Chakraborty A, Fan W (2017) Improved adsorption characteristics data for AQSOA types zeolites and water systems under static and dynamic conditions. Microporous Mesoporous Mater 242:109–117. https://doi.org/10.1016/j.micromeso.2017.01.015

Ulku S (1986) Adsorption heat pumps. J Heat Recover Syst 6:277–284. https://doi.org/10.1016/0198-7593(86)90113-X

Wang LW, Wang RZ, Oliveira RG (2009) A review on adsorption working pairs for refrigeration. Renew. Sustain. Energy Rev. 13:518–534

Wittstadt U, Füldner G, Laurenz E, et al (2017) A novel adsorption module with fiber heat exchangers: Performance analysis based on driving temperature differences. Renew Energy 110:154–161. https://doi.org/10.1016/j.renene.2016.08.061

Zhang LZ, Wang L (1999) Effects of coupled heat and mass transfers in adsorbent on the performance of a waste heat adsorption cooling unit. Appl Therm Eng 19:195–215. https://doi.org/10.1016/S1359-4311(98)00023-4

Zhu LQ, Tso CY, Chan KC, et al (2018) Experimental investigation on composite adsorbent–Water pair for a solar-powered adsorption cooling system. Appl Therm Eng 131:649–659

CHAPTER 3

This Chapter has been published as:

Dias JMS, Costa VAF (2019) Which dimensional model for the analysis of a coated tube adsorber for adsorption heat pumps? Energy 174:1110–1120. https://doi.org/10.1016/j.energy.2019.03.028

3. WHICH DIMENSIONAL MODEL FOR THE ANALYSIS OF A COATED TUBE ADSORBER FOR ADSORPTION HEAT PUMPS?

Abstract

This paper presents the analysis of a coated tube adsorber for adsorption heat pumps (AHP), starting from a well-established physical model and providing information on how many dimensions need to be considered for a given accuracy. A lumped-parameter model, one-dimensional (radial direction) and two-dimensional (radial and longitudinal directions) distributed-parameter models describing the adsorber's dynamics are discussed. The optimal resolution, guaranteeing an accuracy of ≈1% with lower computational efforts is identified. Results obtained with the three dimensional models are compared and their suitability to predict the coefficient of performance (COP) and the specific heating power (SHP) of an AHP is investigated. Results show that the lumped-parameter model is able to predict the COP with minor deviations from the reference model; however, the SHP is overestimated. Furthermore, several sensibility analyses are performed aiming to assess the influence of important parameters, such as the adsorber tube length and heat transfer fluid's (HTF) velocity. In addition, the influence of disregarding the adsorber metal tube mass is evaluated, resulting in deviations up to ≈4.5% for the COP and ≈7% for the SHP, which are considered significant. Results guide researchers to adopt a given dimensional model for the required accuracy.

Keywords: Dimensional models, adsorption heat pump, adsorber, coated tube, coefficient of performance (COP), specific heating power (SHP).

NOMENCLATURE

C	Specific heat (J/kg.K)
C_p	Constant pressure specific heat (J/kg.K)
d	Diameter (m)
D_{ef0}	Effective diffusivity coefficient (m^2.s)
E_a	Activation energy ($J.kg^{-1}$)
H	Enthalpy (J)
$h_{f\rightarrow m}$	Convective heat transfer coefficient between fluid and metal ($W.K^{-1}.m^{-2}$)
$h_{m\rightarrow s}$	Heat transfer coefficient between metal and adsorbent ($W.K^{-1}.m^{-2}$)
k	Thermal conductivity ($W.K^{-1}.m^{-1}$)
k_0	Pre-exponential coefficient ($kg.kg^{-1}.Pa^{-1}$)
k_D	Blake-Kozeny coefficient (m^2)
K_{LDF}	LDF constant (s^{-1})
L	Tube length (m)
m	Mass (kg)
P	Pressure (Pa)
Q	Heat (J)
q_m	Monolayer capacity ($kg.kg^{-1}$)
r	Radial coordinate (m)
R'	Particular gas constant ($J.kg^{-1}K^{-1}$)
t	Time (s)
t_{SG}	Non-dimensional Toth constant
T	Temperature (K)
u	Darcy's velocity ($m.s^{-1}$)
u_f	Heat transfer fluid velocity ($m.s^{-1}$)
X	Adsorbate concentration in the adsorbent ($kg_a.kg_s^{-1}$)
z	Axial coordinate (m)

Greek letters

ΔH_{ads}	Heat of adsorption ($J.kg^{-1}$)
ε	Porosity
μ	Dynamic viscosity (Pa.s)
σ	Thickness (m)
τ	Cycle time (s)

Subscripts

a	Adsorbate
ads	Adsorption
bed	Adsorbent bed
c	Condenser /Cooling
cyc	Cycle
e	Evaporator
eq	Equilibrium
h	Heating
ic	Isosteric cooling
ih	Isosteric heating
l	Liquid adsorbate
m	Metal
p	Particle
reg	Regeneration
s	Adsorbent
v	Vapor/Vaporization

3.1. INTRODUCTION

Heating and cooling is the biggest energy sector in Europe, accounting for 50% of the total energy consumption much of it being wasted. Renewable energies only account for 18% of the total energy used for heating and cooling, to which the most contributions come from fossil fuels (75%) and a tiny part from nuclear sources (7%) (European Commision 2016). Therefore, there is a need for heating/cooling systems driven by renewable energy sources in order to mitigate resources consumption and global warming. Adsorption cooling has been the focus over the last decades with several units for air conditioning, refrigeration and chillers being developed. However, adsorption heating is still at its initial stage (Tokarev et al. 2018). Adsorption heat pumps (AHPs) can provide heat and are a potential viable alternative to the conventional vapor compression heat pumps (VCHPs), which use CFCs, HCFCs and other high global warming potential (GWP) substances, even if important changes are running towards the use of natural refrigerants. AHPs have low environmental impact since they use zero or nearly zero GWP operating substances, significantly contributing to decrease the greenhouse gases emissions (Dawoud 2014). The fact that they can be driven by natural gas (Dawoud 2014), waste heat (Zhang and Wang 1997; Ramji et al. 2014) and renewable energy sources like solar energy (Sakoda and Suzuki 1984, 1986; Fernandes et al. 2016b) gives the technology great potential. In addition, electricity can also be used to drive the system and when/if it is obtained from renewable energy sources, the heating system is considered renewable as well (Sawin et al. 2017).

Heat pumps extract heat from a low temperature level and deliver it at an intermediate temperature level, as long as a third energy source is provided (Ulku 1986). AHPs are driven by higher temperature energy sources that can provide heat to the system, for example, waste heat, gas burners, electricity, geothermal and solar energy. A simple AHP can be built by packing or coating an adsorbent material on a heat exchanger (HEx), a condenser, an expansion valve, an evaporator and a heat transfer system (HTS) or fluid (HTF) to collect/deliver heat from/to the adsorber. Four main configurations for the adsorber can be identified, namely loose grain, consolidated adsorbent, in situ crystalized coatings and binder-based coatings (Freni et al. 2015b). A detailed overview on the AHPs technology can be found in literature (Dias and Costa 2018). The energy scheme of a common AHP system is presented in Figure 3.1.

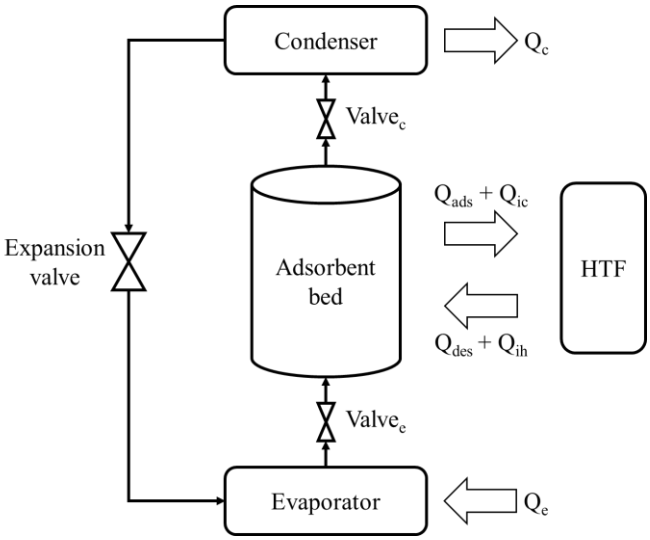

Figure 3.1 – Energy scheme of a common adsorption heat pump (Dias and Costa 2018).

The majority of studies found in literature focus on the adsorbent materials, adsorbers' designing or operating conditions. Comparisons between different dimensional models for the same conditions as well as parametric sensibility studies for the physical models are lacking. Information about the effects of using the same physical models for different system parameters and dimensional models (0D, 1D and 2D) is needed to guide researchers to adopt a given dimensional model for the required accuracy, and mainly to achieve accurate performance predictions. This particular information cannot be found in literature, which forces researchers to perform several sensibility and dimensional analyses before achieving the desired accuracy, wasting lots of time and effort. This paper presents some dimensional and sensibility analyses to well-established AHP's physical models, quantifying their computational cost and accuracy for the system's performance predictions.

Several physical models aiming to describe the adsorber of an AHP system can be found in literature. A comprehensive and detailed review on physical and numerical models for AHPs was presented by Pesaran et al. (2016). The models can be divided in three types: thermodynamic models, lumped-parameter models and distributed-parameter models. Thermodynamic models disregard heat and mass transfer kinetics inside the adsorber, assuming thermodynamic equilibrium between the adsorbent and adsorbate. This type of models can be used to estimate the upper limits of the system's performance. Lumped-parameter models consider heat and mass transfer to/from the adsorber, assuming that the entire adsorber is in thermodynamic equilibrium and at uniform pressure and temperature. Although some models consider the LDF model to account for the internal mass transfer

resistance (Sircar 1983), external mass transfer resistance is neglected. These kind of models are more accurate than thermodynamic models. Distributed-parameter models are the most accurate ones, considering internal and external mass and heat transfer resistances, and pressure and temperature gradients inside the adsorber. These models are more computationally expensive but, given the recent easy access to powerful computers, they have become more appealing (Pesaran et al. 2016). Computational simulation tools like MATLAB R2017b (Massachusetts, USA), MODELICA (Linköping, Sweden) and computational fluid dynamics (CFD) software have recently been used to perform simulations of AHPs (Rezk and Al-Dadah 2012; Ramji et al. 2014; Rivero-Pacho et al. 2017).

Given their high thermal conductivities, higher adsorbent-metal heat transfer coefficients and compact sizes, coated tube adsorbers are nowadays considered the best configuration for AHPs by many researchers (Dias and Costa 2018). Frazzica et al. (2014) performed an experimental characterization of a binder-based coating composed of SAPO-34 as adsorbent and a clay as binder. The experiments were conducted based on the large pressure jump (LPJ) method. The coatings were compared to two loose adsorbent grain configurations, one monolayer and one multilayer. Several coating thicknesses were tested and evaluation based on the volumetric specific cooling power (VSCP). Although the loose grain monolayer showed better kinetic performance, the 0.6 mm thick coating showed an increasing in the VSCP of 65% relatively to the monolayer loose grain. Freni et al. (2015a) also studied the adsorption kinetics of a SAPO-34 based adsorbent coating. They concluded that the binder did not affect the adsorption capacity, and that the mass specific cooling power was greatly improved. However, the VSCP was better for the granular adsorbent. In addition, the stability of the adsorbent coating was also tested for 600 adsorption cycles without degradation of the adsorption capacity. SAPO-34 coatings were also used by Wittstadt et al. (2017) and a COP of 1.4 was reported for heating applications. The effect of the binder used to form the adsorbent coatings on their adsorption capacity was also investigated by Calabrese et al. (2017b). They characterized three silane binder based coatings, and verified that the adsorption capacity of the three adsorbents was not affected by the binders.

Given that adsorbent coatings provide a very promising solution for adsorption heating solutions, three dynamic models for a coated tube adsorber were considered with different dimensions, namely a lumped-parameter model, a one-dimensional (radial direction) distributed-parameter model and a two-dimensional (radial and longitudinal directions)

distributed-parameter model. The considered models take into consideration results reported in literature (Zhang and Wang 1999; Restuccia et al. 2002; Fernandes et al. 2016a) and were adapted and improved for a specific adsorber module design for central and domestic water heating.

Although there are several studies on numerical models for AHPs, and it is guaranteed that lumped-parameter models are less accurate than distributed-parameter ones, it is important to quantify their accuracy differences and computational costs. Only then, researchers can make sustained decisions on which dimensional model should be used considering their desired accuracy and acceptable computational effort. In addition, it is intrinsic to physical models that the more dimensions are considered the better the accuracy will be; but how much? Is the improvement in the model's accuracy worth the additional computational cost? In order to answer these questions it is necessary to quantify the accuracy improvement associated to the consideration of additional spatial dimensions and the associated computational effort and time. Comparisons of different dimensional models based on the same parameters and considerations (which is required to draw useful conclusions) cannot be found in literature. The identification of the best dimensional model (balance between complexity and computational cost versus accuracy) for a particular application can be performed based on the results from this paper, saving a lot of time and effort to those that need to design an AHP system. Thus, decisions can be taken on the necessity of considering all three spatial dimensions or if a lumped-parameter, a one-dimensional or a two-dimensional model is enough to achieve the desired accuracy. In the following sections, different dimensional models for a coated tube adsorber module are presented and discussed. The objective is to analyze the performance of the different dimensional models quantifying the deviations from the most accurate solution. The influence of some parameters on the deviations of the different dimensional models is investigated.

This work focuses on the dimensional models analysis and not on the adsorber characterization itself, aiming to help researchers decide which dimensional model needs to be considered to achieve the desired accuracy. The common lumped-parameter (0D) and distributed-parameter approaches (1D and 2D) are investigated and their main differences quantified. Furthermore, the effects of considering different dimensional models when evaluating the AHP's performance parameters are evaluated and reported. Several comparisons and sensibility analyses of the dimensional models' accuracy to the change of several parameters like the tube length, heat transfer fluid velocity and metal mass are also

carried out. Results presented in this paper can be used to decide which dimensional model needs to be considered and which simplifications can be assumed while still guaranteeing a desired accuracy level. Thus, better agreement between numerical simulations and experimental results can be expected, leading to improved prototype design and faster final application development.

Finally, the adsorber's metal mass is usually disregarded in many studies found in literature (Zhang and Wang 1999; Restuccia et al. 2002; Pinheiro et al. 2016). The quantification of the deviations caused by disregarding that metal mass cannot be found in the literature. It is important to know how much the accuracy is compromised when the metal mass is neglected in order to decide if it is important or not to consider it for each particular application. Therefore, the effects of the adsorber's metal mass are also investigated in this paper, quantifying the deviations on the system's performance predictions when it is not taken into account.

3.2. AHP'S DIMENSIONAL MODELS

The binder-based coated-tube adsorber module represented in Figure 3.2a was designed, which is considered the best hypothesis for a practical adsorber to integrate an AHP system. It is composed by metal tubes externally coated by adsorbent material and by two joints connecting them. For a simpler and clearer visualization, in Figure 3.2 not all the holes of the joints are connected to the correspondent externally coated metal tubes. The joints are linked to the inlet/outlet through which the heat transfer fluid flows, circulating in the interior of the externally coated tubes. The entire component is embedded in a vacuum chamber with connections to the evaporator and condenser, as represented in Figure 3.2b.

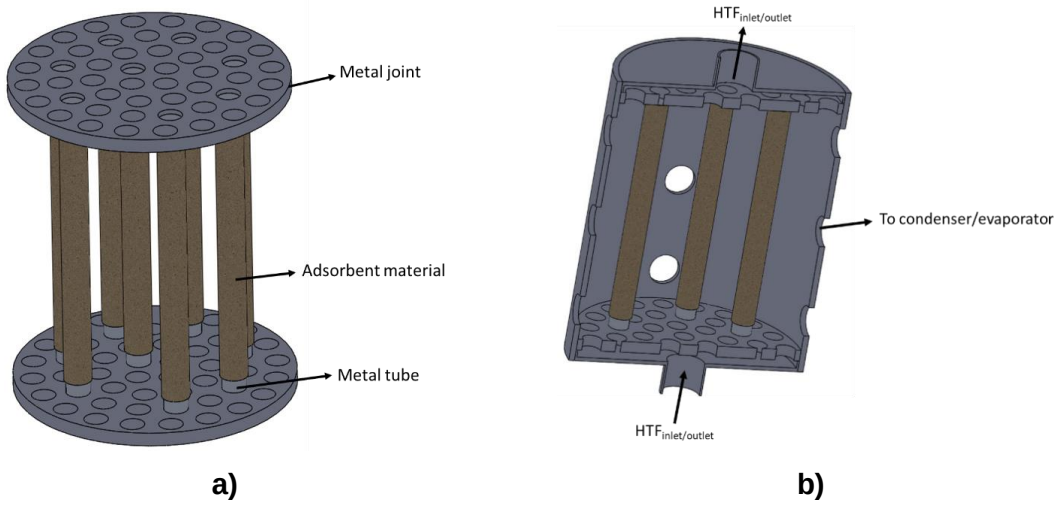

Figure 3.2 – a) Adsorber module containing several metal tubes with an external adsorbent material coating; **b)** Adsorber module cross section view.

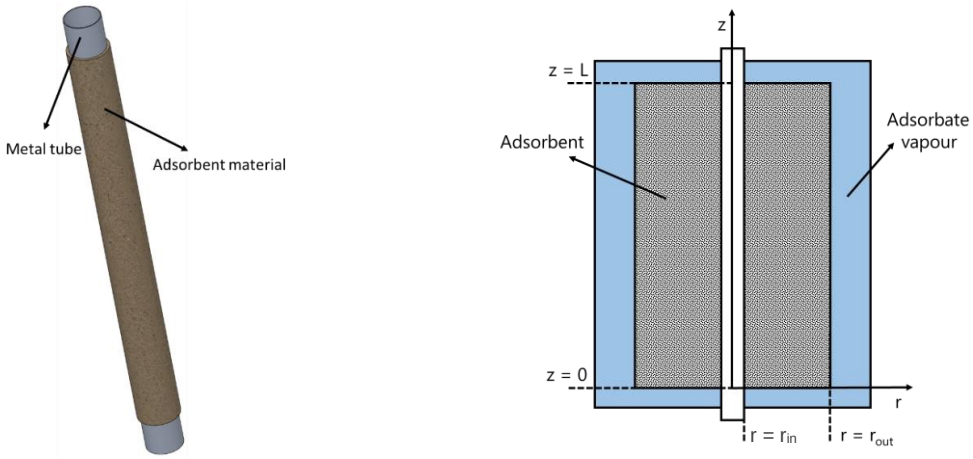

Figure 3.3 – Representative element for the development of the physical models (on the left) and schematics (on the right) (Dias and Costa 2018).

The implemented dimensional models are adapted from Zhang *et al.* (Zhang and Wang 1999) in order to describe the adsorber's behavior. The model was experimentally validated for the zeolite 13X-water pair by Zhang *et al.* (Zhang and Wang 1999) for an adsorption cooling unit, considering the three space dimensions. Since the adsorber contemplated in this work is symmetric along the angular direction for each coated tube, a 2D model is enough to completely describe the adsorber.

All the considered dimensional models describe the dynamics of the representative element from Figure 3.3 to achieve useful comparisons between them. The selected adsorbent-adsorbate working pair is silica gel RD-water since it is well studied and its thermo-physical properties can easily be found in literature. Several applications of the silica gel-water pair for adsorption heat transformation as well as its adsorption isotherms and thermophysical properties are described and experimentally characterized in (Ng et al. 2001; Chua et al. 2002; Di et al. 2007; Wu and Li 2009; Wang et al. 2014; Boman et al. 2017), which are assumed as the experimental validation of the silica gel-water adsorption kinetics. Considering the aforementioned experimental validations of the model itself and the adsorption kinetics for the silica gel-water pair, the 2D model provides trustworthy results for the dimensional models' analysis, which is the objective of this work. However, all the dimensional models are prepared to work with all working pairs that can be described by the LDF model, as long as their equilibrium isotherms and diffusion coefficients are available. Although the use of a binder to apply the coating affects the adsorber's performance, its effect was neglected since the objective is to compare the different dimensional models and not to characterize the adsorber itself. The dimensional models are different spatial implementations of the energy and mass conservation equations, Equations 3.1 and 3.2, respectively, for the selected design.

$$\frac{\partial\left(\rho C_p T_s\right)}{\partial t} + \nabla\left(\rho_v C_{p,v} T_s u\right) - \nabla(k_s \nabla T_s) - \rho_s(1-\varepsilon)\Delta H_{ads}\frac{\partial X}{\partial t} = 0 \qquad 3.1$$

$$\varepsilon\frac{\partial \rho_v}{\partial t} + \nabla(\rho_v u) + \rho_s(1-\varepsilon)\frac{\partial X}{\partial t} = 0 \qquad 3.2$$

with,

$$\rho C_p = \varepsilon\rho_v C_{p,v} + \rho_s(1-\varepsilon)\left(C_s + X C_{p,a}\right) \qquad 3.3$$

and

$$\varepsilon = \varepsilon_{bed} + (1-\varepsilon_{bed})\varepsilon_p \qquad 3.4$$

The momentum balance is described by the Darcy's Law (3.5), and the adsorbent bed permeability is calculated by using the Blake-Kozeny model (3.6) (Wilkes and Birmingham 2006):

$$u = -\frac{k_D}{\mu}\nabla P \tag{3.5}$$

where,

$$k_D = \frac{d_p^2 \varepsilon_{bed}^3}{150(1-\varepsilon_{bed})^2} \tag{3.6}$$

The uptake is described by the linear driving force model (LDF) (Sircar 1983):

$$\frac{dX}{dt} = K_{LDF}\left(X_{eq} - X\right) \tag{3.7}$$

The K_{LDF} constant is a function of temperature and is calculated by (Aristov 2009):

$$K_{LDF} = \frac{15 D_{ef0} e^{-\frac{E_a}{R' T_s}}}{R_p^2} \tag{3.8}$$

For the silica gel RD-water working pair X_{eq} can be obtained by (Chua et al. 2002):

$$X_{eq} = \frac{P k_0 e^{\frac{\Delta H_{ads}}{R' T_s}}}{\left[1 + \left(\frac{P k_0}{q_m} e^{\frac{\Delta H_{ads}}{R' T_s}}\right)^{t_{SG}}\right]^{\frac{1}{t_{SG}}}} \tag{3.9}$$

3.2.1. General assumptions

The following set of assumptions was considered for all dimensional models considered:

- Adsorbent bed is homogenous;
- The evaporator and the condenser are ideal heat exchangers with uniform pressures;
- Adsorbate vapor phase behaves as an ideal gas and the adsorbed phase is considered to be liquid;
- Specific heats for the adsorbate vapor and liquid phases are constants;
- Adsorbate vapor around the adsorbent is always in the saturated conditions;
- Thermophysical properties of solid materials do not change with temperature;
- The pre-heating and pre-cooling phases are terminated when the pressure in the adsorber reaches the condenser and evaporator pressures, respectively.

3.2.2. Lumped parameter model (0D model)

The lumped parameter model results from the mass and energy conservation equations applied to the representative element of the adsorber, under the following additional assumptions:

- Temperature and pressure are uniform in the adsorbent bed;
- Adsorbate is uniformly adsorbed and desorbed by the adsorbent;
- The uptake is constant during pre-heating (isosteric heating) and pre-cooling (isosteric cooling) phases.

The uptake is described by:

$$\frac{dX}{dt} = K_{LDF}\left(X_{eq} - X\right)(\alpha), \qquad 3.10$$

$$\begin{cases} Isosteric\ phases & \rightarrow \alpha = 0 \\ Adsorption/Desorption & \rightarrow \alpha = 1 \end{cases}$$

The adsorbent bed energy balance equation is given by:

$$\left[\rho_s(1-\varepsilon)\left(C_s + XC_{p,a}\right) + \varepsilon\rho_v C_{p,v}\right]\frac{dT_s}{dt} = \\ = (1-\varepsilon)\rho_s \Delta H_{ads}\frac{dX}{dt} + \frac{4d_{out,tube}h_{m\to s}(T_m - T_s)}{d_{out,s}^2 - d_{in,s}^2} \quad 3.11$$

with $d_{in,s} = d_{out,tube}$.

The differential form of the ideal gas law describes the adsorbent bed mass balance:

$$\frac{d\rho_v}{dt} = \frac{P}{T_s^2 R'}\left(-\frac{dT_s}{dt}\right)(\gamma) + \frac{1}{R'T_s^2}\left(T_s\frac{dP}{dt} - \rho_v\frac{dT_s}{dt}\right)(\delta) \quad 3.12$$

$$\begin{cases} Isosteric\ phases & \to \gamma = 0, \quad \delta = 1 \\ Adsorption/Desorption & \to \gamma = 1, \quad \delta = 0 \end{cases}$$

The adsorbent bed pressure is obtained from the Clausius-Clapeyron equation (Do Duong 1998), which can be rearranged as:

$$\frac{dP}{dt} = \frac{PL_v}{R'T_s^2}\left(\frac{dT_s}{dt}\right)(\beta) \quad 3.13$$

$$\begin{cases} Isosteric\ phases & \to \beta = 1 \\ Adsorption/Desorption & \to \beta = 0 \end{cases}$$

The pressure variation with time is considered to be null during adsorption and desorption phases because these processes are considered to be isobaric, at the evaporator and condenser pressures, respectively.

Lastly, the metal tube energy balance equation is:

$$\rho_m C_m\frac{dT_m}{dt} = \frac{4d_{in}h_{f\to m}\left(T_f - T_m\right)}{d_{out}^2 - d_{in}^2} + \frac{4d_{out}h_{m\to s}(T_s - T_m)}{d_{out}^2 - d_{in}^2} \quad 3.14$$

$$\begin{cases} Adsorption/Isosteric\ cooling \to T_f = T_{ads} \\ Desorption/Isosteric\ heating \to T_f = T_{reg} \end{cases}$$

For laminar flow conditions ($Re_f \leq 2300$) of the heat transfer fluid inside the adsorber tubes the Nusselt number is obtained considering the constant heat flux situation (Bergman et al. 2011):

$$Nu_f = 4.36 \tag{3.15}$$

For $2300 < Re_f \leq 5 \times 10^6$ and $0.5 \leq Pr \leq 2000$ the Nusselt number is obtained through the Gnielinsky correlation (Gnielinski 1976) (caution should be taken when using this correlation for $Re_f < 3000$):

$$Nu_f = \frac{\left(f/8\right)\left(Re_f - 1000\right)Pr}{1 + 12.7\left(f/8\right)^{1/2}\left(Pr^{2/3} - 1\right)} \tag{3.16}$$

where f is calculated using the correlation developed by Petukhov (Petukhov 1970):

$$f = \left(0.79ln\left(Re_f\right) - 1.64\right)^{-2} \tag{3.17}$$

The convective heat transfer coefficient between the fluid and the metal tube is obtained as:

$$h_{f\rightarrow m} = \frac{Nu_f k_f}{d_{in}} \tag{3.18}$$

The set of initial conditions is:

$$t_{ini} = 0 \qquad P(t_{ini}) = P_{ini}$$

$$T_m(t_{ini}) = T_s(t_{ini}) = T_{ini} \qquad X(t_{ini}) = X_{eq}$$

The differential equations system was solved numerically in MATLAB R2017b (Massachusetts, USA).

3.2.3. 1D distributed parameter model (radial)

The 1D distributed parameter model was developed considering the following additional assumption:

- Temperature and pressure in the adsorbent bed are uniform over the longitudinal and angular directions;

The uptake is obtained similarly to the lumped parameter model; however, it is now function of the radial coordinate since $T_s(r)$ and $P(r)$ are considered instead. In addition, the uptake is no longer constant during the pre-heating/cooling phases and it is described by equation 3.7. The adsorbent bed energy balance equation is given by:

$$\begin{aligned}\left[\rho_s(1-\varepsilon)(C_s+XC_l)+\varepsilon\rho_v C_{p_v}\right]\frac{dT_s}{dt} = \\ = (1-\varepsilon)\rho_s\Delta H_{ads}\frac{dX}{dt}+\frac{k_s}{r}\left(\frac{\partial T_s}{\partial r}+r\frac{\partial^2 T_s}{\partial r^2}\right) \\ -\frac{C_{p_v}}{r}\left(\rho_v T_s u+rT_s\frac{\partial\rho_v}{\partial r}+r\rho_v u\frac{\partial T_s}{\partial r}+r\rho_v T_s\frac{\partial u}{\partial r}\right)\end{aligned} \quad 3.19$$

The mass conservation equation is:

$$\frac{\partial\rho_v}{\partial t}=-\frac{1}{\varepsilon}\left[\rho_s(1-\varepsilon)\frac{\partial X}{\partial t}+\frac{1}{r}\left(ru\frac{\partial\rho_v}{\partial r}+\rho_v r\frac{\partial u}{\partial r}+\rho_v u\right)\right] \quad 3.20$$

The metal tube thermal energy balance equation is equal to its lumped parameter version because the approximation $\frac{\partial T_m}{\partial r}\approx 0$ is considered, since $k_m \gg k_s$. In addition, the temperature of the heat transfer fluid is considered constant along the radial direction, $\frac{\partial T_f}{\partial r}\approx 0$, assuming that $L_{tube} \gg r_{tube}$.

The initial conditions are:

$$t_{ini} = 0 \qquad P(t_{ini}) = P_{ini}$$

$$T_m(t_{ini}) = T_s(t_{ini}) = T_{ini} \qquad X(t_{ini}) = X_{eq}$$

During the pre-heating/pre-cooling phases, the pressure in the chamber is considered to be equal to the pressure of the external layer of the adsorbent ($P_{chamber} = P_{r=r_{out}}$) within each time step. The boundary conditions for the pressure are:

$$\left.\frac{\partial P}{\partial r}\right|_{r=r_{in}} = 0$$

$$\begin{cases} P|_{r=r_{out}} = P_e, & Adsorption \\ P|_{r=r_{out}} = P_c, & Regeneration \\ \left.\dfrac{\partial P}{\partial r}\right|_{r=r_{out}} = 0, & Cooling/Heating \end{cases}$$

For the temperature, the following boundary conditions apply:

$$-k_s \left.\frac{\partial T_s}{\partial r}\right|_{r=r_{in}} = h_{m\to s}(T_m - T_s)$$

$$\left.\frac{\partial T_s}{\partial r}\right|_{r=r_{out}} = 0$$

In order to solve the physical model's partial differential equations, the method of lines was implemented and the spatial derivatives in the radial coordinate were discretized through the finite difference method. For the first order derivatives, the forward finite difference scheme was used whereas for the second order derivatives, the centered finite difference scheme was implemented. As a result, the partial differential equations were reduced to an ODE system that was solved using MATLAB R2017b (Massachusetts, USA).

3.2.4. 2D distributed parameter model (radial and longitudinal)

The two dimensional distributed parameter model considers the same assumptions as the one-dimensional model, except for the temperature and pressure that will additionally change along the axial (longitudinal) coordinate. Furthermore, the temperature of the heat transfer fluid will depend on the axial coordinate as well. The uptake is also described by the LDF model and it depends on the axial and radial positions through the variables $T_s(r,z)$ and $P(r,z)$. The adsorbent bed energy balance equation in this case is:

$$\begin{aligned}\left[\rho_s(1-\varepsilon)(C_s+XC_l)+\varepsilon\rho_v C_{p_v}\right]\frac{dT_s}{dt} = \\ = (1-\varepsilon)\rho_s\Delta H_{ads}\frac{dX}{dt}+\frac{k_s}{r}\left(\frac{\partial T_s}{\partial r}+r\frac{\partial^2 T_s}{\partial r^2}\right) \\ -\frac{C_{p_v}}{r}\left(\rho_v T_s u_r + rT_s u_r\frac{\partial\rho_v}{\partial r}+r\rho_v u_r\frac{\partial T_s}{\partial r}+r\rho_v T_s\frac{\partial u_r}{\partial r}\right) \\ -C_{p_v}\left(T_s u_z\frac{\partial\rho_v}{\partial z}+\rho_v T_s\frac{\partial u_z}{\partial z}+\rho_v u_z\frac{\partial T_s}{\partial z}\right)+k_s\left(\frac{\partial^2 T_s}{\partial z^2}\right)\end{aligned} \quad 3.21$$

The mass conservation equation is given by:

$$\frac{\partial\rho_v}{\partial t} = -\frac{1}{\varepsilon}\left[\rho_s(1-\varepsilon)\frac{\partial X}{\partial t}+\frac{1}{r}\left(ru_r\frac{\partial\rho_v}{\partial r}+\rho_v r\frac{\partial u_r}{\partial r}+\rho_v u_r\right)+\rho_v\frac{\partial u_z}{\partial z}+u_z\frac{\partial\rho_v}{\partial z}\right] \quad 3.22$$

For the heat transfer fluid, $\frac{\partial T_f}{\partial r}\approx 0$ is assumed since $r_{tube}\ll L_{tube}$ and the fluid velocity, u_f, is constant. The energy balance equation for the heat transfer fluid is given by:

$$\rho_f C_{p,f}\frac{\partial T_f}{\partial t} = k_f\left(\frac{\partial^2 T_f}{\partial z^2}\right)-u_f\rho_f C_{p,f}\frac{\partial T_f}{\partial z}+\frac{4h_{f\to m}}{d_{in}}\left(T_m-T_f\right) \quad 3.23$$

For the metal tube $\frac{\partial T_m}{\partial r}\approx 0$ is also assumed and its energy balance equation is:

$$\rho_m C_m\frac{dT_m}{dt} = k_m\left(\frac{\partial^2 T_m}{\partial z^2}\right)+\frac{4d_{in}h_{f\to m}\left(T_f-T_m\right)}{d_{out}^2-d_{in}^2}+\frac{4d_{out}h_{m\to s}(T_s-T_m)}{d_{out}^2-d_{in}^2} \quad 3.24$$

The initial conditions are:

$$t_{ini} = 0 \qquad P(t_{ini}) = P_{ini}$$

$$T_m(t_{ini}) = T_f(t_{ini}) = T_s(t_{ini}) = T_{ini} \qquad X(t_{ini}) = X_{eq}\left(P_{ini}, T_{s_{ini}}\right)$$

During the pre-heating/pre-cooling phases, the pressure in the chamber is considered to be equal to the pressure of the external layer of the adsorbent ($P_{chamber} = P_{r=r_{out}}$) within each time step. The pressure and temperature boundary conditions that define the selected design for the adsorber are:

$$\left.\frac{\partial P}{\partial r}\right|_{r=r_{in}} = 0$$

$$P|_{r=r_{out}} = P|_{z=0} = P|_{z=L} = P_e, \qquad Adsorption$$

$$P|_{r=r_{out}} = P|_{z=0} = P|_{z=L} = P_c, \qquad Regeneration$$

$$\left.\frac{\partial P}{\partial r}\right|_{r=r_{out}} = \left.\frac{\partial P}{\partial r}\right|_{z=0} = \left.\frac{\partial P}{\partial r}\right|_{z=L} = 0, \qquad Cooling/Heating$$

$$-k_s \left.\frac{\partial T_s}{\partial r}\right|_{r=r_{in}} = h_{m\to s}(T_m - T_s)$$

$$\left.\frac{\partial T_s}{\partial r}\right|_{r=r_{out}} = \left.\frac{\partial T_s}{\partial z}\right|_{z=0} = \left.\frac{\partial T_s}{\partial z}\right|_{z=L} = 0$$

$$T_f\big|_{z=0} = T_{ads}\,, \qquad Adsorption/Cooling$$

$$T_f\big|_{z=0} = T_{reg}\,, \qquad Regeneration/Heating$$

$$\left.\frac{\partial T_f}{\partial z}\right|_{z=L} = 0$$

$$\left.\frac{\partial T_m}{\partial z}\right|_{z=0} = \left.\frac{\partial T_m}{\partial z}\right|_{z=L} = 0$$

In order to solve the physical model's partial differential equations, the method of lines was also implemented and the derivatives in the radial and axial coordinates discretized through the finite difference method. The discretization is performed for the axial coordinate

first and then, every element is discretized along the radial coordinate. As for the 1D model, the forward finite difference and the centered finite difference schemes were used for the first and second order derivatives, respectively. As a result, the partial differential equations were reduced to an ODE system and solved using MATLAB R2017b (Massachusetts, USA).

3.3. COMPARISON AND SENSIBILITY ANALYSIS OF THE DIMENSIONAL MODELS

Results obtained with the three different dimensional models were compared in order to quantify their main differences. The parameters used for the accuracy comparisons are the performance coefficients for heating applications, namely the coefficient of performance (COP) and the specific heating power (SHP), obtained respectively as (Dias and Costa 2018),

$$COP = \frac{Q_c + Q_{4-1} + Q_{1-2}}{Q_{2-3} + Q_{3-4}}, \quad 3.25$$

$$SHP = \frac{Q_c + Q_{4-1} + Q_{1-2}}{m_s \tau_{cyc}}, \quad 3.26$$

Q_c enters the numerators of equations 3.25 and 3.26, as it is assumed to be useful heat for heating applications. The adsorption (1-2), pre-heating (2-3), regeneration (3-4) and pre-cooling (4-1) heats were calculated as follows (Dias and Costa 2018):

$$-Q_{1-2} \approx \int_{T_1}^{T_2} \left[m_s \left(C_s + X C_{p,a} \right) + m_m C_m \right] dT - \int_{X_{min}}^{X_{max}} m_s \Delta H_{ads} dX \quad 3.27$$

$$Q_{2-3} \approx \int_{T_2}^{T_3} \left[m_s \left(C_s + X_{max} C_{p,a} \right) + m_m C_m \right] dT \quad 3.28$$

$$Q_{3-4} \approx \int_{T_3}^{T_4} \left[m_s\left(C_s + XC_{p,a}\right) + m_m C_m\right] dT - \int_{X_{max}}^{X_{min}} m_s \Delta H_{ads} dX \quad 3.29$$

$$-Q_{4-1} \approx \int_{T_4}^{T_1} \left[m_s\left(C_s + X_{min} C_{p,a}\right) + m_m C_m\right] dT \quad 3.30$$

$$Q_c = m_s \Delta X \Delta H_v \quad 3.31$$

The different dimensional models' results are compared to the most accurate model results, which is the 2D distributed-parameter model with the highest spatial resolution. The selected values for the radial and longitudinal spatial resolutions for the highest accuracy model were $\Delta r = 4 \times 10^{-5}\, m$ and $\Delta z = 2.08 \times 10^{-2}\, m$, respectively. Further decreasing of these space steps results in improvements of less than 1 % for the COP and SHP values, which was found unnecessary for the given purposes.

3.3.1. Reference parameters

First, a simple analysis was carried out in order to compare the COP and SHP values obtained by each dimensional model, considering the same parameters for all three models. In Table 3.1 are listed some parameters used in the simulations. These parameters values were taken from several studies available in the literature (Ng et al. 2001; Chua et al. 2002; Di et al. 2007; Chakraborty et al. 2014; Sun and Chakraborty 2015). A modest heat transfer coefficient between the metal tube and the adsorbent material was considered, since the objective is to investigate the dimensional models and not the optimization of the adsorber's performance. However, it must be mentioned that higher heat transfer coefficients for adsorbent coatings can be found in literature (Restuccia et al. 2002).

Table 3.1 – Standard parameters used in the simulations.

Symbol name	Value	Unit
C_m	910	J.kg^{-1}.K^{-1}
C_s	921	J.kg^{-1}.K^{-1}
d_p	3.5×10^{-4}	m
$d_{in,tube}$	0.02	m
E_a	2.3314×10^{6}	J.kg^{-1}
$h_{m \to s}$	100	W.m^{-2}.K^{-1}
k_0	7.3×10^{-13}	kg.kg^{-1}.Pa^{-1}
k_f	0.6	W.m^{-1}.K^{-1}
k_m	205	W.m^{-1}.K^{-1}
k_s	0.198	W.m^{-1}.K^{-1}
L_{tube}	1	m
ΔH_v	2.4×10^{6}	J.kg^{-1}
q_m	0.45	kg.kg^{-1}
t_{ads}	1500	s
T_c	$273.15 + 30$	K
T_e	$273.15 + 12$	K
$T_{f,ads}$	$273.15 + 30$	K
$T_{f,reg}$	$273.15 + 200$	K
t_{reg}	$0.91 \times t_{ads}$	s
t_{SG}	12	-
u_f	0.05	m.s^{-1}
ΔH_{ads}	2.693×10^{6}	J.kg^{-1}
ε	0.4	-
ρ_m	2700	kg.m-^{3}
ρ_s	2561	kg.m-^{3}
σ_s	0.002	m
σ_{tube}	0.001	m

The three dimensional models' results are compared to the high spatial resolution distributed-parameter model results, these used as reference. The criterion for the selection

of the spatial resolution of the reference model was to increase the resolution and compare the results to the previous ones, stopping the process when deviations smaller than 0.5% were achieved. This process was carried out for the radial and longitudinal directions using the standard parameters. The selected resolution for the reference model is $\Delta r = 4 \times 10^{-5}\ m$ and $\Delta z = 2.08 \times 10^{-2}\ m$, for the radial and longitudinal directions respectively. The spatial resolution for the 2D model was chosen guaranteeing deviations relative to the reference lower than 1% for both directions using the standard parameters, which correspond to $\Delta r = 5 \times 10^{-5}\ m$ and $\Delta z = 8.33 \times 10^{-2}\ m$. For the 1D model the same radial resolution as for the 2D model was selected. The simulations were carried out for three different HTF velocities. The selected velocities might seem low, but they were selected in order to achieve useful temperature increases inside the tubes during the adsorption phase. The calculation time was also measured in order to access the computational cost of each dimensional model. The COP and SHP values, as well as the deviations relatively to the reference model, and the calculation times are presented in Table 3.2. For this purpose, the reference model is considered as the ‘exact’ solution. In order to calculate the computational time, the function “tic…toc” from MATLAB R2017b (Massachusetts, USA) was used.

Table 3.2 – Results comparison for the different dimensional models using constant parameters.

Model	v_{HTF} ($m.s^{-1}$)	COP	SHP ($W.kg^{-1}$)	$t_{calc.}$ (min)	Φ_{COP} (%)	Φ_{SHP} (%)
Reference	0.050	1.582	217.97	534.00	-	-
2D		1.583	219.94	21.30	0.04	0.90
1D		1.588	219.64	0.15	0.36	0.77
0D		1.608	262.07	0.01	1.61	20.23
Reference	0.025	1.579	209.01	529.90	-	-
2D		1.580	211.46	23.68	0.06	1.17
1D		1.588	219.64	1.67	0.54	5.09
0D		1.608	262.07	0.02	1.79	25.39
Reference	0.010	1.567	183.93	580.55	-	-
2D		1.570	187.63	30.82	0.19	2.01
1D		1.588	219.64	0.15	1.31	19.41
0D		1.608	262.07	0.02	2.56	42.48

2D – Two-dimensional distributed-parameter

1D – One-dimensional distributed-parameter

0D – Lumped-parameter

Φ – Deviation relatively to the reference

$t_{calc.}$ – Calculation time

By analyzing Table 3.2, it is noticeable that for smaller HTF velocities the deviations relative to the reference increase. For the lumped-parameter model it can be concluded that it is not suitable to describe the adsorber's dynamics since it overestimates the SHP value by more than 20%. Consequently, the lumped-parameter model will not be used for the upcoming analyses. However, it can be a very interesting option to instantaneously provide a first prediction for the system's performance. The lumped-parameter model predicts the system's maximum performance since it is able to obtain the maximum and minimum uptake values. However, being a 0D space model, the temperature and pressure changes along the materials are assumed to occur uniformly and the predicted pre-heating and pre-cooling duration are too low, resulting in cycle times lower than reality, which lead to an overestimation of SHP. The 1D distributed-parameter model can be used for higher HTF velocities, providing good accuracy. As the HTF velocity lowers, the accuracy of the 1D model worsens due to the increase of the temperature differences along the tube length

and the adsorbent, which are not taken into account by the model. Meanwhile, the 2D distributed-parameter model proved to require a reasonable computational effort. On the other hand, the high computational effort required by the 2D reference model is not justified, since the improvement on the results' accuracy is irrelevant.

3.3.2. Metal-adsorbent interface heat transfer coefficient

The heat transfer coefficient at the metal-adsorbent interface has a strong associated uncertainty. Values in the range 100-1000 $W.K^{-1}.m^{-2}$ can be achieved from the literature, depending on the coating technique among other factors. Given this uncertainty, the 1D and 2D models' results were compared using different metal-adsorbent heat transfer coefficients, which are represented in Figure 3.4.

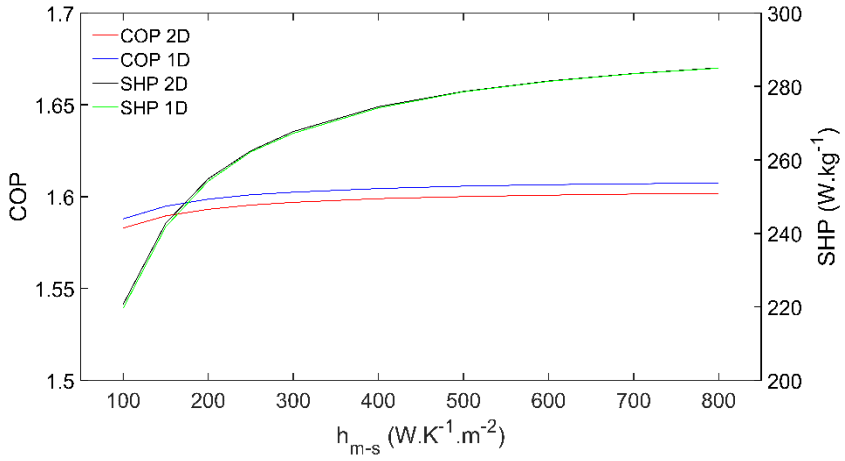

Figure 3.4 – COP and SHP as function of the metal-adsorbent heat transfer coefficient obtained with the 1D and 2D models.

These results prove that the 1D model can be used to evaluate the effect of the metal-adsorbent heat transfer coefficient on the performance parameters, since the difference between its predictions and the 2D model's is insignificant. Furthermore, the COP is not significantly affected by this heat transfer coefficient whereas the SHP shows significant variations. Even though the SHP increases with the heat transfer coefficient, this increase fades for heat transfer coefficients higher than 400 $W.K^{-1}.m^{-2}$.

3.3.3. Adsorber tube length

After performing a first analysis to the considered dimensional models, which resulted in ruling out the lumped-parameter model, the two distributed-parameter models' results

were analyzed for different tube lengths. Thus, a comparison between the 1D and 2D models' results for different tube lengths was carried out. For comparison purposes, the 2D model results were taken as the best results, since the reference model would require enormous computational effort, which was found unnecessary. Figure 3.5 shows the deviations in COP and SHP obtained when using the 1D model.

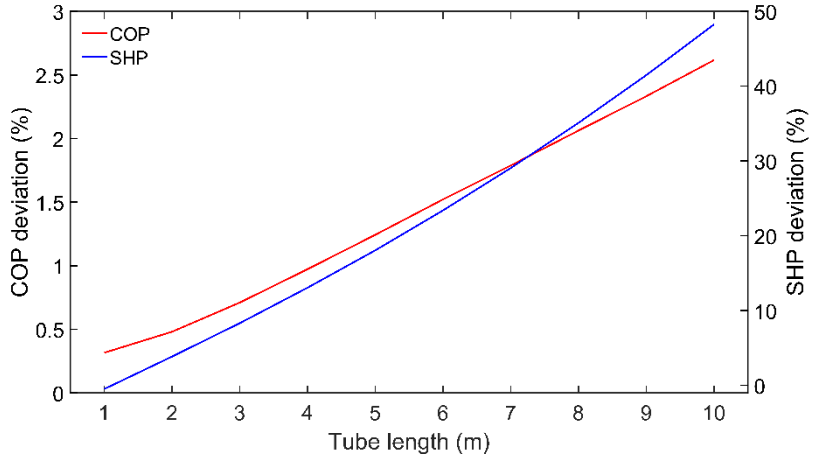

Figure 3.5 – COP and SHP deviations as function of the tube length.

The COP is slightly over-predicted by the 1D model being its deviation of ≈2.5% for a 10 m long tube. Thus, the 1D model is a reliable tool to predict the COP, even for long tubes where the temperature changes along the tube's length are significant. On the other hand, the SHP deviation is too high to be despised since it surpasses the 10% mark if a tube longer than 3 m is used. As depicted in Figure 3.5, for a 10 m long tube the SHP deviation is over-predicted by approximately one-half of its most accurate value. Therefore, the 1D model can provide accurate predictions if the tube length is not too high; however, it cannot be relied on for longer tubes, where significant temperature variation along the length of the tube occur. Thus, in the following sections the analyses will only contemplate the 2D model.

3.3.4. Heat transfer fluid velocity

A resolution analysis for the 2D model has been performed in order to evaluate the minimal spatial resolution needed for the desired deviation relative to its high-resolution version, which has been used as reference on the previous sections. The simulations were conducted for different HTF velocities, and the deviations of the COP and SHP values were investigated for different spatial resolutions. Figure 3.6 and Figure 3.7 show the deviations for the COP and the SHP, respectively, caused by lowering the resolution of the model in

both radial and longitudinal directions. In Figure 3.6 and Figure 3.7, the deviations of the 2D model results relative to the reference results are plotted against the HTF velocity and the radial and longitudinal resolutions, v_{HTF}, Δr and Δz, respectively.

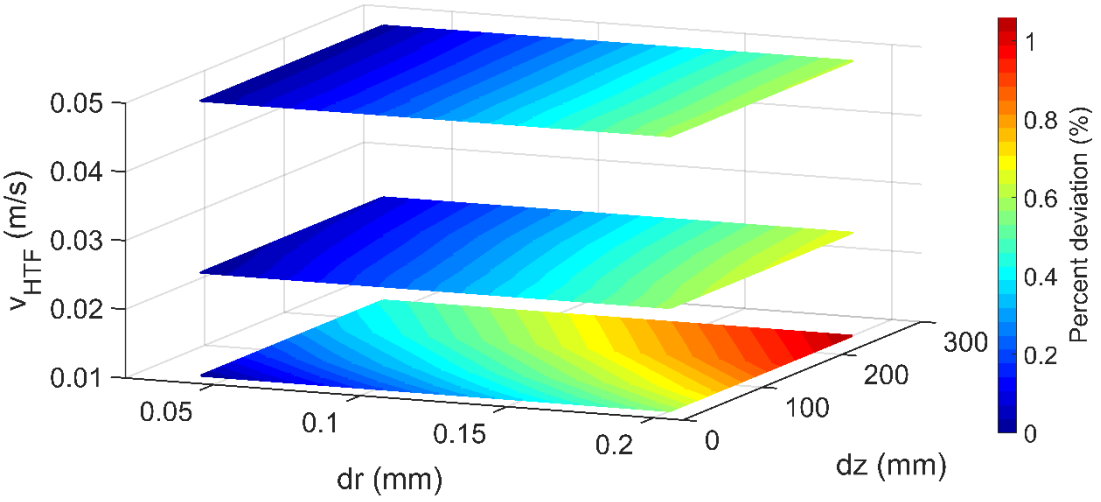

Figure 3.6 – COP percent deviation as function of the axial and radial direction resolutions, respectively Δz and Δr, and the heat transfer fluid velocity.

For higher HTF velocities the COP deviations are affected mainly by the radial resolution; however, for lower HTF velocities the longitudinal resolution also begins to cause COP deviations. Although, even for the smallest HTF velocity, the COP deviations caused by using a lower resolution are small.

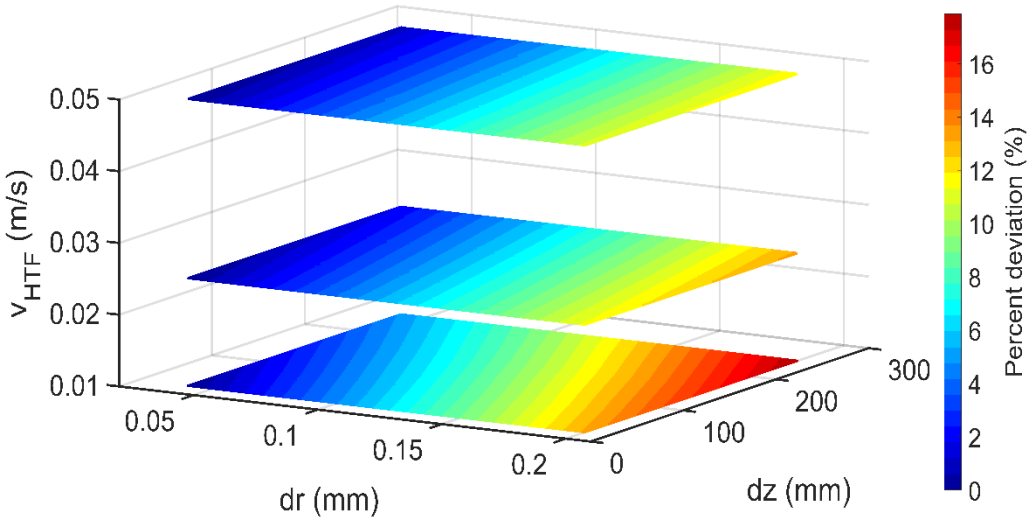

Figure 3.7 – SHP percent deviation as function of the axial and radial direction resolutions, respectively *Δz* and *Δr*, and the heat transfer fluid velocity.

On the other hand, the SHP deviations caused by lowering the resolution are significant. The radial resolution strongly affects the accuracy of the SHP predictions for all HTF velocities tested. The influence of the longitudinal resolution on the accuracy increases as the HTF's velocity decreases, reaching ≈5% for the smallest HTF velocity tested. For the lowest resolution the obtained SHP deviations are 12%, 13% and 18% for the respective HTF velocities of 0.050 m.s^{-1}, 0.025 m.s^{-1} and 0.010 m.s^{-1}. From the analysis it is concluded that a 2D spatial resolution with $\Delta r = 5 \times 10^{-5}\, m$ and $\Delta z = 8.33 \times 10^{-2}\, m$ is enough to guarantee a total SHP deviation of only ≈1% under the worst-case scenario tested (lowest HTF's velocity). It is important to note that there is a difference of 700 min on the calculation time when using the highest and lower spatial resolutions. The difference on the calculation time between the selected best resolution and the highest resolution is of 670 min for the standard parameters. The selected best radial and longitudinal resolution requires much less computational effort, and still provides accurate results.

3.3.5. Metal mass

Although some studies take into consideration the mass of the adsorber's metal tubes (Freni et al. 2016; Sapienza et al. 2016; Kowsari et al. 2017), this parameter is often disregarded or not mentioned in many studies for the calculation of the resultant heat from an AHP cycle (Zhang and Wang 1999; Restuccia et al. 2002; Pinheiro et al. 2016). The effects of considering this metal mass on the physical models were evaluated. In order to

quantify these effects, the 2D distributed-parameter model was used to simulate the AHP cycle. Simulations were carried out considering the metal tube mass and disregarding it ($m_m = 0$), for different inner tube diameters and for two distinct HTF's velocities. The COP and SHP deviations due to disregarding of the tube's metal mass are presented in Table 3.3.

Table 3.3 – Deviations of COP and SHP due to disregarding the tube metal mass.

Inner tube diameter (mm)	HTF velocity = 0.01 m/s		HTF velocity = 0.05 m/s	
	COP deviation	SHP deviation	COP deviation	SHP deviation
5	3.7%	-6.0%	3.4%	-5.3%
10	4.1%	-6.4%	4.0%	-6.1%
20	4.5%	-7.1%	4.5%	-7.0%

By analyzing Table 3.3 it is concluded that not considering the metal mass has a significant impact on the prediction of the system's performance. The COP is always overestimated whereas the SHP is always underestimated, with the SHP prediction being the most affected. On the other hand, the deviations of disregarding the tube metal mass are not significantly affected by the HTF velocity. It is thus concluded that the tube's metal mass should not be disregarded unless deviations up to ≈4.5% on the COP and up to ≈7% on the SHP values can be considered acceptable.

3.4. CONCLUSIONS

Analysis of different transient dimensional models describing a coated tube adsorber for an AHP system was carried out. Three different dimensional models were considered and results compared, namely a 0D lumped-parameter model, a 1D distributed-parameter model and a 2D distributed-parameter model. All the analyses reported help on the selection of the dimensional model that must be used for different adsorption heat pump simulations. Furthermore, parametric sensibility was achieved and an evaluation of the deviations that are associated with each dimensional model was performed. Thus, sustained decisions about which dimensional model must be used in order to achieve suitable accuracies for particular applications can be made, taking into account the deviations and the computational costs associated to each dimensional model.

It was concluded that the lumped-parameter model is not suitable to describe the adsorber's dynamics unless a deviation over 20% can be admitted, since the SHP is overestimated. On the other hand, the results show that the lumped model can be used to predict the COP, with deviations up to ≈2% relative to the high-resolution reference model.

The 1D radially distributed parameter model can be used for a very quick prediction of the adsorber's performance coefficients, providing results with insignificant deviations for the COP. Although the 1D model cannot be relied on for lower HTF's velocities, for higher HTF's velocities that result in low temperature differences along the tube length, the 1D model also provides accurate results for the SHP. However, by carrying out tests for longer tube lengths it was found that this model does not provide accurate predictions for the SHP, with deviations up to 50% for a 10 m long tube due to the high temperature variation along the tube length. Information on whether the utilization of a 1D model is suitable or not depending on the tube length is now available.

From the simulations performed with the 2D (radial and longitudinal) distributed-parameter model for different HTF's velocities, it was concluded that the spatial resolutions tested had no significant impact on the COP predictions. Nevertheless, the SHP predictions are significantly influenced by the spatial resolution since deviations up to ≈17% were obtained using the lowest resolution. In addition, it was found that the radial resolution has greater influence on the accuracy of the model than the longitudinal resolution, which only becomes significant for lower HTF's velocities. Therefore, a spatial resolution of $\Delta r = 5 \times 10^{-5}\ m$ and $\Delta z = 8.33 \times 10^{-2}\ m$ should be used in order to guarantee a total deviation of ≈1% for the SHP value for the worst-case scenario, with the lowest computational cost. It is thus concluded that the 2D distributed-parameter model should be selected if a detailed and accurate description of an AHP system is desired.

Finally, the influence of disregarding the metal mass of the adsorber was investigated. Results show that not accounting for this metal mass leads to significant deviations on the COP and SHP predictions. Deviations up to ≈4.5% for the COP and up to ≈7% for the SHP were obtained due to the disregarding of the metal tube mass.

3.5. REFERENCES

Aristov YI (2009) Optimal adsorbent for adsorptive heat transformers: Dynamic considerations. Int J Refrig. https://doi.org/10.1016/j.ijrefrig.2009.01.022

Bergman TL, Lavigne AS, Incropera FP, Dewitt DP (2011) Fundamentals of Heat and Mass Transfer. John Wiley & Sons

Boman DB, Hoysall DC, Pahinkar DG, et al (2017) Screening of working pairs for adsorption heat pumps based on thermodynamic and transport characteristics. Appl Therm Eng 123:422–434. https://doi.org/10.1016/j.applthermaleng.2017.04.153

Calabrese L, Brancato V, Bonaccorsi L, et al (2017) Development and characterization of silane-zeolite adsorbent coatings for adsorption heat pump applications. Appl Therm Eng 116:364–371. https://doi.org/10.1016/j.applthermaleng.2017.01.112

Chakraborty A, Saha BB, Aristov YI (2014) Dynamic behaviors of adsorption chiller: Effects of the silica gel grain size and layers. Energy 78:304–312. https://doi.org/10.1016/J.ENERGY.2014.10.015

Chua HT, Ng KC, Chakraborty A, et al (2002) Adsorption Characteristics of Silica Gel + Water Systems. https://doi.org/10.1021/je0255067

Dawoud B (2014) On the development of an innovative gas-fired heating appliance based on a zeolite-water adsorption heat pump; System description and seasonal gas utilization efficiency. Appl Therm Eng 72:323–330. https://doi.org/10.1016/j.applthermaleng.2014.09.008

Di J, Wu JY, Xia ZZ, Wang RZ (2007) Theoretical and experimental study on characteristics of a novel silica gel-water chiller under the conditions of variable heat source temperature. Int J Refrig. https://doi.org/10.1016/j.ijrefrig.2006.07.022

Dias JMS, Costa VAF (2018) Adsorption heat pumps for heating applications: A review of current state, literature gaps and development challenges. Renew Sustain Energy Rev 98:317–327. https://doi.org/10.1016/J.RSER.2018.09.026

Do Duong D (1998) Adsorption Analysis: Equilibria And Kinetics (With Cd Containing Computer Matlab Programs). World Scientific

European Commision (2016) Communication from the commission to the European parliament, the council, the European economic and social committee and the committee of the regions. Brussel

Fernandes MS, Brites GJVN, Costa JJ, et al (2016a) A thermal energy storage system provided with an adsorption module – Dynamic modeling and viability study. Energy Convers Manag 126:548–560. https://doi.org/10.1016/j.enconman.2016.08.032

Fernandes MS, Brites GJVN, Costa JJ, et al (2016b) Modeling and parametric analysis of an adsorber unit for thermal energy storage. Energy 102:83–94. https://doi.org/10.1016/j.energy.2016.02.014

Frazzica A, Füldner G, Sapienza A, et al (2014) Experimental and theoretical analysis of the kinetic performance of an adsorbent coating composition for use in adsorption chillers and heat pumps. Appl Therm Eng 73:1020–1029. https://doi.org/10.1016/j.applthermaleng.2014.09.004

Freni A, Bonaccorsi L, Calabrese L, et al (2015a) SAPO-34 coated adsorbent heat exchanger for adsorption chillers. Appl Therm Eng 82:1–7. https://doi.org/10.1016/j.applthermaleng.2015.02.052

Freni A, Dawoud B, Bonaccorsi L, et al (2015b) Characterization of zeolite-based coatings for adsorption heat pumps. Springer

Freni A, Maggio G, Sapienza A, et al (2016) Comparative analysis of promising adsorbent/adsorbate pairs for adsorptive heat pumping, air conditioning and refrigeration. Appl Therm Eng 104:85–95. https://doi.org/10.1016/j.applthermaleng.2016.05.036

Gnielinski V (1976) New Equations for Heat and Mass Transfer in Turbulent Pipe and Channel Flow. Int Chem Eng

Kowsari MM, Niazmand H, Tokarev MM (2017) Bed configuration effects on the finned flat-tube adsorption heat exchanger performance: Numerical modeling and experimental validation. Appl. Energy

Ng KC, Chua HT, Chung CY, et al (2001) Experimental investigation of the silica gel-water adsorption isotherm characteristics. Appl Therm Eng. https://doi.org/10.1016/S1359-4311(01)00039-4

Pesaran A, Lee H, Hwang Y, et al (2016) Review article: Numerical simulation of adsorption heat pumps. Energy 100:310–320

Petukhov BS (1970) Heat Transfer and Friction in Turbulent Pipe Flow with Variable Physical Properties. Adv Heat Transf. https://doi.org/10.1016/S0065-2717(08)70153-9

Pinheiro JM, Salústio S, Rocha JJ, et al (2016) Analysis of equilibrium and kinetic parameters of water adsorption heating systems for different porous metal/metalloid oxide adsorbents. Appl Therm Eng 100:215–226. https://doi.org/10.1016/j.applthermaleng.2016.01.142

Ramji HR, Leo SL, Abdullah MO (2014) Parametric study and simulation of a heat-driven adsorber for air conditioning system employing activated carbon-methanol working pair. Appl Energy 113:324–333. https://doi.org/10.1016/j.apenergy.2013.07.017

Restuccia G, Freni A, Maggio G (2002) A zeolite-coated bed for air conditioning adsorption systems: Parametric study of heat and mass transfer by dynamic simulation. In: Applied Thermal Engineering. pp 619–630

Rezk ARM, Al-Dadah RK (2012) Physical and operating conditions effects on silica gel/water adsorption chiller performance. Appl Energy 89:142–149. https://doi.org/10.1016/J.APENERGY.2010.11.021

Rivero-Pacho AM, Critoph RE, Metcalf SJ (2017) Modelling and development of a generator for a domestic gas-fired carbon-ammonia adsorption heat pump. Renew Energy 110:180–185. https://doi.org/10.1016/j.renene.2017.03.089

Sakoda A, Suzuki M (1984) Fundamental study on solar powered adsorption cooling system. J Chem Eng Japan 17:52–57. https://doi.org/10.1252/jcej.17.52

Sakoda A, Suzuki M (1986) Simultaneous transport of heat and adsorbate in closed type adsorption cooling system utilizing solar heat. J Sol Energy Eng Trans ASME. https://doi.org/10.1115/1.3268099

Sapienza A, Gullì G, Calabrese L, et al (2016) An innovative adsorptive chiller prototype based on 3 hybrid coated/granular adsorbers. Appl Energy 179:929–938. https://doi.org/10.1016/j.apenergy.2016.07.056

Sawin JL, Seyboth K, Sverrisson F (2017) Renewables 2017: Global status report

Sircar S (1983) Linear-driving-force model for non-isothermal gas adsorption kinetics. J Chem Soc Faraday Trans 1 Phys Chem Condens Phases 79:785. https://doi.org/10.1039/f19837900785

Sun B, Chakraborty A (2015) Thermodynamic frameworks of adsorption kinetics modeling: Dynamic water uptakes on silica gel for adsorption cooling applications. Energy. https://doi.org/10.1016/j.energy.2015.02.101

Tokarev MM, Gordeeva LG, Grekova AD, Aristov YI (2018) Adsorption cycle “heat from cold” for upgrading the ambient heat: The testing a lab-scale prototype with the composite sorbent CaClBr/silica. Appl Energy 211:136–145. https://doi.org/10.1016/j.apenergy.2017.11.015

Ulku S (1986) Adsorption heat pumps. J Heat Recover Syst 6:277–284. https://doi.org/10.1016/0198-7593(86)90113-X

Wang D, Zhang J, Yang Q, et al (2014) Study of adsorption characteristics in silica gel-water adsorption refrigeration. Appl Energy. https://doi.org/10.1016/j.apenergy.2013.08.011

Wilkes JO, Birmingham SG (2006) Fluid Mechanics for Chemical Engineers with Microfluidics and CFD. Pearson Education

Wittstadt U, Füldner G, Laurenz E, et al (2017) A novel adsorption module with fiber heat exchangers: Performance analysis based on driving temperature differences. Renew Energy 110:154–161. https://doi.org/10.1016/j.renene.2016.08.061

Wu JY, Li S (2009) Study on cyclic characteristics of silica gel–water adsorption cooling system driven by variable heat source. Energy 34:1955–1962. https://doi.org/10.1016/J.ENERGY.2009.08.003

Zhang LZ, Wang L (1997) Performance estimation of an adsorption cooling system for automobile waste heat recovery. Appl Therm Eng. https://doi.org/10.1016/S1359-4311(97)00039-2

Zhang LZ, Wang L (1999) Effects of coupled heat and mass transfers in adsorbent on the performance of a waste heat adsorption cooling unit. Appl Therm Eng 19:195–215. https://doi.org/10.1016/S1359-4311(98)00023-4

CHAPTER 4

This Chapter has been published as:

Dias JMS, Costa VAF (2021) Modeling and Analysis of a Coated Tube Adsorber for Adsorption Heat Pumps. Energies 14:6878. https://doi.org/https://doi.org/10.3390/en14216878

4. MODELING AND ANALYSIS OF A COATED TUBE ADSORBER FOR ADSORPTION HEAT PUMPS

Abstract

This work investigates the effects of several parameters on the coefficient of performance (COP) and the specific heating power (SHP) of a coated-tube adsorber for adsorption heat pumps (AHP) suitable for water heating (space and/or domestic water heating). The COP and SHP are obtained based on physical models that have already proven to adequately describe this type of adsorbers. Several parameters are tested namely, the regeneration, condenser and evaporator temperatures, the heat transfer fluid velocity, the tube diameter, the adsorbent coating thickness, the metal-adsorbent heat transfer coefficient, and the cycle time. Two different scenarios were tested, corresponding to distinct working conditions. The working conditions for Scenario A are suitable for pre-heating water in mild climates. Scenario B's working conditions are based on the European standard EN16147. The maximum COP is obtained for regeneration temperatures of 75 °C and 95 °C for Scenarios A and B, respectively. The COP increases for longer cycle times (more complete adsorption and desorption processes) whilst the SHP decreases (less complete cycles per unit time). Hence, the right balance between the COP and the SHP must be found for each particular scenario to have the best whole performance of the AHP. A metal-adsorbent heat transfer coefficient lower than 200 $W.m^{-2}.K^{-1}$ leads to reduced SHP. Lower adsorbent coating thicknesses lead to higher SHP and can still provide reasonably high COP. However, low coating thicknesses would require a too high number of tubes to achieve the desired adsorbent mass to deliver the required useful heating power, resulting in too large systems. Due to that, the best relation between the SHP and the size of the system must be selected for each specific application.

Keywords: Adsorption heat pump; adsorption heat; coated tube adsorber; coefficient of performance; specific heating power.

NOMENCLATURE

C	Specific heat (J.kg^{-1}.K^{-1})
C_p	Constant pressure specific heat (J.kg^{-1}.K^{-1})
d	Diameter (m)
D_{ef0}	Effective diffusivity coefficient (m^2.s^{-1})
E_a	Activation energy (J.kg^{-1})
H	Enthalpy (J)
$h_{f\rightarrow m}$	Fluid-metal heat transfer coefficient (W.K^{-1}.m^{-2})
$h_{m\rightarrow s}$	Adsorbent-metal heat transfer coefficient (W.K^{-1}.m^{-2})
k	Thermal conductivity (W.K^{-1}.m^{-1})
k_0	Pre-exponential coefficient (kg.kg^{-1}.Pa^{-1})
k_D	Blake-Kozeny coefficient (m^2)
K_{LDF}	LDF constant (s^{-1})
L	Tube length (m)
m	Mass (kg)
P	Pressure (Pa)
Q	Heat (J)
q_m	Monolayer capacity (kg.kg^{-1})
r	Radial coordinate (m)
R'	Steam particular gas constant (J.kg^{-1}K^{-1})
t	Time (s)
t_{SG}	Dimensionless Toth's constant (-)
T	Temperature (K)
u	Darcy's velocity (m.s^{-1})
u_f	Heat transfer fluid velocity (m.s^{-1})
X	Adsorbate concentration in the adsorbent (kg$_a$.kg$_s^{-1}$)
z	Axial coordinate (m)

Greek letters

ΔH_{ads}	Heat of adsorption (J.kg^{-1})
ε	Adsorbent bed porosity (-)
μ	Dynamic viscosity (Pa.s)
σ	Thickness (m)
τ	Cycle time (s)

Subscripts

a	Adsorbate
ads	Adsorption
bed	Adsorbent bed
c	Condenser /Cooling
cyc	Cycle
e	Evaporator
eq	Equilibrium
f	Fluid
h	Heating
ic	Isosteric cooling
ih	Isosteric heating
l	Liquid adsorbate
m	Metal
p	Particle
reg	Regeneration
s	Adsorbent
v	Vapor/Vaporization

4.1. INTRODUCTION

About 50% of Europe's total energy consumption is channelled for heating and cooling, much of it being inefficiently used (European Commision 2016). Over 35% of the overall energy consumption is directed to the building sector, from which 75% is used for space and domestic water heating (Pinheiro et al. 2016). Nowadays, much of this energy is still being wasted through inefficient processes and heat losses. In addition, only 18% of the total energy used for heating and cooling comes from renewables, 75% coming from fossil fuels burning and 7% from nuclear power plants (European Commision 2016). Furthermore, the residential sector accounts for 17% of global CO2 emissions (Kieft et al. 2021). Efforts must be made to increase the share of renewables for heating and cooling, contributing towards a sustainable and greener future. Considering the intermittent nature of renewable energy sources, energy storage technologies can improve the effectiveness of the use of renewables (Gaeini et al. 2018). Adsorption heat pumps (AHPs) can play a significant role towards the achievement of a green World. Unlike conventional vapor compression heat pumps (VCHPs) that use high global warming potential (GWP) fluids, AHPs can work with natural refrigerants like water or ammonia. Furthermore, contrarily to the VCHPs, which are electrically driven, AHPs may be driven directly by thermal energy such as waste or surplus heat (Zhang and Wang 1997; Ramji et al. 2014), renewable energy sources like solar energy (Sakoda and Suzuki 1984, 1986; Fernandes et al. 2016), or even with heat from natural gas (Dawoud 2014).

By 2016, combustible fuels (coal, oil, natural gas, biofuels, industrial and municipal waste, etc.) represented 67.3% of the total electricity production worldwide. Pressurized steam, generated from combustion heat, is used to drive an electric generator by spinning a steam turbine. Most power plants worldwide still use this system to produce electricity. A large amount of energy is wasted since only a fraction of the heat generated by burning the fuels is converted into electricity (Kaushik et al. 2011). This must be considered when comparing the coefficient of performance (COP) of AHPs and VCHPs. The significantly lower COP of AHPs is usually interpreted as a major disadvantage. However, for VCHPs the COP is obtained as the ratio between the thermal energy output (useful effect) and the electrical energy input required to drive the system. Thus, for comparison purposes, the fraction of energy that is lost in the above referred electricity generation process should also be considered as an energy consumption for VCHPs, for a fair comparison between these two technologies. Therefore, when this energy loss is accounted for the COP of

conventional VCHPs is significantly lower than what is commonly presented. Taking this into account, the lower COP of AHPs is not as lower as when usually compared with that of the VCHPs, and it should not be seen as such a high disadvantage. There are systems being developed that are addressing this handicap of VCHPs by using photovoltaic panels but the compressors are always electricity dependent (James et al. 2021; Mahmoudi et al. 2021).

Several advancements in AHPs technologies have recently been reported. Gluesenkamp et al. carried out an experimental study on the thermal mass of adsorption heat exchangers with several designs (Gluesenkamp et al. 2020). The combination of compression units with adsorption based systems is being considered, aiming to achieve a system that can integrate the best of each technology (Vasta et al. 2018). Different control methods for AHPs have been recently investigated through two different approaches (Robbins et al. 2020). One of the methods is to control the system based on the refrigerant concentration in the adsorbent bed. The second method is to consider the adsorbent bed temperature as the control variable. For source temperatures lower than the design value a 5-50% improvement in the overall COP is reported. Pan et al. investigated a cascaded cycle which integrates four adsorbers (Pan et al. 2018). This cycle resulted in an improved COP by increasing the refrigerant quantity that is adsorbed within each cycle. The performance improvements are more notorious for low heat source temperature, high heat sink temperature, and high evaporation temperature working conditions. Adsorption systems based on cascaded cycles are also being used for cooling applications (Aprile et al. 2020). Furthermore, adsorption systems are being tested not only for heating and cooling but also for desalination purposes (Sztekler 2021).

The interest on the implementation of adsorption systems as energy storage devices has been increasing over the last 5 years (Palomba et al. 2021). Adsorption systems can store heat in several forms. The adsorbent material can be regenerated when a heat source is available, keeping a potential to release heat of adsorption when required, simply by opening a valve. The latent heat captured in the evaporator from a free energy source during adsorption phase can also be released in the condenser during regeneration. Furthermore, sensible heat is stored as hot water inside an isolated reservoir.

This paper presents an analysis to a coated tube adsorber for AHPs suitable for space and water heating, and heat storage applications. The dependence of the system from various governing parameters like the evaporator’s and condenser’s temperature, cycle time, metal-adsorbent heat transfer coefficient, regeneration temperature metal tube

diameter, coating thickness and heat transfer fluid (HTF) velocity on the adsorber's performance is investigated and discussed for two sets of working conditions. The working conditions for Scenario A are suitable for pre-heating water in mild climates, whereas those for Scenario B are based on the European standard EN16147.. Understanding the dynamics of these systems will lead to better control strategies as well as effective integration with renewable energy sources.

Improving the overall performance of AHP systems requires detailed numerical models capable of identifying the optimal values for the several governing parameters, configurations, and designs. Computational power has been increasing, allowing the implementation of numerical models with higher detail level, both in the parameters considered, the space dimensions and resolution along each dimension, and time resolution, leading to improved accuracy. This paper makes use of a physical model that has proven to be highly accurate implemented on a coated tube adsorber for AHP to investigate the effect of the several governing parameters on the adsorber performance. This high level of detail if often used for materials studies, only accounting for small amounts of adsorbent. The use of detailed models on real scale applications is of major importance towards the achievement of improved and market ready AHP.

The research for new adsorbent materials with enhanced characteristics and new adsorber designs are important for further advancements in AHP technology and have recently been the focus of several studies (AL-Dadah et al. 2020; Pahinkar et al. 2020; Makhanya et al. 2021). On the other hand, system level studies involving models that deal with all the components of an AHP system are lacking in literature (Pesaran et al. 2016). Moreover, experimental studies reporting the properties and parameters with sufficient detail to allow the experimental validation of detailed models by other researchers for real scale applications cannot be found in the literature. Development of compact, affordable, and sustainable AHP systems is extremely important to increase the relevance of AHPs in the market. Therefore, a complete AHP system suitable for domestic water heating is proposed, what is a step forward on the literature related with adsorption heat pumps, usually dealing with some isolated components of the AHPs.

4.2. ADSORBER'S DESIGN

Several adsorber configurations and adsorbent packing techniques can be found in the literature, namely shell packing (Pinheiro et al. 2016), plate-finned, tube, finned tube, fin

plate, flat pipe, spiral plate and coated tube (Li et al. 2015). The adsorber configuration that promises the best performance for AHPs is the coated tube setup due to the improved adsorbent-metal tube wall heat transfer and the higher thermal conductivity of adsorbent coatings (Dias and Costa 2018). The major advantages of the coated tube configuration are the high adsorbent-metal heat transfer coefficient, the high adsorbent-metal surface area, and the compact size of the resulting construction, which results in higher heat exchanges between the HTF and the adsorbent material. Furthermore, it allows the inclusion of a greater adsorbent mass in a smaller volume, giving a higher energy storage density to the system. Therefore, the coated tube adsorber is the subject of this performance analysis.

As other adsorption applications, silica gel has been selected as adsorbent material and water as adsorbate (Chen et al. 2010). Given its availability, ease of handling and environmental friendship, the usage of water as adsorbate is straightforward. On the other hand, silica gel was chosen based on its low regeneration temperature (60-100 °C), market availability and relatively low cost. The use of an adsorbent material that could be regenerated at temperatures under 95 °C is mandatory since water is also used as HTF, limiting the regeneration temperature to guarantee that the HTF remains in its liquid state. Furthermore, silica gel has a significant water adsorption capacity under space and domestic water heating working conditions, and information on its thermophysical properties and adsorption kinetics is already available from the open literature (Ng et al. 2001b; Chua et al. 2002, 2004; Vodianitskaia et al. 2017).

The adsorber used in this study consists of a set of metal tubes with a coating of adsorbent material on their outer surfaces. The RD2060 silica gel type from Fuji Silysia Chemical LTD is considered. It is mixed with a binder and then layered on the outer metal tubes' surfaces until obtaining the desired thickness. The effect of the binder is accounted for by adjusting the heat and mass transfer coefficients, based on values reported in the literature for such coatings. The silica gel mixing with a binder to form an external coating on the metal tubes improves the metal-adsorbent heat transfer coefficient and the coating thermal conductivity. On the other hand, the mass transfer resistance is increased by mixing the silica gel with the binder. However, since the coating thickness is small, mixing the adsorbent with the binder will have more benefits than hindrances on the system's performance (Frazzica et al. 2014). An air thermal treatment is applied to dry and stabilize the so obtained coating. The so coated tubes are enclosed into a cylindrical metal structure and connected to two metal joints, which seal them up in a vacuum chamber. The joints connect the interior of the tubes to the HTF's circuit, enabling it to flow through the inside of

the metal tubes. The vacuum chamber is alternately connected to an evaporator and a condenser during the adsorption and regeneration phases, respectively. A schematic of the aforementioned adsorber and the ideal thermodynamic cycle of the AHP are represented in Figure 4.1. Not all the tubes are represented in order to keep the schematics clearer, and more compact and perceptible.

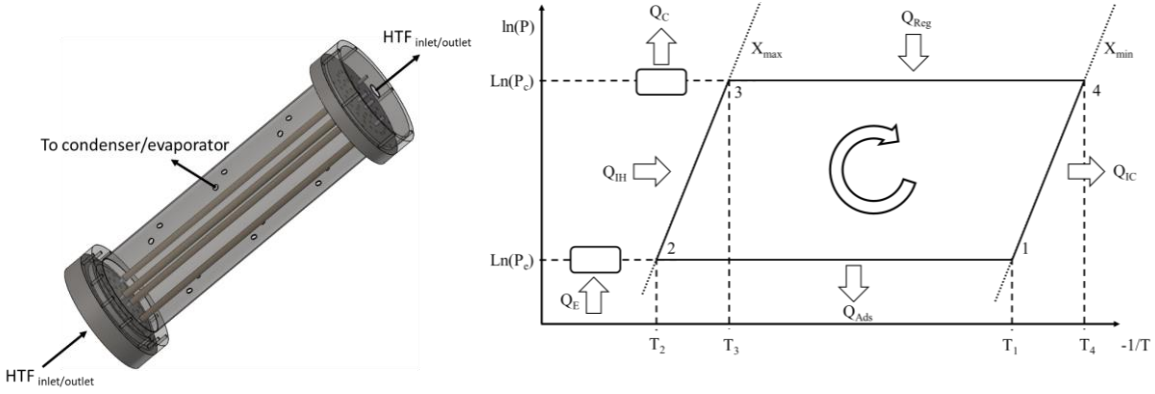

Figure 4.1 – a) Coated tube adsorber schematics. **b)** Ideal thermodynamic cycle of the AHP (Adapted from (Dias and Costa 2018) with permission from Elsevier).

Figure 4.2 depicts the adsorber without the top lid, showing its core construction. Table 4.1 reports some important dimensions of the coated tube adsorber, giving an idea of its size.

Table 4.1 – Dimensions of the coated tube adsorber.

Important dimensions	Value (mm)
Cylindrical structure inner diameter	290
Cylindrical structure length	980
Cylindrical structure thickness	3
Joint thickness	30
Joint diameter	363
Coated metal tube inner diameter	10
Coated metal tube length	1180
Coating length	1000
Coated metal tube thickness	1
Adsorbent coating thickness	2
Adsorbent coating length	1000
Adsorber height	1226

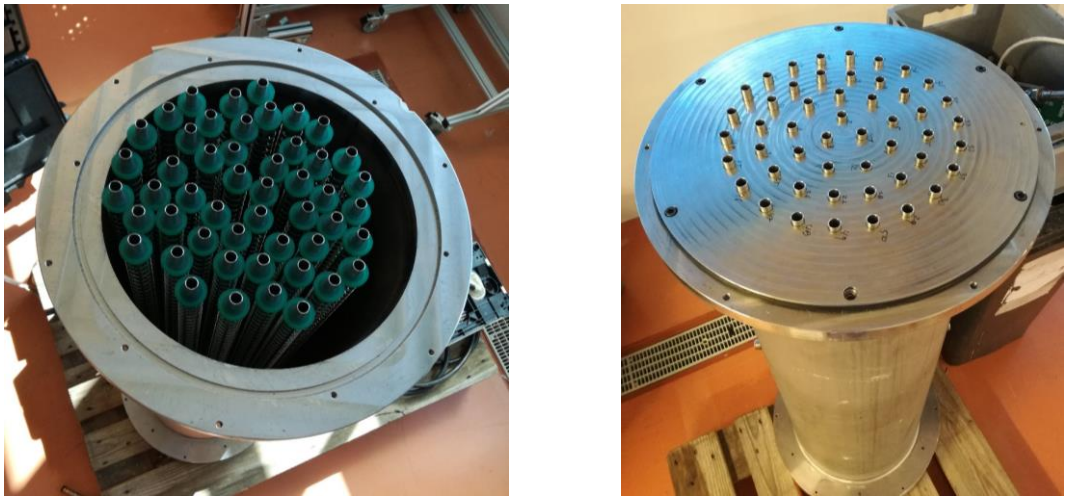

Figure 4.2 – The AHP coated tube adsorber, without the sealing metal joint (left) and with the sealing metal joint (right).

4.3. PHYSICAL MODEL

The adsorber's dynamics are described by a distributed parameter model that considers two dimensions, which is extensively described in (Dias and Costa 2019). The

physical model has already been used for adsorption cooling applications (Dias and Costa 2020). The model resorts on the energy and mass conservation equations considering the developed adsorber, which give, respectively,

$$\frac{\partial(\rho C_p T_s)}{\partial t} + \nabla\left(\rho_v C_{p,v} T_s u\right) - \nabla(k_s \nabla T_s) - \rho_s(1-\varepsilon)\Delta H_{ads}\frac{\partial X}{\partial t} = 0 \quad (4.1)$$

$$\varepsilon\frac{\partial \rho_v}{\partial t} + \nabla(\rho_v u) + \rho_s(1-\varepsilon)\frac{\partial X}{\partial t} = 0 \quad (4.2)$$

where

$$\rho C_p = \varepsilon\rho_v C_{p,v} + \rho_s(1-\varepsilon)\left(C_s + X C_{p,a}\right) \quad (4.3)$$

and

$$\varepsilon = \varepsilon_{bed} + (1-\varepsilon_{bed})\varepsilon_p \quad (4.4)$$

Darcy's Law,:

$$u = -\frac{k_D}{\mu}\nabla P \quad (4.5)$$

is used to describe the momentum balance, the Blake-Kozeny model, giving the adsorbent bed permeability (Wilkes and Birmingham 2006),

$$k_D = \frac{d_p^2 \varepsilon_{bed}^3}{150(1-\varepsilon_{bed})^2} \quad (4.6)$$

The evolution of the concentration of adsorbate in the adsorbent material is obtained through the linear driving force (LDF) model (Sircar 1983)

$$\frac{dX}{dt} = K_{LDF}\left(X_{eq} - X\right) \tag{4.7}$$

where K_{LDF} coefficient is obtained as

$$K_{LDF} = \frac{15 D_{ef0} e^{-\frac{E_a}{R' T_s}}}{R_p^2} \tag{4.8}$$

By its own turn, the equilibrium adsorbate concentration in the adsorbent, X_{eq}, for the silica gel RD-water working pair is obtained as

$$X_{eq} = \frac{P k_0 e^{\frac{\Delta H_{ads}}{R' T_s}}}{\left[1 + \left(\frac{P k_0}{q_m} e^{\frac{\Delta H_{ads}}{R' T_s}}\right)^{t_{SG}}\right]^{\frac{1}{t_{SG}}}} \tag{4.9}$$

The following main assumptions, which have already been used in previous studies, are considered in the model (Dias and Costa 2020):

- Adsorbent bed is homogenous;
- The evaporator and the condenser are ideal heat exchangers with uniform pressures;
- Adsorbate vapor phase behaves as an ideal gas and the adsorbed phase is considered to be liquid;
- Specific heats of the adsorbate vapor and liquid phases are constants;
- Adsorbate vapor around the adsorbent is saturated vapor;
- Thermophysical properties of solid materials do not change with temperature;
- Temperature, adsorbent content and pressure in the adsorbent bed do not change along the angular direction;

Considering these assumptions, the energy and mass conservation equations can be rearranged:

$$\begin{aligned}\left[\rho_s(1-\varepsilon)(C_s+XC_l)+\varepsilon\rho_v C_{p_v}\right]\frac{dT_s}{dt} = \\ =(1-\varepsilon)\rho_s\Delta H_{ads}\frac{dX}{dt}+\frac{k_s}{r}\left(\frac{\partial T_s}{\partial r}+r\frac{\partial^2 T_s}{\partial r^2}\right) \\ -\frac{C_{p_v}}{r}\left(\rho_v T_s u_r + rT_s u_r\frac{\partial\rho_v}{\partial r}+r\rho_v u_r\frac{\partial T_s}{\partial r}+r\rho_v T_s\frac{\partial u_r}{\partial r}\right) \\ -C_{p_v}\left(T_s u_z\frac{\partial\rho_v}{\partial z}+\rho_v T_s\frac{\partial u_z}{\partial z}+\rho_v u_z\frac{\partial T_s}{\partial z}\right)+k_s\left(\frac{\partial^2 T_s}{\partial z^2}\right)\end{aligned} \quad 4.10$$

$$\frac{\partial\rho_v}{\partial t}=-\frac{1}{\varepsilon}\left[\rho_s(1-\varepsilon)\frac{\partial X}{\partial t}+\frac{1}{r}\left(ru_r\frac{\partial\rho_v}{\partial r}+\rho_v r\frac{\partial u_r}{\partial r}+\rho_v u_r\right)+\rho_v\frac{\partial u_z}{\partial z}+u_z\frac{\partial\rho_v}{\partial z}\right] \quad 4.11$$

Given that $r_{tube} \ll L_{tube}$, the variation of the HTF temperature along the radial direction is neglected, $\frac{\partial T_f}{\partial r} \approx 0$. Considering that the HTF velocity is constant, the energy balance for the HTF is expressed as:

$$\rho_f C_{p,f}\frac{\partial T_f}{\partial t}=k_f\left(\frac{\partial^2 T_f}{\partial z^2}\right)-u_f\rho_f C_{p,f}\frac{\partial T_f}{\partial z}+\frac{4h_{f\to m}}{d_{in}}\left(T_m-T_f\right) \quad 4.12$$

Since the metal tubes have high thermal conductivity and their thickness is small, their temperature is assumed constant along the radial direction, $\frac{\partial T_m}{\partial r} \approx 0$. Thus, the energy balance equation for the metal tube is:

$$\rho_m C_m\frac{dT_m}{dt}=k_m\left(\frac{\partial^2 T_m}{\partial z^2}\right)+\frac{4d_{in}h_{f\to m}\left(T_f-T_m\right)}{d_{out}^2-d_{in}^2}+\frac{4d_{out}h_{m\to s}(T_s-T_m)}{d_{out}^2-d_{in}^2} \quad 4.13$$

By using the method of lines, discretizing the partial derivatives in the axial and radial coordinates through finite difference methods, the set of partial differential equations is transformed in a set of ordinary differential equations. The resultant set of ordinary differential equations is solved using a solver suitable for stiff systems, ode15s, from Matlab R2020b (Shampine and Reichelt 1997). To obtain the solution for the ordinary differential equations, the following set of initial and boundary conditions were considered.

$$t_{ini} = 0 \qquad P(t_{ini}) = P_{ini}$$

$$T_m(t_{ini}) = T_f(t_{ini}) = T_s(t_{ini}) = T_{ini} \qquad X(t_{ini}) = X_{eq}\left(P_{ini}, T_{s\,ini}\right)$$

$$\left.\frac{\partial P}{\partial r}\right|_{r=in} = 0$$

$$P|_{r=r_{out}} = P|_{z=0} = P|_{z=L} = P_e, \qquad Adsorption$$

$$P|_{r=r_{out}} = P|_{z=0} = P|_{z=L} = P_c, \qquad Regeneration$$

$$\left.\frac{\partial P}{\partial r}\right|_{r=r_{out}} = \left.\frac{\partial P}{\partial r}\right|_{z=0} = \left.\frac{\partial P}{\partial r}\right|_{z=L} = 0, \qquad Cooling/Heating$$

$$-k_s \left.\frac{\partial T_s}{\partial r}\right|_{r=r_{in}} = h_{m\to s}(T_m - T_s)$$

$$\left.\frac{\partial T_s}{\partial r}\right|_{r=r_{out}} = \left.\frac{\partial T_s}{\partial z}\right|_{z=0} = \left.\frac{\partial T_s}{\partial z}\right|_{z=L} = 0$$

$$T_f\big|_{z=0} = T_{ads}\,, \qquad Adsorption/Cooling$$

$$T_f\big|_{z=0} = T_{reg}\,, \qquad Regeneration/Heating$$

$$\left.\frac{\partial T_f}{\partial z}\right|_{z=L} = 0$$

$$\left.\frac{\partial T_m}{\partial z}\right|_{z=0} = \left.\frac{\partial T_m}{\partial z}\right|_{z=L} = 0$$

The adsorber's performance is assessed through the evaluation of the COP and the SHP, evaluated respectively as:

$$COP = \frac{Q_c + Q_{ic} + Q_{ads}}{Q_{ih} + Q_{reg}}, \quad 4.14$$

$$SHP = \frac{Q_c + Q_{ic} + Q_{ads}}{m_s \tau_{cyc}}, \quad 4.15$$

where the adsorption, pre-heating, regeneration and pre-cooling heats are calculated using the equations below, where the integration temperatures are those of the AHP's thermodynamic cycle (Figure 4.1 b) (Dias and Costa 2018)

$$-Q_{ads} \approx \int_{T_1}^{T_2} \left[m_s\left(C_s + XC_{p,a}\right) + m_m C_m\right] dT - \int_{X_{min}}^{X_{max}} m_s \Delta H_{ads} dX \quad 4.16$$

$$Q_{ih} \approx \int_{T_2}^{T_3} \left[m_s\left(C_s + X_{max} C_{p,a}\right) + m_m C_m\right] dT \quad 4.17$$

$$Q_{reg} \approx \int_{T_3}^{T_4} \left[m_s\left(C_s + XC_{p,a}\right) + m_m C_m\right] dT - \int_{X_{max}}^{X_{min}} m_s \Delta H_{ads} dX \quad 4.18$$

$$-Q_{ic} \approx \int_{T_4}^{T_1} \left[m_s\left(C_s + X_{min} C_{p,a}\right) + m_m C_m\right] dT \quad 4.19$$

$$Q_c = m_s \Delta X \Delta H_v \quad 4.20$$

4.4. RESULTS AND DISCUSSION

The analysis on the effect of the evaporator's and condenser's temperature, cycle time, metal-adsorbent heat transfer coefficient, regeneration temperature, metal tube diameter, coating thickness and heat transfer fluid (HTF) velocity on the COP and SHP of the adsorber is presented. A series of reference parameters consistent with space and domestic water heating operating conditions was selected, which are summarized in Table 4.2. Some properties were obtained from detailed material studies available in the open literature (Ng et al. 2001a; Chua et al. 2002; Di et al. 2007; Chakraborty et al. 2014; Sun and Chakraborty 2015). All parameters assume their reference value except for the one being studied, which

will be varied within a reasonable range. The analysis was carried out for two different operating conditions which translates into different heat sources and heat sinks temperatures. Scenario A corresponds to pre-heating water in mild climates, the evaporator and condenser temperatures being set to T_e = 12 °C and T_c = 30 °C, respectively. For Scenario B, the working conditions were based on the European standard EN16147, which sets the testing and requirements for domestic hot water units. This standard applies to common (whole system) heat pumps. Since this work focuses on the adsorber, the working conditions have been adapted to allow its analysis. The temperature for the evaporator has been selected according to EN16147, considering an outside air unit at the mean temperature of 7 °C. The condenser temperature is set to 40 °C, which is considered as the reference hot water supply temperature in EN16147. Comparing the results obtained in this study to others available in literature could not be carried out in detail given that no similar application with sufficient details on all the parameters and coefficients could be found. In general, the COP values are in line with the values reported in the literature for silica gel-water working pair under the reference temperatures. As for the specific heating power, it can be fine-tuned by changing the heat and mass transfer coefficients, cycle times, and phase change timings. These are the details that are not completely reported in the literature, preventing the authors from performing a useful and fair comparison.

Table 4.2 – Reference values for the parameters and thermophysical properties used in the simulations.

Parameter	Value	Unit
C_m	910	J.kg^{-1}.K^{-1}
C_s	921	J.kg^{-1}.K^{-1}
d_p	3.5×10^{-4}	m
$d_{in,tube}$	0.01	m
E_a	2.3314×10^{6}	J.kg^{-1}
$h_{m \to s}$	200	W.m^{-2}.K^{-1}
k_0	7.3×10^{-13}	kg.kg^{-1}.Pa^{-1}
k_f	0.6	W.m^{-1}.K^{-1}
k_m	205	W.m^{-1}.K^{-1}
k_s	0.198	W.m^{-1}.K^{-1}
L_{tube}	1	m
ΔH_v	2.3×10^{6}	J.kg^{-1}
q_m	0.45	kg.kg^{-1}
t_{ads}	1500	s
$T_{f,ads}$	$273.15 + 30$	K
$T_{f,reg}$	$273.15 + 90$	K
t_{reg}	$0.91 \times t_{ads}$	s
t_{SG}	12	-
v_{HTF}	0.05	m.s^{-1}
ΔH_{ads}	2.693×10^{6}	J.kg^{-1}
ε	0.4	-
ρ_m	2700	kg.m^{-3}
ρ_s	2027	kg.m^{-3}
σ_s	0.002	m
σ_{tube}	0.001	m

4.4.1. Influence of the evaporator temperature

During the adsorption phase, the pressure inside the system is determined by the evaporator temperature, which has thus a significant influence on the adsorber's performance. Figure 4.3 represents the impact of the evaporator temperature on the COP and SHP within the 0-30 °C temperature range. As well-known from Thermodynamics, the COP of a heat pump increases for higher evaporator temperatures. Low evaporator temperatures are associated with lower pressures in the adsorber during the adsorption phase, which reduces the adsorbing capacity and leads to low adsorbate flows. In addition, for lower pressures the adsorption process is slower; thus, for the same cycle time, the

amount of adsorbate that flows from the evaporator to the adsorber is significantly reduced. Notwithstanding the performance for Scenario B is lower, which was expected from Thermodynamics, the influence of the evaporator temperature is similar for Scenarios A and B. For low evaporator temperatures (<5 °C) it might happen that the temperature of the HTF is not sufficiently low to reduce the adsorber's pressure to the level of the evaporator's pressure. In this case, the adsorbate cannot flow from the evaporator to the adsorber and the AHP can no longer work properly, resulting in a null heat pumping from the ambient to the hot water storage tank.

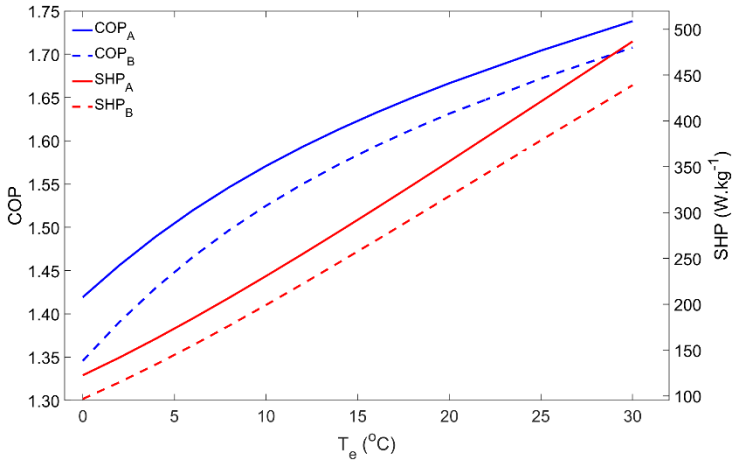

Figure 4.3 – Effect of the evaporator temperature on the adsorber performance for scenarios A and B.

4.4.2. Influence of the condenser temperature

For domestic water heating applications, the condenser temperature is usually the temperature of the water inside the hot water storage tank. Thus, the condenser temperature was varied from 15 °C up to 70 °C and the results are reproduced in Figure 4.4. Until approximately 40 °C for Scenario A and 30 °C for Scenario B, the COP and SHP slightly decrease with the condenser temperature. However, in both cases, for higher condenser temperatures the adsorber's performance greatly decreases and becomes very low when the water reaches its maximum temperature. The condenser temperature determines the pressure of the regeneration phase. The higher the pressure the more time is required to raise the adsorber's pressure from the evaporator pressure level up to the condenser pressure level, which along with the slower adsorption kinetics for higher pressures causes the SHP to fall down. On the other hand, for the same regeneration

temperature, an increase on the pressure in the adsorber during the regeneration phase means that less adsorbate is desorbed, reducing the adsorbate flow in each cycle, which results on a lower COP. In an extreme scenario, the pressure in the condenser can be so high that the available regeneration temperature is not high enough to raise the adsorber's pressure to that of the condenser, becoming impossible to regenerate the adsorbent material, and properly operate the AHP. This issue was confirmed in Scenario B for condenser temperatures above 60 °C, when the highest temperature of the HTF during the regeneration phase is not able to increase the pressure in the adsorber to match the condenser's pressure, resulting in an operating failure.

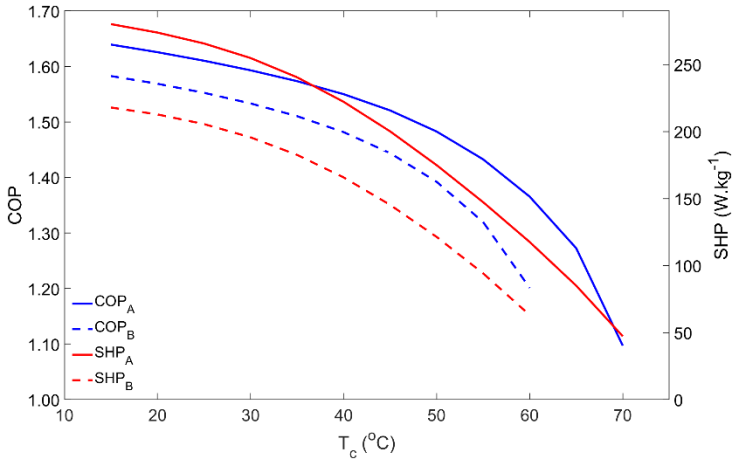

Figure 4.4 – Influence of the condenser temperature on the adsorber performance for scenarios A and B.

4.4.3. Influence of the regeneration temperature

The dependence of the adsorber's performance on the regeneration temperature is represented in Figure 4.5. Regeneration temperatures in the range of 70 °C to 130 °C were investigated. For Scenario A, COP reaches its maximum using regeneration temperatures around 75 °C and then it slightly decreases. For the silica gel-water working pair, it is not worth to use regeneration temperatures above 75 °C if the objective is to maximize the output/input energy ratio. Nonetheless, using higher temperatures can be interesting since the SHP is increased due to the higher heat transfer rates (and faster heat transfer process) between the adsorbent material and the HTF. Using a higher regeneration temperature can reduce the size of the AHP system, while providing the same heating power with only a slight penalty on its COP. Meanwhile, increasing the regeneration temperature beyond the

vaporization point of the HTF will require safety valves and a pressurized system to keep the HTF in the liquid phase in order to maintain high heat transfer rates. Concerning the Scenario B, the maximum COP occurs for regeneration temperatures of approximately 95 °C, significantly decreasing for lower temperatures due to the higher pressure that is required during regeneration, which is associated to the higher condenser temperature when comparing with Scenario A. Despite its lower values, SHP under the working conditions considered in Scenario B shows a similar behavior as in Scenario A.

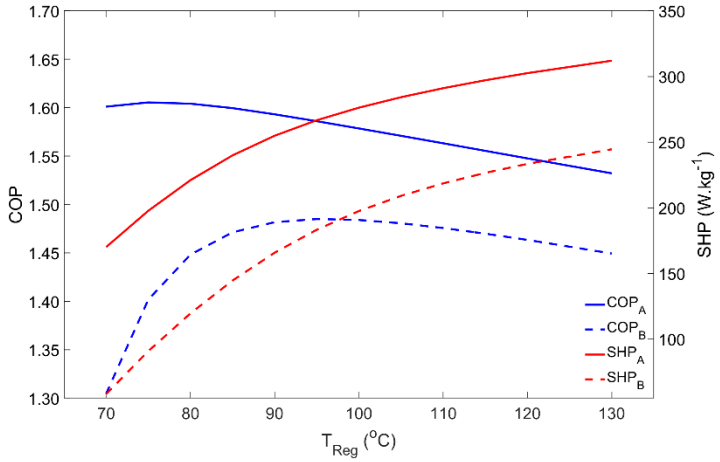

Figure 4.5 – Adsorber performance as a function of the regeneration temperature for scenarios A and B.

4.4.4. Influence of the cycle time

The cycle time is a key parameter since it allows the control and tuning of an AHP system. Moreover, as it is shown in Figure 4.6, the COP and SHP have opposite behaviors when the cycle time is changed. In both Scenarios A and B, for low cycle times the COP is minimal whilst the SHP is the highest (apart the small increase for very short cycle times that do not allow the proper transition between the four phases of the adsorption cycle). Increasing the cycle time results on higher COP until saturation occurs for cycle times nearly above 40 min, meaning that the adsorbent is adsorbing the maximum amount of adsorbate for the given operating conditions, leading to the maximum adsorbate flow within each cycle. On the other hand, when the cycle time increases the SHP decreases, since the extra energy that is obtained by running longer (and more complete) cycles does not compensate for the increase on the cycle duration. Thus, a balance between the COP and the SHP must be found for the best AHP performance, which may be different for each application.

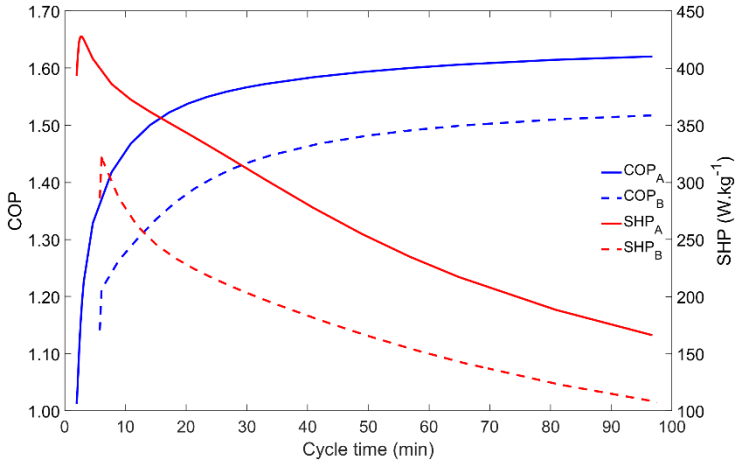

Figure 4.6 – Influence of the cycle time on the adsorber performance for scenarios A and B.

4.4.5. Influence of the metal-adsorbent heat transfer coefficient

The metal-adsorbent heat transfer coefficient is a measure of the heat exchange effectiveness between the metal tube outer surface and the inner layer of adsorbent material coating the external surface of the adsorber's tubes. Increased values of this parameter is one of the main reasons for using the coated tube setup. In addition, applying a thermal binder in the metal-adsorbent interface leads to increased values this parameter. Figure 4.7 represents the impact of changing the metal-adsorbent heat transfer coefficient from 25 $W.m^{-2}.K^{-1}$ up to 600 $W.m^{-2}.K^{-1}$ on the adsorber's performance for Scenarios A and B. Since a long cycle time was selected, based on a long adsorption time (t_{ads} in Table 4.1), even low values of the metal-adsorbent heat transfer coefficient are enough to allow the achievement of approximately the maximum adsorption capacity, which results on insignificant impact on the COP. Nonetheless, the influence of this parameter on the COP is more pronounced under the Scenario B conditions, due to the higher difference between the evaporator and condenser temperatures. However, since this heat transfer coefficient greatly conditions the rate of heat exchange between the HTF and the adsorbent material, the SHP greatly increases until the metal-adsorbent heat transfer coefficient attains approximately 200 $W.m^{-2}.K^{-1}$, and only slightly increases for $h_{m\to s}$ in the 200 to 350 $W.m^{-2}.K^{-1}$ range. Further increasing $h_{m\to s}$ does not have significant impact on the adsorber's performance since the adsorption kinetics becomes the limiting factor instead of the metal-adsorbent heat transfer coefficient. Apart from the inherent reduced performance under Scenario B conditions, there are no significant differences on the adsorber dynamics when operating under the different working conditions.

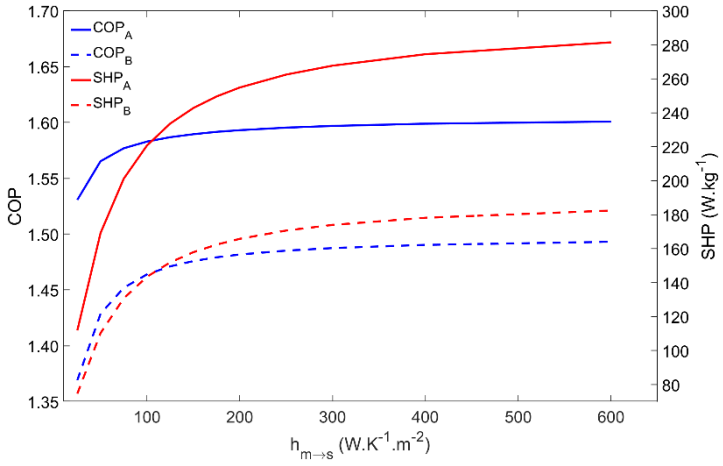

Figure 4.7 – COP and SHP as function of the metal-adsorbent heat transfer coefficient for scenarios A and B.

4.4.6. Influence of the adsorbent coating thickness

Besides influencing the COP and SHP, the adsorbent coating thickness also changes the mass of adsorbent material that externally covers each tube. The influence of the adsorbent coating thickness on the performance of the adsorber is represented in Figure 4.8. The COP is maximum for coating thicknesses in the 1.5-2-mm range, whereas the SHP decreases when increasing the coating thickness. Apart from the inherent performance reduction, the adsorber dynamics is similar under the Scenarios A and B conditions. Considering these performance indicators, there is no advantage in increasing the adsorbent coating thickness over 2 mm. Nonetheless, increasing the adsorbent thickness increases the mass of adsorbent that externally covers each tube, which results on higher heating power, leading to a more compact adsorber but with a lower energy efficiency. Depending on the AHP system's requirements, the adsorbent thickness can be adjusted in order to result on higher SHP, providing more heating power per unit mass of adsorbent, or to achieve higher energy efficiency by increasing the COP. However, one must be prudent not to reduce the thickness too much, since it will result on a tiny mass of adsorbent per tube, requiring a huge, and maybe unrealistic, number of tubes to satisfy the necessary heating power.

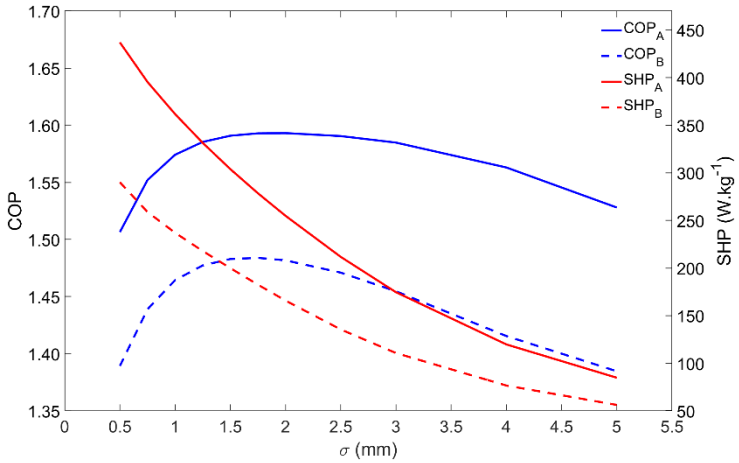

Figure 4.8 – Effect of the adsorbent coating thickness on the adsorber performance for scenarios A and B.

4.4.7. Influence of the tube diameter

Similar to the metal-adsorbent heat transfer coefficient, the metal tube's inner diameter also affects other parameters. The heat transfer between the HTF and the metal tube, and also between the metal tube and the adsorbent material, is directly affected by the heat transfer areas, being thus affected by the metal tube's diameter. Once the HTF's velocity is set, the HTF's mass flow rate increases as increases the tube's diameter. The adsorbent mass that externally covers each tube also increases as the tube's diameter increases. The influence of the tube diameter on the adsorber performance is represented in Figure 4.9. There are no evident differences on the adsorber dynamics when comparing the two tested Scenarios A and B. The most noticeable aspect is the performance increase that occurs when increasing the tube's diameter from 35 mm to 40 mm. This behavior is due to the change on the HTF flow conditions in the tube from laminar to turbulent, which highly increases the heat transfer rate between the HTF and the inner surface of the metal tube. Even though the variations on the COP are not significant, the SHP has a maximum value for a diameter of 10 mm, while under laminar flow conditions, which results from the optimal combination of the HTF's mass flow rate and the adsorbent mass. For turbulent flow conditions, since the HTF mass flow rate is more than enough to provide/withdraw heat from the adsorber due to the more effective (and faster) heat exchange between the HTF and the metal tube, the SHP is higher. Increasing the tube's diameter above 40 mm causes no significant impact on the performance of the adsorber. Although these results suggest the use of higher tube diameters, it might not be the best option since higher diameters lead

to large adsorbers containing low adsorbent mass, most of its volume being filled with the HTF.

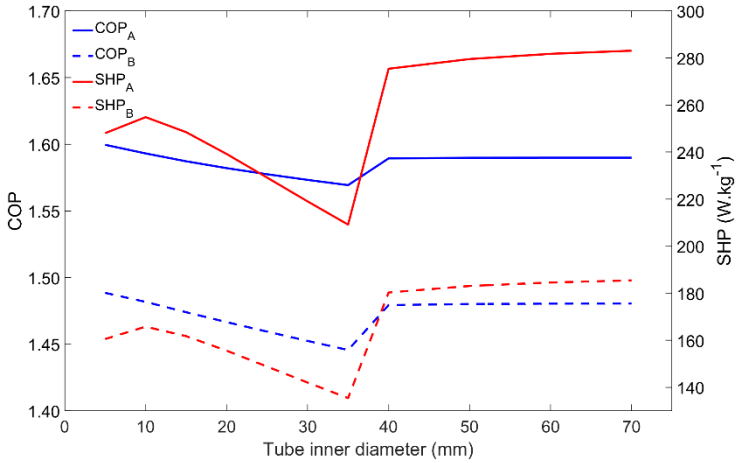

Figure 4.9 – Impact of the inner tube's diameter on the adsorber performance for scenarios A and B.

4.4.8. Influence of the heat transfer fluid velocity

The last parameter to be analyzed is the HTF's velocity, results being depicted in Figure 4.10. The adsorber behavior is coincident for both Scenarios A and B. For the simulated conditions, the COP is not significantly affected by the HTF's velocity since the adsorption and regeneration temperatures can always be achieved. However, the quickness of the process is highly affected, what is confirmed by the increase on the SHP with the HTF's velocity. The SHP highly increases for HTF velocities within 0.005 $m.s^{-1}$ and 0.02 $m.s^{-1}$, slightly increases for HTF velocities from 0.02 $m.s^{-1}$ to 0.04 $m.s^{-1}$, and above that it does not show significant increases. For higher HTF's velocities, the adsorption kinetics becomes the dominant mechanism and further increasing the HTF velocity has no useful effect.

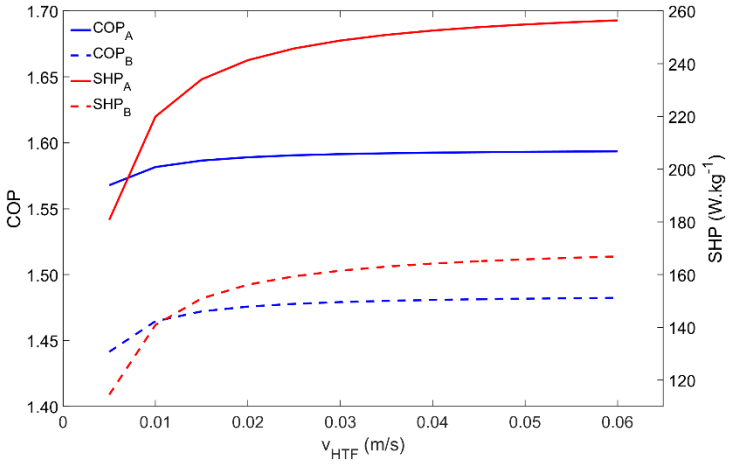

Figure 4.10 – Influence of the heat transfer fluid's velocity on the adsorber performance for scenarios A and B.

4.5. ADSORPTION HEAT PUMP SYSTEM

The design of an AHP system suitable for space and domestic water heating is proposed, which contains the coated tube adsorber described and studied above and also the following main components: evaporator, condenser, heating element, water reservoir, expansion valve, centrifugal pump and the control valves. Condenser is placed inside the hot water reservoir, in this particular case the heating element is a natural gas burner; however, any other heating element can be used under the condition that heat is provided at a temperature above the regeneration temperature. The AHP system is represented in Figure 4.11 and Figure 4.12 during the adsorption and regeneration phases, respectively. The adsorbate flow is represented by green arrows, and the HTF (water) flow is represented by orange arrows. During the adsorption phase, the adsorbate flows from the evaporator to the adsorber. Cold water is taken from the bottom of the reservoir, circulated through the adsorber's tubes to be heated and returned back to the top of the reservoir, transferring the adsorption heat from the adsorber to the water reservoir. During the regeneration phase, valves V_1 and V_2 are closed, valves V_3 and V_4 are opened, and the three-way valve shifts the flow from the reservoir towards valve V_3. The water flows from the adsorber to the gas burner, which is switched on, and back through the adsorber as hot HTF, providing heat to regenerate the adsorbent. At the end of the regeneration phase, the remaining circulating hot water is delivered to the top of the water reservoir. The supply water enters the reservoir

at its bottom and the hot water is withdrawn from the top, where its temperature is higher, taking advantage of the thermal stratification effect.

The proposed AHP system resorts on a gas burner as high temperature heat source. The gas-heated water can be used to regenerate the adsorbent or to be directly discharged into the hot water reservoir, depending on the temperature of the water in the reservoir. When the AHP effect is used to heat the water in the reservoir, the proposed heat pump system has the advantage of using the low temperature heat received for free from the ambient in addition to the heat received from the heating element. Another feature of the proposed system is that it can work as a direct gas water heater to provide hot water faster, when a high or unpredicted hot water demand occurs, in this case without taking advantage of the heat pumping effect. The hot water leaving the reservoir can then be distributed through space heating circuits or be used as domestic hot water.

The development of a model that considers all components of the AHP system, describing the entire system's dynamics, will allow to obtain the whole system's performance. The adsorber's performance when integrated in a real AHP system will probably be different than when considering constant temperature and pressure in the evaporator and in the condenser during each of the different phases within each cycle. Additionally, in a real system the adsorption and regeneration temperatures within each cycle are also changing. In the future, efforts will be made to develop a model capable of predicting the COP and SHP of the complete AHP system.

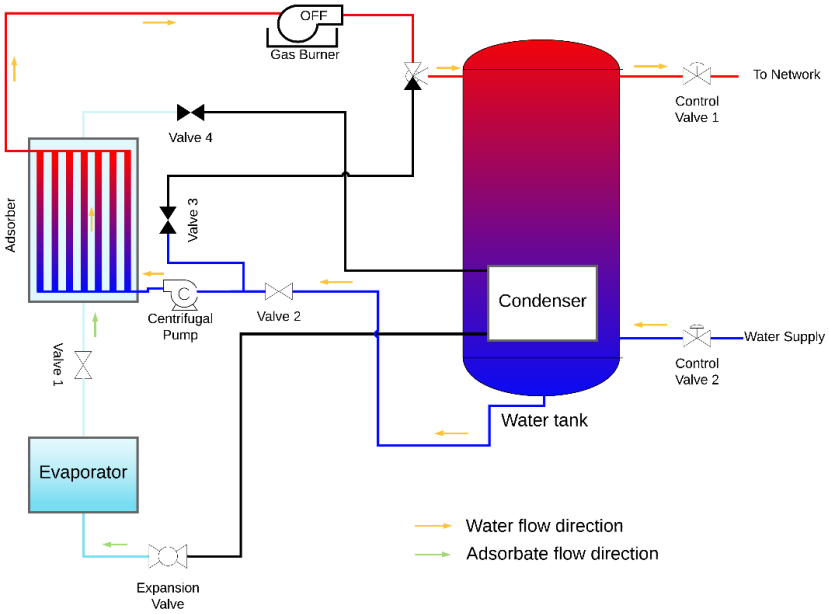

Figure 4.11 – AHP system during the adsorption phase.

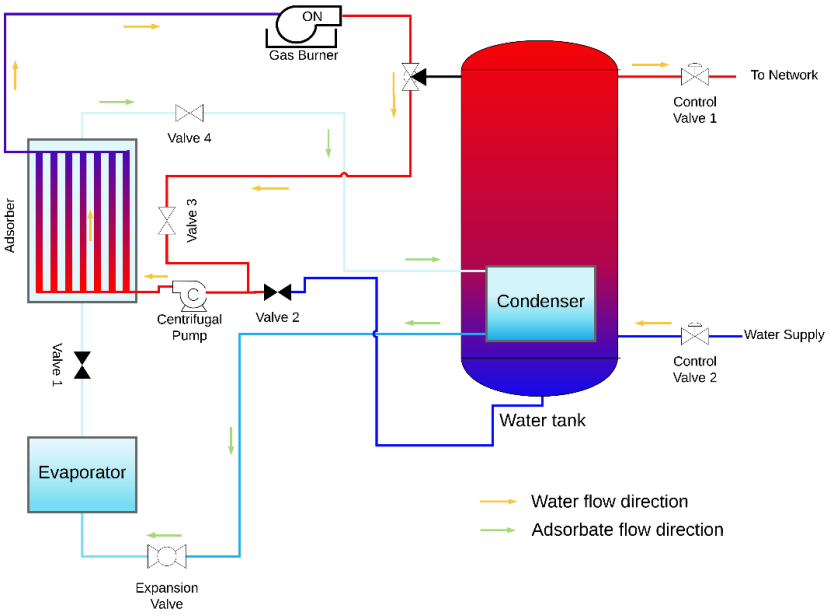

Figure 4.12 – AHP system during the regeneration phase.

The developed system can also be operated in a heat storage mode. When operated in subsequent cycles, the AHP is continuously storing sensible heat in the water reservoir. In many countries worldwide, the price for electricity or natural gas varies for different hours during the day, being cheaper during the hours with lower energy demand and more

expensive during the peaks of daily energy consumption. An effective way to reduce the energy cost of households is to use energy during low demand periods. The proposed system can be regenerated during these periods, releasing condensation heat that is stored in the water reservoir, closing valve V_4 when the adsorbent material is fully regenerated, keeping the system on halt and ready to later release heat of adsorption. When hot water is demanded during high energy price periods, the system can begin the adsorption phase by opening the valve V_1 and provide heat that was stored during cheaper periods. During adsorption, latent heat is captured in the evaporator and stored in the adsorbent bed, being released in the when the subsequent regeneration phase is started. This strategy of integrating adsorption technologies with the common instant heating devices is an effective way of reducing the energy costs of households.

4.6. CONCLUSIONS

Several governing parameters of a coated tube adsorber for an AHP suitable for space and domestic water heating were analyzed under different sets of working conditions. Results show that high evaporator temperatures and low condenser temperatures lead to better performances, which was already expected considering the Thermodynamic lessons. However, kinetics of the adsorption process and the heat transfer between the heat transfer fluid and the adsorbent material need to be considered, as the AHP operates out of the equilibrium conditions considered in those Thermodynamics lessons. For all parameters investigated, the adsorber performs worse under the working conditions of Scenario B working conditions, which could be foreseen by a thermodynamic evaluation due to the increased evaporator-condenser temperature difference between the evaporator and con-denser. The adsorber's dynamics are consistent among the two tested Scenarios for all parameters, except for the regeneration and condenser temperatures. The adsorber cannot operate for condenser temperatures above 70 °C and 60 °C, respectively for Scenarios A and B, respectively, since the pressure inside the adsorber cannot be sufficiently increased to achieve the pressure inside the condenser. The maximum COP is obtained for a regeneration temperature of about 75 °C and 95 °C, respectively for Scenarios A and B, respectively, whilst the SHP increases with the regeneration temperature. The COP and the SHP have opposite behaviors with the change of the cycle time. Short cycle times lead to higher SHP but lower COP, whereas long cycle times result on higher COP and lower SHP. The cycle time must be adjusted in order to achieve the

optimal balance between the COP and the SHP, to give to the AHP the best performance depending on its specific application.

Although the metal-adsorbent heat transfer coefficient does not significantly affect the COP, the SHP highly increases until it reaches 200 $W.m^{-2}.K^{-1}$. This is the main reason for the use of adsorbent coatings since they can provide metal-adsorbent heat transfer coefficients up to ten times higher than packed beds. The SHP can also be improved by using thinner adsorbent coatings but requiring an adsorber with a larger number of tubes. The inner diameter of the metal tube and the HTF's velocity can both be used to improve the performance of an AHP system. Turbulent flow conditions result on higher SHP; however, in order to set this condition using low HTF's velocities, the tube's diameter needs to be too large, which will result on high volume adsorbers.

Future developments include a model that considers the whole AHP system illustrated in Figure 4.11 and Figure 4.12, and not only the adsorber. Understanding the dynamics of the complete AHP system and predicting its performance considering several working modes and conditions will contribute to improved AHP systems that can be made available in the market faster and at lower costs. The heat storage capacity of AHP systems can be used to reduce household's energy costs as well as to boast the effectiveness of using intermittent renewable energy sources.

4.7. REFERENCES

AL-Dadah R, Mahmoud S, Elsayed E, et al (2020) Metal-organic framework materials for adsorption heat pumps. Energy. https://doi.org/10.1016/j.energy.2019.116356

Aprile M, Freni A, Toppi T, Motta M (2020) Modelling and performance assessment of a thermally-driven cascade adsorption cycle suitable for cooling applications. Therm Sci Eng Prog 19:100602. https://doi.org/10.1016/j.tsep.2020.100602

Chakraborty A, Saha BB, Aristov YI (2014) Dynamic behaviors of adsorption chiller: Effects of the silica gel grain size and layers. Energy 78:304–312. https://doi.org/10.1016/J.ENERGY.2014.10.015

Chen CJ, Wang RZ, Xia ZZ, Kiplagat JK (2010) Study on a silica gel-water adsorption chiller integrated with a closed wet cooling tower. Int J Therm Sci. https://doi.org/10.1016/j.ijthermalsci.2009.09.009

Chua HT, Ng KC, Chakraborty A, et al (2002) Adsorption Characteristics of Silica Gel + Water Systems. https://doi.org/10.1021/je0255067

Chua HT, Ng KC, Wang W, et al (2004) Transient modeling of a two-bed silica gel-water adsorption chiller. Int J Heat Mass Transf. https://doi.org/10.1016/j.ijheatmasstransfer.2003.08.010

Dawoud B (2014) On the development of an innovative gas-fired heating appliance based on a zeolite-water adsorption heat pump; System description and seasonal gas utilization efficiency. Appl Therm Eng 72:323–330. https://doi.org/10.1016/j.applthermaleng.2014.09.008

Di J, Wu JY, Xia ZZ, Wang RZ (2007) Theoretical and experimental study on characteristics of a novel silica gel-water chiller under the conditions of variable heat source temperature. Int J Refrig. https://doi.org/10.1016/j.ijrefrig.2006.07.022

Dias JMS, Costa VAF (2018) Adsorption heat pumps for heating applications: A review of current state, literature gaps and development challenges. Renew Sustain Energy Rev 98:317–327. https://doi.org/10.1016/J.RSER.2018.09.026

Dias JMS, Costa VAF (2019) Which dimensional model for the analysis of a coated tube adsorber for adsorption heat pumps? Energy 174:1110–1120. https://doi.org/10.1016/J.ENERGY.2019.03.028

Dias JMS, Costa VAF (2020) Evaluating the performance of a coated tube adsorber for adsorption cooling. Int J Refrig. https://doi.org/10.1016/j.ijrefrig.2020.06.023

European Commision (2016) Communication from the commission to the European parliament, the council, the European economic and social committee and the committee of the regions. Brussel

Fernandes MS, Brites GJVN, Costa JJ, et al (2016) A thermal energy storage system provided with an adsorption module – Dynamic modeling and viability study. Energy Convers Manag 126:548–560. https://doi.org/10.1016/j.enconman.2016.08.032

Frazzica A, Füldner G, Sapienza A, et al (2014) Experimental and theoretical analysis of the kinetic performance of an adsorbent coating composition for use in adsorption chillers and heat pumps. Appl Therm Eng 73:1020–1029. https://doi.org/10.1016/j.applthermaleng.2014.09.004

Gaeini M, van Alebeek R, Scapino L, et al (2018) Hot tap water production by a 4 kW sorption segmented reactor in household scale for seasonal heat storage. J Energy Storage 17:118–128. https://doi.org/10.1016/j.est.2018.02.014

Gluesenkamp KR, Frazzica A, Velte A, et al (2020) Experimentally measured thermal masses of adsorption heat exchangers. Energies. https://doi.org/10.3390/en13051150

James A, Srinivas M, Mohanraj M, et al (2021) Experimental studies on photovoltaic-thermal heat pump water heaters using variable frequency drive compressors. Sustain Energy Technol Assessments. https://doi.org/10.1016/j.seta.2021.101152

Kaushik SC, Reddy VS, Tyagi SK (2011) Energy and exergy analyses of thermal power plants: A review. Renew. Sustain. Energy Rev.

Kieft A, Harmsen R, Hekkert MP (2021) Heat pumps in the existing Dutch housing stock: An assessment of its Technological Innovation System. Sustain Energy Technol Assessments. https://doi.org/10.1016/j.seta.2021.101064

Li XH, Hou XH, Zhang X, Yuan ZX (2015) A review on development of adsorption cooling - Novel beds and advanced cycles. Energy Convers. Manag. 94:221–232

Mahmoudi M, Dehghan M, Haghgou H, Keyanpour-Rad M (2021) Techno-economic performance of photovoltaic-powered air-conditioning heat pumps with variable-speed and fixed-speed compression systems. Sustain Energy Technol Assessments. https://doi.org/10.1016/j.seta.2021.101113

Makhanya N, Oboirien B, Ren J, et al (2021) Recent advances on thermal energy storage using metal-organic frameworks (MOFs). J. Energy Storage 34:102179

Ng KC, Chua HT, Chung CY, et al (2001a) Experimental investigation of the silica gel-water adsorption isotherm characteristics. Appl Therm Eng. https://doi.org/10.1016/S1359-4311(01)00039-4

Ng KC, Chua HT, Chung CY, et al (2001b) Experimental investigation of the silica gel–water adsorption isotherm characteristics. Appl Therm Eng 21:1631–1642. https://doi.org/10.1016/S1359-4311(01)00039-4

Pahinkar DG, Boman DB, Garimella S (2020) High performance microchannel adsorption heat pumps. Int J Refrig 119:184–194. https://doi.org/10.1016/j.ijrefrig.2020.07.020

Palomba V, Nowak S, Dawoud B, Frazzica A (2021) Dynamic modelling of Adsorption systems: a comprehensive calibrateddataset for heat pump and storage applications. J Energy Storage 33:102148. https://doi.org/10.1016/j.est.2020.102148

Pan Q, Wang R, Vorayos N, Kiatsiriroat T (2018) A novel adsorption heat pump cycle: Cascaded mass recovery cycle. Int J Refrig. https://doi.org/10.1016/j.ijrefrig.2018.08.004

Pesaran A, Lee H, Hwang Y, et al (2016) Review article: Numerical simulation of adsorption heat pumps. Energy 100:310–320

Pinheiro JM, Salústio S, Rocha JJ, et al (2016) Analysis of equilibrium and kinetic parameters of water adsorption heating systems for different porous metal/metalloid oxide adsorbents. Appl Therm Eng 100:215–226. https://doi.org/10.1016/j.applthermaleng.2016.01.142

Ramji HR, Leo SL, Abdullah MO (2014) Parametric study and simulation of a heat-driven adsorber for air conditioning system employing activated carbon-methanol working pair. Appl Energy 113:324–333. https://doi.org/10.1016/j.apenergy.2013.07.017

Robbins T, Kini G, Garimella S (2020) Alternate control methods for adsorption heat pumps. Int J Refrig. https://doi.org/10.1016/j.ijrefrig.2020.08.018

Sakoda A, Suzuki M (1984) Fundamental study on solar powered adsorption cooling system. J Chem Eng Japan 17:52–57. https://doi.org/10.1252/jcej.17.52

Sakoda A, Suzuki M (1986) Simultaneous transport of heat and adsorbate in closed type adsorption cooling system utilizing solar heat. J Sol Energy Eng Trans ASME. https://doi.org/10.1115/1.3268099

Shampine LF, Reichelt MW (1997) The MATLAB ode suite. SIAM J Sci Comput. https://doi.org/10.1137/S1064827594276424

Sircar S (1983) Linear-driving-force model for non-isothermal gas adsorption kinetics. J Chem Soc Faraday Trans 1 Phys Chem Condens Phases 79:785. https://doi.org/10.1039/f19837900785

Sun B, Chakraborty A (2015) Thermodynamic frameworks of adsorption kinetics modeling: Dynamic water uptakes on silica gel for adsorption cooling applications. Energy. https://doi.org/10.1016/j.energy.2015.02.101

Sztekler K (2021) Optimisation of operation of adsorption chiller with desalination function. Energies. https://doi.org/10.3390/en14092668

Vasta S, Palomba V, La Rosa D, Mittelbach W (2018) Adsorption-compression cascade cycles: An experimental study. Energy Convers Manag. https://doi.org/10.1016/j.enconman.2017.11.061

Vodianitskaia PJ, Soares JJ, Melo H, Gurgel JM (2017) Experimental chiller with silica gel: Adsorption kinetics analysis and performance evaluation. Energy Convers Manag 132:172–179. https://doi.org/10.1016/j.enconman.2016.11.028

Wilkes JO, Birmingham SG (2006) Fluid Mechanics for Chemical Engineers with Microfluidics and CFD. Pearson Education

Zhang LZ, Wang L (1997) Performance estimation of an adsorption cooling system for automobile waste heat recovery. Appl Therm Eng. https://doi.org/10.1016/S1359-4311(97)00039-2

CHAPTER 5

This Chapter has been published as:

Dias JMS, Costa VAF (2020) Evaluating the performance of a coated tube adsorber for adsorption cooling | Évaluation de la performance d'un adsorbeur à tube enrobé pour le refroidissement par adsorption. Int J Refrig 118:21–30. https://doi.org/10.1016/j.ijrefrig.2020.06.023

5. EVALUATING THE PERFORMANCE OF A COATED TUBE ADSORBER FOR ADSORPTION COOLING

Abstract

Adsorption cooling (AC) is an environmentally friendly alternative to conventional vapor compression cooling. In this paper, the performance of a coated tube adsorber suitable for AC systems is numerically evaluated. The developed adsorber uses silica gel-water as adsorbent-adsorbate working pair. A numerical model is used to analyze the influence of several governing parameters such as the evaporator, condenser and regeneration temperatures, cycle time, metal-adsorbent heat transfer coefficient, metal tube diameter, coating thickness and heat transfer fluid (HTF) velocity on the adsorber's performance. It is confirmed that increasing the evaporator temperature results on a performance increase whereas increasing the condenser temperature hindrances the system's performance. A regeneration temperature close to 70 °C results on the highest cooling coefficient of performance (COP_c). The cycle time can be used as a system-controlling parameter to tune the COP_c and the specific cooling power (SCP). The adsorber performs better when the regeneration time is 35% shorter than the adsorption time. The maximum COP_c occurs when the metal-adsorbent heat transfer coefficient reaches values of 100 $W.m^{-2}.K^{-1}$. The SCP greatly increases until this coefficient reaches 350 $W.m^{-2}.K^{-1}$. The adsorbent coating thickness severely influences the performance of an AC system. It was found that the maximum COP_c corresponds to a coating thickness of 1.75 mm and, the smaller the coating thickness the smaller the SCP. The metal tube's diameter and the HTF's velocity mainly influence the SCP since they have direct impact on the heat transfer rate exchanged between the HTF and the adsorbent material.

Keywords: Adsorption cooling, coated tube adsorber, adsorbent material, adsorbate vapor, cooling coefficient of performance (COPc), specific cooling power (SCP).

NOMENCLATURE

AC	Adsorption cooling
C	Specific heat (J.kg^{-1}.K^{-1})
C_p	Constant pressure specific heat (J.kg^{-1}.K^{-1})
COP_c	Cooling coefficient of performance
d	Diameter (m)
D_{ef0}	Effective diffusivity coefficient (m^2.s^{-1})
E_a	Activation energy (J.kg^{-1})
HTF	Heat transfer fluid
$h_{f\rightarrow m}$	Fluid-metal convective heat transfer coefficient (W.K^{-1}.m^{-2})
$h_{m\rightarrow s}$	Adsorbent-metal heat transfer coefficient (W.K^{-1}.m^{-2})
k	Thermal conductivity (W.K^{-1}.m^{-1})
k_0	Pre-exponential coefficient (kg.kg^{-1}.Pa^{-1})
k_D	Blake-Kozeny coefficient (m^2)
K_{LDF}	LDF constant (s^{-1})
L	Tube length (m)
m	Mass (kg)
P	Pressure (Pa)
Q	Heat (J)
q_m	Monolayer capacity (kg.kg^{-1})
r	Radial coordinate (m)
R_p	Particle radius (m)
R'	Adsorbate specific gas constant (J.kg^{-1}K^{-1})
SCP	Specific cooling power
t	Time (s)
t_{SG}	Non-dimensional Toth constant
T	Temperature (K)
u	Adsorbate velocity (m.s^{-1})
v	Velocity (m.s^{-1})
X	Adsorbate concentration in the adsorbent (kg$_a$.kg$_s^{-1}$)
z	Axial coordinate (m)

Greek letters

ΔH_{ads}	Heat of adsorption (J.kg^{-1})
ΔH_v	Heat of vaporization (J.kg-^{1})
ε	Adsorbent bed porosity (-)
μ	Dynamic viscosity (Pa.s)
ρ	Adsorbate density (kg.m-^{3})
σ	Thickness (m)
τ	Cycle time (s)

Subscripts

a	Adsorbate
ads	Adsorption
bed	Adsorbent bed
c	Condenser /Cooling
cyc	Cycle
e	Evaporator
eq	Equilibrium
f	Fluid
h	Heating
ic	Isosteric cooling
ih	Isosteric heating
in	Inner
ini	Initial
m	Metal
max	Maximum
min	Minimum
out	Outer
p	Particle
reg	Regeneration
s	Adsorbent
v	Vapor/Vaporization

5.1. INTRODUCTION

The global energy demand for space cooling has been increasing yearly by 6% for the residential sector (Palomba et al. 2017b). Most of the cooling demands are fulfilled by conventional vapor compression cooling systems that rely on high global warming potential (GWP) refrigerants (HFCs and HCFCs). In addition, electrical energy is required to drive these systems, which contributes to the increase of greenhouse gases (GHG) emissions, since 43% of the gross electricity production is still obtained from fossil fuels combustion (European Environment Agency 2018). In order to avoid catastrophic consequences of anthropogenic climate change 197 Parties signed the Paris Agreement, in which each party pledged to severely reduce greenhouse gases emissions (European-Commission 2015). Therefore, the European Union aims to cut GHG emissions by 40% by 2030 relatively to the 1990 levels. Adsorption cooling (AC) technology is an environmentally friendly alternative to vapor compression systems. It works based on natural refrigerants with zero or nearly zero GWP such as water, ammonia, ethanol and methanol. Furthermore, AC systems are driven by thermal energy (solar, waste heat, biomass heat, natural gas, etc.), only requiring electricity to power small pumps and electronic control valves. As no moving parts are required for the refrigerant circulation, AC systems generate very low noise and no vibrations, making them appealing for quiet and household applications.

Combustible fuels (coal, oil, natural gas, biofuels, industrial and municipal waste, etc.) accounted for 66.8% of the total World gross electricity production in 2017 (International Energy Agency (IEA) 2019). Combustion's heat is used to produce steam driving electric generators through the spinning of steam turbines. This process is used in the majority of worldwide thermal power plants. Only approximately 30% heat generated from the fuels' combustion is converted into electricity, being the remaining wasted heat (Kaushik et al. 2011). One of AC major limits is the low coefficient of performance (COP) when compared to the conventional vapor compression systems. Nonetheless, this should be carefully considered since it is commonly overrated. The COP for vapor compression systems is defined as the ratio between the thermal energy withdrawn (cooling production) and the electrical energy needed to drive the cooling system. However, when comparing an electrically driven system with a thermally driven one, it has to be noticed that 70% of the total heat is lost in its conversion to electricity, which also must be accounted for in electrically driven systems. Therefore, if the efficiency of electricity generation from heat is considered, the COP of compression refrigeration systems is much lower than the

commonly reported one. In fact, from this perspective care is needed when comparing the COP of adsorption and vapor compression refrigeration systems, and the low COP of AC systems should not be considered such a huge disadvantage.

One of the most interesting features of AC systems is that they require heat to produce the cooling effect. In several cases, the need for cooling occurs when and where some excess heat exists, as waste heat from industrial processes and machine working, ambient heat, or solar heat. The thermal energy available can be used to drive AC systems by itself or to reduce the costs of the energy required to drive these systems. Advanced systems' configurations can be implemented in order to exploit the usage of available heat. Moreover, compressor dependent systems cannot provide cooling without electricity whereas AC systems can function resorting to very small batteries only to power their small pumps and electronic valves. Since most households do not have a backup electricity generator, an energy failure during an extreme hot period (like heat waves, which are becoming more intense and frequent) can bring disastrous consequences to human health and wellbeing. AC can help to overcome these situations, if driven by solar energy and resorting to very small batteries only.

A lot of research has been carried out over the last decade on AC technologies (Wang et al. 2010; Aristov 2017; Vasta et al. 2018; Mohammed et al. 2019; Abd-Elhady and Hamed 2020). Mohamed *et al.* carried out a scaling study of heat diffusion and vapor adsorption in an adsorbent silica gel packed bed (Mohammed et al. 2018). Valuable information on the influence of heat transfer resistances, intra and interparticle mass resistances, particle diameter and adsorbent thickness on the adsorbent bed performance was presented. Several studies are focused on the adsorbent-adsorbate working-pairs and their state equations, that can be used as database for future works (Hassan et al. 2015; Shmroukh et al. 2015; Younes et al. 2017, 2019; Elsayed et al. 2019). Mohamed and Askalany developed an advanced system that integrates adsorption cooling and desalination (Mohammed and Askalany 2019). The studied cycle achieved a specific daily water production of 25 $kg_{water}/kg_{adsorbent}$. Frazzica *et al.* (Frazzica et al. 2016b) built an adsorption refrigerator for air conditioning and refrigeration purposes, activated carbon and methanol being used as the working pair. The specific cooling power (SCP) achieved was 95 W/kg and 50 W/kg for air conditioning and refrigeration operating conditions, respectively. However, the achieved COP was in the range of 0.09-0.11, which is considerably low. In addition, the authors used a thermodynamic model to predict the COP and select the best adsorbent material. The COP predicted by the model, for the working pair used to build the

prototype, was 0.63 and 0.55 respectively for air conditioning and refrigeration conditions, which are far from the considerably lower experimental results. From these results, it can be concluded that thermodynamic (equilibrium) models are not suitable to predict the performance of AC systems. In Ref. (Vodianitskaia et al. 2017) is presented an experimental adsorption chiller using the silica gel-water working pair. Grains of silica gel were packed in a finned tube heat exchanger. Different grain sizes were tested, and results showed that smaller grain sizes perform better considering the COP and SCP. The performance improvements obtained with smaller particle diameters have paved the way to the implementation of adsorbent coatings, which is nowadays acknowledged as the most promising technique to achieve more performant adsorption systems (Dias and Costa 2018). The enhancement of the SCP as a result of reducing particle diameter and bed thickness has also been reported in (Mohammed et al. 2017). Building AC systems with multiple adsorbent beds is also leading to improvements in the SCP (Rouf et al. 2020). An up-to-date review on performance enhancing techniques for adsorption air conditioning systems can be found in Ref. (Alahmer et al. 2019).

An interesting feature of the adsorption refrigeration is the capability of regenerating the adsorbent using solar thermal energy. Fernandes *et al.* (Fernandes et al. 2014) elaborated a comprehensive review on solar adsorption refrigeration systems. Given the low regeneration temperatures associated with silica gel, it has been a widely used adsorbent for solar adsorption refrigeration applications. A parametric analysis of a solar adsorption refrigerator was carried out by Brites *et al.* (Brites et al. 2016). The influence of several parameters on the overall system's performance was investigated. A prototype was developed and tested, and experimental results used to validate the numerical model. Among the many governing parameters, whose best numerical values need to be evaluated, are the adsorbent mass, the number of metallic fins in the adsorbent bed and the thermal contact resistance between the solar collector plate and the adsorbent. Recently, a silica gel-water adsorption air conditioning system has been developed and tested by Pan *et al.* (Pan et al. 2019). Experimental tests were carried out under different operating conditions. The study reported a cooling power of 3.98 kW and a COP_c of 0.63 operating with a regeneration temperature of 85.1 °C, a condenser temperature of 30.3 °C and an evaporator temperature of 22.8 °C. In addition, the authors reported that the water used to cool the adsorber can reach a temperature of 39.9 °C, making it suitable for domestic water pre-heating or heating purposes.

In order to improve the overall performance of AC systems, detailed numerical models enabling the identification of optimal values for the several governing parameters, configurations and designs are required. The increase of the computational capacities allows implementation of a higher level of detail in the numerical models, and detailed analyses of adsorption cooling systems.

This work considers a coated tube adsorber module, which was used for heating applications in previous works, and evaluates its performance when used for cooling purposes. The coated tube adsorber is presented as well as a physical model that has already been validated for heating purposes in previous studies (Zhang and Wang 1999; Dias and Costa 2019). Analysis of the impact of several governing parameters such as the evaporator, condenser and regeneration temperatures, cycle time, metal-adsorbent heat transfer coefficient (heat transfer coefficient between the outer tube wall and the adsorbent material), metal tube diameter, coating thickness and HTF's velocity on the adsorber's performance is performed. The reported results enable the identification of the key parameters and their best values for the use of the coated tube adsorber module in AC applications.

5.2. COATED TUBE ADSORBER

Coated tube adsorbers are nowadays considered the most promising configuration for adsorption applications (Dias and Costa 2018), with the main advantages of high adsorbent-metal heat transfer coefficients and compact sizes. These improved characteristics have a significant impact on the cooling power of the AC systems due to more effective heat exchanges between the HTF and the adsorbent material. In addition, the compactness of the coated tube adsorbers allows the incorporation of higher adsorbent mass in smaller volumes.

Given the advantages of the coated tube design, a coated tube adsorber was selected for analysis in this paper. The adsorber consists of several cylindrical metal tubes, which outer surface is coated with the adsorbent material. These tubes are enclosed inside a sealed chamber, which is connected to the evaporator or condenser through several holes during adsorption and regeneration phases, respectively. Thus, adsorbate vapor flows from the evaporator to the chamber during the adsorption phase (heat release) and from the chamber to the condenser during the regeneration phase (heat reception). The HTF circulates inside the metal tubes in order to retrieve the heat released during the adsorption

phase and provide heat to the adsorbent during the regeneration phase. The metal tubes are linked to two joints, which separate the adsorbate chamber from the HTF's inlet and outlet ports. The coated tube adsorber is depicted in Figure 5.1, which does not include all the tubes in order to keep the picture clear and perceptible.

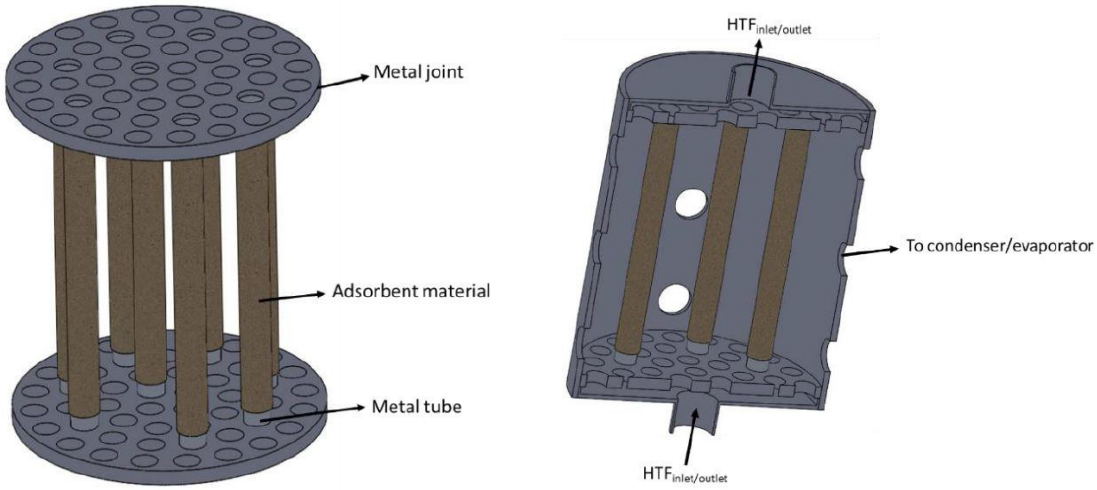

Figure 5.1 – a) Schematics of the adsorber module containing several metal tubes with an external adsorbent coating; **b)** Adsorber module cross section view. (Reproduced from (Dias and Costa 2019) with permission from Elsevier).

Silica gel was used as adsorbent material due to its low regeneration temperature (<100 ºC), readiness to market, low cost, and good capacity of water adsorption, which was selected as adsorbate. The selected silica gel is of the RD2060 type from Fuji Silysia Chemical LTD. The silica gel is mixed with a binder to form an external coating on the metal tubes, improving the metal-adsorbent heat transfer coefficient and the coating thermal conductivity. The mass transfer resistance is increased by mixing the silica gel with the binder. However, since the coating thickness is small, mixing the adsorbent with the binder will have more benefits than hindrances on the system's performance (Frazzica et al. 2014).

5.3. ADSORBER MODEL

This work implemented a two-dimensional distributed parameter model. The implemented model resorts on general mass and energy conservation laws, and on

particular constitutive laws and thermophysical properties that are well documented and that were previously validated. Although the situation/system presented in this work is different, the constitutive laws and thermophysical properties, as well as the adsorption data, remain the same for each particular adsorbent-adsorbate working pair, which makes the model a validated tool that can be applied for adsorption systems in general. Since the geometry is symmetric over the angular direction, only the radial and axial coordinate directions are considered. This model was studied in a previous work, where it was found which dimensional model must be used for the analysis of the coated tube adsorber for adsorption heat pumps (Dias and Costa 2019). Although lumped parameter models can accurately predict the COP of a coated tube adsorber under particular scenarios, that study concluded that the implementation of a two-dimensional distributed parameter model is necessary to achieve accurate predictions for the specific heating power. As all adsorber tubes are equal, the physical model describes the dynamics of a single representative tube only, and the overall results depend on the adsorber's number of tubes. The representative metal tube with the external adsorbent coating and its schematics are presented in Figure 5.2.

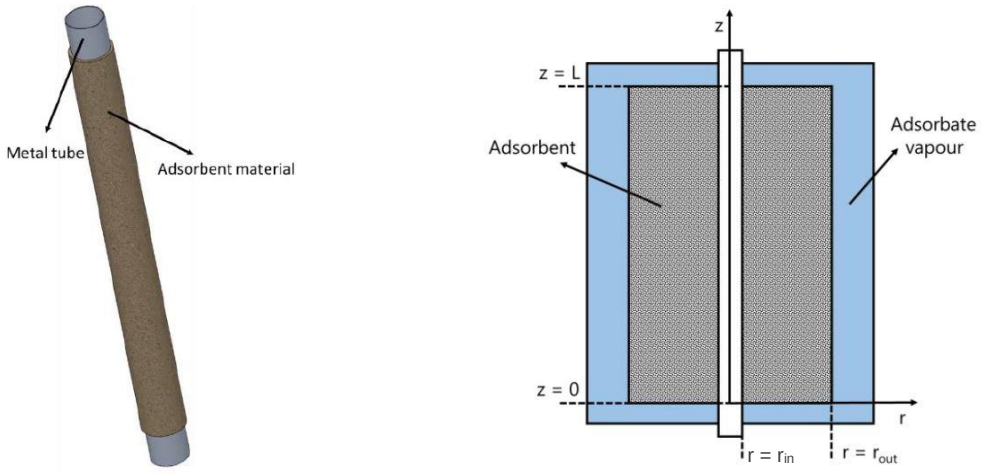

Figure 5.2 – a) Representative metal tube externally coated with the adsorbent material; **b)** Coated tube schematics. (Reproduced from (Dias and Costa, 2018) with permission from Elsevier).

The implemented model results from the application of the energy and mass balance equations to the coated tube geometry, respectively Equations 5.1 and 5.2:

$$\frac{\partial(\rho C_p T_s)}{\partial t} + \nabla(\rho_v C_{p,v} T_s u) - \nabla(k_s \nabla T_s) - \rho_s(1-\varepsilon)\Delta H_{ads}\frac{\partial X}{\partial t} = 0 \quad (5.1)$$

$$\varepsilon\frac{\partial \rho_v}{\partial t} + \nabla(\rho_v u) + \rho_s(1-\varepsilon)\frac{\partial X}{\partial t} = 0 \quad (5.2)$$

where

$$\rho C_p = \varepsilon\rho_v C_{p,v} + \rho_s(1-\varepsilon)(C_s + X C_{p,a}) \quad (5.3)$$

and

$$\varepsilon = \varepsilon_{bed} + (1-\varepsilon_{bed})\varepsilon_p \quad (5.4)$$

Darcy's Law is used to express the momentum balance:

$$u = -\frac{k_D}{\mu}\nabla P \quad (5.5)$$

and the Blake-Kozeny model is used to obtain the adsorbent bed permeability (Wilkes and Birmingham 2006):

$$k_D = \frac{d_p^2 \varepsilon_{bed}^3}{150(1-\varepsilon_{bed})^2} \quad (5.6)$$

The linear driving force (LDF) model is adopted to describe the adsorbate uptake (Sircar 1983):

$$\frac{dX}{dt} = K_{LDF}(X_{eq} - X) \quad (5.7)$$

where K_{LDF} coefficient can be obtained as:

$$K_{LDF} = \frac{15 D_{ef0} e^{-\frac{E_a}{R' T_s}}}{R_p^2} \quad 5.8$$

For the silica gel-water working pair, the adsorbate concentration in the adsorbent at equilibrium, X_{eq}, can be obtained as:

$$X_{eq} = \frac{P k_0 e^{\frac{\Delta H_{ads}}{R' T_s}}}{\left[1 + \left(\frac{P k_0}{q_m} e^{\frac{\Delta H_{ads}}{R' T_s}}\right)^{t_{SG}}\right]^{\frac{1}{t_{SG}}}} \quad 5.9$$

The physical model is implemented considering the following main assumptions:

- Adsorbent bed is homogenous;
- The evaporator and the condenser are ideal heat exchangers with uniform internal pressures;
- Adsorbate vapor phase behaves as an ideal gas and the adsorbed phase is considered to be liquid;
- Specific heats of the adsorbate vapor and liquid phases are constants;
- Adsorbate vapor around the adsorbent is always in the saturation conditions;
- Thermophysical properties of solid materials do not change with temperature;
- Temperature and pressure in the adsorbent bed are uniform along the angular direction;

The adsorbate uptake is obtained through the LDF model, Equation 5.7, and it depends on the pressure and temperature along the adsorbent bed, $P(r,z)$ and $T(r,z)$. The energy conservation equation for the adsorbent bed can be written as:

$$\begin{aligned}\left[\rho_s(1-\varepsilon)(C_s+XC_l)+\varepsilon\rho_v C_{p_v}\right]\frac{dT_s}{dt} = \\ = (1-\varepsilon)\rho_s\Delta H_{ads}\frac{dX}{dt}+\frac{k_s}{r}\left(\frac{\partial T_s}{\partial r}+r\frac{\partial^2 T_s}{\partial r^2}\right) \\ -\frac{C_{p_v}}{r}\left(\rho_v T_s u_r + rT_s u_r\frac{\partial\rho_v}{\partial r}+r\rho_v u_r\frac{\partial T_s}{\partial r}+r\rho_v T_s\frac{\partial u_r}{\partial r}\right) \\ -C_{p_v}\left(T_s u_z\frac{\partial\rho_v}{\partial z}+\rho_v T_s\frac{\partial u_z}{\partial z}+\rho_v u_z\frac{\partial T_s}{\partial z}\right)+k_s\left(\frac{\partial^2 T_s}{\partial z^2}\right)\end{aligned} \quad 5.10$$

For the mass conservation, Equation 5.2 can be rearranged as:

$$\begin{aligned}\frac{\partial\rho_v}{\partial t} = -\frac{1}{\varepsilon}\Big[\rho_s(1-\varepsilon)\frac{\partial X}{\partial t}+\frac{1}{r}\left(ru_r\frac{\partial\rho_v}{\partial r}+\rho_v r\frac{\partial u_r}{\partial r}+\rho_v u_r\right)+\rho_v\frac{\partial u_z}{\partial z} \\ +u_z\frac{\partial\rho_v}{\partial z}\Big]\end{aligned} \quad 5.11$$

Since $r_{tube} \ll L_{tube}$, the HTF temperature variation along the radial coordinate can be neglected, $\frac{\partial T_f}{\partial r} \approx 0$. As the HTF velocity is constant, the energy balance equation for the HTF is:

$$\rho_f C_{p,f}\frac{\partial T_f}{\partial t} = k_f\left(\frac{\partial^2 T_f}{\partial z^2}\right)-u_f\rho_f C_{p,f}\frac{\partial T_f}{\partial z}+\frac{4h_{f\to m}}{d_{in}}\left(T_m-T_f\right) \quad 5.12$$

The temperature of the metal tube is considered constant along the radial direction due to the small thickness and metal's high thermal conductivity, $\frac{\partial T_m}{\partial r} \approx 0$. The energy balance equation for the metal tube is given by:

$$\rho_m C_m\frac{dT_m}{dt} = k_m\left(\frac{\partial^2 T_m}{\partial z^2}\right)+\frac{4d_{in}h_{f\to m}\left(T_f-T_m\right)}{d_{out}^2-d_{in}^2}+\frac{4d_{out}h_{m\to s}(T_s-T_m)}{d_{out}^2-d_{in}^2} \quad 5.13$$

The partial differential equation's system is solved using the method of lines by discretizing the derivatives in the radial and axial coordinates using the finite difference method. The resultant system of ordinary differential equations is solved resorting to the

Matlab R2018b ode15s solver. The initial conditions used to obtain the presented results are:

$$t_{ini} = 0 \qquad P(t_{ini}) = P_{ini}$$

$$T_m(t_{ini}) = T_f(t_{ini}) = T_s(t_{ini}) = T_{ini} \qquad X(t_{ini}) = X_{eq}\left(P_{ini}, T_{s_{ini}}\right)$$

The temperature and pressure boundary conditions used to solve the model's equations are as follows:

$$\left.\frac{\partial P}{\partial r}\right|_{r=r_{in}} = 0$$

$$P|_{r=r_{out}} = P|_{z=0} = P|_{z=L} = P_e, \qquad Adsorption$$

$$P|_{r=r_{out}} = P|_{z=0} = P|_{z=L} = P_c, \qquad Regeneration$$

$$\left.\frac{\partial P}{\partial r}\right|_{r=r_{out}} = \left.\frac{\partial P}{\partial r}\right|_{z=0} = \left.\frac{\partial P}{\partial r}\right|_{z=L} = 0, \qquad Cooling/Heating$$

$$-k_s \left.\frac{\partial T_s}{\partial r}\right|_{r=r_{in}} = h_{m\to s}(T_m - T_s)$$

$$\left.\frac{\partial T_s}{\partial r}\right|_{r=r_{out}} = \left.\frac{\partial T_s}{\partial z}\right|_{z=0} = \left.\frac{\partial T_s}{\partial z}\right|_{z=L} = 0$$

$$T_f\big|_{z=0} = T_{ads}\,, \qquad Adsorption/Cooling$$

$$T_f\big|_{z=0} = T_{reg}\,, \qquad Regeneration/Heating$$

$$\left.\frac{\partial T_f}{\partial z}\right|_{z=L} = 0$$

$$\left.\frac{\partial T_m}{\partial z}\right|_{z=0} = \left.\frac{\partial T_m}{\partial z}\right|_{z=L} = 0$$

The physical model is described with extensive detail in reference (Dias and Costa 2019).

5.4. RESULTS AND DISCUSSION

The coated tube adsorber's performance is investigated considering several parameters, which are suitable for cooling applications such as air conditioning and water chillers. The adsorber's performance is analyzed resorting on the cooling coefficient of performance (COP_c) and the specific cooling power (SCP), defined respectively as:

$$COP_c = \frac{Q_e}{Q_{\text{ih}} + Q_{reg}} \quad 5.14$$

$$SCP = \frac{Q_e}{m_s \tau_{cyc}} \quad 5.15$$

Heats provided during the isosteric heating (Q_{ih}) and regeneration (Q_{reg}) are calculated through Equations 5.16 and 5.17, respectively:

$$Q_{ih} \approx \int_{T_{initial}}^{T_{final}} \left[m_s\left(C_s + X_{max}C_{p,a}\right) + m_m C_m\right] dT \quad 5.16$$

$$Q_{reg} \approx \int_{T_{initial}}^{T_{final}} \left[m_s\left(C_s + XC_{p,a}\right) + m_m C_m\right] dT - \int_{X_{max}}^{X_{min}} m_s \Delta H_{ads} dX \quad 5.17$$

where the $T_{initial}$ and T_{final} refer the initial and final temperatures of the isosteric heating and regeneration phases, respectively. Finally, the heat drawn by the evaporator (Q_e), which is the useful cooling effect, is obtained as:

$$Q_e = m_s \Delta X \Delta H_v + \int_{T_c}^{T_e} m_s \Delta X C_{p,a} dT \quad 5.18$$

where T_c and T_e are the condenser and evaporator temperatures, respectively. The influence of the evaporator, condenser and regeneration temperatures, cycle times, metal-adsorbent heat transfer coefficient, metal tube diameter, coating thickness and HTF's velocity on the COP_c and SCP of the coated tube adsorber are analyzed. A set of reference parameters suitable for cooling applications was selected, which is summarized in Table 5.1. Throughout the analyses, one parameter is varied at a time whilst the others assume their reference values (segregated approach).

Table 5.1 – Parameters used as references.

Parameter	Value	Unit
C_m	910	J.kg^{-1}.K^{-1}
C_s	921	J.kg^{-1}.K^{-1}
d_p	3.5×10^{-4}	m
$d_{in,tube}$	0.01	m
E_a	2.3314×10^{6}	J.kg^{-1}
$h_{m \to s}$	200	W.m^{-2}.K^{-1}
k_0	7.3×10^{-13}	kg.kg^{-1}.Pa^{-1}
k_f	0.6	W.m^{-1}.K^{-1}
k_m	205	W.m^{-1}.K^{-1}
k_s	0.198	W.m^{-1}.K^{-1}
L_{tube}	1	m
ΔH_v	2.3×10^{6}	J.kg^{-1}
q_m	0.45	kg.kg^{-1}
R_p	1.75×10^{-4}	m
t_{ads}	600	s
T_c	$273.15 + 22$	K
T_e	$273.15 + 10$	K
$T_{f,ads}$	$273.15 + 20$	K
$T_{f,reg}$	$273.15 + 90$	K
t_{reg}	$0.91 \times t_{ads}$	s
t_{SG}	12	-
v_{HTF}	0.05	m.s^{-1}
ΔH_{ads}	2.693×10^{6}	J.kg^{-1}
ε_{bed}	0.4	-
ρ_m	2700	kg.m^{-3}
ρ_s	2027	kg.m^{-3}
σ_s	0.002	m
σ_{tube}	0.001	m

5.4.1. Evaporator temperature

The evaporator temperature directly determines the adsorber's pressure during the adsorption phase. The adsorber's performance was evaluated for evaporator temperatures in the 0-20 °C range, suitable for several cooling applications. The influence of the evaporator temperature on the COP_c and SCP is represented in Figure 5.3. As expected, for higher evaporator temperatures the COP_c and the SCP increase. The performance decreases for low evaporator temperatures due to the lower pressure during adsorption, which results in lower adsorption capacity. Thus, low evaporator temperatures cause

reduced refrigerant flowing in each cycle. In order to reduce the pressure inside the adsorber, the adsorber must be cooled down. The temperature of the cooling HTF dictates the lowest pressure that can be reached in the adsorbent bed. Therefore, if the temperature of the cooling HTF is not low enough, the adsorber cannot be sufficiently cooled down to reach the reduced evaporator pressure, precluding the adsorbate adsorption. Therefore, the temperature of the HTF cooling fluid will limit the lowest pressure that can be reached in the adsorber and, consequently, the lowest evaporator temperature (relevant for producing the useful cooling effect) for the system's proper operation.

It might seem that setting $T_e = T_c$ would not make sense as no heat transfer occurs for equal temperatures. However, the system's evolution is unsteady, the implemented model is dynamic, and the evaporator and condenser pressures are equal just at the beginning of each cycle. Although the adsorption and regeneration phases are theoretically isobaric, in practice the pressure during adsorption phase is lower that the initial P_e and the pressure during regeneration phase is higher than P_c. Consequently, the evaporator and condenser temperatures over each cycle are respectively lower and higher than the operating conditions set at the beginning of each cycle. Although not represented in Figure 5.3, it is possible to evaluate non-zero adsorber's performance for $T_e = T_c$, which are only equal at the initial instant of each cycle.

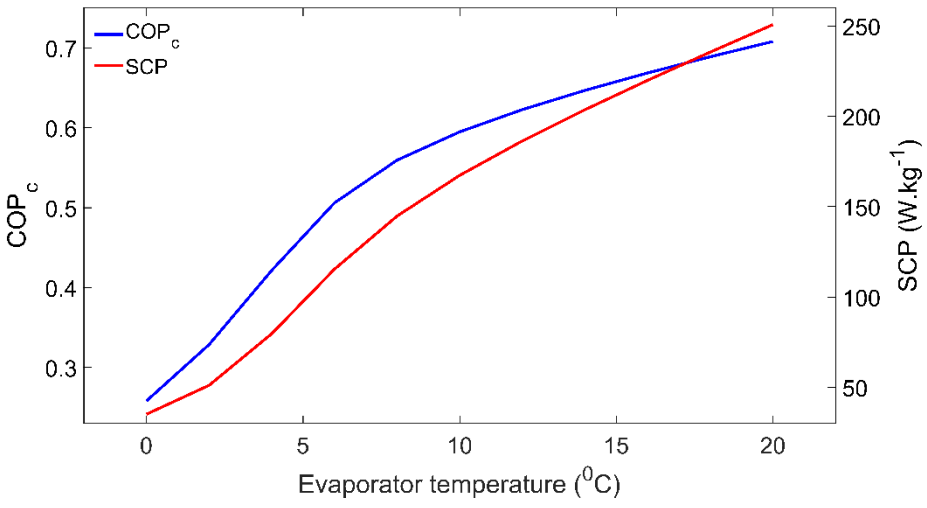

Figure 5.3 – Influence of the evaporator temperature on the adsorber's performance.

5.4.2. Condenser temperature

The adsorber's pressure during the regeneration phase is set by the condenser temperature. Simulations were carried out considering that the condenser would reject heat in a temperature range of 15-41 °C. The effect of the condenser temperature on the adsorber's performance is presented in Figure 5.4. Both COP_c and SCP are reduced when the condenser temperature increases, which is inherent to both adsorption and conventional cooling systems. The decrease of the SCP is almost linear; however, with the increase of the condenser temperature the decrease of COP_c becomes more abrupt. This is due to the pressure increase during the regeneration phase for higher condenser temperatures, which increases the amount of adsorbate in the adsorbent for the same regeneration temperature. In a limit scenario, if the regeneration temperature is not high enough to increase the adsorber's pressure to the level of the condenser pressure, the adsorbent material is not regenerated.

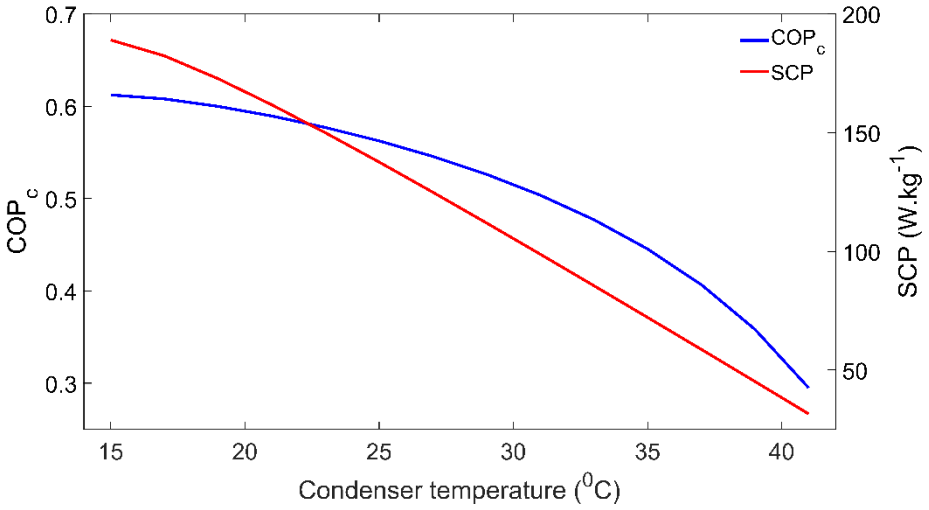

Figure 5.4 – Effect of the condenser temperature on the adsorber's performance.

5.4.3. Regeneration temperature

The required regeneration temperature highly depends on the adsorbent-adsorbate working pair. For the investigated working pair, silica gel-water, regeneration temperatures between 60 °C and 90 °C are commonly used. In this work, the adsorber's performance was evaluated for regeneration temperatures in the 50-90 °C range. The COP_c and SCP as a function of the regeneration temperature are represented in Figure 5.5. The COP_c reaches

its maximum for a regeneration temperature of approximately 70 °C. According to these results, from the energy output/input ratio, it is not worth to regenerate the adsorbent with temperatures higher than 75 °C, since the adsorbate flow increase does not compensate the additional energy input required to heat the HTF up to 90 °C. Concerning the SCP, its value increases with the regeneration temperature since higher regeneration temperatures result on faster heat transfer (higher heat transfer rate) between the HTF and the adsorbent material. Since water is used as HTF, regeneration temperatures higher than 90 °C were not considered, preventing boiling and the use of a pressurized system, including safety devices like a pressure relief valve.

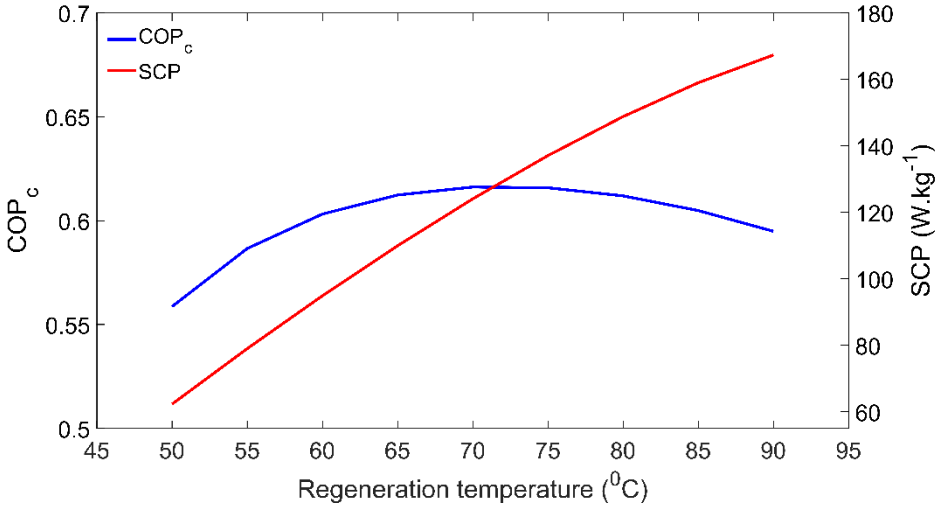

Figure 5.5 – COP_c and SCP as function of the regeneration temperature.

5.4.4. Cycle time

The cycle time is one of the most relevant parameters since it directly controls the system dynamics. The cycle time depends on the adsorption time set for each simulation. The adsorption time was varied from 50 s up to 3000 s, resulting in the cycle times that are the abscissas of Figure 5.6, demonstrating its relevance on the adsorber's performance. When the cycle time is too low, COP_c and SCP are minimal since there is not enough time for heat exchange between the adsorbent material and the HTF, resulting in an almost zero adsorbate flow. However, for longer cycle times COP_c and SCP present opposite behaviors. As the cycle time increases, the COP_c also increases reaching a maximum for the highest cycle times, as long cycle times allow the maximum adsorption capacity to be reached for a given combination of temperature and pressure. On the other hand, the SCP reaches its

peak for a cycle time of approximately 17 min and significantly decreases for longer cycle times. Longer cycle times allow higher COP_c (more complete heat and mass transfers), but only few cycles per unit time, and thus lower powers. The right balance between the COP_c and the SCP must be selected, depending on the priority for the AC system to provide more power (higher SCP) or to have a higher energy performance (higher COP_c).

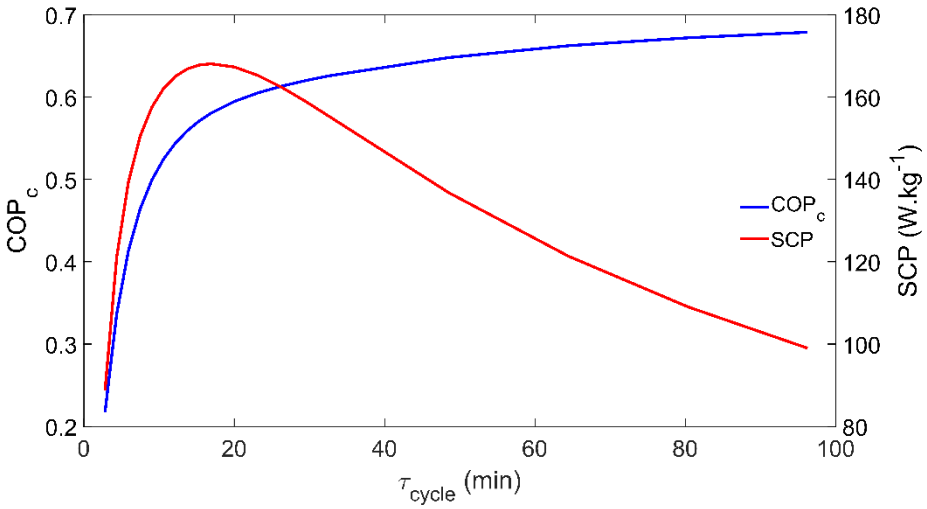

Figure 5.6 – Influence of the cycle time on the adsorber's performance.

5.4.5. Regeneration time

Regeneration phase is normally faster than the adsorption phase. In addition, the regeneration phase of an adsorption system occurs when the major (driving) energy is provided to the system. In Figure 5.7 is presented the influence of the regeneration time on the adsorber's performance. The regeneration time is taken as a fraction of the adsorption time. By analyzing these results, it can be seen that the COP_c is not significantly affected by reducing the regeneration time. Although the SCP shows a peak when the regeneration phase lasts for 65% of the adsorption time, it does not reflect severe variations as occurring for other parameters. Nonetheless, if a large mass of adsorbent material is used, small changes on the SCP will result on significant changes on the system's (absolute) cooling power.

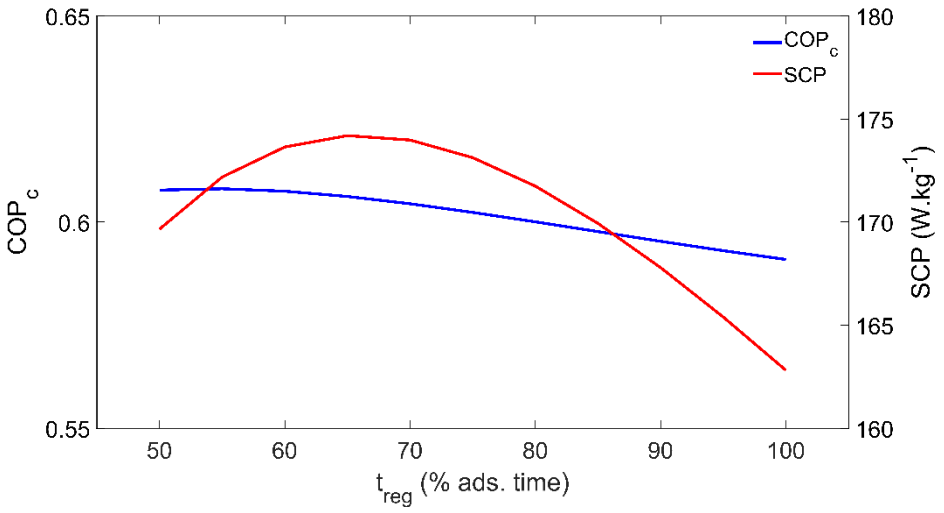

Figure 5.7 – Effect of the regeneration time on the adsorber's performance.

5.4.6. Tube-adsorbent heat transfer coefficient

The heat transfer between the external metal wall and the adsorbent coating has major influence on the adsorber's performance. This is the main reason for the use of coatings over granular beds. Value of this heat transfer coefficient is hard to measure and, and it is commonly estimated or used as a calibration parameter for the simulation models. Applying a thermal paste to the external metal tube's wall enables higher metal-adsorbent heat transfer coefficients. Values higher than 400 W.m-2.K-1 have been reported in the literature for adsorbent coatings (Restuccia et al. 2002; Frazzica et al. 2014). Simulations were carried out varying this parameter from 25 $W.m^{-2}.K^{-1}$ up to 600 $W.m^{-2}.K^{-1}$ and the results are presented in Figure 5.8. Both COP_c and SCP greatly increase with the metal-adsorbent heat transfer coefficient, for lower values of this coefficient. Increasing this coefficient beyond 100 $W.m^{-2}.K^{-1}$ will not have significant impact on the COP_c. However, in order to obtain the highest SCP this coefficient should be at least 350 $W.m^{-2}.K^{-1}$. Further increase of this heat transfer coefficient will have only an insignificant impact on the system's performance.

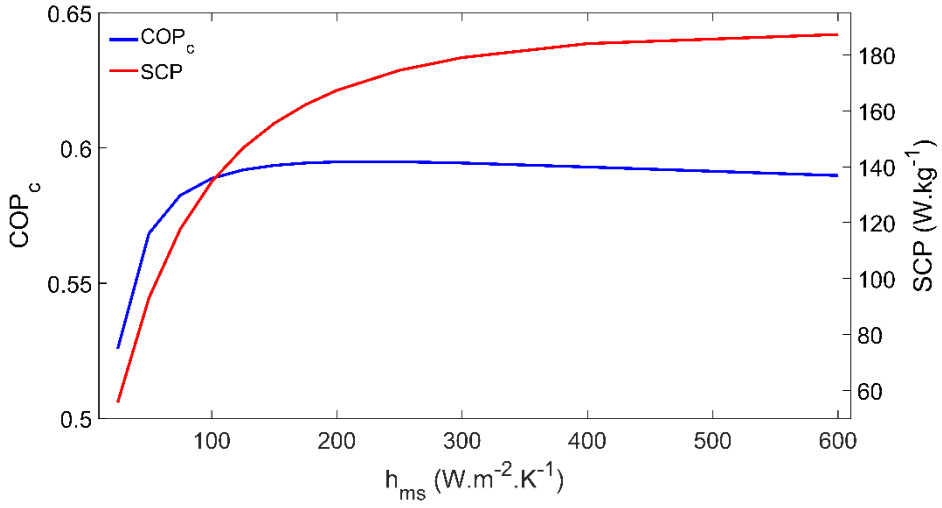

Figure 5.8 – Tube-adsorbent heat transfer coefficient's impact on the adsorber's performance.

5.4.7. Adsorbent coating thickness

Thickness of the adsorbent coating is very important for the adsorber's design since it will not only influence the COP_c and the SCP, but also the mass of adsorbent material coating each metal tube (and thus the total mass of adsorbent material in the adsorber). Figure 5.9 depicts the adsorber's performance as function of the adsorbent coating thickness. Results show that coating thicknesses higher than 3 mm lead to very low values of COP_c and SCP. The COP_c reaches its maximum for a thickness of approximately 1.75 mm, whereas the SCP is highest for the lowest coating thickness. Given the inverse behavior of these two performance coefficients, the thickness of the adsorbent coating must be selected accordingly to the AC system application. If the maximum COP_c is desired, the adsorbent coating thickness should be in the range of 1.5-2 mm; however, if high SCP is preferable, the coating thickness must be smaller. Nevertheless, caution must be taken when greatly reducing the adsorbent coating thickness since the mass of adsorbent coating each metal tube will be tiny, which may require an impracticable number of tubes to achieve the demanded total (absolute) cooling power.

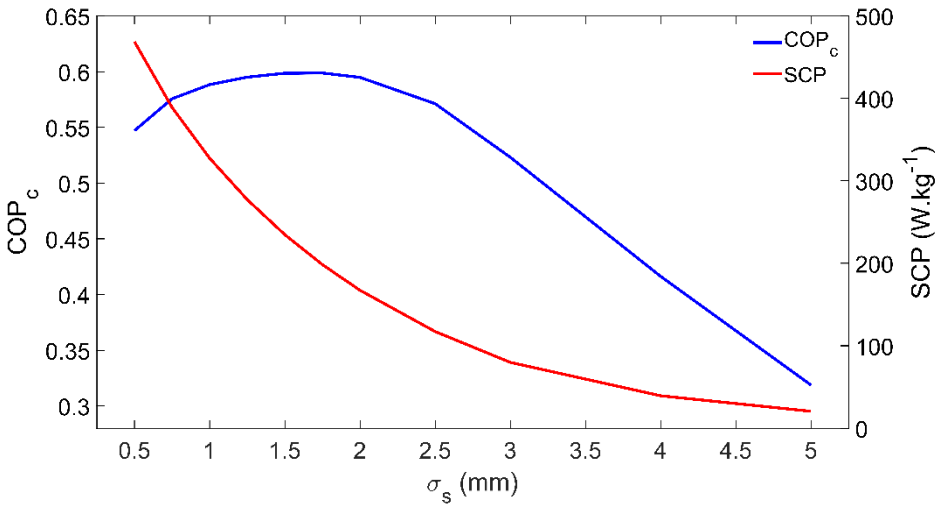

Figure 5.9 – Adsorber's performance as function of the adsorbent coating thickness.

5.4.8. Tube diameter

The tube's diameter, conjugated with the coating thickness, has a direct influence on the amount of adsorbent material coating each tube and on the contact area between the adsorbent coating and the tube wall. The tube's inner diameter was varied from 5 mm up to 70 mm. The velocity of the HTF was kept constant, resulting in different mass flow rates for the different tube diameters. The adsorber's performance for the different tube diameters tested is presented in Figure 5.10. First, a noticeable performance increase occurs for diameters over 35 mm due to the HTF flow regime transition from laminar to turbulent. The COP_c is not significantly affected by the changes on the tube's diameter. Under the HTF laminar flow conditions, the SCP is highest for a diameter of 10 mm, resulting from the best combination between the HTF mass flow rate and the adsorbent coating mass. Shifting to turbulent flow regime, the HTF mass flow rate is sufficient to provide/withdraw heat to/from the adsorber, and the influence of the tube's diameter on the adsorber's performance becomes insignificant. Meanwhile, it might be counterproductive to use large tube diameters since it will result in large adsorbers containing low adsorbent mass, which may become too large and impracticable if medium to high cooling powers are required.

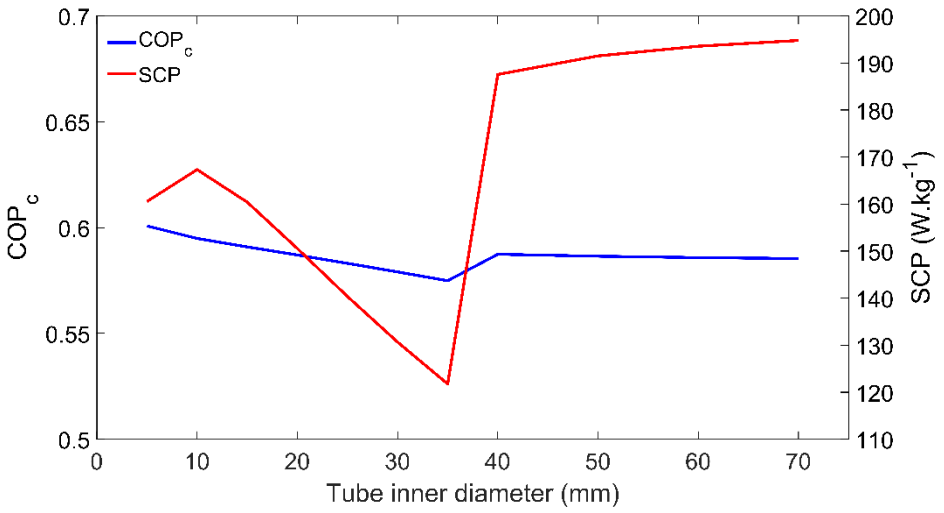

Figure 5.10 – Influence of the tube's diameter on the adsorber's performance.

5.4.9. Heat transfer fluid velocity

At last, the influence of the HTF's velocity on the adsorber's performance was investigated and the results presented in Figure 5.11. The COP_c does not present significant changes for the tested flow velocities since the adsorption and regeneration temperatures did not change. On the other hand, as the HTF's velocity directly influences the heat exchange inside the adsorber, it will affect the system's SCP. The SCP greatly increases with the flow velocity in the velocity range 0.005 $m.s^{-1}$ up to 0.02 $m.s^{-1}$, moderately increases in the velocity range 0.02 $m.s^{-1}$ up to 0.04 $m.s^{-1}$, and for HTF velocities beyond 0.04 $m.s^{-1}$ only residually changes, meaning that for these highest HTF velocities the adsorption kinetics becomes the limiting factor. For cooling applications, the HTF's velocity should be high enough so that the limits for the heat transfer in the adsorber are dictated by the adsorption kinetics of the selected working pair, guaranteeing it is not the HTF's velocity the performance limiting factor.

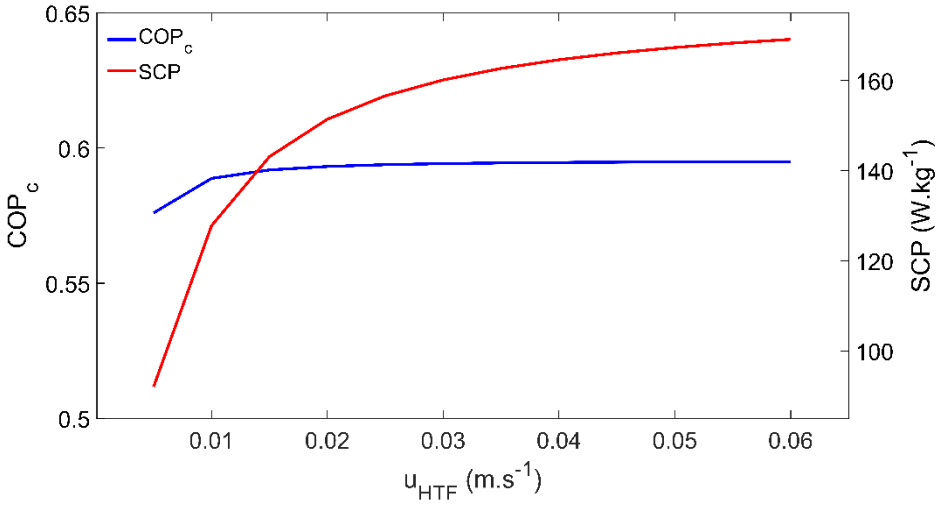

Figure 5.11 – HTF's velocity impact on the adsorber's performance.

5.5. CONCLUSIONS

The influence of several governing parameters on the performance of a coated tube adsorber for cooling applications was numerically analyzed. Some results were already anticipated, such as better adsorber's performance for higher evaporator temperatures and lower condenser temperatures. Nevertheless, a detailed characterization enables the better tuning of an AC system, whose behavior is inherently unsteady. Higher regeneration temperatures result in higher cooling powers, although the highest COP_c occurs when using a regeneration temperature of approximately 70 °C. Despite the fact that long cycle times allow maximum COP_c, the SCP becomes low or even very low. The cycle time must be carefully selected in order to provide the best combination between the COP_c and the SCP for each specific application of the AC system. Use of a regeneration time close to 65% of the adsorption time allows the best performance for the tested coated tube adsorber.

The external tube wall-adsorbent coating heat transfer coefficient should be higher than 100 $W.m^{-2}.K^{-1}$ in order to provide satisfactory SCP. The highest COP_c and SCP occur when this heat transfer coefficient has values of 100 $W.m^{-2}.K^{-1}$ and 350 $W.m^{-2}.K^{-1}$, respectively. An adsorbent coating thickness of approximately 1.75 mm will allow the highest COP_c; however, the SCP is higher for the smaller coating thicknesses. Although these results might suggest the use of small coating thicknesses to obtain high SCP values, decreasing the coating thickness excessively means that only a small mass of adsorbent is coating

each tube, which may require a large number of tubes to achieve the required (absolute) cooling power. The tube's inner diameter must be carefully selected as it influences the adsorbent mass per tube, the contact area between the external tube wall and the adsorbent coating, and the HTF mass flow rate. While under laminar flow regime, simulations suggest that an inner diameter of 10 mm is the best solution. When the inner tube diameter is high enough for HTF turbulent flow to develop, further increase on the tube diameter has an insignificant impact on the adsorber's performance. Increasing the HTF's velocity causes minimal improvements on the COP_c. Nonetheless, its increase until approximately 0.03 $m.s^{-1}$ leads to higher SCP, but no further significant changes on the system's performance are observed if the HTF velocity increases above 0.03 $m.s^{-1}$.

Generally, the working temperatures have major influence on the COP_c, a well-known main message from Thermodynamics. However, due to the unsteady nature of the involved processes, only dynamic studies of this type can provide detailed information on how they influence the AC systems' performance. On the other hand, parameters related to the cycle duration or to the heat transfer between the adsorbent material and the HTF have a major impact on the SCP. Longer cycle times allow more complete heat and mass transfers, and thus higher COP_c. However, longer cycle times allow only a lower number of cycles per unit time, and thus lower SCP. Thus, a balance of these two performance parameters is required for the best performance of a coated tube adsorber, depending on the specific AC application. The additional balance between the investment and working costs of each AC system can provide the additional information needed to set the better COP_c and SCP combination.

5.6. REFERENCES

Abd-Elhady MM, Hamed AM (2020) Effect of fin design parameters on the performance of a two-bed adsorption chiller. Int J Refrig. https://doi.org/10.1016/j.ijrefrig.2020.01.006

Alahmer A, Ajib S, Wang X (2019) Comprehensive strategies for performance improvement of adsorption air conditioning systems : A review. Renew Sustain Energy Rev 99:138–158. https://doi.org/10.1016/j.rser.2018.10.004

Aristov YI (2017) Adsorptive transformation and storage of renewable heat: Review of current trends in adsorption dynamics. Renew Energy 110:105–114. https://doi.org/10.1016/j.renene.2016.06.055

Brites GJVN, Costa JJ, Costa VAF (2016) Influence of the design parameters on the overall performance of a solar adsorption refrigerator. Renew Energy. https://doi.org/10.1016/j.renene.2015.07.099

Dias JMS, Costa VAF (2018) Adsorption heat pumps for heating applications: A review of current state, literature gaps and development challenges. Renew Sustain Energy Rev 98:317–327. https://doi.org/10.1016/J.RSER.2018.09.026

Dias JMS, Costa VAF (2019) Which dimensional model for the analysis of a coated tube adsorber for adsorption heat pumps? Energy 174:1110–1120. https://doi.org/10.1016/J.ENERGY.2019.03.028

Elsayed E, AL-Dadah R, Mahmoud S, et al (2019) Adsorption cooling system employing novel MIL-101(Cr)/CaCl2 composites: Numerical study. Int J Refrig. https://doi.org/10.1016/j.ijrefrig.2019.08.004

European-Commission (2015) Paris Agreement | Climate Action. Eur. Comm. Clim. Action

European Environment Agency (2018) Overview of electricity production and use in Europe. https://www.eea.europa.eu/data-and-maps/indicators/overview-of-the-electricity-production-2/assessment-4

Fernandes MS, Brites GJVN, Costa JJ, et al (2014) Review and future trends of solar adsorption refrigeration systems. Renew. Sustain. Energy Rev.

Frazzica A, Füldner G, Sapienza A, et al (2014) Experimental and theoretical analysis of the kinetic performance of an adsorbent coating composition for use in adsorption chillers and heat pumps. Appl Therm Eng 73:1020–1029. https://doi.org/10.1016/j.applthermaleng.2014.09.004

Frazzica A, Palomba V, Dawoud B, et al (2016) Design, realization and testing of an adsorption refrigerator based on activated carbon/ethanol working pair. Appl Energy 174:15–24. https://doi.org/10.1016/j.apenergy.2016.04.080

Hassan HZ, Mohamad AA, Alyousef Y, Al-Ansary HA (2015) A review on the equations of state for the working pairs used in adsorption cooling systems. Renew Sustain Energy Rev 45:600–609. https://doi.org/10.1016/j.rser.2015.02.008

International Energy Agency (IEA) (2019) Electricity Information: Overview. Stat iea

Kaushik SC, Reddy VS, Tyagi SK (2011) Energy and exergy analyses of thermal power plants: A review. Renew. Sustain. Energy Rev.

Mohammed RH, Askalany AA (2019) Productivity Improvements of Adsorption Desalination Systems. In: Kumar A, Prakash O (eds) Solar Desalination Technology. Springer Singapore, Singapore, pp 325–357

Mohammed RH, Mesalhy O, Elsayed ML, Chow LC (2019) Performance enhancement of adsorption beds with silica-gel particles packed in aluminum foams. Int J Refrig. https://doi.org/10.1016/j.ijrefrig.2019.03.013

Mohammed RH, Mesalhy O, Elsayed ML, Chow LC (2018) Scaling analysis of heat and mass transfer processes in an adsorption packed bed. Int J Therm Sci. https://doi.org/10.1016/j.ijthermalsci.2018.07.017

Mohammed RH, Mesalhy O, Elsayed ML, Chow LC (2017) Novel compact bed design for adsorption cooling systems: Parametric numerical study. Int J Refrig. https://doi.org/10.1016/j.ijrefrig.2017.04.028

Palomba V, Vasta S, Freni A, et al (2017) Increasing the share of renewables through adsorption solar cooling: A validated case study. Renew Energy. https://doi.org/10.1016/j.renene.2016.12.016

Pan Q, Peng J, Wang H, et al (2019) Experimental investigation of an adsorption air-conditioner using silica gel- water working pair. Sol Energy 185:64–71. https://doi.org/10.1016/j.solener.2019.04.054

Restuccia G, Freni A, Maggio G (2002) A zeolite-coated bed for air conditioning adsorption systems: Parametric study of heat and mass transfer by dynamic simulation. In: Applied Thermal Engineering. pp 619–630

Rouf RA, Jahan N, Alam KCA, et al (2020) Improved cooling capacity of a solar heat driven adsorption chiller. Case Stud Therm Eng 17:100568

Shmroukh AN, Ali AHH, Ookawara S (2015) Adsorption working pairs for adsorption cooling chillers: A review based on adsorption capacity and environmental impact. Renew Sustain Energy Rev 50:445–456. https://doi.org/10.1016/j.rser.2015.05.035

Sircar S (1983) Linear-driving-force model for non-isothermal gas adsorption kinetics. J Chem Soc Faraday Trans 1 Phys Chem Condens Phases 79:785. https://doi.org/10.1039/f19837900785

Vasta S, Brancato V, La Rosa D, et al (2018) Adsorption Heat Storage: State-of-the-Art and Future Perspectives. Nanomaterials. https://doi.org/10.3390/nano8070522

Vodianitskaia PJ, Soares JJ, Melo H, Gurgel JM (2017) Experimental chiller with silica gel: Adsorption kinetics analysis and performance evaluation. Energy Convers Manag 132:172–179. https://doi.org/10.1016/j.enconman.2016.11.028

Wang DC, Li YH, Li D, et al (2010) A review on adsorption refrigeration technology and adsorption deterioration in physical adsorption systems. Renew Sustain Energy Rev 14:344–353. https://doi.org/10.1016/j.rser.2009.08.001

Wilkes JO, Birmingham SG (2006) Fluid Mechanics for Chemical Engineers with Microfluidics and CFD. Pearson Education

Younes MM, El-sharkawy II, Kabeel AE, et al (2019) Synthesis and characterization of silica gel composite with polymer binders for adsorption cooling applications. Int J Refrig. https://doi.org/10.1016/j.ijrefrig.2018.09.003

Younes MM, El-Sharkawy II, Kabeel AE, Saha BB (2017) A review on adsorbent-adsorbate pairs for cooling applications. Appl Therm Eng 114:394–414. https://doi.org/10.1016/j.applthermaleng.2016.11.138

Zhang LZ, Wang L (1999) Effects of coupled heat and mass transfers in adsorbent on the performance of a waste heat adsorption cooling unit. Appl Therm Eng 19:195–215. https://doi.org/10.1016/S1359-4311(98)00023-4

CHAPTER 6

This Chapter has been published as:

Dias JMS, Costa VAF (2022) Modelling and analysis of a complete adsorption heat pump system. Appl Therm Eng 118782. https://doi.org/https://doi.org/10.1016/j.applthermaleng.2022.118782

6. MODELLING AND ANALYSIS OF A COMPLETE ADSORPTION HEAT PUMP SYSTEM

Abstract

Adsorption heat pumps (AHPs) can play a significant role in the future energy transition policies. However, the technology still needs to be matured and further research is still necessary. In this paper, the detailed model of a whole AHP system for domestic water heating is presented aiming to fulfil the literature gap for models that can simulate the dynamics of these complete heating systems, while maintaining a high level of modeling detail for the adsorbent bed. The model integrates all the main components of the AHP system, namely the evaporator, the condenser, the heater, the water reservoir and the adsorber. The adsorber is modeled by a 2D distributed parameter model with dynamic boundary conditions since the evaporator and condenser's temperatures vary in a cycle as well as from cycle to cycle. The novel model obtains the detailed temperature, pressure, and uptake fields in the adsorbent bed when integrated in a complete AHP system. Real scale AHP systems should not be accurately modelled by lumped-parameter models due to the heterogeneities on the temperature, pressure, and uptake in the adsorbent bed. The time evolution of the system's variables over five simulated cycles is obtained, as well as the coefficient of performance (COP) and specific heating power (SHP) of the whole system. For working conditions suitable for domestic water heating the system's COP is 1.35 and the SHP is 79.3 $W.kg^{-1}$.

Keywords: Adsorption heat pump; water heating; complete system; dynamic simulation; system performance.

NOMENCLATURE

A	Area (m^2)
C	Specific heat ($J.kg^{-1}.K^{-1}$)
C_p	Constant pressure specific heat ($J.kg^{-1}.K^{-1}$)
d	Diameter (m)
D_{ef0}	Effective diffusivity coefficient ($m^2.s^{-1}$)
E_a	Activation energy ($J.kg^{-1}$)
H	Enthalpy (J)
$h_{f\rightarrow m}$	Fluid-metal heat transfer coefficient ($W.m^{-2}.K^{-1}$)
$h_{m\rightarrow s}$	Adsorbent-metal heat transfer coefficient ($W.m^{-2}.K^{-1}$)
k	Thermal conductivity ($W.m^{-1}.K^{-1}$)
k_0	Pre-exponential coefficient ($kg.kg^{-1}.Pa^{-1}$)
k_D	Blake-Kozeny coefficient (m^2)
K_{LDF}	LDF constant (s^{-1})
L	Tube length (m) / Specific latent heat ($J.kg^{-1}$)
m	Mass (kg)
P	Pressure (Pa)
Q	Heat (J)
q_m	Monolayer capacity ($kg.kg^{-1}$)
r	Radial coordinate (m)
R'	Steam particular gas constant ($J.kg^{-1}.K^{-1}$)
t	Time (s)
t_{SG}	Dimensionless Toth's constant (-)
T	Temperature (K)
u	Velocity ($m.s^{-1}$)
U	Overall heat transfer coefficient ($W.m^{-2}.K^{-1}$)
V	Volume (m^3)
X	Adsorbate concentration in the adsorbent ($kg_a.kg_s^{-1}$)
z	Axial longitudinal coordinate (m)

Greek letters

ΔH_{ads}	Adsorption heat ($J.kg^{-1}$)
ε	Adsorbent bed porosity (-)
μ	Dynamic viscosity (Pa.s)
σ	Thickness (m)
τ	Cycle time (s)

Subscripts

a	Adsorbate
ads	Adsorption
amb	Ambient
bed	Adsorbent bed
c	Condenser/Condensation
cyc	Cycle
e	Evaporator/Evaporation
eh	Electrical heater
eq	Equilibrium
f	Fluid
h	Heating
m	Metal
net	Water net
p	Particle
reg	Regeneration
s	Solid/Adsorbent
t	Total
v	Vapor/Vaporization
w	Water

6.1. INTRODUCTION

The achievement of a greener planet is mandatory to maintain and improve citizens' life quality worldwide. The European Union (EU) is focused on a new growth strategy that aims to achieve zero greenhouse gases (GHG) emissions by 2050. Towards that goal, the European Commission has set as a priority for 2019-2024 to work for a European Green Deal, focusing on several key actions like environmentally friendly technologies, decarbonization of the energy sector, and improvement of buildings' energy efficiency, among others (European Commission 2019). Heating/cooling is the biggest energy end-use sector in Europe, accounting for 51% of the EU's energy consumption in 2019, from which approximately 75% are obtained from burning fossil fuels. In 2017, buildings represented 33% of the EU total energy consumption, from which 86.4% still come from non-renewable sources (REN21 2020). Space and water heating account for 79% of European households' final energy consumption (European Commission 2021). Most focus is being addressed to include and increase the share of renewables in the energy sector; however, the heating and cooling sector is causing a bigger impact on the environment. Efforts must be strengthened to reduce the harmful impacts of thermal needs and move towards the achievement of the energy goals set for the upcoming years, by introducing new technologies and perfecting those that are already available.

Heat pumps are among of the most environmentally friendly technologies suitable to be integrated with intermittent renewable energy sources (Yunna and Ruhang 2013). Given that heat pumps can contribute to reduce GHG emissions, its importance has been recently increasing. Despite their market share being still very low, only accounting for 5% of the heating sector in buildings in 2019, it is required to triple under the Sustainable Development Scenario by 2030, which will require several technological improvements, installation and purchase cost reduction, increased energy performance, removal of market barriers, and implement the use of alternative refrigerants (International Energy Agency (IEA) 2020). Policy makers from several countries are setting incentives towards the adoption and diffusion of heat pumps, recognizing the benefits they can provide to the low carbon future, in the transition to a more sustainable energy society (Gaur et al. 2021).

Most of the heat pumps in the market are electricity driven conventional vapor compression heat pumps (VCHP). Although many efforts have been carried out to reduce their global warming potential (GWP), VCHP still mostly rely on refrigerants with significant GWP. An alternative and relatively recent technology are adsorption heat pumps (AHP),

driven by thermal energy and that can rely on natural refrigerants like water or ammonia, with zero GWP. However, the high manufacturing costs, lower coefficient of performance (COP) and lower power density of AHP contribute to its shy presence on the market. Nonetheless, the COP for adsorption technologies should not be directly compared to that of VCHP since there is a significant difference between them. AHP are directly driven by thermal energy that can be freely obtained, or obtained from processes with high energy efficiencies close to 100% (e.g., waste heat, solar collectors, gas and biomass burners). On the other hand, VCHP rely on electricity and their COP is obtained as the ratio between the thermal energy delivered for heating and the electric energy required to operate the heat pump, disregarding the thermal energy lost during the electric energy generation processes, which have low efficiencies (approximately 30% for steam turbines and 10-14% for photovoltaic panels). To truly compare the AHP's and VCHP's COPs, the energy lost during electric energy production should be included as an input for the VCHP, which will result in much lower COPs than those commonly reported. Only under these conditions the COP comparison between these two different heat pump technologies can be effectively made. This reality must be taken into consideration and it is important to make use of the financial incentives, provided by policy makers, to carry out further research on AHP technology to minimize their well-identified disadvantages and improve their technology readiness level (TRL). Adsorption technologies are not only used in AHP, being used also in energy hybrid systems with VCHP, solar collectors and electricity generation systems (Vasta et al. 2018; Wang et al. 2018; Alsagri et al. 2020; Zhao et al. 2020). Yang *et al.* presented a semi-coupled solid desiccant heat pump system, using a desiccant coated evaporator in series with a conventional evaporator to obtain lower supply air temperatures and temperature variation (Yang et al. 2020). A parametric study was carried out to investigate the effects of the coating density and the area ratio of both evaporators. The optimal combination of a coating surface density of 0.25 kg.m-2 and an area ratio of 50% allows the achievement of the required performance under summer conditions.

Several contributions have been made recently on AHP technology, which mainly target adsorption materials and kinetics, adsorbent bed design, and control techniques. Shabir et al. presented a recent review on the adsorption capacity of adsorbent-adsorbate working pairs (Shabir et al. 2020). Among the adsorbent materials reviewed are activated carbons, zeolite, silica gel, composites, and metal organic frameworks (MOF), which are paired with several adsorbates like water, carbon dioxide, ethanol, methanol, and some synthetic refrigerants usual in VCHPs. Recent studies contemplate the research on new adsorbent materials and improvement of the physical properties of the already existing ones (Pan and

Wang 2017; Mohammed et al. 2018; Pal et al. 2019; Rupam et al. 2020). As promising as these improved adsorbents may be, they are still far from being used in full scale AHP. Graf et al. used the large temperature jump (LTJ) method along with an infrared camera to determine the heat and mass transfer coefficients of silica gel Siogel (Graf et al. 2017). Li et al. used a binder-based adsorbent coating using silica gel powder in a heat exchanger (Li et al. 2016). The heat and mass transfer rates of the new silica gel coating were higher than those of granular adsorbers, resulting in shorter cycle times and improved performance. Ammann *et al.* also investigated the heat and mass transfer on silica gels, comparing different grain configurations (Ammann et al. 2018). These studies have in common a tiny amount of adsorbent material used. It would be important to carry out similar studies capable of analyzing heat and mass transfer performances of real scale adsorbers, or of their representative elements, although it is difficult to have experimental setups suitable for real scale analyses.

Investigation on adsorbent bed design has also been the focus of a handful of studies. Wittstadt *et al.* developed an adsorption module with fiber heat exchangers (Wittstadt et al. 2017). The adsorption module was tested for several working conditions and the COP, cycled adsorbate mass and heat exchangers performance were reported. Al-Mousawi *et al.* have realized a study on the performance of an adsorption system, comparing several bed configurations and different time ratios for three adsorbent materials (Al-Mousawi et al. 2017). A lumped parameter model was used to model the adsorption system and obtain the performance results. An adsorber for a domestic gas fired AHP was presented by Rivero-Pacho *et al.* (Rivero-Pacho et al. 2017). The adsorber uses the carbon-ammonia working pair in a shell and tube design. The carbon is packed around cylindrical tubes and sealed in a vacuum chamber that is filled with ammonia vapor. Water is circulated inside the tubes to heat up and cool down the adsorber module. Besides the design itself, the packing methods and the resulting bed thickness play an important role in the AHP performance, being the target of some investigations that have recently been reported in the literature (Bendix et al. 2017; Gediz Ilis and Demir 2018).

Given its low cost, environmental friendliness, and well known thermophysical properties, silica gel-water has been used as the working pair in several studies. Ng *et al.* presented a performance analysis of an adsorption cycle capable of providing cooling power and desalinated potable water (Ng et al. 2012). The adsorption cycle is driven by waste heat and can produce 3.6 m3 of potable water and a cooling power of 23 Rton for chilled water at 10 °C, using hot water at 85 °C to regenerate the adsorbent. Alam *et al.* carried out

a parametric study by evaluating the performance of a two-bed silica gel-water adsorption refrigeration system (Alam et al. 2000). The influence of the cycle time on the system's COP and specific cooling capacity was investigated by changing the switching frequency of the adsorption refrigerator. It was concluded that both performance indicators were not optimized for the same value of the switching frequency. Different cycle times must be used depending on the performance indicator that must be maximized. The performance indicators are strongly dependent on the cycle time, which is strongly dependent on the adsorption details inside the adsorbent bed. Thus, it is of major importance to implement numerical models for the complete AHP systems simulation, accurately and detailly describing the dynamics inside the adsorbent bed.

The control of an AHP system plays a crucial role in its performance. Robbins *et al.* implemented alternative control methods for AHP based on the adsorbent bed temperature and on the adsorbate concentration in the adsorbent bed (Robbins et al. 2020). Results have shown that for non-optimal conditions, with lower heat source temperature, the COP can be improved by 5-50% using the adsorbate concentration method, when compared to using a fixed cycle time. Mitra *et al.* presented a scaling analysis for the heat and mass transfer characteristics of a silica gel-water system, validated by two-dimensional simulation results (Mitra et al. 2016). A comprehensive and direct literature review on the silica gel-water working pair is reported. The adsorption dynamics was analyzed for a rectangular domain that represent the adsorbent bed. The implementation of numerical models that simulate the dynamics of AHP systems can significantly contribute to improve their control, leading to noticeable performance enhancements. There are some models available in the literature that simulate and predict the performance of AHP (Brites et al. 2016; Fernandes et al. 2016; Pesaran et al. 2016; Krzywanski et al. 2017; Azahar et al. 2018). However, most models are thermodynamic (lumped parameter) models, suitable for predicting the system's performance limits, but that are not able to account for the heterogeneities and dynamics of the adsorbent bed. There are a few distributed parameters models that capture the dynamics of the adsorbent bed, yet considering fixed boundary conditions, what is not real since the adsorption cycles are slow and the conditions among the remaining system components (e.g. evaporator, condenser, heat transfer fluid) vary within the cycle, and from cycle to cycle. Pesaran *et al.* have presented a complete and detailed review on numerical models used to simulate AHP (Pesaran et al. 2016). This study has categorized the models available in the literature as thermodynamic models, lumped parameter models, and distributed parameter models. The more recent models are distributed parameter models that deal with the heat and mass transfer processes in the adsorbent bed. The external

mass transfer resistance is commonly described by Darcy's Law and the internal mass transfer resistance is modeled using the Linear Driving Force (LDF) model. Details and comparisons between several models available in the literature can be found in Ref. (Pesaran et al. 2016). Most of the models are focused on the adsorbent bed or on the operating parameters. System level studies simultaneously considering the working conditions and the adsorber designs are lacking. Models capable of simulating the dynamics of whole AHP systems, simultaneously considering the operating conditions and the adsorber specifications are lacking in the literature, which may have been avoided in the past due mainly to the required computational resources and time. Studies available in the literature that simulate complete AHP systems use lumped parameters models (Pesaran et al. 2016). Considering the advancements in computational power, it is now possible to carry out complex and detailed simulations much faster than some years ago, enabling the development of extensive models that consider the dynamics of the whole AHP systems.

An improved model for an AHP system for domestic water heating, that considers the dynamics of the whole AHP system, is proposed in this work. To capture the details inside the adsorbent bed and provide more accurate results, distributed parameters models must be used (Dias and Costa 2019b). The few distributed parameter models available in the literature, which describe the dynamics inside the adsorber module, use fixed boundary conditions (evaporator, condenser, and regeneration temperatures) within each cycle. Given that adsorption cycles are long, these temperatures are not constant throughout the cycle. Simulation of the complete AHP systems require dynamic boundary conditions and distributed parameters models. This novel approach implements a validated and detailed distributed parameter model to the adsorber, and that deals with all the main components of the complete AHP system, connecting and integrating all the components considering all the interactions and dynamics. Every main component of the AHP has its own dynamics, contributing to and being influenced by the dynamics of the whole AHP system. This kind of approach provides a deeper understanding and more accurate performance prediction of AHP that cannot be captured when testing each single/separate component. It aims to fulfil the identified gap in the literature for detailed models capable of simulating the entire dynamics of whole AHPs, providing better insights on how to design and control these systems and contributing to future performance improvements and manufacturing costs reductions. The presented model is also a useful tool to test new adsorbent materials, different working pairs, several condenser and evaporator designs, water reservoir sizes, water consumption profiles, positions of the condenser in the reservoir, heating powers (for

the adsorbent regeneration), heat transfer fluid's velocities, system layouts, integration with other heating systems, among others. This tool is not only able to provide details on the time evolution of all the relevant variables, but it is also capable of more accurate performance predictions, what is of major importance on the scaling of small prototypes to ready to market AHP systems, considering particular requirements and specifications.

There are several papers available in the literature that detailly describe and explain the adsorption working principles; so, this will not be the target of this paper (Demir et al. 2008; Dias and Costa 2018, 2020). It describes the developed AHP system that uses silica gel-water as the working pair. The physical model for the AHP that integrates all its main components is detailed. The temperature, pressure and uptake distributions inside the adsorbent bed are reported as one of the model outputs. The time evolution of the relevant system's variables for five consecutive complete cycles is presented and discussed. Finally, the system's performance evaluation is reported, and some conclusions drawn. drawn.

6.2. ADSORPTION HEAT PUMP SYSTEM

The proposed air to water AHP system was developed with the objective of providing domestic hot water. It consists of an adsorber, an evaporator, a condenser, a heating element, a water reservoir, an expansion valve, a water pump and control valves and sensors. Granular silica gel RD-2060 from Fuji Silysia Chemical LTD was selected as the adsorbent material, given that it is well studied and its data can be easily found in the literature. It is also commercially available at a relatively low cost. The selected adsorbate is water, due to its several advantages: low cost, environmental friendliness, well know properties, ease of use, and harmless in case of leakage to the ambient and/or to the domestic water reservoir. The condenser is a copper coil made of a tube with internal diameter of 5 mm, thickness of 1 mm, and 15 m length, which is placed inside the domestic hot water reservoir. This ensures that heat can only be transferred from the condenser to the domestic hot water, thus eliminating heat losses from the condenser to the ambient, what is only possible as the used adsorbate is harmless in case of water leakage from the condenser. This is a relevant issue for commercially available systems since the condenser is often ruptured due to exposure to treated domestic water at high temperatures. The condenser is placed between 0.25 m and 0.75 m relatively to the reservoir's height. A commercial aluminum finned tube evaporator with a blower is used. The AHP system resorts to an electric water heater as heating element, allowing easy heating available on demand, being easy to work in the laboratory, without requiring extra safety measures that

would be required by other possible heating systems, like combustion heating systems. For practical purposes, thermal energy from other sources, like solar thermal, residual heat, or biomass combustion heat can be used as the AHP driving thermal energy input.

The core of the AHP system is the adsorber, which consists of a set of 50 tubular units enclosed in a vacuum chamber. Each tubular unit is formed by an inner metal tube concentric with an external perforated tube. The space between the outer surface of the inner tube and the inner surface of the outer tube is filled with an annularly shaped silica gel layer. The outer perforated tube is wrapped with a steel mesh, with holes smaller than the silica gel particles size but still large enough to allow the water vapor to easily pass through. Two rubber rings are used to ensure the concentricity of the inner and outer tubes of each tubular unit. In this way, the outer surface of the silica gel layer is exposed to the adsorbate vapor. The heat transfer fluid (HTF) is circulated inside the inner tube, providing heat for the silica gel regeneration during the desorption phase, and withdrawing the adsorption heat during the adsorption phase. Figure 6.1 depicts an individual tubular unit, where are observable the inner tube (top) and the steel mesh externally covering the outer perforated tube, the annularly shaped silica gel layer residing between the inner tube and the outer perforated tube. The schematic of this individual tube is presented in Figure 6.6.

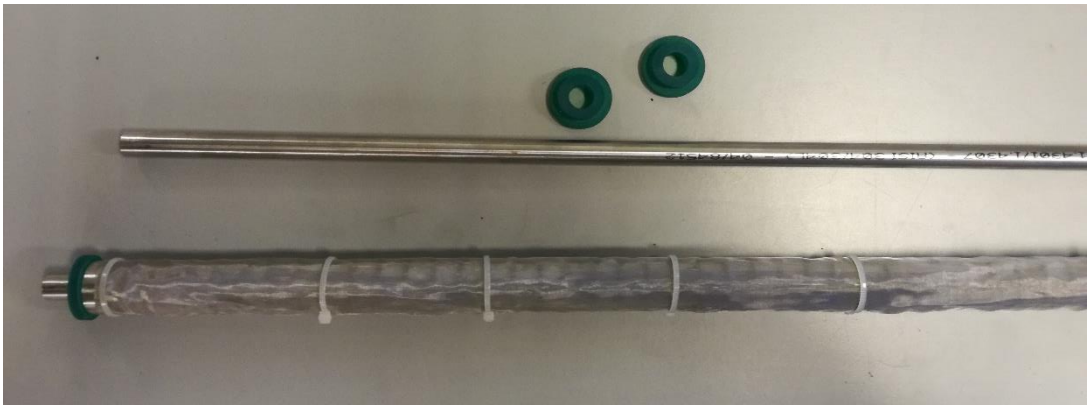

Figure 6.1 – Inner metal tube and an assembled adsorber tubular unit.

The The 50 tubular units are assembled on a steel structure designed and constructed for this purpose. This structure assumes the form of a cylinder with two flanges welded on its ends. The structure is then sealed on both ends by screwing a joint on each side using rubber sealings in between. These joints have holes that fit the inner tube of each tubular unit. Steel lids are attached to the ends of the adsorber, acting as HTF collectors connected to the domestic water circuit. A schematic of the adsorber is presented in Figure 6.2.

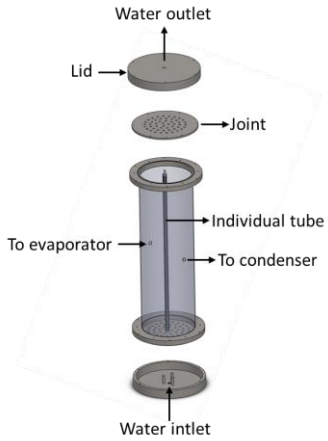

Figure 6.2 – Schematics of the adsorber built and modelled.

Figure 6.3 contains some pictures of the developed adsorber. Two holes are made in the main body of the adsorber, at its middle length and diametrically opposed, with vacuum fittings for connection with the evaporator and the condenser.

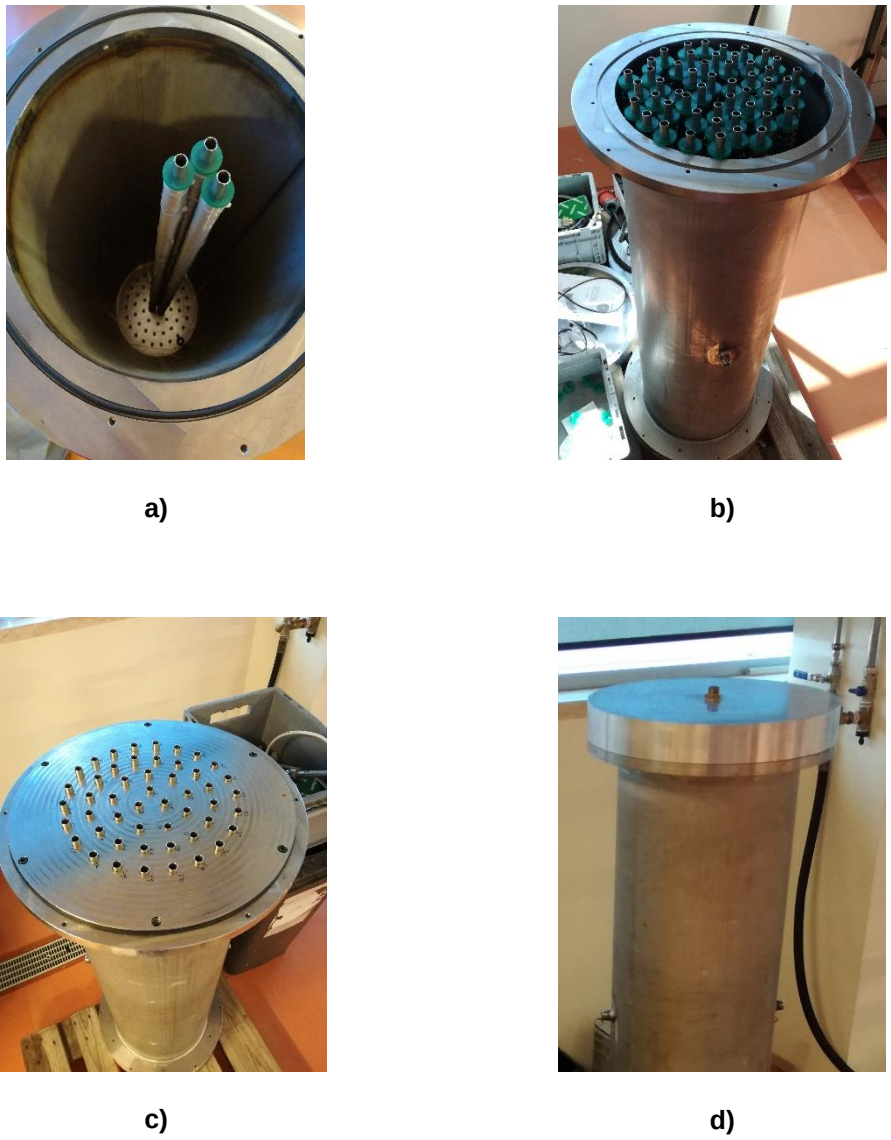

a) **b)**

c) **d)**

Figure 6.3 – Pictures of the developed adsorber: **a)** Three assembled tubular units assembled in the adsorber; **b)** Fifty tubular units assembled in the adsorber; **c)** Adsorber sealed with the sealing joint; **d)** Adsorber assembled with the top HTF collector steel lid.

The configuration of the entire AHP system is presented in Figure 6.5, during the adsorption phase in Figure 6.5.a and during the regeneration phase in Figure 6.5.b. When the adsorption phase starts, pressure in the adsorber is equal to that in the evaporator. Absorbing the low temperature level ambient heat, the adsorbate evaporates in the evaporator and flows into the adsorber through valve V_1, which remains open during the adsorption phase. The adsorbate vapor is adsorbed by the silica gel in the adsorber, a process that releases heat to the HTF. To collect this adsorption heat, the water HTF is

withdrawn from the domestic water reservoir and circulated by a pump inside the inner tubes of the adsorber's tubular elements, receiving the adsorption heat and returning at an increased temperature to the top of the water reservoir. The adsorption process duration, t_{ads}, is one of the system's control parameters. When the adsorption phase ends valve V_1 closes and separates the adsorber from the evaporator. Isosteric heating phase begins and there is no adsorbate flowing in or out the adsorber. Valve V_2 closes, valve V_3 opens, and the 3-way valve shifts the HTF flow from the reservoir to the circulator pump inlet, closing the HTF circuit. The electric heater is turned on, providing heat to the HTF water that, flowing in the inner tubes of the adsorber releases heat there, that is used to increase the adsorber temperature. Consequently, pressure in the adsorber increases, which is monitored by the pressure sensor P_a. When the pressure read by sensor P_a is equal to the condenser's pressure, this measured by sensor P_c, the isosteric heating phase ends. Valve V_4 opens, connecting the adsorber to the condenser, and the system evolves to the subsequent regeneration phase. The adsorbate vapor flows from the adsorber to the condenser, where it condenses and releases heat to the domestic water. During this regeneration (desorption) phase, pressure inside the adsorber is equal to that in the condenser. The duration of the regeneration phase, t_{reg}, is also a control parameter of the system. Valve V_4 is closed to stop the regeneration phase, and the adsorber is separated from the condenser and from the evaporator once more. The isosteric cooling phase begins and during it there is no adsorbate flowing in or out the adsorber. The electric heater is turned off during this phase, valve V_3 closes, valve V_2 opens, and the 3-way valve redirects the circulating HTF water flow into the reservoir. The cooler water collected from the bottom of the reservoir is circulated through the adsorber's tubes, reducing the temperature of the adsorbent. As a result, pressure inside the adsorber also reduces. This phase runs until the pressure measured by sensor P_a equals that in the evaporator, this measured by sensor P_e. Once these pressures are equal, the system is ready to start a new cycle by opening valve V_1. The system is designed to minimize the heat losses since the condenser can only exchange heat with the domestic water in the reservoir. Additionally, any excess heat generated by the electric heater ends up inside the water reservoir. If a high hot water demand occurs, it is possible to use the electric heater to directly heat the water and provide instantaneous hot water, setting aside the adsorption cycle and thus without taking advantage of the heat pumping effect.

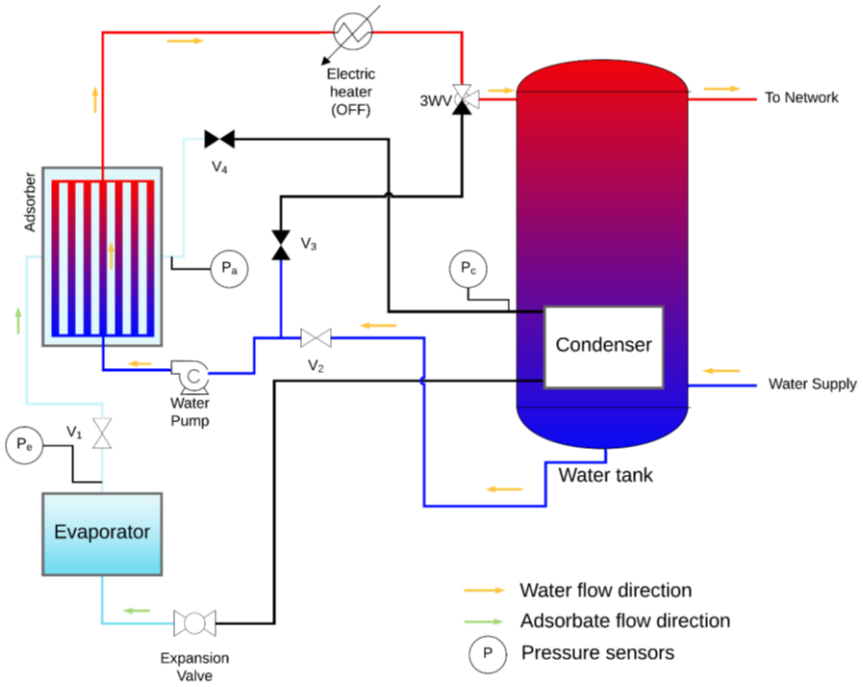

a)

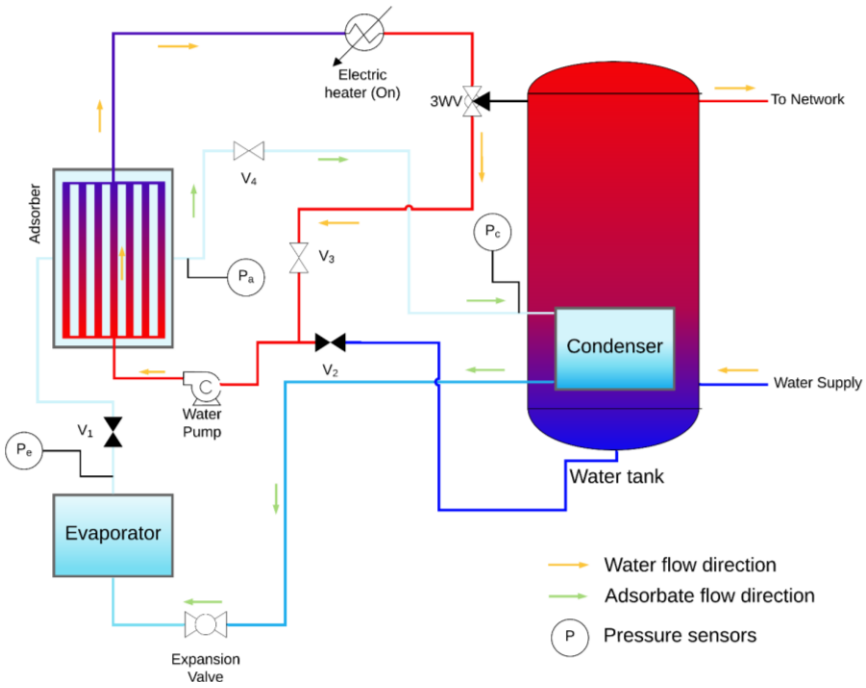

b)

Figure 6.4 – The AHP system: **a)** During the adsorption phase, and **b)** During the regeneration (desorption) phase.

Despite the developed AHP system is using electricity for the adsorbent regeneration, by the reasons discussed in the beginning of this section, it can work based on other driving thermal energies such as from gas burners, or even on renewable energies such as solar thermal energy, waste heat or biomass burners.

6.3. PHYSICAL MODEL

A physical model was developed capable of simulating the dynamics of the whole AHP system, considering and integrating all its main components. Usual models available in the literature consider the dynamics of the adsorber only, assuming as constants the variables and properties for the remaining system's components (Pesaran et al. 2016), and thus also the adsorber boundary conditions. The model presented and described in what follows is an evolution from a previously existing model discussed in Ref (Dias and Costa 2019a), which now considers the dynamics of all the main components of the whole AHP system, thus allowing more complete, more accurate, and deeper analyses and understandings of the complete system's dynamics, instead of the usual lumped parameter and segregated approaches (Pesaran et al. 2016; Verde et al. 2016; Seol et al. 2020). The main components considered in the physical model include the adsorber, the water reservoir, the evaporator, the condenser, and the water heater. The equations that result from modelling each of these components are all integrated at once, being connected by the boundary conditions for each component and by the interaction through the HTF. As this model considers the dynamics of all the involved variables and components, its predictions are closer to reality, allowing more complete, more accurate, and deeper analyses, developments, and improvements of the AHP systems.

The physical model is based on the mass and energy balances for each of the main components of the AHP system, and within some of them for slices/parts when a distributed parameters' analysis is considered. Since the adsorber is the heart of the system, a 2D distributed parameters model is used aiming to describe its dynamics with higher reliability. The domestic water reservoir is modelled through a 1D distributed parameters model. The remaining main components are modelled through lumped parameter approaches, as the involved variables are essentially uniform in each of them. It is also to be mentioned that the design and optimization of evaporators, condensers and electric heaters is not the objective of this work, several models suitable for that being available in the literature. Although different spatial approaches (2D, 1D and 0D (lumped)) are assumed for the AHP's main components, all of them are linked with each other in the resulting model for the

complete AHP system, thus allowing the dynamic simulation of the complete AHP system as whole.

The models for each of the AHP components are well established and accepted in the literature. The adsorber model equations are not new and have been proven to describe its dynamics. The main innovation of this work is to integrate all the validated models together and being able to get results that consider the complete adsorption heat pump system. Given that experimental studies for full scale adsorption heat pumps do not report all the necessary information (e.g. material properties, measured heat and mass transfer coefficients/resistances, among others), a true comparison cannot be made. However, the obtained results are in line with other experimental results found in the literature for full-scale AHP systems, and all the material properties as well as heat and mass transfer coefficients were taken from experimental measurements by other researchers, as specified in Section 6.4.

The developed model considers the following main assumptions:

- Geometry of the adsorbent layer is homogenous;
- Temperature and pressure are uniform along the angular direction of the annularly-shaped adsorbent layer;
- Temperatures are uniform in the evaporator and in the condenser;
- Pressures are uniform in the evaporator and in the condenser;
- There is no accumulation of adsorbate in the condenser, since it immediately flows to the evaporator after condensation (the desorption process duration is much longer than the time required for the adsorbate to drain from the condenser to the evaporator);
- Adsorbate vapor phase behaves like an ideal gas, and the adsorbed phase is in the liquid phase;
- Specific heats of the adsorbate vapor and liquid phases are constants;
- Adsorbate vapor surrounding the adsorbent is under saturated conditions;
- Thermophysical properties of solid materials remain constants;
- The pre-heating and pre-cooling phases end when pressure in the adsorber equals the condenser and evaporator pressures, respectively;
- Conditions are the same in all the adsorber tubular units.

6.3.1. Evaporator

The adsorbate mass balance equation for the evaporator of the whole AHP system may be expressed as:

$$\frac{dm_a}{dt} = -\left[m_s \frac{dX}{dt} + \varepsilon V_{s,t} \frac{d\rho}{dt}\right] \quad 6.1$$

and the energy balance equation for the evaporator is:

$$[m_e C_e + m_a C_a]\frac{dT_e}{dt} = U_e A_e (T_{amb} - T_e) + \frac{dm_a}{dt} L_e(\gamma) + \frac{dm_a}{dt} C_a (T_c - T_e)(\alpha) \quad 6.2$$

The global heat transfer conductance for the evaporator is $U_e A_e = 540\ \mathrm{W.K^{-1}}$. During the isosteric heating and cooling phases there is no adsorbate flowing into the evaporator, and the mass of adsorbent in the evaporator remains constant during these phases, that is, $\frac{dm_a}{dt} = 0$. Since during the adsorption phase the adsorbate only flows from the evaporator to the adsorber, $\gamma = 1$ and $\alpha = 0$ during this phase. During the regeneration phase the adsorbate flows to the evaporator after being condensed in the condenser, and thus $\gamma = 0$ and $\alpha = 1$ during this phase.

6.3.2. Condenser

Having already expressed the adsorbate mass balance equation (Eq. 6.1), and as no adsorbate accumulation occurs in the condenser, the condenser's energy balance equation can be written as:

$$m_c C_c \frac{dT_c}{dt} = U_c A_c (T_w - T_c) + \frac{dm_a}{dt}\left[L_c + C_{p,v}(T_s - T_c)\right](\beta) \quad 6.3$$

where,

$$U_c A_c = \frac{1}{\frac{1}{h_{\mathrm{in},c} A_{\mathrm{in,c}}} + \frac{ln\left(d_{\mathrm{out},c}/d_{\mathrm{in,c}}\right)}{2\pi k_c L_c} + \frac{1}{A_{\mathrm{out,c}} h_{\mathrm{out,c}}}} \quad 6.4$$

During adsorption and isosteric phases there is no adsorbate flow in the condenser, and it is $\beta = 0$. During the regeneration phase it is $\beta = 1$.

6.3.3. Electric heater

It is considered that all the thermal energy generated by the electric heater is transferred to the HTF water, the thermal efficiency of the electric water heater being approximately 100%. The heat rate in the electric heater is related with the HTF temperature increase as:

$$\dot{Q}_f = \dot{m}_f \, C_f \left(T_{f,out} - T_{f,in}\right) \tag{6.5}$$

$\dot{Q}_f = 0$ during the adsorption and isosteric cooling phases, and if $T_{f,in} \geq T_{reg}$, since the electric water heater is switched off in that case.

6.3.4. Water reservoir

The water reservoir is modeled using the finite volume method. Since $r_{\text{tank}} \ll L_{\text{tank}}$, the water temperature is considered not changing along the radial and angular directions in the tank. The reservoir is divided in N_h finite volumes as illustrated in Figure 6.5. The HTF water is taken from the bottom of the reservoir and returns to the reservoir at this top; thus, the HTF water flows downwards in the reservoir. The net supply (cold) water enters at the bottom of the reservoir, the demanded hot water leaving from the top of the reservoir; thus, the useful water flows upwards in the reservoir. The water reservoir has an internal diameter of 0.5 m and a height of 1.5 m. The energy and mass balance inside the water reservoir are modeled inside the solver by the finite volume method, taking into consideration the mass flow rate and temperature of the HTF, supply water, and domestic hot water inlets/outlets. Due to that, the balance equations for the water reservoir are presented considering the implementation of the finite volume method.

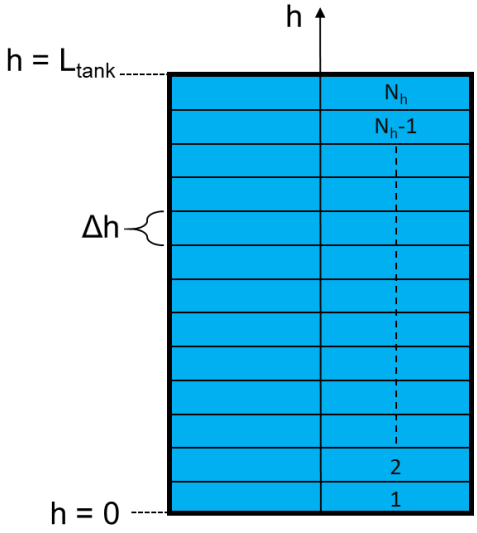

Figure 6.5 – Finite volume discretization of the water reservoir.

The energy balance equation for the bottom control volume of the reservoir is:

$$\frac{V_{tank}}{N_h}\rho_w C_w \frac{dT_w}{dt} = \pi U_{tank}\left(\frac{d_{tank}^2}{4} + d_{tank}\Delta h\right)\left(T_{amb,tank} - T_{w,1}\right) + \pi k_w \frac{d_{tank}^2}{4\Delta h}\left(T_{w,2} - T_{w,1}\right) + \dot{m}_{net} C_w \left(T_{w,net} - T_{w,1}\right) + \dot{m}_f C_f \left(T_{w,2} - T_{w,1}\right) \quad 6.6$$

for the upper control volume of the reservoir is:

$$\frac{V_{tank}}{N_h}\rho_w C_w \frac{dT_w}{dt} = \pi U_{tank}\left(\frac{d_{tank}^2}{4} + d_{tank}\Delta h\right)\left(T_{amb,tank} - T_{w,N_h}\right) + \pi k_w \frac{d_{tank}^2}{4\Delta h}\left(T_{w,N_h-1} - T_{w,N_h}\right) + \dot{m}_{net} C_w \left(T_{w,N_h-1} - T_{w,N_h}\right) + \dot{m}_f C_f \left(T_{f,z=L} - T_{w,N_h}\right) \quad 6.7$$

and for the internal control volumes of the reservoir is:

$$\frac{V_{tank}}{N_h}\rho_w C_w \frac{dT_{w,n}}{dt} = U_{tank}\pi d_{tank}\Delta h\left(T_{amb,tank} - T_{w,n}\right) + \pi k_w \frac{d_{tank}^2}{4\Delta h}\left(T_{w,n+1} - 2T_{w,n} + T_{w,n-1}\right) + \dot{m}_{net}C_w\left(T_{w,n-1} - T_{w,n}\right) + \dot{m}_f C_f\left(T_{w,n+1} - T_{w,n}\right) + UA_{c,n}\left(T_{c,n} - T_{w,n}\right)(\varphi) \quad 6.8$$

Depending on the size and position of the condenser, $\varphi = 1$ when the control volume includes part of the condenser and $\varphi = 0$ for the control volumes that do not include part of the condenser. The volume occupied by the condenser in each control volume where it is placed is neglected, as it is much smaller than the volume of the control volume and of the volume of water contained in it, and overall, the volume of the condenser is much smaller than the reservoir's internal volume.

6.3.5. Adsorber

The adsorber consists of several individual tubular units, a tubular unit being represented by the schematics in Figure 6.6. The physical model is applied to the layout of a single tubular unit, and it is assumed that all tubular units have similar behaviors. A 2D (radial and longitudinal) model is considered for the adsorber tubular unit.

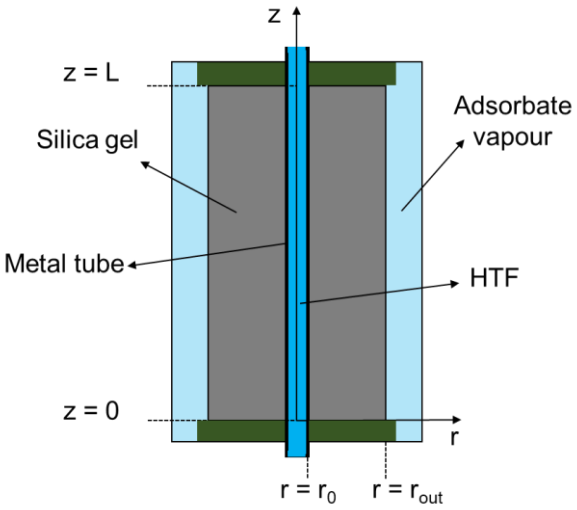

Figure 6.6 – Schematics of an adsorber's single tubular unit (figure not to scale).

The energy and mass balance equations that describe the adsorber dynamics are, respectively:

$$\frac{\partial\left(\rho C_p T_s\right)}{\partial t} + \nabla\left(\rho_v C_{p,v} T_s u\right) - \nabla(k_s \nabla T_s) - \rho_s(1-\varepsilon)\Delta H_{\text{ads}} \frac{\partial X}{\partial t} = 0 \qquad 6.9$$

$$\varepsilon \frac{\partial \rho_v}{\partial t} + \nabla(\rho_v u) + \rho_s(1-\varepsilon)\frac{\partial X}{\partial t} = 0 \qquad 6.10$$

where

$$\rho C_p = \varepsilon \rho_v C_{p,v} + \rho_s(1-\varepsilon)(C_s + X C_l) \qquad 6.11$$

and

$$\varepsilon = \varepsilon_{\text{bed}} + (1-\varepsilon_{\text{bed}})\varepsilon_p \qquad 6.12$$

Equations 6.9 and 6.10 can be rearranged as:

$$\begin{aligned}\left[\rho_s(1-\varepsilon)(C_s+XC_l)+\varepsilon\rho_v C_{p_v}\right]\frac{dT_s}{dt} = \\ = (1-\varepsilon)\rho_s\Delta H_{\text{ads}}\frac{dX}{dt}+\frac{k_s}{r}\left(\frac{\partial T_s}{\partial r}+r\frac{\partial^2 T_s}{\partial r^2}\right) \\ -\frac{C_{p_v}}{r}\left(\rho_v T_s u_r + rT_s u_r\frac{\partial\rho_v}{\partial r}+r\rho_v u_r\frac{\partial T_s}{\partial r}+r\rho_v T_s\frac{\partial u_r}{\partial r}\right) \\ -C_{p_v}\left(T_s u_z\frac{\partial\rho_v}{\partial z}+\rho_v T_s\frac{\partial u_z}{\partial z}+\rho_v u_z\frac{\partial T_s}{\partial z}\right)+k_s\left(\frac{\partial^2 T_s}{\partial z^2}\right)\end{aligned} \quad 6.13$$

$$\frac{\partial\rho_v}{\partial t} = -\frac{1}{\varepsilon}\left[\rho_s(1-\varepsilon)\frac{\partial X}{\partial t}+\frac{1}{r}\left(ru_r\frac{\partial\rho_v}{\partial r}+\rho_v r\frac{\partial u_r}{\partial r}+\rho_v u_r\right)+\rho_v\frac{\partial u_z}{\partial z}+u_z\frac{\partial\rho_v}{\partial z}\right] \quad 6.14$$

The momentum balance is described by the Darcy's Law, equation 6.15, using the Blake-Kozeny model, equation 6.16, to obtain the permeability of the annularly-shaped adsorbent bed (Wilkes and Birmingham 2006).

$$u = -\frac{k_D}{\mu}\nabla P \quad 6.15$$

$$k_D = \frac{d_p^2\varepsilon^3}{150(1-\varepsilon)^2} \quad 6.16$$

The time rate of change of the adsorbate concentration in the adsorbent, also referred to as uptake, is described by the Linear Driving Force (LDF) model as (Sircar 1983):

$$\frac{dX}{dt} = K_{LDF}\left(X_{eq}-X\right) \quad 6.17$$

The K_{LDF} constant is obtained as (Aristov 2009):

$$K_{LDF} = \frac{15 D_{ef0} e^{-\frac{E_a}{R' T_s}}}{R_p^2} \tag{6.18}$$

The equilibrium adsorbate concentration in the adsorbent, X_{eq}, depends on the adsorbent-adsorbate working pair. For the silica gel-water working pair it can be obtained as (Chua et al. 2002):

$$X_{eq} = \frac{P k_0 e^{\frac{\Delta H_{ads}}{R' T_s}}}{\left[1 + \left(\frac{P k_0}{q_m} e^{\frac{\Delta H_{ads}}{R' T_s}}\right)^{t_{SG}}\right]^{\frac{1}{t_{SG}}}} \tag{6.19}$$

The heat exchanges between the HTF water and the adsorbent are obtained from the energy balance equations for the HTF and for the inner tube, which are, respectively:

$$\rho_f C_{p,f} \frac{\partial T_f}{\partial t} = k_f \left(\frac{\partial^2 T_f}{\partial z^2}\right) - u_f \rho_f C_{p,f} \frac{\partial T_f}{\partial z} + \frac{4 h_{f \to m}}{d_{in}} \left(T_m - T_f\right) \tag{6.20}$$

$$\rho_m C_m \frac{dT_m}{dt} = k_m \left(\frac{\partial^2 T_m}{\partial z^2}\right) + \frac{4 d_{in} h_{f \to m} \left(T_f - T_m\right)}{d_{out}^2 - d_{in}^2} + \frac{4 d_{out} h_{m \to s} (T_s - T_m)}{d_{out}^2 - d_{in}^2} \tag{6.21}$$

The HTF velocity, u_f, is constant along the tube, and it is assumed that $\frac{\partial T_f}{\partial r} \approx 0$ given that $r_{tube} \ll L_{tube}$. The same applies to the inner metal tube, for which $\frac{\partial T_m}{\partial r} \approx 0$.

The convection heat transfer coefficient between the HTF and the inner surface if the inner tube is expressed as:

$$h_{f\to m} = \frac{Nu_f k_f}{d_{in}} \quad 6.22$$

When the HTF flows is in the laminar regime, corresponding to $Re_f \leq 2300$, the Nusselt number is evaluated using the correlation for a uniform heat transfer flux as (Bergman et al. 2011):

$$Nu_f = 4.36 \quad 6.23$$

For HTF turbulent flow conditions, corresponding to $Re_f > 2300$, if $Re_f \leq 5 \times 10^6$ and $0.5 \leq Pr \leq 2000$ the Gnielinsky correlation may be used to evaluate the Nusselt number as (Gnielinski 1976):

$$Nu_f = \frac{\left(f/8\right)\left(Re_f - 1000\right)Pr}{1 + 12.7\left(f/8\right)^{1/2}\left(Pr^{2/3} - 1\right)} \quad 6.24$$

the friction factor *f* being obtained from the Petukhov's correlation (Petukhov 1970):

$$f = \left(0.79ln\left(Re_f\right) - 1.64\right)^{-2} \quad 6.25$$

The spatial resolution has significant influence on the accuracy of the adsorber's AHP models (Dias and Costa 2019a). The resolutions used on the radial and axial directions are $\Delta r = 5 \times 10^{-5}\ m$ and $\Delta z = 8.33 \times 10^{-2}\ m$, respectively. The initial and boundary conditions are prescribed below. The water temperature at the inlet of the adsorber, $T_f\big|_{\mathrm{z=0}}$, is equal to the temperature at the outlet of the water reservoir, $T_{w,1}$, during the adsorption and pre-cooling phases, and equal to the temperature at the outlet of the water heater, $T_{f,\mathrm{out}}$, during the regeneration and pre-heating phases. The water temperature at the inlet of the water reservoir is equal to the temperature at the outlet of the adsorber, $T_f\big|_{\mathrm{z=L}}$, since the electric heater is turned off when water is being sent to the reservoir. Unlike as in many of the

previous models in the literature, the evaporator and condenser pressures are not constant when considering the whole system operation but, instead, are changing in time, what significantly affects the adsorber dynamics.

$$t_{ini} = 0 \qquad P(t_{ini}) = P_{ini}$$

$$T_m(t_{ini}) = T_f(t_{ini}) = T_s(t_{ini}) = T_{ini} \qquad X(t_{ini}) = X_{eq}\left(P_{ini}, T_{s_{ini}}\right)$$

$$\left.\frac{\partial P}{\partial r}\right|_{r=r_{in}} = \left.\frac{\partial P}{\partial r}\right|_{z=0} = \left.\frac{\partial P}{\partial r}\right|_{z=L} = 0$$

$$P|_{r=r_{out}} = P_e, \qquad Adsorption$$

$$P|_{r=r_{out}} = P_c, \qquad Regeneration$$

$$\left.\frac{\partial P}{\partial r}\right|_{r=r_{out}} = 0, \qquad Cooling/Heating$$

$$-k_s \left.\frac{\partial T_s}{\partial r}\right|_{r=r_{in}} = h_{m\to s}(T_m - T_s)$$

$$\left.\frac{\partial T_s}{\partial r}\right|_{r=r_{out}} = \left.\frac{\partial T_s}{\partial z}\right|_{z=0} = \left.\frac{\partial T_s}{\partial z}\right|_{z=L} = 0$$

$$T_f\big|_{z=0} = T_{w,1}\,, \qquad Adsorption/Cooling$$

$$T_f\big|_{z=0} = T_{reg}\,, \qquad Regeneration/Heating$$

$$\left.\frac{\partial T_f}{\partial z}\right|_{z=L} = 0$$

$$\left.\frac{\partial T_m}{\partial z}\right|_{z=0} = \left.\frac{\partial T_m}{\partial z}\right|_{z=L} = 0$$

6.3.6. Model's solution

The equations that result from modelling each component, some of them modeled through their decomposition in control volumes, are all interconnected. The pipes and hoses used to connect components are assumed to be perfectly insulated and imposing negligible pressure drops, thus having insignificant impact on the system's dynamics and behavior. The water temperature at the inlet of the electric heater, $T_{f,\mathrm{ini}}$, is assumed to be equal to its temperature when exiting the adsorber, $T_f\big|_{\mathrm{z=L}}$. The pressure in the evaporator and in the condenser depend on the temperature in each of these heat exchangers, being obtained according to reference (Lemmon et al. 2017).

The physical models result in a set of partial differential equations that require significant computational efforts to be solved. The longitudinal derivatives in the water reservoir and the radial and longitudinal derivatives in the adsorber module are discretized (within each time step) using the method of lines. Finite difference method is used to express radial and axial derivatives, transforming the set of partial differential equations in a set of ordinary differential equations, solved using the adaptative timestep solver "ode15s" from Matlab R2020b, adequate for solving stiff ordinary differential equations (Shampine and Reichelt 1997). A grid independence study for the adsorbent bed has already been carried out, concluding that a spatial resolution of $\Delta r = 5 \times 10^{-5}\ \mathrm{m}$ and $\Delta z = 8.33 \times 10^{-2}\ \mathrm{m}$ is suitable for detailed and accurate adsorber description (Dias and Costa 2019a). The domestic hot water reservoir was divided in 150 control volumes, resulting in a resolution of 0.01 m. To make the results independent from the initial conditions, the model performs pre-starting simulations for ten successive cycles assuming a very high value for U_{tank}, allowing the stabilization of the entire system. The warming up period for the uptake (selected as an example) is presented in Figure 6.7, where it is noticeable that the system is stable enough and independent from the initial conditions. After this warming up, the U_{tank} value is set to its realistic value and the next cycle is thus independent from the selected initial conditions. This approach makes the model more robust and eliminates the difficulty of selecting realistic initial conditions, what is hard to accomplish given the complexity of adsorption process and the interlinks between the involved variables.

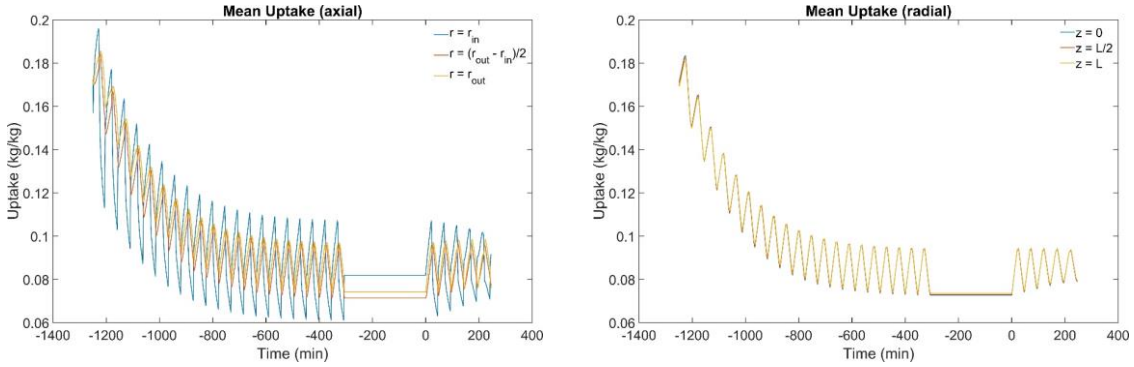

a) **b)**

Figure 6.7 – Time evolution of the uptake, including the warming up period, for the bottom, middle, and top layers, **a)** mean axial uptake; **b)** mean radial uptake.

6.4. RESULTS AND DISCUSSION

Two Two sets of results are presented and discussed, obtained from simulating five complete cycles of the complete proposed system. The first set of results includes the dynamics of the adsorbent bed as given by temperature, pressure, and uptake at selected instants of pre-cooling, adsorption, pre-heating, and regeneration phases. The time evolution of these variables throughout the adsorption bed for the first cycle is presented in video format as supplementary material (Link to video1). The second set of results includes the time evolution of all the meaningful system components for the same five cycles. The set of parameters, thermophysical properties and working conditions that were adopted for the simulations are summarized in Table 6.1. Some of these parameters and thermophysical properties were gathered from several studies on the silica gel-water working pair available in literature (Ng et al. 2001; Chua et al. 2002; Di et al. 2007; Chakraborty et al. 2014; Sun and Chakraborty 2015).

Table 6.1 – Reference parameters used in the simulations.

Parameter	Value	Units
C_{m}	910	J.kg^{-1}.K^{-1}
C_{l}	4184	J.kg^{-1}.K^{-1}
C_{pv}	1869	J.kg^{-1}.K^{-1}
C_{s}	921	J.kg^{-1}.K^{-1}
d_{p}	3.5×10^{-4}	m
$d_{\mathrm{in,c}}$	0.005	m
$d_{\mathrm{out,c}}$	0.007	m
$d_{\mathrm{in,tube}}$	0.01	m
d_{tank}	0.5	m
E_a	2.3314×10^{6}	J.kg^{-1}
$h_{\mathrm{in,c}}$	750	W.m^{-2}.K^{-1}
$h_{\mathrm{out,c}}$	750	W.m^{-2}.K^{-1}
$h_{\mathrm{m\rightarrow s}}$	30	W.m^{-2}.K^{-1}
k_0	7.3×10^{-13}	kg.kg^{-1}.Pa^{-1}
k_{c}	205	W.m^{-1}.K^{-1}
k_{f}	0.6	W.m^{-1}.K^{-1}
k_{m}	205	W.m^{-1}.K^{-1}
k_{s}	0.198	W.m^{-1}.K^{-1}
L_{c}	15	m
L_{tube}	1	m
L_{tank}	1.5	m
$m_{\mathrm{s,\ tube}}$	0.325	kg
ΔH_{v}	2.3×10^{6}	J.kg^{-1}
q_{m}	0.45	kg.kg^{-1}
$\dot{Q}_f$	5000	W
t_{ads}	1250	s
$T_{\mathrm{w,\ ini}}$	$273.15 + 20$	K
$T_{\mathrm{amb,e}}$	$273.15 + 12$	K
$T_{\mathrm{f,reg}}$	$273.15 + 90$	K
t_{reg}	$0.9 \times t_{ads}$	s
t_{SG}	12	-
u_{f}	0.05	m.s^{-1}
ΔH_{ads}	2.693×10^{6}	J.kg^{-1}
ε	0.4	-
ρ_{m}	2700	kg.m^{-3}
ρ_{s}	2027	kg.m^{-3}
σ_{s}	0.005	m
σ_{tube}	0.001	m

The duration of the pre-heating and pre-cooling phases is indirectly controlled by the pressure sensors P_c and P_e, respectively. These phases end when the pressure in the outer layer of the adsorbent bed at $z = \frac{L}{2}$ is equal to the condenser and evaporator pressure, respectively for the pre-heating and pre-cooling phases. Consequently, the duration of pre-heating and pre-cooling phases depend on several parameters such as water flow rate, regeneration temperature, electric heater power, tube diameters and the heat transfer coefficient between the metal tube and the adsorbent material. Thermodynamically, it depends on the condenser's temperature since the higher the temperature in the condenser the higher the pressure lift that must be achieved before moving onto the regeneration phase.

6.4.1. Temperature, pressure, and uptake fields

The temperature, pressure and uptake distributions in the adsorbent bed are critical to understand the AHP system's dynamics. These distributions are presented in Figure 6.8 for the pre-cooling and adsorption phases, and in Figure 6.9 for the pre-heating and regeneration phases. It is evidenced that the temperature, pressure, and uptake changes in the adsorbent bed occur at different paces. Although the temperature and pressure in the adsorbent bed are attached to each other, pressure's evolution is faster than temperature's during each of the four phases, as expected. The HTF water circulates in the positive direction of *z* axis during the entire cycle. In the graphics are just represented the variables' distributions in the adsorbent bed, although they are calculated for the remaining components as described in the previous section.

Temperature and pressure differences along the adsorbent bed are higher during the pre-cooling and pre-heating phases. When these phases end, there are high heterogeneities on the temperature, pressure, and uptake values along the bed, which can only be reliably simulated using a distributed parameter model. Even during the adsorption and regeneration phases, there is a noticeable heterogeneity on the uptake value throughout the adsorbent bed. One of the most important conclusions that can be taken from the analysis of the temperature, pressure and uptake distributions in the adsorbent bed is that a real scale system cannot be accurately modelled through lumped parameter models. As it can be seen, even for small adsorbent bed thicknesses under 5 mm, there are significant heterogeneities on the temperature, pressure, and uptake distributions in the adsorbent bed. The uptake is the most heterogeneous variable since it is locally influenced not only by temperature and pressure but also by the mass transfer rate inside the bed. This

is evident at the instant t = 160 s, during the adsorption phase, the uptake in the middle of the adsorbent bed being significantly lower than in the bed's inner and outer zones.

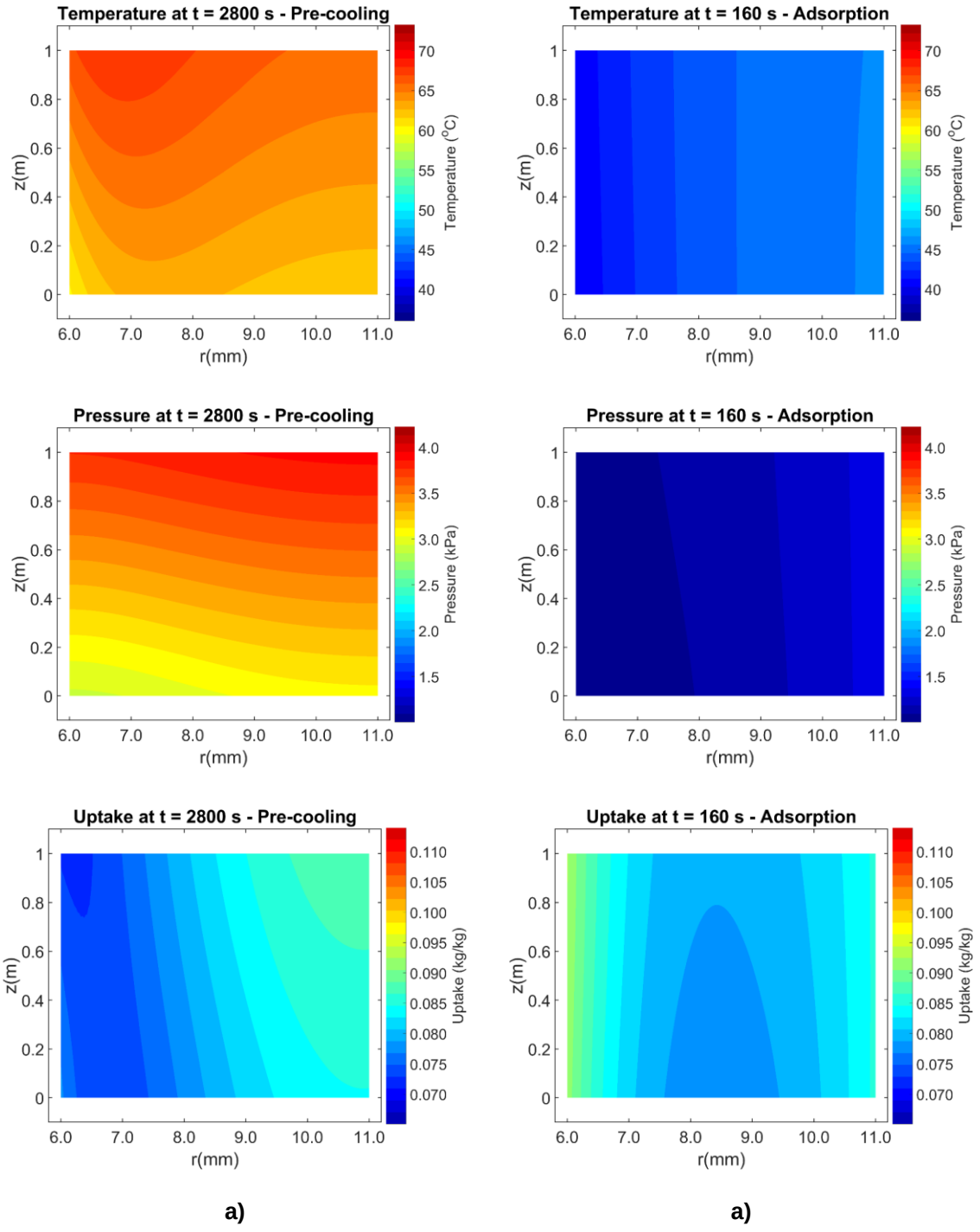

Figure 6.8 – Temperature, pressure, and uptake distributions in the adsorbent bed at selected instants **a)** during pre-cooling; **b)** during adsorption.

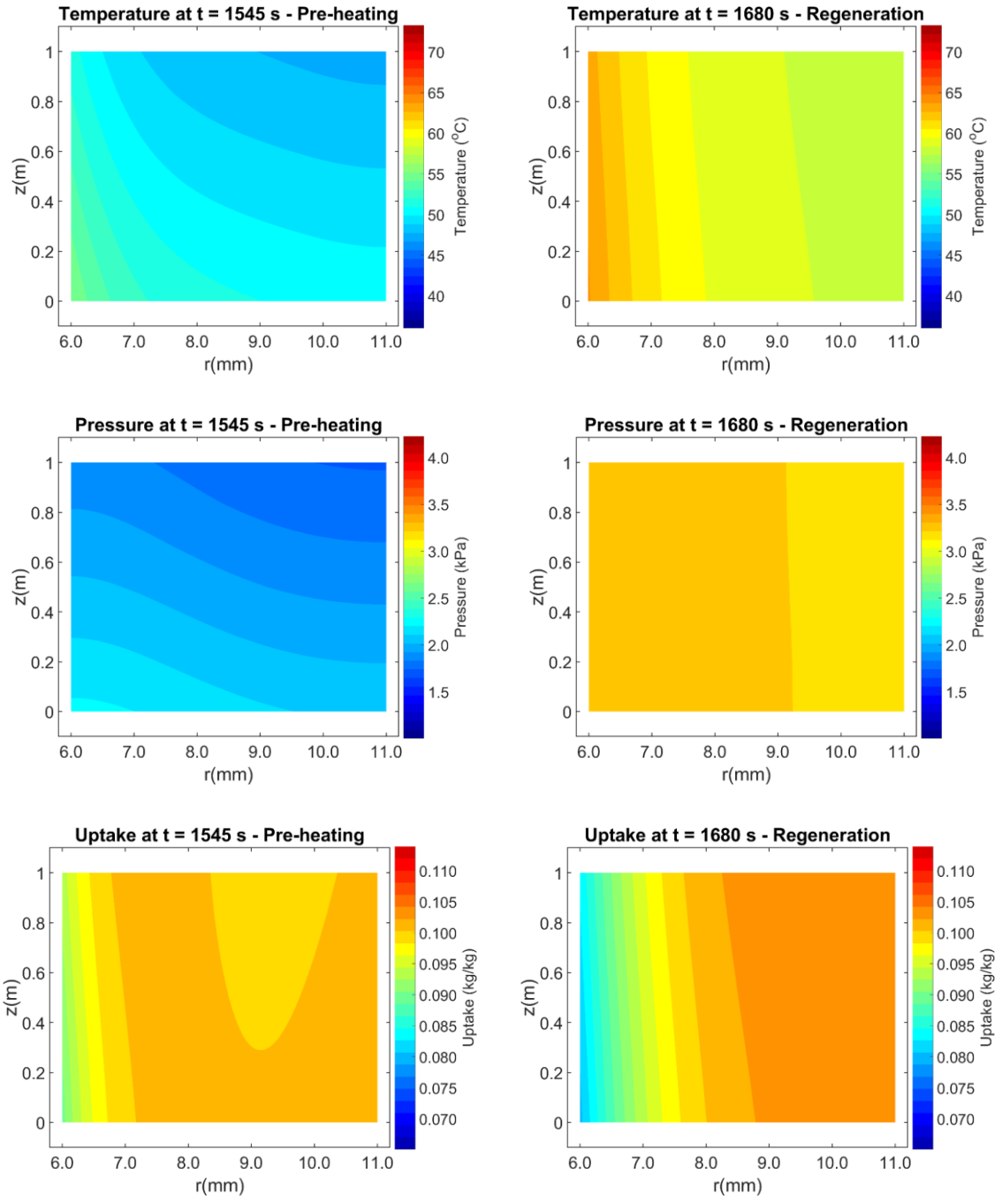

Figure 6.9 – Temperature, pressure, and uptake distributions in the adsorbent bed at selected instants, **a)** during pre-heating **b)** during regeneration.

6.4.2. System's time evolution

The time evolution of the complete proposed AHP system was simulated for five complete cycles and the uptake, bed temperature and pressure, evaporator and condenser temperatures, adsorbate mass and domestic water temperature were analyzed. Concerning the adsorbent bed, the uptake, temperature, and pressure are represented by their axial and radial means. The axial mean of a variable is obtained as its mean along the axial direction for a given radial position. Analogously, the radial mean of a variable is obtained as its mean along the radial direction for a particular axial position. The five cycles sequence starts at the instant t = 0 s, corresponding to the beginning of the adsorption phase.

The temperature time evolution in the adsorbent bed is represented in Figure 6.10. It can be seen that the bed temperature does not significantly change along the axial direction, for the considered HTF's velocity. However, along the radial direction there are meaningful changes. The lowest and highest temperatures are always achieved in the adsorbent bed's inner layer. The temperature difference achieved in the adsorbent bed decreases along the radial direction, since it is affected by the bed's thermal resistance. There are two interesting points that result from considering the whole AHP system, which are worth pointing out in Figure 6.10. Analyzing the mean axial bed temperature for $r = r_0$ it is noticeable that the bed's temperature assumes a smooth decreasing rate during the first adsorption phase. As the cycle develops, in the following adsorption phase the bed's temperature decreases and then starts to increase even during the adsorption phase. This behavior results from the increase on the water temperature in the reservoir, as the water in the reservoir is being used as the HTF. At the beginning of the adsorption phase, the colder water from the bottom of the reservoir is circulated through the adsorber. As the adsorption phase carries on, the warmer water stored in the upper layers of the reservoir starts to move down, which means that after some time the water taken from the bottom of the reservoir is warmer than when the adsorption phase started and will lead to the increase of the bed's temperature even during the adsorption phase. The other issue that results from considering the whole system is that the minimum bed's temperature, achieved during the adsorption phase, increases from cycle to cycle, since the water temperature in the reservoir will be also increasing from cycle to cycle. In addition, setting the HTF regeneration temperature to 90 °C is not enough to raise the bed's temperature to that same temperature due to heat transfer resistances in between. The maximum temperature achieved during regeneration is around 70-75 °C at the inner layer of the adsorbent bed. To increase this temperature, the HTF must be heated

to a higher temperature level. However, heating water close to or over 100 °C would require extra safety precautions due to its probable liquid-vapor phase change, and therefore the HTF's temperature was limited to 90 °C.

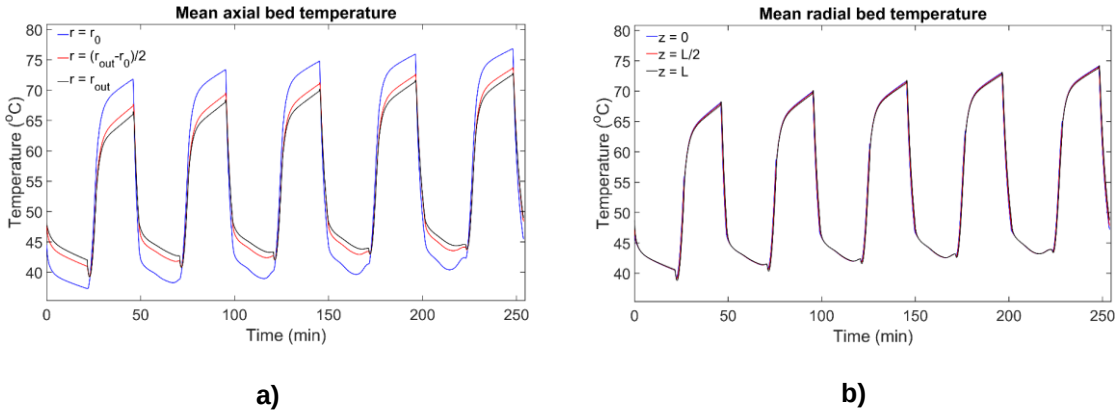

a) **b)**

Figure 6.10 – Time evolution of the adsorbent's bed temperature for the bottom, middle and top layers, **a)** mean axial temperature; **b)** mean radial temperature.

The effect of the water reservoir temperature dynamics is even more noticeable when analyzing the adsorbent bed's pressure. As it is shown in Figure 6.11, the maximum mean pressure, achieved during the regeneration phase, increases from cycle to cycle due to the increase of the condenser's pressure caused by its temperature increase. The same effect is not observed for the minimum mean pressure as its value is dictated by the evaporator's pressure, which does not significantly change in the simulated scenario. Similarly, as to the temperature case, there are no meaningful pressure variations along the axial direction, but they are significant along the radial direction. The effect of the decreasing and then slightly increasing pressure during the adsorption phase is, as already explained, more notorious in the inner layers of the adsorbent bed, since the outer layers are directly exposed to the evaporator's pressure. Although the pressure and temperature are attached, naturally, pressure changes occur much faster than temperature changes. Small sharp variations in the pressure occur when the system moves from adsorption/regeneration phases to the pre-heating/pre-cooling phases. After the adsorption phase ends, the adsorber is immediately isolated from the condenser and the evaporator by closing the valve V_1, but it still takes some time for the HTF to heat up, what means that for a short period the adsorber is still being cooled and isolated from the heat exchangers, causing its slight pressure decrease. This effect is more noticeable in the outer layers of the adsorbent bed since it

takes even longer times for the heat to reach them due to the heat resistance of the adsorbent bed itself. When moving from the regeneration phase to the pre-cooling phase the effect appears in the inverse order. Although this effect can be seen in the temperature (Figure 6.9), it is much more noticeable in the pressure graphics as the pressure changes happen much quicker than temperature changes, especially when the adsorber is isolated from the remaining components.

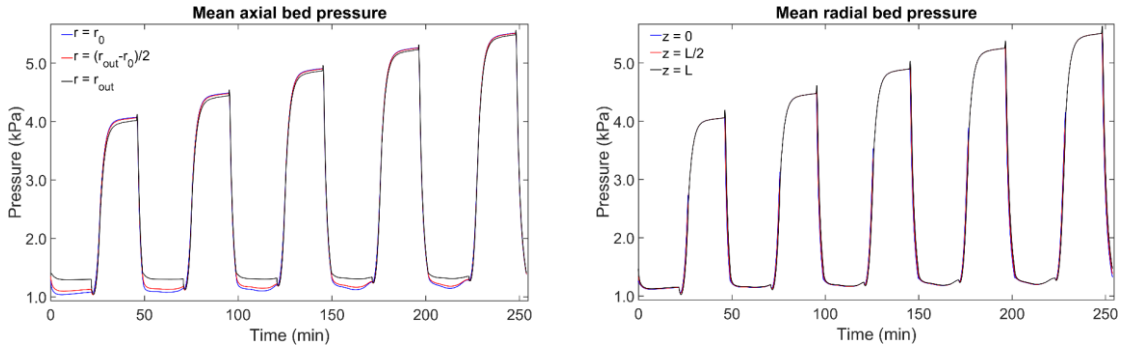

a) **b)**

Figure 6.11 – Time evolution of the adsorbent's bed pressure for the bottom, middle and top layers, **a)** mean axial pressure; **b)** mean radial pressure.

The uptake time evolution is represented in Figure 6.12, where it is obvious that its distribution is different along the axial and radial directions. The uptake variation along the axial direction is only noticeable during the pre-cooling phase, for the HTF velocity considered. For lower HTF velocities, the uptake difference along the axial direction may start to increase. On the other hand, the uptake variation is notorious over the radial direction, specially right after a phase change in the cycle. This variation depends on the adsorbent bed thermal conductivity and on the mass transfer resistance. Moreover, the uptake change throughout the adsorbent bed is not linear, which leads to inaccurate values when evaluating a mean uptake and using it as a representative value of the entire adsorbent bed for performance predictions. This inaccuracy is increased by the fact that the mass of adsorbent varies with the square of the annularly shaped bed radius. By closely analyzing the mean axial uptake from Figure 6.10 there are interesting points that can be observed. Given that the minimum and maximum bed temperatures always occur at the adsorbent bed's inner layer, the minimum and maximum uptake follows the same tendency. However, even though the outer layer temperature is lower, the uptake is higher there than on the middle layer since the outer layer is directly exposed to the adsorbate vapor and is

thus not affected by the bed's mass transfer resistance. In addition, the fact that the heat exchange occurs on the adsorbent bed's inner layers, and the adsorbate exchange on its outer layers leads to an unexpected inflection and increase on the outer and middle layers' uptake, respectively, after the end of the adsorption phase. Also, at the beginning of the pre-cooling phase the uptake starts to increase at the inner layer while it is still decreasing in the middle and outer layers. Finally, the effect of the increasing temperature of the water in the reservoir over the cycles is notorious on the uptake time evolution. The increasing temperature of the water circulated through the adsorber reduces the maximum uptake that can be reached from cycle to cycle. Furthermore, as the reservoir's water temperature increases, the condenser's pressure rises and leads to a higher minimum uptake over the cycles. Consequently, the adsorbate flow during each cycle slowly decreases from one cycle to the next, while the AHP system is heating the water in the reservoir. One last aspect is that the system could benefit from using a higher regeneration temperature to compensate for the heat transfer resistances between the HTF and the adsorbent bed but, as previously mentioned, it would require safety measures or a different HTF with a higher boiling point. Increasing the cycle time would also result in higher uptake variations, but it would result in lower specific heating powers.

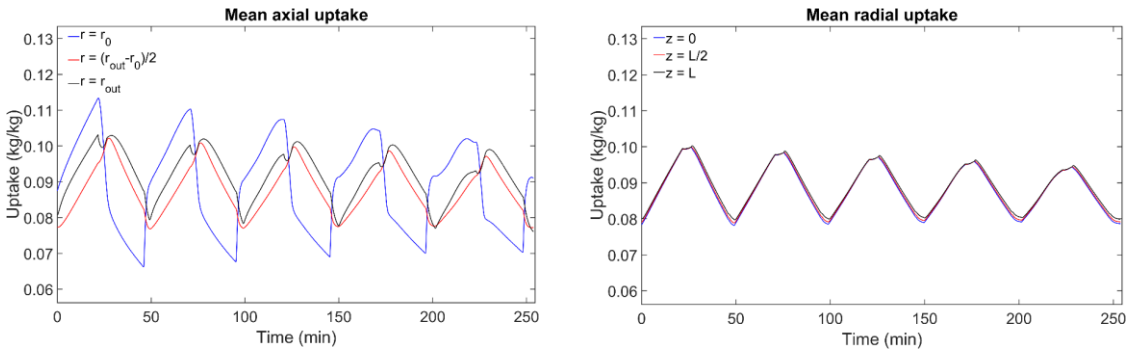

a) **b)**

Figure 6.12 – Time evolution of the adsorbent's bed uptake for the bottom, middle and top layers, **a)** mean axial uptake; **b)** mean radial uptake.

The evaporator temperature does not experience significant changes. The reason for the evaporator temperature being almost constant is that it is externally exposed to the ambient temperature, which was constant. In addition, the selected evaporator heat transfer capacity (conductance) was intentionally oversized, so that it would not limit the

performance of the system. Thus, evaporating the adsorbate during the adsorption phase only causes an evaporator slight temperature reduction, and it rapidly returns to ambient temperature after the phase ends due to the high heat transfer conductance of the evaporator. Given its high heat transfer conductance and the low adsorbate flow rate, the evaporator can exchange heat with the ambient without significantly changing its temperature. Figure 6.13.a) shows a decrease on the evaporator's temperature, of slightly over 1 °C, right after the opening of the valve V_1, which quickly returns to the ambient temperature once the adsorption phase ends. However, the decrease on the evaporator's temperature consequently lowers its pressure, which influences the pressure inside the adsorber during the adsorption phase. This effect is observable on the time evolution of the adsorbent bed pressure from Figure 6.9. As time evolves, the decrease on the evaporator's temperature during the adsorption phase becomes smaller due to the reduced amount of adsorbate that is changing phase from cycle to cycle, what is observable from Figure 6.13.b). During the first cycle approximately 0.33 kg of adsorbate changes phase, whereas in the last cycle the adsorbate changing phase is only of about 0.22 kg. Analogously to the uptake, to increase the adsorbate changing phase without changing the adsorbent-adsorbate working pair, the cycle time or the regeneration temperature must increase. The other option is to increase the mass of adsorbent by increasing the size of the adsorber, but maintaining the annularly shaped adsorbent bed thickness, which could be achieved by increasing the number of tubes or increasing the length of each tube, since the changes along the tube's length are not significant. It is also noticeable that the periods when there is no adsorbate mass change in the evaporator slightly increase from cycle to cycle. These periods correspond to the pre-cooling (top levels) and pre-heating (bottom levels) phases. Pre-heating and pre-colling periods increase from cycle to cycle due to the inherent water temperature (condenser temperature) increase. The higher the temperature difference between the evaporator and condenser, the longer the pre-cooling/pre-heating period will be, leading to longer cycle times. The increase of the cycle time will hindrance the SHP, meaning that each consecutive cycle will have lower SHP then the previous one, until the reservoirs water is used and replaced by colder supply water.

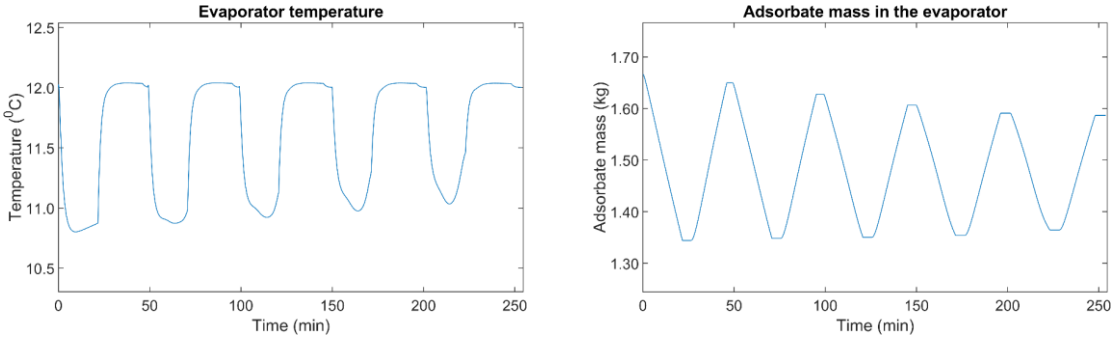

a) **b)**

Figure 6.13 – Time evolution of, **a)** the evaporator's temperature; and **b)** the adsorbate mass in the evaporator.

The condenser's temperature highly influences the dynamics of the AHP system, as its increase also increases its pressure, forcing that the regeneration phase occurs at higher pressures, requiring more thermal energy. Furthermore, the desorption process is less efficient for higher pressures, considering the same regeneration temperature. **Figure 6.14** The time evolution of the condenser temperature and the average water temperature of the reservoir's control volumes that contain the condenser are presented in Figure 6.14.a). The condenser is placed at a height of 0.25 m relatively to the bottom of the reservoir and extends until 0.75 m, occupying 50 finite volumes of the reservoir. The temperature of the condenser mainly increases during the regeneration phase due to the adsorbate condensation, resulting in higher temperature differences between the condenser and the reservoir's water. It is evident that over the cycles the condenser's temperature increases, decreasing the temperature difference that drives the heat transfer from the condenser to the water in the reservoir, thus penalizing the system's performance. Even within each regeneration phase, it is noticeable that the condenser's temperature is slightly increasing, leading to the pressure increase that is seen in the adsorbent bed pressure graphics (Figure 6.10). During the remaining phases, the temperature of the condenser is naturally the same as that of the water around it since the condenser thermal inertia is very low and its heat transfer conductance very high. During the pre-cooling and adsorption phases the temperature of the water in the reservoir varies along its height due to the HTF water circulation, which causes temperature variations in the zone where the condenser is placed, and consequently causing changes its temperature. This deserves additional attention and should be considered in future studies.

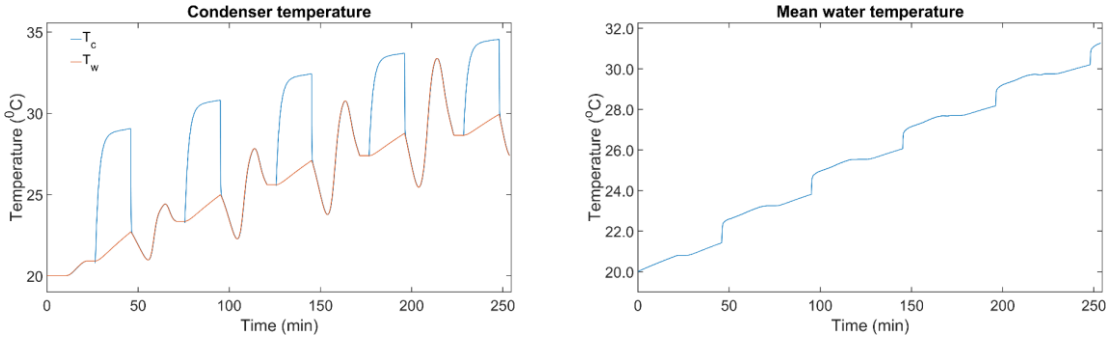

a) **b)**

Figure 6.14 – Time evolution of, **a)** the condenser's temperature and mean water temperature in the reservoir's control volumes that contain the condenser; and **b)** the reservoir's mean water temperature.

The main objective of the AHP system is to heat the water in the reservoir, requiring an amount of thermal energy to operate the system that is smaller than that delivered to the hot water. Figure 6.14 shows the reservoir's mean water temperature over the considered five cycles. The water inside the reservoir was heated from 20 °C to 31 °C in approximately 4h. A fast water temperature lift occurs when the hot water used to regenerate the adsorbent is returned to the water reservoir. The heat obtained from the adsorption process decreases as the water temperature in the reservoir increases due to two main reasons. Firstly, as previously mentioned, the condenser's temperature increase diminishes the regeneration effectiveness. Secondly, the water taken from the reservoir to cool down the adsorber during the pre-cooling and adsorption phases becomes warmer from cycle to cycle, what slightly increases the adsorbent bed's temperature during the adsorption phase. This means that systems with higher heating powers will have lower COPs for the same heat requirements, since the water temperature (condenser temperature) will have a higher increase within each cycle, meaning that the difference between the evaporator and condenser temperatures will be higher Achieving the optimal balance between the COP and the heating power of an AHP system can be challenging and would deserve to be explored. In addition, the size of the water tank has a significant impact on the whole system's performance, given that small tanks will increase their temperature faster, making the AHP system work further away from the optimal performance conditions.

6.4.3. System's performance evaluation

The performance of the proposed complete AHP was evaluated considering two separate approaches. Calculation of the performance of AHP systems based on the heat involved in the adsorption process is a common approach, that gives a good insight on the adsorber's performance. However, in order to get the whole system's real performance, the ratio between the heat delivered to the water in the reservoir and the energy used to drive the system must be considered. Thus, the COP and SHP were calculated for the adsorber and for the whole system.

For the adsorber, the conventional formulas that derive from the energy analysis of the cycle were used (Demir et al. 2008; Dias and Costa 2018):

$$COP_{adsorber} = \frac{Q_c + Q_{pre-cooling} + Q_{ads}}{Q_{pre-heating} + Q_{reg}} \quad 6.26$$

$$SHP_{adsorber} = \frac{Q_c + Q_{pre-cooling} + Q_{ads}}{m_s \tau_{cyc}} \quad 6.27$$

To evaluate the whole system's performance, the heat delivered to the reservoir's water and the heat required from the electric heater were considered. The necessary energy to drive the water pump and all the sensors and valves was not taken into account since it stands for just a tiny fraction of the energy requirements to operate the whole AHP system.

$$COP_{system} = \frac{Q_w}{Q_{eh}} \quad 6.28$$

$$SHP_{system} = \frac{Q_w}{m_s \tau_{cyc}} \quad 6.29$$

TThe performance evaluation was carried out considering the five cycles analyzed in the Section 4.2. The adsorber performance parameters when included in the AHP system are $COP_{\text{adsorber}} = 1.58$ and $SHP_{\text{adsorber}} = 57.6$ W.kg^{-1}. Regarding the complete system, the performance parameters obtained for the considered conditions are $COP_{\text{system}} = 1.35$ and $SHP_{\text{system}} = 79.3$ W.kg^{-1}. As expected, the COP is higher for the adsorber than for the whole

system since there is some delay on the energy delivering from the adsorber to the water in the reservoir, and a small portion of it may not be used for the useful purpose of water heating. In addition, when calculating the COP_{adsorber}, not all the energy required from the electric heater is considered but only that portion that was truly involved in the adsorbent regeneration, whereas the COP_{system} includes the total energy delivered by the electric heater. An interesting result is the higher SHP obtained for the complete system when compared to the one obtained for the adsorber. This extra power results from the hot water that was being used to regenerate the adsorber, which is returned to the water reservoir after the regeneration phase. The energy that was used to heat this water is provided by the electric heater; thus, it is not included in the adsorber's performance calculations, which only considers the energy that was in fact used for the pre-heating and regeneration processes. Analyzing and comparing these two approaches for evaluating the performance of AHPs allows for a more comprehensible understanding of the system dynamics, enabling researchers to more finely tune each particular AHP application.

6.5. CONCLUSIONS

An innovative physical model for a complete AHP system was proposed, implemented, and solved. The dynamics of the AHP system, including the detailed analysis of the adsorber, was simulated under variable working conditions within each adsorption cycle. The integrated consideration of all the main system components, and of real operating conditions, provides more accurate results and improves the reliability of the simulation results, leading to faster development of ready to market AHP systems.

The temperature, pressure and adsorbate concentration in the adsorbent bed were analysed. Their distributions in the adsorbent bet are far from homogeneous, the usually used lumped parameter models not considering important inhomogeneities and dynamics that affect the quality of the obtained results. The slight change on the adsorbent bed temperature, pressure, and uptake along the length of the adsorber tubes indicate that the heat and mass transfers along the radial direction are the performance limiting factors. This effect is highly dependent on the adsorbent layer thickness. If the adsorbent bed thickness is too large it will take longer to get all the adsorbent material at the desired temperature. Longer tubes and smaller adsorbent bed thicknesses lead to better performances. Thus, any increase of the adsorbent mass should be done by using longer tubes instead of thicker adsorbent layers. However, if the tubes' length is significantly increased, the HTF velocity may also be higher to prevent significant changes on the temperature, pressure, and uptake

along the axial direction. The placement of the condenser inside the water reservoir is a key parameter that is worthy of a closer analysis, as well as the influence of the HTF flow rate. For the working conditions considered in this study, the values obtained for the COP_{adsorber} and COP_{system} are 1.58 and 1.35, respectively, and the SHP_{adsorber} and SHP_{system} are 57.6 $W.kg^{-1}$ and 79.3 $W.kg^{-1}$, respectively. The COP is higher for the adsorber, whereas the SHP is higher for the complete system.

The proposed model can be used in the future for detailed parametric analysis, aiming to find the optimal performances of similar AHP systems, leading to faster improved prototyping and AHP systems development. In addition, it is a valuable tool to evaluate the performance of new adsorbent materials operating in real systems, as well as to test control techniques and integration of AHP systems with other heating devices and technologies.

6.6. REFERENCES

Al-Mousawi FN, Al-Dadah R, Mahmoud S (2017) Different bed configurations and time ratios: Performance analysis of low-grade heat driven adsorption system for cooling and electricity. Energy Convers Manag. https://doi.org/10.1016/j.enconman.2017.06.062

Alam KCA, Saha BB, Kang YT, et al (2000) Heat exchanger design effect on the system performance of silica gel adsorption refrigeration systems. Int J Heat Mass Transf. https://doi.org/10.1016/S0017-9310(00)00072-7

Alsagri AS, Alrobaian AA, Almohaimeed SA (2020) Concentrating solar collectors in absorption and adsorption cooling cycles: An overview. Energy Convers. Manag.

Ammann J, Ruch P, Michel B, Studart AR (2018) Quantification of heat and mass transport limitations in adsorption heat exchangers: Application to the silica gel/water working pair. Int J Heat Mass Transf. https://doi.org/10.1016/j.ijheatmasstransfer.2018.02.076

Aristov YI (2009) Optimal adsorbent for adsorptive heat transformers: Dynamic considerations. Int J Refrig. https://doi.org/10.1016/j.ijrefrig.2009.01.022

Azahar FHM, Mitra S, Yabushita A, et al (2018) Improved model for the isosteric heat of adsorption and impacts on the performance of heat pump cycles. Appl Therm Eng. https://doi.org/10.1016/j.applthermaleng.2018.07.131

Bendix P, Füldner G, Möllers M, et al (2017) Optimization of power density and metal-to-adsorbent weight ratio in coated adsorbers for adsorptive heat transformation applications. Appl Therm Eng. https://doi.org/10.1016/j.applthermaleng.2017.05.165

Bergman TL, Lavigne AS, Incropera FP, Dewitt DP (2011) Fundamentals of Heat and Mass Transfer. John Wiley & Sons

Brites GJVN, Costa JJ, Costa VAF (2016) Influence of the design parameters on the overall performance of a solar adsorption refrigerator. Renew Energy. https://doi.org/10.1016/j.renene.2015.07.099

Chakraborty A, Saha BB, Aristov YI (2014) Dynamic behaviors of adsorption chiller: Effects of the silica gel grain size and layers. Energy 78:304–312. https://doi.org/10.1016/J.ENERGY.2014.10.015

Chua HT, Ng KC, Chakraborty A, et al (2002) Adsorption Characteristics of Silica Gel + Water Systems. https://doi.org/10.1021/je0255067

Demir H, Mobedi M, Ülkü S (2008) A review on adsorption heat pump: Problems and solutions. Renew. Sustain. Energy Rev. 12:2381–2403

Di J, Wu JY, Xia ZZ, Wang RZ (2007) Theoretical and experimental study on characteristics of a novel silica gel-water chiller under the conditions of variable heat source temperature. Int J Refrig. https://doi.org/10.1016/j.ijrefrig.2006.07.022

Dias JMS, Costa VAF (2019a) Which dimensional model for the analysis of a coated tube adsorber for adsorption heat pumps? Energy 174:1110–1120. https://doi.org/10.1016/j.energy.2019.03.028

Dias JMS, Costa VAF (2019b) Which dimensional model for the analysis of a coated tube adsorber for adsorption heat pumps? Energy 174:1110–1120. https://doi.org/10.1016/J.ENERGY.2019.03.028

Dias JMS, Costa VAF (2018) Adsorption heat pumps for heating applications: A review of current state, literature gaps and development challenges. Renew Sustain Energy Rev 98:317–327. https://doi.org/10.1016/J.RSER.2018.09.026

Dias JMS, Costa VAF (2020) Evaluating the performance of a coated tube adsorber for adsorption cooling. Int J Refrig. https://doi.org/10.1016/j.ijrefrig.2020.06.023

European Commission (2019) A European Green Deal. https://ec.europa.eu/info/strategy/priorities-2019-2024/european-green-deal_en

European Commission (2021) Heating and Cooling. https://ec.europa.eu/energy/topics/energy-efficiency/heating-and-cooling_en

Fernandes MS, Brites GJVN, Costa JJ, et al (2016) A thermal energy storage system provided with an adsorption module – Dynamic modeling and viability study. Energy Convers Manag 126:548–560. https://doi.org/10.1016/j.enconman.2016.08.032

Gaur AS, Fitiwi DZ, Curtis J (2021) Heat pumps and our low-carbon future: A comprehensive review. Energy Res. Soc. Sci. 71:101764

Gediz Ilis G, Demir H (2018) Influence of bed thickness and particle size on performance of microwave regenerated adsorption heat pump. Int J Heat Mass Transf. https://doi.org/10.1016/j.ijheatmasstransfer.2018.02.063

Gnielinski V (1976) New Equations for Heat and Mass Transfer in Turbulent Pipe and Channel Flow. Int Chem Eng

Graf S, Lanzerath F, Bardow A (2017) The IR-Large-Temperature-Jump method: Determining heat and mass transfer coefficients for adsorptive heat transformers. Appl Therm Eng. https://doi.org/10.1016/j.applthermaleng.2017.06.054

International Energy Agency (IEA) (2020) Heat Pumps. In: IEA, Paris. https://www.iea.org/reports/heat-pumps

Krzywanski J, Grabowska K, Herman F, et al (2017) Optimization of a three-bed adsorption chiller by genetic algorithms and neural networks. Energy Convers Manag. https://doi.org/10.1016/j.enconman.2017.09.069

Lemmon EW, McLinden MO, Friend and DG (2017) NIST Chemistry WebBook, NIST Standard Reference Database

Li A, Thu K, Ismail A Bin, et al (2016) Performance of adsorbent-embedded heat exchangers using binder-coating method. Int J Heat Mass Transf. https://doi.org/10.1016/j.ijheatmasstransfer.2015.08.097

Mitra S, Aswin N, Dutta P (2016) Scaling analysis and numerical studies on water vapour adsorption in a columnar porous silica gel bed. Int J Heat Mass Transf. https://doi.org/10.1016/j.ijheatmasstransfer.2015.12.011

Mohammed RH, Mesalhy O, Elsayed ML, et al (2018) Physical properties and adsorption kinetics of silica-gel/water for adsorption chillers. Appl Therm Eng. https://doi.org/10.1016/j.applthermaleng.2018.03.088

Ng KC, Chua HT, Chung CY, et al (2001) Experimental investigation of the silica gel-water adsorption isotherm characteristics. Appl Therm Eng. https://doi.org/10.1016/S1359-4311(01)00039-4

Ng KC, Thu K, Saha BB, Chakraborty A (2012) Study on a waste heat-driven adsorption cooling cum desalination cycle. Int J Refrig. https://doi.org/10.1016/j.ijrefrig.2011.01.008

Pal A, Uddin K, Thu K, Saha BB (2019) Activated carbon and graphene nanoplatelets based novel composite for performance enhancement of adsorption cooling cycle. Energy Convers Manag. https://doi.org/10.1016/j.enconman.2018.10.092

Pan QW, Wang RZ (2017) Study on boundary conditions of adsorption heat pump systems using different working pairs for heating application. Energy Convers Manag. https://doi.org/10.1016/j.enconman.2017.11.023

Pesaran A, Lee H, Hwang Y, et al (2016) Review article: Numerical simulation of adsorption heat pumps. Energy 100:310–320

Petukhov BS (1970) Heat Transfer and Friction in Turbulent Pipe Flow with Variable Physical Properties. Adv Heat Transf. https://doi.org/10.1016/S0065-2717(08)70153-9

REN21 (2020) Renewables 2020 Global Status Report. Paris

Rivero-Pacho AM, Critoph RE, Metcalf SJ (2017) Modelling and development of a generator for a domestic gas-fired carbon-ammonia adsorption heat pump. Renew Energy 110:180–185. https://doi.org/10.1016/j.renene.2017.03.089

Robbins T, Kini G, Garimella S (2020) Alternate control methods for adsorption heat pumps. Int J Refrig. https://doi.org/10.1016/j.ijrefrig.2020.08.018

Rupam TH, Islam MA, Pal A, Saha BB (2020) Adsorption thermodynamics and performance indicators of selective adsorbent/refrigerant pairs. Appl Therm Eng. https://doi.org/10.1016/j.applthermaleng.2020.115361

Seol SH, Nagano K, Togawa J (2020) Simulation on annual performance of solar adsorption heat pump system using composite natural mesoporous material in different metrological conditions. Renew Energy. https://doi.org/10.1016/j.renene.2020.09.119

Shabir F, Sultan M, Miyazaki T, et al (2020) Recent updates on the adsorption capacities of adsorbent-adsorbate pairs for heat transformation applications. Renew. Sustain. Energy Rev.

Shampine LF, Reichelt MW (1997) The MATLAB ode suite. SIAM J Sci Comput. https://doi.org/10.1137/S1064827594276424

Sircar S (1983) Linear-driving-force model for non-isothermal gas adsorption kinetics. J Chem Soc Faraday Trans 1 Phys Chem Condens Phases 79:785. https://doi.org/10.1039/f19837900785

Sun B, Chakraborty A (2015) Thermodynamic frameworks of adsorption kinetics modeling: Dynamic water uptakes on silica gel for adsorption cooling applications. Energy. https://doi.org/10.1016/j.energy.2015.02.101

Vasta S, Palomba V, La Rosa D, Mittelbach W (2018) Adsorption-compression cascade cycles: An experimental study. Energy Convers Manag. https://doi.org/10.1016/j.enconman.2017.11.061

Verde M, Harby K, de Boer R, Corberán JM (2016) Performance evaluation of a waste-heat driven adsorption system for automotive air-conditioning: Part I – Modeling and experimental validation. Energy. https://doi.org/10.1016/j.energy.2016.09.113

Wang Y, Li M, Du W, et al (2018) Performance comparative study of a solar-powered adsorption refrigerator with a CPC collector/adsorbent bed. Energy Convers Manag. https://doi.org/10.1016/j.enconman.2018.07.080

Wilkes JO, Birmingham SG (2006) Fluid Mechanics for Chemical Engineers with Microfluidics and CFD. Pearson Education

Wittstadt U, Füldner G, Laurenz E, et al (2017) A novel adsorption module with fiber heat exchangers: Performance analysis based on driving temperature differences. Renew Energy 110:154–161. https://doi.org/10.1016/j.renene.2016.08.061

Yang TY, Ge TS, Lu FL, et al (2020) A novel semi-coupled solid desiccant heat pump system - Part 1: Simulation study. Int J Refrig. https://doi.org/10.1016/j.ijrefrig.2020.09.005

Yunna W, Ruhang X (2013) Green building development in China-based on heat pump demonstration projects. Renew. Energy 53:211–219

Zhao Y, Li M, Long R, et al (2020) Dynamic modelling and analysis of an adsorption-based power and cooling cogeneration system. Energy Convers Manag. https://doi.org/10.1016/j.enconman.2020.113229

CHAPTER 7

This Chapter has been submitted and is under revision as:

Costa VAF, **Dias JMS** (2022) On the best coefficient of performance and specific heating or cooling power combination for adsorption refrigerators and heat pumps. Energy Conversion and Management

7. ON THE BEST COEFFICIENT OF PERFORMANCE AND SPECIFIC HEATING OR COOLING POWER COMBINATION FOR ADSORPTION REFRIGERATORS AND HEAT PUMPS

Abstract

Performance parameters of adsorption refrigerators and heat pumps are the coefficient of performance (*COP*) and the specific cooling power (*SCP*) or specific heating power (*SHP*). Higher *COP*s are associated with the longer cycle times required for more complete desorption and adsorption processes, thus resulting in a lower number of cycles per unit time and to lower *SCP* or *SHP*, unless the adsorption systems have large masses of adsorbent material and are of large sizes. The inverse occurs for shorter cycle times, associated with smaller *COP*s and higher *SCP* or *SHP*. An objective criterion is lacking to set the best balance between *COP* and *SCP* of adsorption refrigerators and heat pumps, which corresponds to their best whole performances. This work proposes such a criterion, based on the minimum cost of the unit of the obtained useful effect of the refrigerators or heat pumps. For a system operating under a given set of operating conditions it can be obtained the dependence of *COP* and *SCP* or *SHP* on the cycle time from numerical simulations, and once known these dependencies it is found the cycle time leading to the minimum cost of the unit of the obtained useful effect. The best balance between *COP* and *SCP* or *SHP* corresponds to the *COP* and *SHP* corresponding to that cycle time. Two examples are presented to show the application of the proposed criterion.

Keywords: Adsorption refrigerators; Adsorption heat pumps, Coefficient of performance, Specific cooling or heating power; Best balance between *COP* and *SCP* or *SHP*

NOMENCLATURE

C	Dimensionless cooling or heating COP [-]
C	Cost [€]
C_e	Specific energy cost [€/J]
C_0	Operation cost [€]
COP	Coefficient of performance [-]
F	Dimensionless specific cost function [-]
m	Mass [kg]
N	Number of cycles [-]
Q	Heat [J]
S	Dimensionless specific cooling or heating power [-]
SCP	Specific cooling power [W/kg]
SHP	Specific heating power [W/kg]
T	Lifetime [s]
P	Pressure (Pa)
Q	Heat (J)
q_m	Monolayer capacity ($kg.kg^{-1}$)
r	Radial coordinate (m)
R'	Steam particular gas constant ($J.kg^{-1}.K^{-1}$)
t	Time (s)
t_{SG}	Dimensionless Toth's constant (-)
T	Temperature (K)
u	Velocity ($m.s^{-1}$)
U	Overall heat transfer coefficient ($W.m^{-2}.K^{-1}$)
X	Adsorbate concentration in the adsorbent ($kg_a.kg_s^{-1}$)
z	Axial longitudinal coordinate (m)

Greek letters

α_i	Specific investment cost [J/kg]
β	Dimensionless factor [-]
γ	Dimensionless factor [-]
τ	Time [s]

Subscripts

ads	Adsorption
c	Cycle
e	Energy
i	Investment
in	Input
o	Operation
s	Adsorbent
T	Total
u	Useful
vc	Vapor compression

7.1. INTRODUCTION

Adsorption refrigerators and heat pumps are receiving increasing attention, as they allow obtaining cooling and heating, respectively, without using global warming potential (GWP) gases, and may be driven by heat obtained from renewable energy sources or that otherwise would be lost heat (Dias and Costa 2018; Gupta and Puri 2021; Pan et al. 2021). It is true that adsorption refrigerators and heat pumps have low coefficient of performance (COP) when comparing with vapor compression refrigerators and heat pump systems, those requiring electrical energy to operate and many times involving operating substances with considerably high GWP. However, these considerable COP differences need to be carefully taken into consideration. The adsorption refrigerators and heat pumps are heat driven systems and not electrically driven systems, Thermodynamics teaching that the amount of heat is considerably higher than the mechanical work (or electricity) that can be obtained from it. Additionally, it needs to be taken into consideration that the heat used to operate adsorption refrigerators and heat pumps may be low temperature heat, obtained from renewable energy sources, or that it can be residual heat that otherwise would be wasted. Thus, attention needs to be given to the fact that the denominator on the definition of the COP of adsorption systems is heat obtained at null or only residual cost, and that the denominator on the definition of the COP of vapor compression systems is mechanical work or electrical energy.

It is well known that the COP is the best way to express the energy performance of refrigerators or heat pumps. In mathematical terms, the COP of a vapor compression system must be expressed as

$$COP_{vc} = \frac{Q_u}{W} = \frac{Q_u}{Q_{in}} \times \frac{1}{\eta} \tag{7.1}$$

where Q_u is the useful heat (removed heat for cooling purposes by refrigerators, or released heat for heating purposes by heat pumps) obtained in one cycle, W is the mechanical work that needs to be invested for the vapor compression system to execute one cycle, and $\eta = \frac{W}{Q_{in}}$ is the energy efficiency of the heat-to-work conversion process. By its own turn, the COP of an adsorption system may be expressed as

$$COP_{ads} = \frac{Q_u}{Q_{in}} \quad 7.2$$

where Q_u has the same meaning as in Eq. 7.1, and Q_{in} is the heat that needs to be invested for the adsorption system to execute one cycle. Thus, when comparing the COP of adsorption systems, COP_{ads}, and of vapor compression systems, COP_{vc}, a more fair comparison must be made comparing $\frac{Q_u}{Q_{in}}$ in both situations, the COP_{vc} appearing multiplied by $\frac{1}{\eta}$, that is, multiplied by a factor higher than 2, when evaluated as given by Eq. 7.1, since the heat to work conversion efficiency is usually lower than 50%.

However, when dealing with adsorption systems the time required for the desorption and adsorption processes to occur leads to cycle times that are much longer than the short cycle times required by vapor compression systems. This results on a reduced number of cycles executed by adsorption systems per unit time, and thus to low available useful powers, unless they are big systems, capable of obtaining a huge useful effect per each long cycle. The useful power of adsorption systems is usually referred to the mass of used adsorbent, the specific (heating or cooling) power (S(H,C)P) being defined as

$$S(H,C)P = \frac{Q_u}{m_s \tau_c} \quad 7.3$$

For an adsorption system with a given mass of adsorbent m_s, longer cycle times allow more complete adsorption and desorption processes, thus allowing also higher adsorbent uptakes and thus a better use of the adsorbent desorption/adsorption capacity, higher useful heats Q_u, and higher COPs (Dias and Costa 2020, 2021). This up to a saturation limit, from which no more desorption or adsorption occurs even if additional time is allowed for that. Higher *COPs* mean higher thermal performance of adsorption systems, in the sense that more units of the useful effect Q_u are obtained per each unit of the invested heat Q_{in} in each cycle. However, longer cycle times imply low numbers of cycles per unit time, and thus lower ratios $\frac{Q_u}{\tau_c}$, or, in other words, lower (S(H,C)P). By its own turn, lower (S(H,C)P) mean lower useful effect of the system per unit time (lower effectiveness). Due to that, an adsorption system with a high COP will have a low (S(H,C)P), and an adsorption system

with a high (S(H,C)P) will have a low COP. It is to be retained that for a system to have a high (S(H,C)P) the cycle time may not be sufficiently long for the adsorption and desorption processes to occur in all their possible extensions, and that the adsorbent desorption/adsorption capacities are not fully advantageously used.

The COP and (S(H,C)P) are usually analyzed separately in the parametric studies and performance evaluations available in literature. It is common to plot the COP and the (S(H,C)P) against the cycle time, referring to the maximum value for each of these performance parameters. However, usually these maximum values occur for different cycle times, depending on the bed design and working conditions, among other factors. Sapienza *et al*. presented the COP and the average cooling power as function of the cycle time in the same graphics for several working conditions (Sapienza et al. 2016). It is evident that the maximum COP and average cooling power are obtained for different cycle times, leaving the doubt on which cycle time should be selected to obtain the best overall performance. The optimal cycle time was identified as the one that maximizes the COP or the cooling power, depending on the specific application. Choosing to maximize the COP or the cooling power might not provide the whole optimal performance for a given adsorption system. Frazzica *et al*. carried out a study reporting the COP and the SCP as a function of the cycle time for different working conditions (Frazzica et al. 2016). Their results are another example of the maximum COP and SCP occurring for different cycle times, leaving the doubt on which cycle time should be used. Even in more detailed analyses where the adsorption and desorption times are investigated, it remains to be defined the best COP and (S(H,C)P) balance/combination. Graf *et al.* chose to select the COP that corresponded to the maximum SCP (Graf et al. 2016). To use the results from their study to achieve the best performance of an adsorption refrigerator or heat pump, the best balance between COP and (S(H,C)P) must be found. The inverse behavior of COP and when increasing the cycle time is recurrent in the literature (Grisel et al. 2010; San and Tsai 2014; Chen et al. 2018; Pinheiro et al. 2018; Dias and Costa 2020, 2021). A simultaneous analysis that includes the balance between COP and (S(H,C)P) leading to the best overall performance of the adsorption systems cannot be found in the literature, and criteria or methods for selecting the optimal cycle time for each adsorption system are lacking.

A criterion is thus required to obtain the best balance/combination between COP and (S(H,C)P) of the adsorption refrigerators and heat pumps. This work proposes such a criterion, based on the minimum unit cost of the obtained useful cooling effect (by refrigerators) or heating effect (by heat pumps). From numerical simulations it is obtained

how the COP and the (S(H,C)P) depend on the cycle time, the proposed formulation allowing to obtain the cycle times that lead to the minimum unit cost of the obtained cooling or heating useful effect, and thus also allowing to obtain the best suitable combination of COP and (S(H,C)P) based on that minimum cost criterion. To the best of the authors' knowledge, and based on the literature, no such a criterion or similar approach has been proposed and/or used before.

7.2. PROPOSED METHODOLOGY AND CRITERION

The total cost of an adsorption system, that is expected to operate during a given lifetime period T_0, is obtained as the sum of the operation and investment costs.

The operation cost may be expressed as

$$C_0 = C_e \times Q_{in} \times N_c \tag{7.4}$$

where C_e is the unit cost of the energy (as heat) required to operate the system, expressed in €/J, Q_{in} is the heat required to operate the adsorption system during one cycle, and N_c is the total number of cycles that the system will operate during its expected operation lifetime T_0. If Q_{in} is obtained from nonrenewable energy sources it has a cost, as well as the equipment required to obtain it, this investment cost being diluted by each unit of the product $Q_{in} \times N_c$. If Q_{in} is obtained from renewable energy sources only the cost of the required equipment is considered, this investment cost being diluted by each unit of the product $Q_{in} \times N_c$. Thus, for a system that is expected to operate N_c cycles during its whole lifetime, C_e is set as the ratio between the sum of the investment costs on the necessary equipment to obtain the required invested energy, $Q_{in} \times N_c$, plus the cost of the $Q_{in} \times N_c$ invested energy itself. It is to be noted that, under this perspective, one thing are the investment costs needed to obtain the energy (heat) required to operate the adsorption system, and a different thing are the investment costs associated to the construction and installation of the adsorption system itself.

The investment costs on the adsorption system itself may be taken as being proportional to the mass of adsorbent,

$$C_i = C_{i,0} \times \alpha_i \times m_s \quad 7.5$$

where $C_{i,0}$ is the investment cost that is independent on the size of the system, and α_i, with units of €/kg, is the proportionality factor, assuming the investment costs are proportional to the mass of adsorbent. Any adsorption system is much more than its adsorbent, and it is being assumed as a good approximation that the investment costs on the whole adsorption system are proportional to the mass of adsorbent, which can be taken as a measure of the size of the adsorption system.

As the balance between COP and (S(H,C)P) is required when a high number of cycles per unit time is required for a high (S(H,C)P), and long cycle times are required for a high COP, analysis is conducted considering the adsorption system is operating over the whole operation time period T_0, related with the total number of cycles N_c through the cycle time τ_c as

$$N_c = \frac{T_0}{\tau_c} \quad 7.6$$

From the foregoing equations it can be obtained that the total cost, corresponding to the whole lifetime of the system, can be expressed as

$$C_0 + C_i = \left(C_e \times T_0 \times \frac{1}{COP} + \alpha_i \times \frac{1}{S(H,C)P} + C_{i,0} \left(\frac{Q_u}{\tau_c} \right)^{-1} \right) \times \left(\frac{Q_u}{\tau_c} \right) \quad 7.7$$

During the whole adsorption system's lifetime T_0 the useful obtained heat may be expressed as

$$Q_{u,T} = N_c Q_u = T_0 \left(\frac{Q_u}{\tau_c} \right) \quad 7.8$$

and thus, the total (operation plus investment) unit cost of useful heat $Q_{u,T}$ may be obtained as

$$\frac{C_0 + C_i}{Q_{u,T}} = C_e \left(\frac{1}{COP} + \frac{\alpha_i}{T_0 \times C_e} \times \frac{1}{S(H,C)P} + \frac{C_{i,0}}{C_e \times Q_u \times T_0} \right) \times \tau_c \quad (7.9)$$

Defining the dimensionless variables

$$\tau = \frac{\tau_c}{(\tau_c)_{max}} \quad (7.10a)$$

$$C = \frac{COP}{(COP)_{max}} \quad (7.10b)$$

$$S = \frac{S(H,C)P}{(S(H,C)P)_{max}} \quad (7.10c)$$

Eq. 7.9 may be rewritten as

$$F = \frac{C_0 + C_i}{Q_{u,T}(C_e/(COP)_{max})} = \frac{1}{C} + \beta \times \frac{1}{S} + \gamma \times \tau \quad (7.11)$$

where the dimensionless coefficient β is obtained as

$$\beta = \frac{\alpha_i \times (COP)_{max}}{T_o \times C_e \times (S(H,C)P)_{max}} \quad (7.12)$$

And the dimensionless coefficient γ is defined as

$$\gamma = \frac{C_{i,0} \times (COP)_{max} \times (\tau_c)_{max}}{T_o \times C_e \times Q_u} \quad (7.13)$$

It must be noted that τ, C, and S dimensionless variables are all of them in the [0;1] interval, and that they can thus be treated and/or compared on a common basis through Eq. 7.11.

For a whole adsorption system, with a given mass of adsorbent, numerical simulation tests can be conducted in order to obtain how the COP and (S(H,C)P) depend on the cycle time. From these tests are also obtained the (maximum) reference parameters $(\tau_c)_{max}$, $(COP)_{max}$ and $(S(H,C)P)_{max}$, where it is implicitly assumed that $(\tau_c)_{max}$ is the cycle time long enough to have the most complete possible adsorption, desorption and uptake for the considered operating conditions.

A cycle time exists that minimizes the unit cost of the obtained useful effect. Thus, the next step of the proposed method is to obtain the cycle time that minimizes the dimensionless function $(C_0 + C_i)/\left[Q_{u,T}(C_e/(COP)_{max})\right]$ as given by Eq. 7.11, based on the COP and (S(H,C)P) values as functions of the cycle time. In this paper those values were obtained from numerical simulation, as detailed in Section 3. The COP and (S(H,C)P) for that cycle time are their best combination, in the sense that it is the cycle time leading to the minimum unit cost of the obtained useful effect.

Eq. 7.11 allows obtaining the cycle time leading to the best COP and (S(H,C)P) combination, and additionally it allows to extract some relevant conclusions:

i) Term $\gamma \times \tau$ introduces a linear contribution of τ on F, the proportionality constant γ being proportional to the investment costs $C_{i,0}$ that are independent on the size of the system, and inversely proportional to the unit energy costs C_e, to the useful heat Q_u in one cycle, and to the operation lifetime T_0 of the system. Small investment costs $C_{i,0}$ that are independent on the size of the system, high unit energy costs C_e and long operation lifetime T_0, lead to investment costs that are independent on the size of the system, which are low when comparing with the energy costs required to operate the system during its useful long lifetime, decreasing the relevance of the linear contribution of τ on F. In the inverse situation, high investment costs $C_{i,0}$ that are independent on the size of the system, low unit energy costs C_e and short operation lifetime T_0 mean that the investment costs that are independent on the size of the system are high when comparing with the energy costs required to operate the system during its useful lifetime, increasing the relevance of the linear contribution of τ on F;

ii) Given the dimensionless character of $(C_0 + C_i)/\left[Q_{u,T}(C_e/(COP)_{max})\right]$ and τ, and the upper limit $\tau = 1$ of τ, influence of the linear term $\gamma \times \tau$ on F linearly increases as τ increases, introducing the highest contribution of γ on F in the upper limit situation of $\tau = 1$;

iii) If the dimensionless factor β takes a low value, what means low investment costs (low proportionality factor α_i), high unit energy costs C_e, or long operation lifetime T_0, or a low $(COP)_{max}/(S(H,C)P)_{max}$ ratio, the right hand side of Eq. 7.11 is dominated by $1/C$, and under these conditions the minimum unit cost of the obtained useful effect is obtained for the highest value of C, what is the same as to say that it is obtained for the highest COP. This is a situation for which COP is much more relevant than (S(H,C)P) as the adsorption system's performance index. By the reasons explained before, in this case long cycle times lead to the best whole performance of the adsorption systems;

iv) If the dimensionless factor takes a high value, what means high investment costs (high proportionality factor α_i), or low unit energy costs C_e, short operation lifetime T_0, or a high ratio, the right hand side of Eq. 7.11 is dominated by β/C, and under these conditions the minimum unit cost of the obtained useful effect is achieved for the highest value of S, what is the same as to say that it is obtained for the highest value of (S(H,C)P). This is a situation for which (S(H,C)P) is much more relevant than COP as the adsorption systems' performance index. By the reasons explained before, in this case short cycle times lead to the best whole performance of the adsorption systems;

v) The same general equation may be used to obtain the best COP and (S(H,C)P) combination for adsorption refrigerators or heat pumps, as the combination leading to the minimum value of F, that is, to the combination that leads to the minimum unit cost of the obtained useful cooling or heating effect;

vi) Criterion leading to the minimum unit cost of the obtained useful cooling or heating effect is based on the linear combination of the inverse of the two usual performance indices of adsorption systems, that linear combination resulting from arguments grounded on the overall cost minimization.

7.3. APPLICATION EXAMPLES

Several physical models that simulate the dynamics of adsorption heat pump or refrigerators can found in literature (Li et al. 2015; Fernandes et al. 2016; Pesaran et al. 2016; Pan and Wang 2017; Vodianitskaia et al. 2017). The most accurate models are distributed parameter models, which can provide accurate predictions for the *COP* and *S(H,C)P* (Dias and Costa 2019). Some application examples of the proposed methodology and criterion are presented. As application example, the data resulting from an accurate

physical model of a complete adsorption heat pump (AHP) system, described in (Dias and Costa 2022) was selected. More details on the considered AHP system and physical model can be found in that reference. The set of parameters used to obtain the *COP* and *SHP* data is summarized in Table 7.1. There are two application examples presented in this work, which consider different adsorbent thicknesses, σ_s.

Table 7.1 – Set of parameters used to obtain the *COP* and *SHP*.

Parameter	*Value*	*Unit*
C_m	910	J.kg^{-1}.K^{-1}
C_s	921	J.kg^{-1}.K^{-1}
d_p	3.5×10^{-4}	m
$d_{in,tube}$	0.01	m
E_a	2.3314×10^{6}	J.kg^{-1}
$h_{m \to s}$	30	W.m^{-2}.K^{-1}
k_0	7.3×10^{-13}	kg.kg^{-1}.Pa^{-1}
k_f	0.6	W.m^{-1}.K^{-1}
k_m	205	W.m^{-1}.K^{-1}
k_s	0.198	W.m^{-1}.K^{-1}
L_{tube}	1	m
$m_{s,\,tube}$	≈0.325	kg
ΔH_v	2.3×10^{6}	J.kg^{-1}
q_m	0.45	kg.kg^{-1}
$T_{w,\,ini}$	$273.15 + 20$	K
$T_{amb,e}$	$273.15 + 12$	K
$T_{amb,\,tank}$	$273.15 + 20$	K
$T_{f,reg}$	$273.15 + 90$	K
t_{reg}	$0.91 \times t_{ads}$	=
t_{SG}	12	-
u_f	0.05	m.s^{-1}
V_{tank}	≈293	L
ΔH_{ads}	2.693×10^{6}	J.kg^{-1}
ε	0.4	-
ρ_m	2700	kg.m^{-3}
ρ_s	2027	kg.m^{-3}
σ_{tube}	0.001	m

7.3.1. Application example 1

Figure 7.1 is the graphical representation of the dependence of the dimensionless *COP (C)* and *SHP (S)* on the dimensionless cycle time τ for this application example, based on the previously referred conditions. The used data correspond to ten individual tubes with a bed thickness $\sigma_s = 2\,mm$ and a heat transfer fluid's velocity $u_f = 0.05\ m/s$, resulting in

$(COP)_{max} = 1.50$ for $\tau_c = 5322.9\ s$, $(SHP)_{max} = 440.35\ W/kg$ for $\tau_c = 1041.1\ s$, and $(\tau_c)_{max} = 5322.9\ s$. From Figure 7.1 it is clear that the longest cycle times lead to the highest *COPs* and to the lowest *SHPs*, and that the shortest cycle times lead to the highest *SHPs* and to the lowest *COP*. It is also to be noted that very short cycle times are not the best option in what concerns both *COP* and *SHP*, as not enough time exists for the right sequence of the adsorption cycle phases to take place, the maximum *SHP* occurring for the dimensionless cycle time of 0.196.

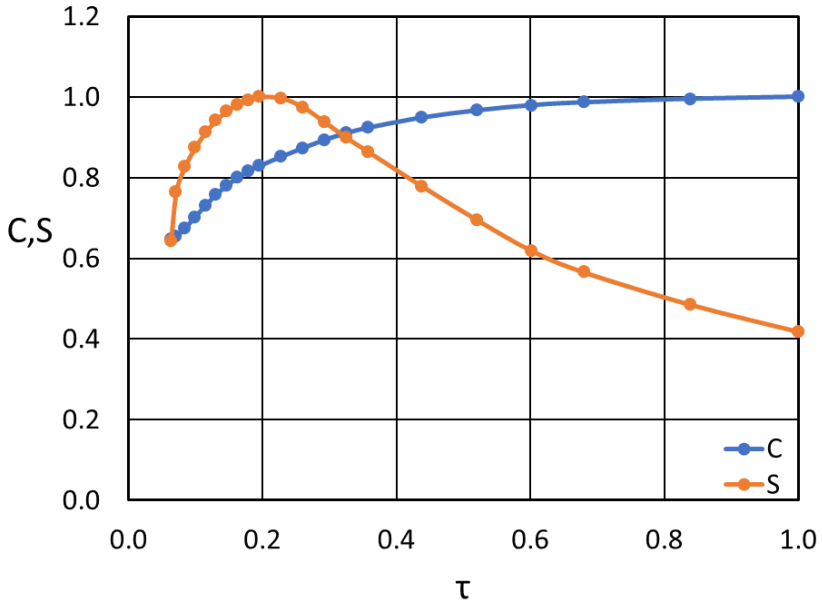

Figure 7.1 – Dependence of the dimensionless *COP (C)* and *SHP (S)* on the dimensionless cycle time (τ).

Figure 7.2 represents the dimensionless function F as given by Eq. 7.11 for the data in Figure 7.1, for some values of dimensionless coefficient β as defined by Eq. 7.12, considering $\gamma = 0.1$. It can be clearly seen that for low values of the dimensionless coefficient β the minimum of the dimensionless function F corresponds to the higher values of the dimensionless *COP*, C. For high values of dimensionless coefficient β the minimum of dimensionless function F corresponds to the maximum of the dimensionless specific heating power S. As for intermediate values of coefficient β, the minimum of dimensionless function F corresponds to a given dimensionless cycle time to which correspond intermediate values of S and C.

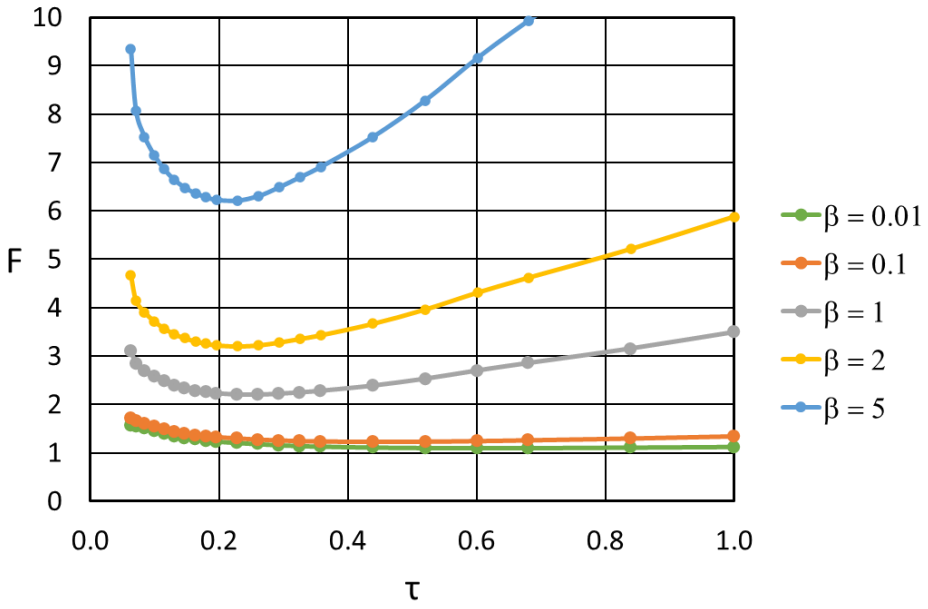

Figure 7.2 – Dependence of the dimensionless function F on the dimensionless cycle time (τ) for some selected values of β, for $\gamma = 0.1$.

Figure 7.3 highlights what happens for the lowest values considered for coefficient β, showing that for $\beta = 1$ the minimum of the dimensionless function F is obtained for $\tau = 0.261$, that for $\beta = 0.1$ the minimum of the dimensionless function F is obtained for $\tau = 0.438$, and that for $\beta = 0.01$ the minimum of the dimensionless function F is obtained for $\tau = 0.602$. Additionally, it is observed that as coefficient β decreases the minimum of the dimensionless function F curve becomes less pronounced, and that it almost disappears for sufficiently low values of this parameter, that is the situation for which *COP* becomes the most important performance parameter that must be taken into consideration when assessing the benefit/cost performance of the adsorption systems.

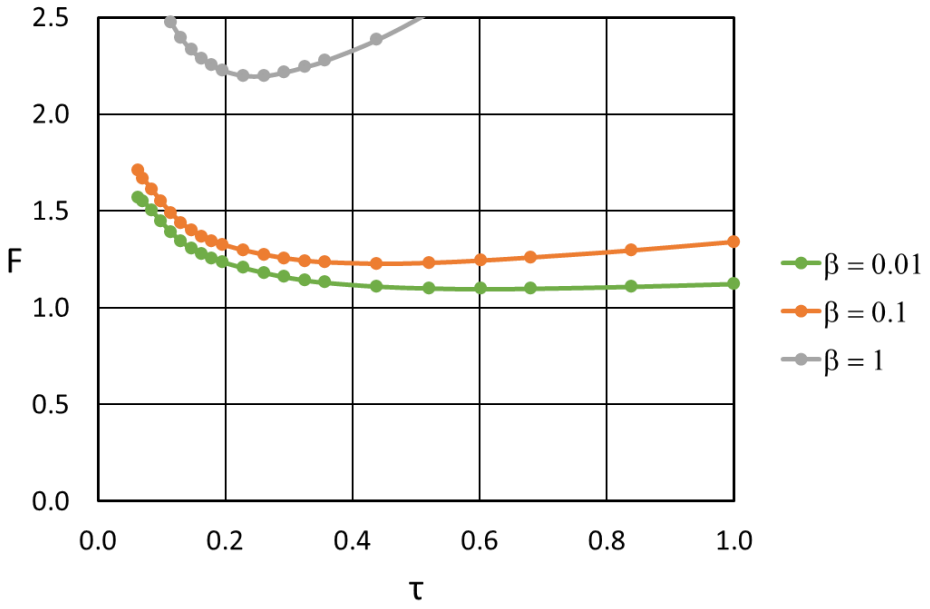

Figure 7.3 – Dependence of the dimensionless function F on the dimensionless cycle time (τ) for some selected values of β, for $\gamma = 0.1$.

The dependence of the dimensionless function F on the dimensionless coefficient γ is represented in Figure 7.4 for $\beta = 1$. Function F is much more sensitive to changes on the coefficient β than to changes on the coefficient γ, meaning that in this case the costs dependence on the size of the system causes greater impact than the costs that are independent from the system's size.

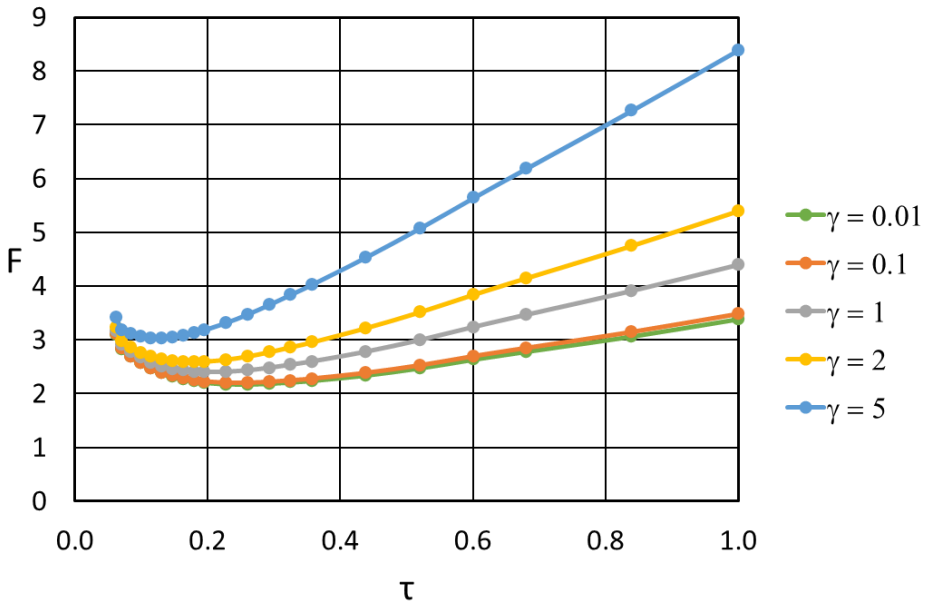

Figure 7.4 – Dependence of the dimensionless function F on the dimensionless cycle time (τ) for some selected values of γ for $\beta = 1$.

7.3.2. Application example 2

Figure 7.5 is the graphical representation of the dependence of the dimensionless *COP* (C) and *SHP* (S) on the dimensionless cycle time τ considering fifty individual tubes with a bed thickness $\sigma_s = 5\,mm$ and a heat transfer fluid's velocity $u_f = 0.05\ m/s$, which results in $(COP)_{max} = 1.42$ for $\tau_c = 6378.5\,s$, $(SHP)_{max} = 133.6\ W/kg$ for $\tau_c = 636.3\,s$, and $(\tau_c)_{max} = 6378.5\,s$. For this application example, and as expected from the foregoing arguments, longer cycle times lead to higher *COP* and that shorter cycles lead to higher *SHP*.

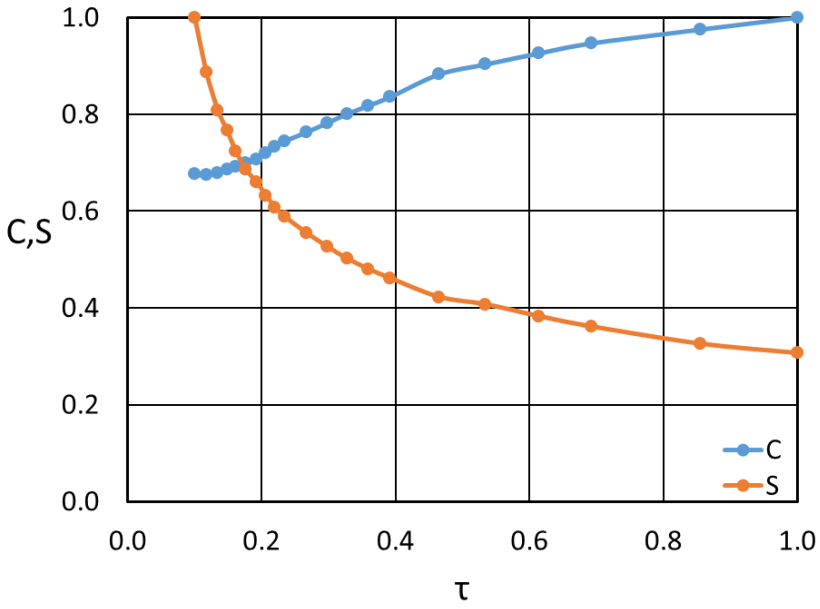

Figure 7.5 – Dependence of the dimensionless *COP* (C) and *SHP* (S) on the dimensionless cycle time (τ).

Figure 7.6 represents the dimensionless function F, using the data from Figure 7.5, for different values of the dimensionless coefficient β, for $\gamma = 0.1$. For higher values of β the minimum of the dimensionless function F occurs when the cycle time is shorter, while for small values of β the minimum of the dimensionless function F corresponds to longer cycle times. For the β values up to $\beta = 0.2$, neither long nor short cycles lead to the minimum of the dimensionless function F. In Figure 7.7 are represented the data corresponding to $\beta = 0.20$ and $\beta = 0.25$. For these β values, the minimum of the dimensionless function F is respectively obtained for the dimensionless cycle times of $\tau = 0.534$ and $\tau = 0.100$.

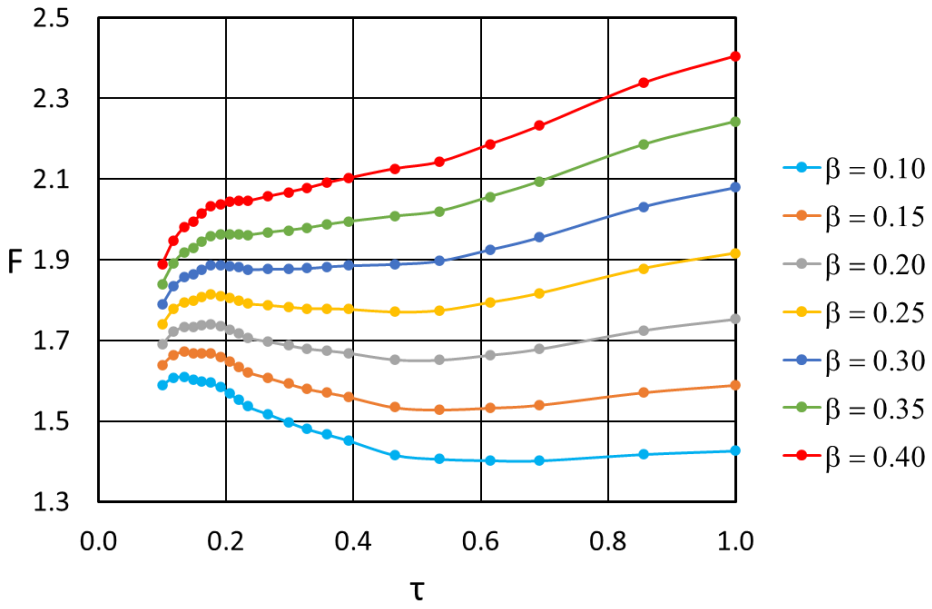

Figure 7.6 – Dependence of the dimensionless function F on the dimensionless cycle time (τ) for some selected values of β, for $\gamma = 0.1$.

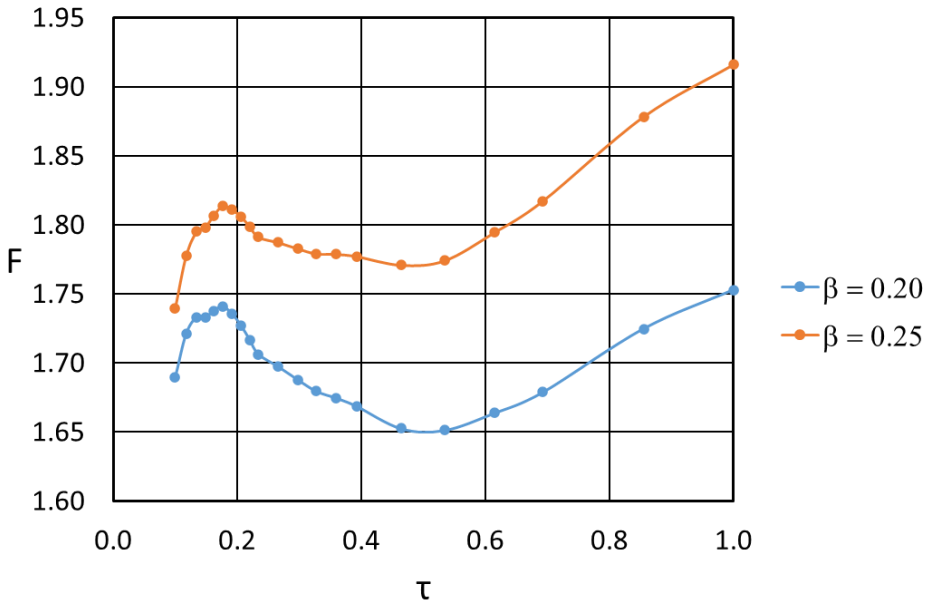

Figure 7.7 – Dependence of the dimensionless function F on the dimensionless cycle time (τ) for some selected values of β, for $\gamma = 0.1$.

The influence of the dimensionless coefficient γ on the dimensionless function Dependence of the dimensionless function F on the dimensionless cycle time (τ) for some

selected values of β, for F in this case, considering $\beta = 0.2$, is represented in Figure 7.8. As for the coefficient β, higher values of γ lead to a minimum of the function F for smallest cycle times. Lower γ values yield the minimum of dimensionless function F for approximately half of the maximum cycle time.

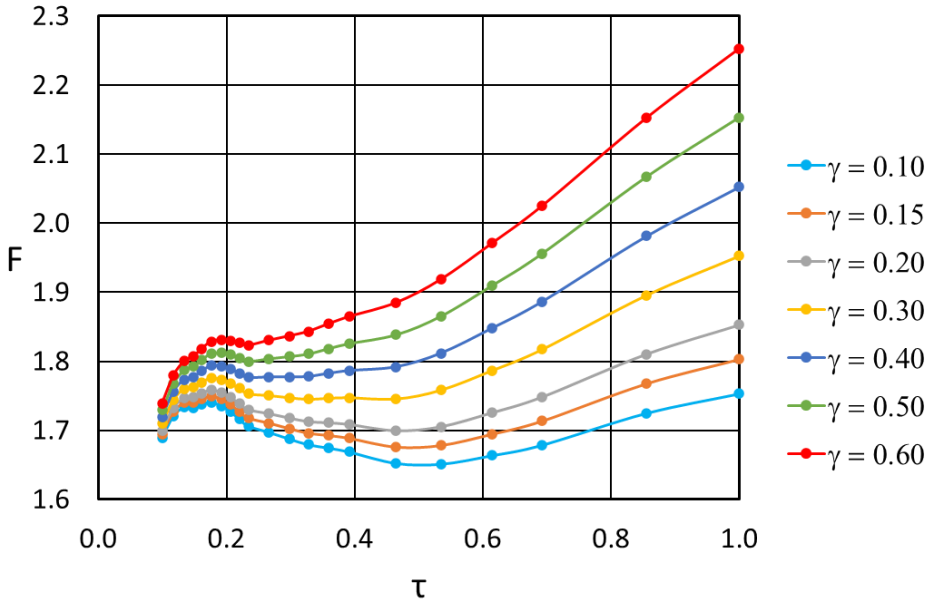

Figure 7.8 – Dependence of the dimensionless function F on the dimensionless cycle time (τ) for some selected values of γ, for $\beta = 0.2$.

This investigation has been conducted considering two more examples, in which the heat transfer fluid's velocity was increased ten times in one of the examples and the adsorbent mass was reduced five times in the other. Although the resulting values of the dimensionless function F were different, these data are not presented here since the shapes of the data curves for the dimensionless function F are similar and lead to the same main conclusions as the previous ones. For higher values of β the dimensionless function F has its minimum for the smallest cycle times, and lower values of β provide the minimum F for longer cycle times. For middle range β values, it is not the maximum nor the minimum cycle times that provide the minimum value of the dimensionless function F. Higher γ values drag the minimum of the dimensionless function F for the smallest cycle times, whereas lower values of γ provide the minimum of the dimensionless function F for approximately half of the longest cycle time.

7.4. CONCLUSIONS

A criterion to set the best balance between *COP* and *SCP* or *SHP* of adsorption systems cannot be based only on energy or efficiency arguments, as the *COP* and *SCP* or *SHP* present a somewhat opposite dependence on the cycle time. High *COPs* require long cycle times and are associated with low cooling or heating powers, unless large masses of adsorbent and large sized systems are used, whereas low *COPs* are associated with high *SCPs* or *SHPs. COP* is an energy efficiency performance index, relating the thermal energy useful effect of the adsorption refrigerators or heat pumps and the thermal energy required to operate the system. By their own turn, *SCP* or *SHP* are power performance indices, relating the thermal energy useful effect of the adsorption refrigerators or heat pumps and the product of the mass of adsorbent and the cycle time. What is more important, the best energy efficiency performance or the best power performance?

A deterministic criterion is proposed in this work to find the best balance between *COP* and *SCP* or *SHP*, based on the minimum unit cost of the thermal useful effect of the adsorption refrigerators or heat pumps. Once known how the *COP* and the *SCP* or *SHP* depend on the cycle time, it is possible to find the cycle time that corresponds to the minimum unit cost of the thermal energy useful effect of the adsorption refrigerators or heat pumps, the best *COP* and *SCP* or *SHP* being those corresponding to that cycle time. To the best of the authors' knowledge, based on the open literature, this is the first time such a criterion is being proposed.

7.5. REFERENCES

Chen QF, Du SW, Yuan ZX, et al (2018) Experimental study on performance change with time of solar adsorption refrigeration system. Appl Therm Eng. https://doi.org/10.1016/j.applthermaleng.2018.04.061

Dias J, Costa VAF (2021) Modeling and Analysis of a Coated Tube Adsorber for Adsorption Heat Pumps. Energies 14:6878. https://doi.org/https://doi.org/10.3390/en14216878

Dias JMS, Costa VAF (2019) Which dimensional model for the analysis of a coated tube adsorber for adsorption heat pumps? Energy 174:1110–1120. https://doi.org/10.1016/j.energy.2019.03.028

Dias JMS, Costa VAF (2018) Adsorption heat pumps for heating applications: A review of current state, literature gaps and development challenges. Renew Sustain Energy Rev 98:317–327. https://doi.org/10.1016/J.RSER.2018.09.026

Dias JMS, Costa VAF (2020) Evaluating the performance of a coated tube adsorber for adsorption cooling. Int J Refrig. https://doi.org/10.1016/j.ijrefrig.2020.06.023

Dias JMS, Costa VAF (2022) Modelling and analysis of a complete adsorption heat pump system. Appl Therm Eng 118782. https://doi.org/https://doi.org/10.1016/j.applthermaleng.2022.118782

Fernandes MS, Brites GJVN, Costa JJ, et al (2016) Modeling and parametric analysis of an adsorber unit for thermal energy storage. Energy 102:83–94. https://doi.org/10.1016/j.energy.2016.02.014

Frazzica A, Palomba V, Dawoud B, et al (2016) Design, realization and testing of an adsorption refrigerator based on activated carbon/ethanol working pair. Appl Energy 174:15–24. https://doi.org/10.1016/j.apenergy.2016.04.080

Graf S, Lanzerath F, Sapienza A, et al (2016) Prediction of SCP and COP for adsorption heat pumps and chillers by combining the large-temperature-jump method and dynamic modeling. Appl Therm Eng 98:900–909

Grisel RJH, Smeding SF, Boer R de (2010) Waste heat driven silica gel/water adsorption cooling in trigeneration. Appl Therm Eng 30:1039–1046. https://doi.org/10.1016/J.APPLTHERMALENG.2010.01.020

Gupta R, Puri IK (2021) Waste heat recovery in a data center with an adsorption chiller: Technical and economic analysis. Energy Convers Manag. https://doi.org/10.1016/j.enconman.2021.114576

Li XH, Hou XH, Zhang X, Yuan ZX (2015) A review on development of adsorption cooling - Novel beds and advanced cycles. Energy Convers. Manag. 94:221–232

Pan Q, Peng J, Wang R (2021) Application analysis of adsorption refrigeration system for solar and data center waste heat utilization. Energy Convers Manag. https://doi.org/10.1016/j.enconman.2020.113564

Pan QW, Wang RZ (2017) Study on boundary conditions of adsorption heat pump systems using different working pairs for heating application. Energy Convers Manag. https://doi.org/10.1016/j.enconman.2017.11.023

Pesaran A, Lee H, Hwang Y, et al (2016) Review article: Numerical simulation of adsorption heat pumps. Energy 100:310–320

Pinheiro JM, Salústio S, Valente AA, Silva CM (2018) Adsorption heat pump optimization by experimental design and response surface methodology. Appl Therm Eng. https://doi.org/10.1016/j.applthermaleng.2018.03.091

San J-Y, Tsai F-K (2014) Testing of a lab-scale four-bed adsorption heat pump. Appl Therm Eng 70:274–281. https://doi.org/10.1016/J.APPLTHERMALENG.2014.05.014

Sapienza A, Gullì G, Calabrese L, et al (2016) An innovative adsorptive chiller prototype based on 3 hybrid coated/granular adsorbers. Appl Energy 179:929–938. https://doi.org/10.1016/j.apenergy.2016.07.056

Vodianitskaia PJ, Soares JJ, Melo H, Gurgel JM (2017) Experimental chiller with silica gel: Adsorption kinetics analysis and performance evaluation. Energy Convers Manag 132:172–179. https://doi.org/10.1016/j.enconman.2016.11.028

CHAPTER 8

8. GENERAL CONCLUSIONS

The conclusions and remarks of the PhD work are presented in this Chapter. The conclusions of all the scientific publications resultant from this PhD work are summarized.

8.1. SUMMARY OF RESEARCH AND FINDINGS

Adsorption heating and cooling technologies can play an important role towards the achievement of a greener and sustainable future. The ability to use natural refrigerants as well as being driven by low or just moderate temperature level thermal energy are two strong remarks that justify further efforts to develop the technology and improve its TRL. The low COP and power density when compared to vapour compression systems are considered as the major hindrances of AHP. Nonetheless, it is important to note that a direct comparison between the COP from AHP and VCHP must not be considered, unless the efficiency from transforming thermal energy into mechanical work is contemplated, which can be between 30%-50%.

Having identified the asset that adsorption systems can be to the heating and cooling sectors, the technology was selected to be used for space and domestic water heating in the scope of the SGH project. The first step of this investigation comprised a review on AHP technologies and deeply understanding its working principle. The different types of system designs, physical models used to describe the dynamics of AHP, adsorption equilibrium and kinetics of conventional and new adsorbent-adsorbate working pairs, and operating conditions were studied (Chapter 2). Notwithstanding all the research carried out on new adsorbent-adsorbate working pairs, few are ready to market, easily accessed and produced, proven to be hydrothermal stable, and tested for long life cycles with high numbers of adsorption-desorption cycles. Adsorbent-adsorbate working pairs with low heat and mass transfer resistances, which also have the capacity of being regenerated at lower temperatures, would be ideal for the most applications. These characteristics are mostly achieved by using adsorbent coatings, but it is hard to obtain the adsorbent mass required to produce significant heating powers. Most studies on adsorbent materials solely focus on the material physical and thermodynamical properties and deal with very small-scale samples. It is important to focus the investigation of future adsorbent-adsorbate working pairs on creating bridges to real scale applications, where larger amounts of adsorbent must be used. Thus, detailed system level studies are becoming even more important to increase the TRL of AHP. From the literature review, it was concluded that physical models that consider the whole AHP system are lacking. In the models found in the literature, the internal mass transfer resistance is most commonly described by the LDF model, whereas the external mass transfer resistance is usually described by Darcy's Law. Most experimental studies and numerical simulations available in the literature do not provide detailed

information suitable for validating new models. Moreover, the simultaneous optimization of the bed specifications, operating conditions and adsorbent material thermodynamic and physical properties cannot be found in the literature.

Since adsorbent coatings were identified as suitable to be used in AHP for space and domestic water heating, a coated tube adsorber was modelled as the first step towards modelling a complete AHP system. Several transient dimensional models describing a coated tube adsorber were analysed and discussed (Chapter 3). The analyses considered a lumped (0D) parameter model, a 1D distributed parameter model (radial direction), and a 2D distributed parameter model (radial and longitudinal directions). It was concluded that lumped-parameter models are not suitable to accurately describe the adsorber's dynamics, unless a deviation over 20% can be admitted, since these models overestimate the SHP of AHP. On the other hand, it was found that the lumped model can be used to predict the COP, with deviations up to ≈2% relative to the highest resolution 2D reference model that was considered. The 1D distributed parameter model can be used to obtain a reasonable prediction of the adsorber's performance coefficients while requiring low computational efforts, providing results with insignificant deviations for the COP. For high HTF velocities or low tube lengths, the prediction of the SHP also comes out with reasonable accuracy. However, for lower HTF velocities and/or long coated tubes the 1D distributed parameter model fails to accurately predict the SHP of AHP. According to the tests that were carried out, for a 10 m long tube the value for the SHP showed deviations up to 50% due to high temperature variations along the tube length.

Given that in several cases the 1D distributed parameter model failed to accurately predict the performance of AHPs, the 2D model was selected as the base model for the next stages of this PhD work. A grid independence study for the 2D distributed parameter model was conducted. The SHP was identified as the performance indicator that is most affected by changes in the spatial resolution of the model. For an AHP using silica gel-water as working pair, a spatial resolution of $\Delta r = 5 \times 10^{-5}\ m$ and $\Delta z = 8.33 \times 10^{-2}\ m$ should be used to ensure a maximum total deviation of ≈1% for the SHP value with the lowest computational cost, considering the worst-case scenario. The consideration of the mass of the metal tubes that make up the adsorber in the physical model was found to be useful. Although most studies disregard this mass, it was proven that it can cause significant deviations on the COP and SHP predictions, more specifically up to ≈4.5% for the COP, and up to ≈7% for the SHP.

Since adsorbent coatings are capable of achieving better performance coefficients, a coated tube adsorber for an AHP suitable for space and domestic water heating was designed and investigated (Chapter 4). The coated tube adsorber was modelled using the 2D distributed parameter model presented in Chapter 3. Several governing parameters were investigated under two different sets of working conditions. The working conditions for Scenario A are suitable for pre-heating water in mild climates, whereas those for Scenario B are based on the European standard EN16147. Results are in line with the Thermodynamics principles since high evaporator temperatures and/or low condenser temperatures lead to better performances for both scenarios. The adsorber performed worse for B Scenarios' working conditions, which was expected since the temperature difference between the evaporator and condenser is higher. The adsorber is limited by a maximum condenser temperature of 70 °C for Scenario A and of 60 °C for Scenario B, since the pressure inside the adsorber cannot be increased to the pressure level of the condenser, unless the regeneration temperature is increased. Thus, there is a connection between the regeneration temperature and the maximum operating condenser temperature. Higher condenser temperatures will require higher regeneration temperatures for the adsorber's proper working. The maximum COP is obtained for regeneration temperatures of about 75 °C and 95 °C for Scenarios A and B, respectively, whilst the SHP increases with the regeneration temperature. The COP and the SHP have opposite behaviours with the change of the cycle time. Short cycle times lead to higher SHPs but lower COPs, whereas long cycle times result on higher COPs and lower SHPs. This opposite behaviour is inherent to AHP systems and the crossing point will be a characteristic of each induvial system. It is important to deeply analyse this aspect and decide which cycle time should be used. It was found that the metal-adsorbent heat transfer coefficient highly affects the SHP until it reaches 200 $W.m^{-2}.K^{-1}$, considering the working conditions investigated. This is the main reason for the use of adsorbent coatings since they can provide metal-adsorbent heat transfer coefficients up to ten times higher than packed beds. The SHP can also be improved by using thinner adsorbent coatings but requiring an adsorber with a larger number of the so coated tubes to have the required mass of adsorbent material.

The possibility to use the AHP principle for cooling applications appeared naturally during this PhD work. The capacity of producing the cooling effect using heat as the energy input was found to be interesting as low or moderate medium and/or high temperature waste heat is available in from many cooling applications. The influence of the previously identified key parameters on the performance of the adsorber was investigated for cooling

applications (Chapter 5). The results confirmed the already expected better adsorber's performance for higher evaporator temperatures and lower condenser temperatures. The maximum COP_c was obtained for a regeneration temperature of approximately 70 °C. On the other hand, high cooling powers require higher regeneration temperatures. The cycle time steps out as a crucial control parameter once more as a crucial control parameter, long cycle times providing the maximum COP_c and very low SCP, and short cycles resulting in higher SCP and lower COP_c. The cycle time must be specifically selected aiming to provide the best combination between the COP_c and the SCP for each specific application of AC systems. The heat transfer coefficient of the tube wall-adsorbent material interface has great impact on the SCP. The highest COP_c and SCP are obtained for values of this heat transfer coefficient of 100 $W.m^{-2}.K^{-1}$ and 350 $W.m^{-2}.K^{-1}$ for this heat transfer coefficient, respectively. The adsorbent coating thickness has a heavy impact on the performance of AC systems, due to the increased heat and mass transfer resistances associated with thicker coatings. On the other hand, the excess decrease of the coating thickness leads to a small adsorbent mass per tube, which will require a large number of tubes, resulting in a huge sized and expensive system. The inner diameter of each individual tube has generated significant changes in the impact on the system's performance since the HTF mass flow rate, heat transfer area, and adsorbent mass depend on this dimension. While under laminar flow regime, results have shown that an inner diameter of 10 mm is the best solution. When the inner tube diameter is high enough for HTF turbulent flow to develop, further increase on the tube diameter has an insignificant impact on the adsorber's performance. Increasing the HTF's velocity causes minimal improvements on the COP_c. Nonetheless, its increase until approximately 0.03 $m.s^{-1}$ leads to higher SCP, but no further meaningful changes on the system's performance are observed if the HTF velocity increases above 0.03 $m.s^{-1}$. Longer cycle times allow more complete heat and mass transfer processes, and thus higher COPc. However, longer cycle times translates into lower number of cycles by per unit time, and thus into lower SCP. Thus, a balance between these two performance parameters is required for the best performance of a coated tube adsorber, depending on the specific application. The additional balance between the investment and working costs of each AC system can provide the additional information needed to set the better COP_c and SCP combination.

Having developed and established a reliable physical model for the adsorber component, the next step consisted of developing and implementing a model that considered all the main components of an a complete AHP system and its dynamics. An innovative physical model for a complete AHP system was proposed, implemented, and

solved (Chapter 6). The dynamics of the AHP system, including the detailed analysis of the adsorber resultant from the previous chapters, were simulated under variable working conditions within the adsorption cycle, representing a significant contribution to the present literature. The developed model integrates and considers all the main AHP system components, and real operation conditions, to provide more accurate results, improving the reliability of the simulation outputs and leading to faster and sustainable development of ready to market ready AHP systems. Most studies on adsorbent coatings report better performance when compared to granular beds, but the coating thicknesses that are used are very small. Thus, to obtain a real system with useful cooling/heating power would lead to huge machines that are not accepted by the market. Furthermore, the mechanical strength and stability of adsorbent coatings is too weak to implement in real scale systems machines, not to mention the associated costs with the coating process. This is just another consequence of the lacking bridge that exists between material and system level studies. Therefore, granular silica gel was used in the simulations for the complete AHP system and used on the AHP prototype. The developed model considers a detailed distributed parameter model for the adsorber, integrating the all the main system components and considering all the interactions and dynamics. It was shown that the temperature, pressure, and uptake distribution inside the adsorbent bed are far from homogeneous, proving that using lumped parameter models that do not consider these inhomogeneities and dynamics will affect the quality of the obtained results. Heat and mass transfer along the radial direction have proven to be performance limiting factors, hindering the performance more severely for higher adsorbent bed thicknesses. Longer tubes and smaller adsorbent bed thicknesses result in better performances.

A criterion to set the best balance between COP and SCP or SHP of adsorption systems cannot be based only on energy or efficiency arguments, as the COP and SCP or SHP present a somewhat opposite dependence on the cycle time. High COPs require long cycle times and are associated with low cooling or heating powers, unless large masses of adsorbent and large sized systems are used, whereas shorter cycle times are associated with high SCPs or SHPs and low COPs. Finding the best balance between the COP and the SHP or SCP for AHP systems is not obvious. A criterion capable of finding the best balance between COP and SCP or SHP was developed, based on the minimum unit cost of the thermal useful effect of the adsorption refrigerators or heat pumps (Chapter 7). Based on the literature, this is the first time that such a criterion is being proposed. The model for a complete AHP system developed in Chapter 6 was used to investigate the dependence of the COP and SHP on the cycle time. The established criterion identifies the cycle times

that correspond to the minimum unit cost of the thermal energy useful effect of AHPs or adsorption refrigerators, the best COP and SCP or SHP combinations being those corresponding to that cycle time.

Overall, there are a few aspects that should be retained when dealing with AHPs or adsorption refrigerators. The COP of adsorption heating or cooling technologies cannot be directly compared to the COP of vapor compressions systems unless the heat to mechanical work energy conversion efficiency is considered. In terms of physical properties, the metal-adsorbent heat transfer coefficient along with the heat transfer resistance of the adsorbent itself are often the limiting factor. Investigations on adsorbent materials should put more effort on achieving adsorbent materials that can be easily handled outside the lab so they can be used in real scale systems. It is better to have and adsorbent that can be used in a real system than an adsorbent with a theoretical COP one or two decimates higher, but that cannot be used beyond the small-scale laboratory research just to carry, which carry out tests using a few grams of material. There is room for performance improvement of adsorption heating or cooling systems by using more complex configurations with several adsorbers and working configurations and strategies. However, perhaps the major performance improvements might be accomplished by finding smart ways of harvesting waste heat or using surplus heat, combining adsorption heating and cooling systems with other technologies like solar thermal collectors. Even though a given adsorption heating and or cooling system has a lower COP, its significance must be put into perspective if the energy that is being used to drive the system is surplus heat or heat freely obtained. Implementing strategies to use thermal energy freely available might play the most important role towards the implementation of adsorption heating and cooling systems in the market. Adsorption HPs systems may be more competitive when used in cooling applications since it is commonly that excess heat exists when cooling is required. As vapor compression heat pumps are electrically driven only work with electricity, they cannot use heat to generate the cooling effect, which makes the ability of adsorption refrigerators for using excess heat to produce the cooling effect a major advantage that should be extensively explored.

8.2. FUTURE CHALLENGES

In the scope of this PhD work, a prototype of an AHP for water heating purposes has been built. Since there is no market for AHP applications and its components, every part had to be customized and produced specifically for the prototype, which resulted in high

costs and several component faults throughout the building process. Nonetheless, it was possible to build-up a prototype that is expected to provide a heating power of several hundreds of watts with a COP of approximately 1.35. The AHP prototype has been described in Chapter 6 and is currently being worked on. After assembling, the adsorber, leakages were identified that prevent the achievement and maintenance of a suitable vacuum level for the AHP's operation. In the future, efforts will be made to try and solve this issue, which is crucial for the AHP to work properly. The prototype is already equipped with several sensors that will allow the evaluation of its performance, more specifically the COP and SHP for the complete AHP system. Several experimental tests are planned to be made once the AHP system is functional, aiming to obtain experimental data that will be use also for comparison with the numerical data. This comparison will allow a detailed experimental validation of the models developed in this work.

A study that evaluates and compares an AHP or refrigerator with a vapor compression heat pump or refrigerator can also be carried out. It will be interesting to fairly compare the COP for both technologies over a year, considering the heat to mechanical work conversion efficiency. This would provide a clearer view on the value of adsorption heating and cooling technologies when compared to the common vapor compression systems.

The development of an adsorption system for cooling applications seems very promising and closer to compete with vapor compression cooling systems, both economically and environmentally. The knowledge that was acquired during this PhD work can be used to design and develop such a system. Finding a way of capturing heat that is freely available and to use it to drive an adsorption cooling system to provide cooling for industrial processes, residential and industrial buildings, data centres, agriculture, fish and animal farms, among other applications, is another challenging work that deserves to be made. Furthermore, it is possible to use adsorption cooling systems in a hybrid way for simultaneous sea water desalination and cooling providing. The perspectives for further investigation on adsorption heating and cooling technologies are high, which may lead to new solutions and/or products that are environmentally friendly and more economically competitive.